A Role for Dopamine Neuron NMDA Receptors in Learning and Decision-Making

by

Emily Hueske

Submitted to the Department of Brain and Cognitive Sciences
in partial fulfillment of the requirements for the degree of

DOCTOR OF PHILOSOPHY IN NEUROSCIENCE

at the

MASSACHUSETTS INSTITUTE OF TECHNOLOGY

June 2011

Author .....
.....
Department of Brain and Cognitive Sciences
May 6, 2011

Certified by..
.....
Susumu Tonegawa
Picower Professor of Biology and Neuroscience
Thesis Supervisor

Accepted by..
.....
Earl K. Miller
Picower Professor of Neuroscience
Director, BCS Graduate Program

A Role for Dopamine Neuron NMDA Receptors in Learning and Decision-Making

by

Emily Hueske

Submitted to the Department of Brain and Cognitive Sciences
on May 6, 2011, in partial fulfillment of the
requirements for the degree of
DOCTOR OF PHILOSOPHY IN NEUROSCIENCE

Abstract

Midbrain dopamine has demonstrated roles in locomotion, motivation, associative learning, habit formation, action selection and cognition. The many functions of dopamine can be attributed to the multiple projection targets of midbrain dopaminergic nuclei and to the multiple characteristic modes of dopamine neuron firing, tonic and phasic. Phasic transients of midbrain dopamine neurons are widely reported to signal errors conveying discrepancies between predicted and actual reward. Knocking out NMDARs in dopamine neurons has been shown to attenuate dopaminergic phasic firing providing a potential model for delineating the functions of tonic and phasic dopamine. In order to study the role of dopamine neuron NMDARs in reward-contingent learning, we developed an auditory-cued binary choice task using complex auditory stimuli that lend themselves to efficient learning as well as morphing. We report that mice lacking NMDARs in dopamine neurons have a deficit in learning an auditory two-alternative choice task, in the absence of changes in response vigor.

Dopamine neurons respond phasically to rewards as well as reward predictive cues. Updating the reward predictive value of cues is fundamental to shaping adaptive patterns of behavior and decision-making. Given the hypothesized role of dopamine in the updating of reward predictive cues, we were interested to see if an influence of reward history would be evident in the choices made by mice lacking dopamine neuron NMDARs. In an auditory-cued binary choice task, we find an influence of the difficulty of prior successes on subsequent decisions when mice are challenged with varying degrees of discrimination difficulty. In mice lacking dopamine neuron NMDARs, we find a lack of influence of prior decision difficulty. Our results identify a modulation of choices by prior decision difficulty in mice, and demonstrate the dopamine-dependent nature of this modulation. These findings are consistent with a role for dopamine neuron phasic firing in the trial-by-trial shaping of reward contingent learning.

Thesis Supervisor: Susumu Tonegawa
Title: Picower Professor of Biology and Neuroscience

Acknowledgements

There are many colleagues and friends to whom I am grateful, and several without whom this thesis would not exist.

Gishnu Das has been one of my closest friends, often an advocate, an entertaining colleague and a dynamic collaborator in establishing mouse behavioral paradigms and circuit-dissecting viral vectors. Gishnu has a true talent for generating the interest and enthusiasm to forge new methodological and new conceptual directions and for identifying and acquiring new reagents and resources. He is responsible for initiating a host of collaborative efforts from which I have benefited, including a collaboration with the lab of Naoshige Uchida, the results of which are the primary topic of this thesis. In addition, Gishnu inspired our lab's early connection with the Allen Brain Institute, as well as several other collaborations in the field of viral vectors.

Arvind Govindarajan enabled my transition from cellular electrophysiology to molecular biology. Arvind has similarly been a friend for many years, and a trusted colleague whose brain seems able to engage any problem and summon an elegant solution, and whose memory for the broad to the minute is a common marvel. In particular, I have personally appreciated the ability of Arvind to make even the most complex concepts accessible.

Specific contributors to the work described in this thesis are acknowledged in Chapter 1 and are noted here with immense gratitude for their expertise and training. In relation to the work described in this thesis, I extend specific and sincerest thanks to my wonderful bench-mate Xiaoning Zhou, and my exceptional colleagues Lisa Sultzman, Wenjiang Xu, Chanel Lovett, Tobias Denninger, Ed Soucy, and Mitsuko Uchida. Not mentioned in Chapter 1 is the sage advice provided by Gonzalo Otazu and Katharine Borges of the lab of Tony Zador at Cold Spring Harbor Laboratory, two compatriots in the battle to coax feats of man out of mere mice!

The behavioral studies I describe in this thesis, I could not have accomplished without the generous demonstration and continual discussion of Mitusko Uchida and the encouragement and feedback of Nao Uchida. To carry out analyses, I had to

learn Matlab, a process made immeasurably more pleasant thanks to the patience and insights of my husband, Nathan Wilson, who took the time to teach and help me with all aspects from data storage and manipulation to plotting and statistics. Dan Bendor has consistently provided advice and helpful discussions regarding auditory perception. Finally, Mark Histed, Srini Turaga and Jeremiah Cohen, and recently, Emery Brown, all lent an ear and their expertise to helping me arrive at a concise summary statistic inspired by regression analyses in single monkeys but adapted to the world of cohorts of multiple mice.

Finally, future studies already underway include a host of in vivo electrophysiological recordings of the mice described here. This work has already required the substantial expertise and coordination on the part of Corey Puryear, our resident expert in rodent dopamine recordings.

During an early phase of my time in the Tonegawa lab, my focus was on the development of novel methods to dissect dopamine function using viral and RNAi-based strategies. I extend grateful thanks to Arvind, Hae-Yoon Jung and Inbal Israely from whom I learned molecular cloning, in addition to Carlos Lois, Sanjay Magavi, Wolfgang Kelsch and Ben Scott, who taught me how to generate lentiviral vectors, and to perform stereotactic injections in mice.

I have had the pleasure of working with several talented students during my time at MIT including Lauren LeBon, now a graduate student at CalTech, Dien Le, currently deciding on which medical school to attend, Ni Ji, a graduate student in this department, and Shani Isaac, now at Harvard Medical School. Lastly, Drew Friedman, now in graduate school at Berkeley, was a technician in our lab and, for a few lucky years, our secret weapon of innovative cloning and construct design. I was lucky to work closely with him, Gishnu, Gishnu's virologist collaborators, and Shu Huang on bringing to fruition an adenoviral viral packaging methodology for Cre-dependent constructs.

I would like to thank my committee members. Nao Uchida has generously devoted substantial time, space and thought to the experiments described here. Through the collaboration between our labs, Nao has become a second advisor on the main topic of

my thesis work, providing a combination of incredibly well-conceived ideas, novel behavioral tools and a remarkable phenomenon to explore using a mouse genetic model which requires vast amounts of time, resources and expertise to generate. Working between the Tonegawa and Uchida labs has been an incredible opportunity for scientific inquiry made truly seamless by the sheer scientific interest displayed on the part of my advisors. Carlos Lois was also a mentor as much as a committee member, and in TAing for him, working next door to his lab, discussing my research many times one-on-one with him, and having him sit on my committee, I learned a great deal about conducting science. Earl Miller and Sebastian Seung, my most recent committee members, have provided critical perspective on this work from the computational, cognitive and behavioral realms, and I am grateful for their pragmatism in the committee meeting environment. They have both been linked to specific inspirations of mine: David Freedman's work in Earl's lab on category learning was the first thesis defense I took in after moving to Boston, and has provided something of a template for some analyses described here. Sebastian's father happens to have been one of my favorite college professors, a wonderful teacher who served up an introduction to the philosophical questions surrounding volition that continues to drive my scientific interest in the subject. Finally, I would like to thank my advisor, Susumu Tonegawa, for his constant support and encouragement, his genuine interest with regard to my thesis work and his fearless pursuit of new directions. In addition, I am extremely grateful for having been welcomed into his lab and onto such an incredibly interesting project at a critical juncture in my graduate training. I have especially appreciated the ease and insistence with which Susumu advocates on behalf of his students, and am grateful for the active role he plays in seeking the resources, reagents and collaborations necessary to drive scientific progress. I have greatly benefited from Susumu's constant push for clarity of the broader ramifications and implications of data and details in a field new to many in our lab.

I am also grateful to the early advice and influence of my first PhD advisor, Guosong Liu. I learned from him many of the realities of science related to mentorship, grant-writing and publishing. A part of the work I did while in his lab is repre-

sented in two co-authored publications reproduced (with permission of the journals) in Appendices II. and III.

No dissertation project occurs in a vacuum. I have seen many people come and go over the years, and those who have stuck, and have been sources of inspiration include my close friends Neville Sanjana and Tevye Rachelson and our renegade band of classmates including Theresa, Jen, Julie, Jon and Cansu. In addition to those already mentioned, my close friends, Brandon, Inbal, Rui, Ned, Nicole, Christine, Amanda, Simon, Tim, Marjorie, Ben, Aaron, Wrenn, Asha, Jesse, Elisabeth, Jennie, Marnie, Travis, Liz, Monique, Mick, Boris and Safa, have kept science social and provided lifts during the inevitable ruts of graduate work. Denise Heintze has similarly helped smooth my journey, as has the recent help of Michael Enos. Lastly, I would like to highlight the awesome support and motivation provided in recent years by the graduate students of the Tonegawa lab, in particular, by Bridget Dolan and Alex Rivest who have traveled the long distance with me to the ends of our theses. This thesis is written in LaTex due entirely to a concise and information-dense education provided by Alex.

I would like to thank my family, my parents Horst and Virginia Hüske, and my brother Jason Hueske, for the ever-interesting and always supportive environment they provide, and for their constant love and encouragement throughout my time here. This thesis is dedicated to them. My more recent initiation into Nathan's wonderful family has provided joy and inspiration at every turn.

And finally, I would like to thank my husband and colleague, Nathan Wilson, from whom I have learned an amazing amount about positive reinforcement-based behavior modification. In the words of one of the faculty in this department, Nathan has been "a beacon of positivity", for me an absolute pillar of support, a kind critic, a structured thinker, a scientist on whose feedback I have often relied, an all-around remarkable human.

This thesis is dedicated to my parents, Horst and Virginia Hüske.

Contents

List of Figures

List of Tables

List of Abbreviations Part 1	
β-Gal	β-Galactosidase; *lacZ* Gene Product
AAV8	Adeno-associated virus serotype 8
AP5	2-amino-5-phosphonopropionic acid
BA	Basolateral Amygdala
BNST	Bed Nucleus of the Stria Terminalis
CA1	Cornu Ammonis Area 1
Cre	Cre-recombinase
Cre$^+$	Cre Expressing
CPP	Conditioned Place Preference
DAT	Dopamine Transporter
DAT-Cre	DAT Promoter Driving Cre-Expression; *Slc6a3$^{+/Cre}$*
DAT/NR1	DAT-Cre and floxed NR1 Mouse Cross
ECFP	Enhanced Cyan Fluorescent Protein
EYFP	Enhanced Yellow Fluorescent Protein
flox	Gene Flanked by loxP Sites
GABA	γ-Aminobutyric Acid
Grin1$^{f/f}$	floxed NR1 Mouse
hSyn1	Human Synapsin I
LDTg	Lateral Dorsal Tegmentum
loxP	Cre-binding Site of Cre-mediated Recombination
LSL	*loxP*-STOP-*loxP* Cassette
LTP	Long-term Potentiation
NMDA	N-methyl-D-aspartate
NMDAR	N-methyl-D-aspartate Receptor
NR1	N-methyl-D-aspartate Receptor Subunit 1
NAcc	Nucleus Accumbens
PFC	Prefrontal Cortex
OFC	Orbitofrontal Cortex
PolII	RNA Polymerase II

List of Abbreviations Part 2	
PPTg	Peduculopontine Tegmentum
RNAi	RNA interference
RRN	Retrorubral Nucleus
ROSA26-LSL-*lacZ*	ROSA26 Promoter Driving β-galactosidase (Reporter Mouse)
RSV	Rous Sarcoma Virus
Slc6a3$^{+/Cre}$	DAT promoter driving Cre Expression Mouse (Cre Mouse Line)
Slc6a3$^{+/Cre}$***;Grin1***$^{\Delta/+}$	Dopamine Neuron NMDAR KO (DAT/NR1 Knockout)
Slc6a3$^{+/Cre}$***;Grin1***$^{\Delta/f}$	Control Mouse (DAT/NR1 Control)
shRNA	short hairpin RNA
siRNA	small interfering RNA
SNc	Substantia Nigra pars compacta
TH	Tyrosine Hydroxylase
TUNEL	Terminal Deoxynucleotidyl Transferase dUTP Nick End Labeling
VTA	Ventral Tegmental Area
VSVG	Vesicular Stomatitis Virus Glycoprotein
WRE	Woodchuck Hepatitis Virus Regulatory Element
X-Gal	bromo-chloro-indolyl-galactopyranoside

Chapter 1

Introduction

Midbrain dopamine has demonstrated roles in locomotion, motivation, associative learning, habit formation, action selection and cognition. In mouse, dopamine has demonstrated roles in behavioral assays of locomotion, motivation, cue-based learning and habit formation (in Pavlovian and operant conditioning tasks), working memory (eg., DMS tasks), models of addiction (behavioral sensitization, conditioned place preference, self-administration and self-stimulation), impulsivity (temporal discounting), perseveration and behavioral flexibility (WCS), attention (5CSRRT), and in diseases including most notably Parkinson's disease and Schizophrenia, as well as Huntington's disease and ADHD. The many roles played by dopamine result at least in part from the diversity of dopamine receptors, the diversity of target structures, the diversity of afferent structures, and the multiple modes of neuronal firing ascribed to midbrain dopamine neurons, ie. tonic and phasic modes.

Phasic dopamine release resulting from dopamine neuron burst-firing occurs in a manner consistent with reward prediction error signaling, and has a demonstrated role in the development of cue-reward associations. Knocking out NMDARs in dopamine neurons has been shown to attenuate dopaminergic phasic firing providing a potential model system for delineating the functions subserved by tonic and phasic dopamine release.

The aim of this thesis is to advance understanding of the role of burst-firing of midbrain dopamine neurons in learning and decision-making by investigation of a

mouse lacking NMDAR function in dopamine neurons in an auditory two-alternative forced choice task.

1.0.1 Contributions of this Thesis

The work in this thesis describes the role of dopamine neuron NMDAR-mediated burst-firing in associative learning and decision-making.

- We describe the development of an auditory two-cue alternative forced choice task and the development of auditory stimuli that lend themselves to efficient learning as well as morphing.
- We report that mice lacking NMDARs in dopamine neurons show impaired acquisition of a two alternative forced choice task.
- We report that mice lacking NMDARs in dopamine neurons retain normal locomotor responses and motivation for acquiring rewards.
- We describe an influence of the difficulty of prior success on subsequent decisions in mice when challenged with varying degrees of discrimination difficulty in an auditory-cued two alternative forced choice task.
- We demonstrate that dopamine neuron NMDARs modulate the influence of prior success on subsequent decisions in a difficulty-dependent manner.

1.0.2 Organization of Thesis

Chapter 2. Background Chapter 2 serves as a review of relevant literature regarding the multiplicity of dopamine functions and how these functions may arise from the vast connectivity and complex firing properties of these neurons.

Chapter 3. Mice Lacking Dopamine Neuron NMDARs Show Learning Impairments Despite Normal Response Vigor Chapter 3 describes the generation of a line of transgenic mice lacking, specifically in dopamine neurons, the obligatory NMDA receptor subunit, NR1. Previous characterizations of mice lacking functional NMDARs in dopamine neurons show selective reduction of burst-firing

in dopamine neurons, the mode of firing specifically proposed to serve as a reward prediction error or "teaching signal." By comparison, previous reports of mice with increased "tonic" dopamine firing have described enhanced motivation in the absence of new learning. We describe the development of an auditory two-cue alternative forced choice task to test reward contingent learning in a mouse line previously reported to show reduced dopamine neuron burst-firing. We describe the development of auditory stimuli that lend themselves to efficient learning as well as morphing. We report that mice lacking dopamine neuron NMDARs demonstrate impaired learning in a two-alternative forced choice task, despite normal response vigor.

Chapter 4. Dopamine Burst-Firing Modulates the Influence of Prior Success on Current Decisions Studies dating back at least to those culminating in Thorndike's Law of Effect have demonstrated the influence of prior choice parameters on future decisions. Recent observations in rat by the Uchida and Mainen labs (manuscript in preparation) have identified an influence of degree of difficulty of prior trials on subsequent decisions in an odor-cued two alternative forced choice task. We report this influence in mice challenged by varying degrees of discrimination difficulty in an auditory-cued two alternative forced choice task. Using mice engineered to selectively lack dopamine neuron NMDARs, we report a dopamine-dependent influence of the difficulty of a prior success on a subsequent decision.

Appendix I. Novel Viral Vector and shRNA-based Circuit Genetic Approaches to Study Dopamine Function Appendix I describes the development of tools aimed at the genetic dissection of dopamine circuits and firing properties using a temporally specific and spatially and cell-type restricted alternative to the transgenic line used in the primary thesis. Specifically described is a virally delivered Cre-mediated shRNA-based strategy for knockdown of gene targets as well as a shRNA-resistant NR1 rescue construct.

Appendix II. Studies of VGLUT1 Appendix II describes a published collaboration of a study of the function of the VGLUT1 vesicular glutamate transporter in

presynaptic function.

Appendix III. Studies of LAR Appendix III describes a published collaboration of a study of the role of the receptor protein tyrosine phosphatase, LAR, in postsynapse formation and function.

1.0.3 Contributors to this Thesis

Please see the Acknowledgements section for extended acknowledgements of others who advised, facilitated and provided the necessary training and mentoring to carry out the work described in this thesis. In particular, Gishnu Das, initiated the collaboration between the Tonegawa and Uchida labs, and worked on a parallel project and parallel pilot experiments to those behavioral experiments described here.

Data Chapters 3-5. E.H., with advice from Arvind Govindarajan and Susumu Tonegawa, developed the breeding strategy, bred, managed and genotyped the first cohort of mice described in all chapters of this thesis. The second of two cohorts of mice described in this thesis was managed and genotyped with the expert help of Xiaoning Zhou. Immunohistochemistry and X-gal staining experiments shown in this thesis were designed and performed by E.H. In situ hybridization experiments were designed by E.H. with the expert advice of Lisa Sultzman and carried out by Lisa Sultzman, Wenjiang Xu and Chanel Lovett. Behavioral experiments were designed by E.H. and Naoshige Uchida with advice from Mitsuko Uchida and members of the Zador lab at Cold Spring Harbor Labs. Auditory stimuli were designed by E.H. with advice from members of the Zador Lab and Naoshige Uchida. Tobias Denninger generated custom Matlab scripts to instantiate the auditory stimulus design. Ed Soucy wrote and provided customized modifications of two generations of LabView software designed to control and acquire data from auditory experiments performed in behavioral training boxes designed for olfactory experiments. All behavioral equipment used in experiments described in this thesis was developed by Naoshige Uchida and Zach Mainen. E.H. performed all behavioral experiments. E.H. wrote all Matlab analysis

scripts used in the analysis of data in this thesis. All analyses were performed by E.H. with advice from many (see Acknowledgements), in particular, Nathan Wilson, Mitsuko Uchida, Naoshige Uchida and Susumu Tonegawa.

Appendix I. E.H. screened and cloned shRNA candidates with training from Arvind Govindarajan and Hae-Yoon Jung. E.H. and Arvind Govindarajan designed an adaptation of a Cre-dependent shRNA construct for use with multiple fluorophores. Critical advice was provided by Carlos Lois. E.H., with training from Carlos Lois, generated lentiviral conditional shRNA vectors and performed stereotactic injections for in vivo assessments of RNAi efficacy, RNAi toxicity and RNAi off-target effects. Gishnu Das and E.H. screened in vivo neuronal transduction efficiencies of lentiviral, AAV, HSV and AD vectors. E.H. cloned conditional shRNA constructs into AAV packaging plasmids. E.H. performed stereotactic injections, immunostaining, X-gal staining and, with the help of Shani Isaac, TUNEL staining for experiments assessing RNAi efficacy, toxicity and off-target effects in conditional AAV-shRNA vectors. Stereotactic injections, immunostaining and X-gal staining experiments for assessment of dose-response and time-course properties of AAV-shRNA vector were designed by E.H. and performed by Xiaoning Zhou. Shani Isaac generated shRNA-resistant target-gene rescue constructs under the guidance of E.H and Arvind Govindarajan. Drew Friedman cloned these target-gene rescue constructs into AAV packaging plasmids.

Appendix II. E.H. contributed immunocytochemical evidence of activity-dependent changes in VGLUT1 expression. E.H., Nathan Wilson and Guosong Liu designed experiments. E.H. performed experiments and analyses of immunocytochemical data.

Appendix II. E.H. contributed electrophysiological assessments of the role of LAR and LAR mutants in synapse function, in particular, the effect of LAR and LAR mutants on measures generally attributed to pre- versus post-synapse function. E.H., Guosong Liu, Anthone Dunah and Morgan Sheng designed experiments. E.H. performed experiments and analyses of whole-cell patch clamp recordings.

Chapter 2

Background

The purpose of this chapter is to provide a review of relevant literature regarding the multiplicity of dopamine functions and how these functions may arise from the vast connectivity and complex firing properties of these neurons. In addition, literature is reviewed relating burst-firing properties of dopamine neurons to theories of dopamine as a prediction error and teaching signal and to behavioral assays of classical and operant conditioning as well as decision-making.

2.1 Introduction

Midbrain dopamine has demonstrated roles in locomotion, motivation, associative learning, habit formation, action selection and cognition. In mouse, dopamine has demonstrated roles in behavioral assays of locomotion, motivation, cue-based learning and habit formation (in Pavlovian and operant conditioning tasks), working memory (eg., delay match/non-match tasks), models of addiction (behavioral sensitization, conditioned place preference, self-administration and self-stimulation), impulsivity (temporal discounting), perseveration and behavioral flexibility (Wisconsin Card Sorting task), attention (5-choice serial reaction time task), and in diseases including most notably Parkinson's disease and Schizophrenia, as well as Huntington's disease and ADHD. The many roles played by

dopamine result at least in part from the diversity of dopamine receptors, the diversity of target structures, the diversity of afferent structures, and the multiple modes of neuronal firing ascribed to midbrain dopamine neurons, ie. tonic and phasic modes.

2.2 Midbrain Dopaminergic Anatomy

Multiple brain targets of midbrain dopamine neurons. Dopamine is produced primarily in neurons of two brain regions, the olfactory bulb and the ventral midbrain; in addition, sparse populations of dopamine producing neurons can be found in the hypothalamic and striatal regions. Within the midbrain, dopamine nuclei are classified based on their projection targets, morphology and neurochemistry as ventral tegmental area (VTA, A10), substantia nigra pars compacta (SNc, A9), and retrorubral (RRN, A8) populations. Midbrain dopamine nuclei comprise a system of modulatory neurons with projections to diverse brain targets. In this section, literature is reviewed, which will highlight brain regions which receive dopaminergic innervation. The goal of this survey is to develop a description of what brain targets of dopamine innervation may be impacted by a perturbation of dopamine neuron burst-firing (Swanson, 1982; Fields et al., 2007; Lammel et al., 2008).

Table 2.1: Percentage of retrogradely labeled cells found in dopamine subregions that were also stained with anti-TH. $*$ indicates no estimate could be obtained. (-) indicates no retrograde labeling. Adapted from Swanson, 1982.

$Site of Injection$	$VTA(\%)$	$SNC(\%)$	$PPN(\%)$
NAcc	85	90	65
Lateral Septum	72	80	-
Amygdala	27	*	*
Entorhinal Areas	46	33	80
Hippocampus	6	67	-
Lateral Hypothalamus	1	-	-
Locus Coeruleus	1	2	0

VTA efferents project via three fiber tracts to distal brain targets. The primary projection ascends via the medial forebrain bundle to terminate in the ventral striatum (in particular the accumbens), the olfactory tubercle, the central, medial and lateral nuclei of the amydgala, and the septal region (including the lateral septal nucleus, the bed nucleus of the stria terminalis (BNST) and the nucleus of the diagonal band), the hippocampal system, entorhinal areas, and hypothalamus. A second fiber projection ascends dorsally from the VTA innervating the areas in the medial thalamus, including the nucleus reunions, the central medial thalamus, mediodorsal thalamus and lateral habenula. A third projection descends from the VTA through the brainstem to innervate the periacquaductal grey, the parabrachial nucleus, the locus coeruleus, and the median raphe (Swanson, 1982). Dopamine projecting to each of these regions may serve to facilitate the particular functions subserved by those target brain regions.

2.3 Midbrain Dopamine Neuron Firing Properties

In vivo studies of dopamine neurons suggest that the activity of dopamine neurons can be parceled into three main patterns of activation: inactive, tonic firing, and, phasic or burst-firing (Grace and Bunney, 1984b,a; Hyland et al., 2002). The afferent circuitry of midbrain dopamine neurons, their intrinsic membrane properties, and their active conductances determine their instantaneous pattern of activity.

Afferent control of multiple modes of dopamine neuron firing. At any given time, 50% of dopamine neurons are held in an inactive state. Studies by Grace and colleagues suggest this is due to a strong, tonically active GABAergic input from the ventral pallidum. Disinhibition of dopamine neurons is proposed to occur when these pallidal inputs are inhibited by a strong GABAergic projection from medium spiny neurons of the striatum.

Tonic firing. Disinhibition of dopamine neurons from this pallidal clamp unmasks a state of irregular single-spike firing at 2-10 Hz characteristic of spontaneously ac-

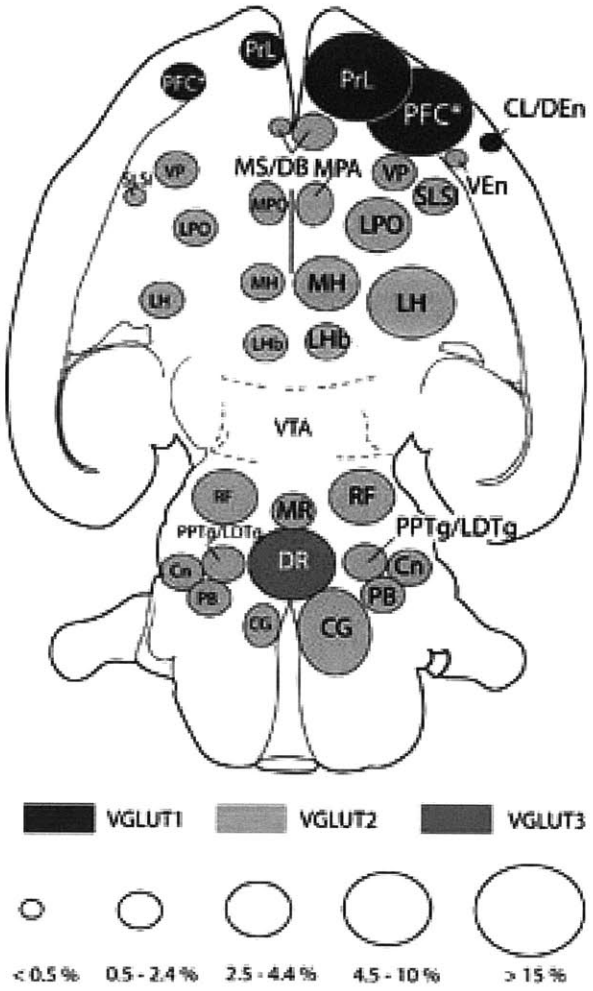

Figure 2-1: **Glutamatergic afferents of VTA.** Diagram of brain nuclei that send glutamatergic projections to VTA. Structures are shaded according to expression of vesicular glutamate transporter, VGLUT1, 2 or 3 (Geisler et al., 2007).

tive dopamine neurons. This baseline firing rate of dopamine activity establishes 'tonic' levels of dopamine in target brain structures. The ventral subiculum has been demonstrated to provide glutamatergic drive to the striatum which can ultimately disinhibit dopamine neurons from an inactive state to this spontaneously active state (Floresco et al., 2001, 2003). (Note: ventral subicular stimulation could also cause activation of dopamine neurons via a polysynaptic excitatory pathway through the PFC. However, Floresco, et al. 2001 and 2003 demonstrate the major effect of ventral subicular stimulation to be a change in numbers of VTA cells firing. They propose that this occurs via disinhibition from pallidal inputs. This is the basis for one leg of

a hippocampal-VTA circuit proposed by John Lisman and Anthony Grace to enable novelty-detection and long-term memory.)

Phasic firing. Burst-firing in dopamine neurons in vivo is classified and defined as three or more spikes with an interspike interval (ISI) of <80ms terminating upon an ISI >160ms (although some studies have included doublets as bursts) (Grace and Bunney, 1984b). These firing modes result in different release profiles in target structures. Dopamine measurements by voltammetry and microdialysis have estimated that tonic firing results in striatal dopamine concentrations of 5-100 nmol/L (Justice, 1993; Suaud-Chagny et al., 1992), while phasic transients thought to result from burst-firing can reach >1μmol/L (Robinson et al., 2001, 2002). In a comparison of afferent drive of midbrain dopamine neurons, burst-firing induced by PPTg stimulation was found to enhances striatal dopamine release 3-fold over tonic firing induced by subicular stimulation. However, burst-firing mediated dopamine transients were only observed following blockade of reuptake mechanisms in the striatum (Floresco et al., 2003). The difference in release concentration and regulation and by reuptake mechanisms highlights differences that undoubtedly underlie function and behavior influenced by these distinct modes of firing.

2.4 The Role of NMDA Receptors in Dopamine Physiology and Function

Dopamine neuron burst-firing as reward prediction error signal. Midbrain dopamine neurons are widely reported to signal errors conveying discrepancies between predicted and actual reward, and, in some cases, punishment (Mirenowicz and Schultz, 1994; Montague et al., 1996; Schultz, 1998; Bayer and Glimcher, 2005; D'Ardenne et al., 2008; Fiorillo et al., 2003; Hollerman and Schultz, 1998; Matsumoto and Hikosaka, 2009; Morris et al., 2006; Pan and Hyland, 2005a; Roesch et al., 2007; Tobler et al., 2005; Ungless et al., 2004; Waelti et al., 2001). Phasic dopamine responses to unexpected rewards and reward predictive cues (Satoh et al., 2003; Naka-

hara et al., 2004; Bayer and Glimcher, 2005; Tobler et al., 2005; Morris et al., 2006; Ravel and Richmond, 2006; Roesch et al., 2007; Kobayashi and Schultz, 2008) are broadcast widely to brain structures where dopamine may contribute to the updating of decision parameters including the predictive value of cues.

Glutamatergic afferents induce dopamine neuron burst-firing. Burst-firing in dopamine neurons can be induced by direct iontophoresis of glutamate onto dopamine neurons *in vivo* (Grace and Bunney, 1984a; Floresco et al., 2003; Chergui et al., 1994). In addition, blocking NMDARs (Chergui et al., 1993; Overton and Clark, 1992) or knocking out NMDARs (Zweifel et al., 2009) has been demonstrated to dramatically reduce spontaneous or evoked burst-firing. While multiple sources of glutamatergic input could account for the induction of burst-firing, the PPTg, a glutamatergic and cholinergic nucleus in the rostral pons, has been repeatedly demonstrated to elicit robust burst-firing in VTA dopamine neurons (Hyland et al., 2002; Pan and Hyland, 2005b; Floresco et al., 2003; Lodge and Grace, 2006; Lokwan et al., 1999). Of note is the observation that *in vitro* midbrain slice preparations lack spontaneous bursting. Instead dopamine neurons show a pacemaker firing pattern reminiscent of tonic firing in vivo. Interestingly, the inactivation of the lateral dorsal tegmentum (LDTg) *in vivo* prevents burst firing of dopamine neurons, suggesting that this LDTg cholinergic input gates burst-firing induced by the largely glutamatergic input of the PPTg (Lodge and Grace, 2006).

Dopamine facilitates plasticity in target regions. One suggested mechanism by which tonic and phasic firing modes may confer differential function is by differential activation of high and low affinity dopamine receptors in dopamine target regions (Richfield et al., 1989). Specifically, low affinity dopamine D1 receptors, activated preferentially by higher concentrations of dopamine such as those resulting from dopamine burst-firing, are implicated in learning as well as synaptic plasticity in dopamine target regions (Dalley et al., 2005; Goto and Grace, 2005; Frey et al., 1990; Huang and Kandel, 1995; Otmakhova and Lisman, 1996).

2.5 The Role of NMDA Receptors in Dopamine Neuron Synaptic Plasticity

NMDA receptors mediate synaptic plasticity in midbrain dopamine neurons: behavioral insights from models of addiction. NMDA receptors mediate synaptic plasticity in dopamine neurons as they do in forebrain regions (Bonci and Malenka, 1999; Overton et al., 1999). This discovery led to a number of investigations of midbrain NMDARs in rodent models of addiction, and a view of addiction as a disease of learning and memory (Hyman, 2005). Research using addiction models has, therefore, informed a broader understanding of the role of dopamine arising from midbrain circuits in the associations formed between cues and rewards. For instance, reinstatement of drug-seeking behavior can occur in response to exposure to drug-associated cues and contexts. Inactivating the VTA blocks cue-induced reinstatement of cocaine-seeking (Di Ciano and Everitt, 2004). This effect is at least partially due to dopamine neurons because blocking D1 receptors in PFC blocks cue-induced reinstatement (McFarland and Kalivas, 2001). A role for glutamatergic afferents to dopamine neurons was suggested when blocking VTA glutamate receptors with kynurenic acid was found to block relapse to cocaine-seeking induced by hippocampal theta burst stimulation (Vorel et al., 2001). Efforts to further dissect the circuitry and mechanisms underlying the role of dopamine in associative learning led to further cellular and behavioral investigations of the role of NMDARs in addiction models. Cocaine exposure induces NMDAR-dependent LTP in VTA (Liu et al., 2005). *In vivo* cocaine exposure occludes NMDAR-dependent LTP in VTA (Ungless et al., 2001).

Acquisition deficits in mice lacking dopamine neuron NMDARs increase with increased task difficulty. Recent studies of mice lacking NMDARs specifically in dopamine neurons have addressed the role of dopamine neuron NMDARs in two paradigms commonly used as models of drug addiction paradigms as well as associative learning: behavioral sensitization, in which locomotor behavior increases

in response to the same dose of reinforcer, and conditioned place preference (CPP), in which cocaine is repeatedly paired with one context and saline with another resulting in a preference for the cocaine-paired context (Zweifel et al., 2008; Engblom et al., 2008). Neither study found a role for dopamine neuron NMDARs in behavioral sensitization. While their CPP results differed, so did the details of their paradigm. Three sessions of cocaine-context pairings revealed a deficit in mice lacking NMDARs, while eight pairings did not, a discrepancy suggested to be the result of saturation of learning by 8 days of training. Further studies support the notion that deficits in mice lacking dopamine neuron NMDARs may be revealed as a function of task difficulty. While a simple Pavlovian conditioned approach training was acquired normally by mice lacking NMDARs, a visually-cued t-maze task performed by the same group showed acquisition deficits (Parker et al., 2010; Zweifel et al., 2009). Consistent with the interpretation that increased task difficulty unmasks greater learning deficits in mice lacking dopamine neuron NMDARs, voltammetry of dopamine release profiles in the nucleus accumbens during conditioned approach training, a task which revealed no acquisition deficit in NMDAR knockout mice, also revealed no difference in the *rate* of change in dopamine responding across training between genotypes. This was seen despite replicating an earlier report of a reduction in dopamine neuron burst-firing (albeit a 3-fold reduction compared a 6-fold reduction reported in response to PPTg-evoked dopamine release). Therefore, while mice lacking dopamine neuron NMDARs show reduced burst-firing, small dopamine transients were seen to task relevant stimuli. And while scaled down in magnitude, these small dopamine transients occurred in response to rewards and developed in response to reward-predictive cues. These findings suggest that a threshold exists in terms of task difficulty above which dopamine neuron NMDARs enable learning.

Further questions regarding the role of dopamine neuron NMDARs. The following questions arise regarding the function of dopamine neuron NMDARs. Is the role of the NMDAR in cue-reward associations, as demonstrated by recent literature, attributable to its role in synaptic plasticity at midbrain dopamine neurons,

or to the facilitation effected by dopamine release in target regions, or both? It is possible that NMDAR-mediated plasticity of inputs to dopamine neurons allows rearrangement of glutamatergic midbrain dopamine afferents, thereby enabling correlated burst firing to reward-predictive cues and salient stimuli. Glutamatergic inputs arising from the PPTg may drive burst-firing in dopamine neurons, subicular or lateral dorsal tegmental inputs may gate this drive by way of disinhibition via the accumbal-pallidal midbrain inputs, prefrontal cortical inputs may provide "top-down" modulation of phasic dopamine activation according to global task parameters. While these differential glutamatergic and GABAeric inputs may confer different types of modulation on midbrain circuits, further dissection using circuit genetic methods is needed to disentangle the many converging glutamatergic contributions, as well as the functional and behavioral consequences of the broadly diverging output of the midbrain dopamine system. Appendix I describes the development of one circuit genetic approach, an effort in that direction, integrating recombinant viral, conditional transgenic and RNAi technologies for the purpose of furthering the dissection of such complex regions as the dopaminergic midbrain.

Bibliography

Bayer, H. M. and P. W. Glimcher (2005). Midbrain dopamine neurons encode a quantitative reward prediction error signal. *Neuron 47*(1), 129–41.

Bonci, A. and R. C. Malenka (1999). Properties and plasticity of excitatory synapses on dopaminergic and gabaergic cells in the ventral tegmental area. *J Neurosci 19*(10), 3723–30.

Chergui, K., H. Akaoka, P. J. Charlety, C. F. Saunier, M. Buda, and G. Chouvet (1994). Subthalamic nucleus modulates burst firing of nigral dopamine neurones via nmda receptors. *Neuroreport 5*(10), 1185–8.

Chergui, K., P. J. Charlety, H. Akaoka, C. F. Saunier, J. L. Brunet, M. Buda, T. H. Svensson, and G. Chouvet (1993). Tonic activation of nmda receptors causes spontaneous burst discharge of rat midbrain dopamine neurons in vivo. *Eur J Neurosci 5*(2), 137–44.

Dalley, J. W., K. Laane, D. E. Theobald, H. C. Armstrong, P. R. Corlett, Y. Chudasama, and T. W. Robbins (2005). Time-limited modulation of appetitive pavlovian memory by d1 and nmda receptors in the nucleus accumbens. *Proc Natl Acad Sci U S A 102*(17), 6189–94.

D'Ardenne, K., S. M. McClure, L. E. Nystrom, and J. D. Cohen (2008). Bold responses reflecting dopaminergic signals in the human ventral tegmental area. *Science 319*(5867), 1264–7.

Di Ciano, P. and B. J. Everitt (2004). Contribution of the ventral tegmental area to

cocaine-seeking maintained by a drug-paired conditioned stimulus in rats. *Eur J Neurosci 19*(6), 1661–7.

Engblom, D., A. Bilbao, C. Sanchis-Segura, L. Dahan, S. Perreau-Lenz, B. Balland, J. R. Parkitna, R. Lujan, B. Halbout, M. Mameli, R. Parlato, R. Sprengel, C. Luscher, G. Schutz, and R. Spanagel (2008). Glutamate receptors on dopamine neurons control the persistence of cocaine seeking. *Neuron 59*(3), 497–508.

Fields, H. L., G. O. Hjelmstad, E. B. Margolis, and S. M. Nicola (2007). Ventral tegmental area neurons in learned appetitive behavior and positive reinforcement. *Annu Rev Neurosci 30*, 289–316.

Fiorillo, C. D., P. N. Tobler, and W. Schultz (2003). Discrete coding of reward probability and uncertainty by dopamine neurons. *Science 299*(5614), 1898–902.

Floresco, S. B., C. L. Todd, and A. A. Grace (2001). Glutamatergic afferents from the hippocampus to the nucleus accumbens regulate activity of ventral tegmental area dopamine neurons. *J Neurosci 21*(13), 4915–22.

Floresco, S. B., A. R. West, B. Ash, H. Moore, and A. A. Grace (2003). Afferent modulation of dopamine neuron firing differentially regulates tonic and phasic dopamine transmission. *Nat Neurosci 6*(9), 968–73.

Frey, U., H. Schroeder, and H. Matthies (1990). Dopaminergic antagonists prevent long-term maintenance of posttetanic ltp in the ca1 region of rat hippocampal slices. *Brain Res 522*(1), 69–75.

Geisler, S., C. Derst, R. W. Veh, and D. S. Zahm (2007). Glutamatergic afferents of the ventral tegmental area in the rat. *J Neurosci 27*(21), 5730–43.

Goto, Y. and A. A. Grace (2005). Dopamine-dependent interactions between limbic and prefrontal cortical plasticity in the nucleus accumbens: disruption by cocaine sensitization. *Neuron 47*(2), 255–66.

Grace, A. A. and B. S. Bunney (1984a). The control of firing pattern in nigral dopamine neurons: burst firing. *J Neurosci 4*(11), 2877–90.

Grace, A. A. and B. S. Bunney (1984b). The control of firing pattern in nigral dopamine neurons: single spike firing. *J Neurosci 4*(11), 2866–76.

Hollerman, J. R. and W. Schultz (1998). Dopamine neurons report an error in the temporal prediction of reward during learning. *Nat Neurosci 1*(4), 304–9.

Huang, Y. Y. and E. R. Kandel (1995). D1/d5 receptor agonists induce a protein synthesis-dependent late potentiation in the ca1 region of the hippocampus. *Proc Natl Acad Sci U S A 92*(7), 2446–50.

Hyland, B. I., J. N. Reynolds, J. Hay, C. G. Perk, and R. Miller (2002). Firing modes of midbrain dopamine cells in the freely moving rat. *Neuroscience 114*(2), 475–92.

Hyman, S. E. (2005). Addiction: a disease of learning and memory. *Am J Psychiatry 162*(8), 1414–22.

Justice, J. B., J. (1993). Quantitative microdialysis of neurotransmitters. *J Neurosci Methods 48*(3), 263–76.

Kobayashi, S. and W. Schultz (2008). Influence of reward delays on responses of dopamine neurons. *J Neurosci 28*(31), 7837–46.

Lammel, S., A. Hetzel, O. Hackel, I. Jones, B. Liss, and J. Roeper (2008). Unique properties of mesoprefrontal neurons within a dual mesocorticolimbic dopamine system. *Neuron 57*(5), 760–73.

Liu, Q. S., L. Pu, and M. M. Poo (2005). Repeated cocaine exposure in vivo facilitates ltp induction in midbrain dopamine neurons. *Nature 437*(7061), 1027–31.

Lodge, D. J. and A. A. Grace (2006). The hippocampus modulates dopamine neuron responsivity by regulating the intensity of phasic neuron activation. *Neuropsychopharmacology 31*(7), 1356–61.

Lokwan, S. J., P. G. Overton, M. S. Berry, and D. Clark (1999). Stimulation of the pedunculopontine tegmental nucleus in the rat produces burst firing in a9 dopaminergic neurons. *Neuroscience 92*(1), 245–54.

Matsumoto, M. and O. Hikosaka (2009). Two types of dopamine neuron distinctly convey positive and negative motivational signals. *Nature 459*(7248), 837–41.

McFarland, K. and P. W. Kalivas (2001). The circuitry mediating cocaine-induced reinstatement of drug-seeking behavior. *J Neurosci 21*(21), 8655–63.

Mirenowicz, J. and W. Schultz (1994). Importance of unpredictability for reward responses in primate dopamine neurons. *J Neurophysiol 72*(2), 1024–7.

Montague, P. R., P. Dayan, and T. J. Sejnowski (1996). A framework for mesencephalic dopamine systems based on predictive hebbian learning. *J Neurosci 16*(5), 1936–47.

Morris, G., A. Nevet, D. Arkadir, E. Vaadia, and H. Bergman (2006). Midbrain dopamine neurons encode decisions for future action. *Nat Neurosci 9*(8), 1057–63.

Nakahara, H., H. Itoh, R. Kawagoe, Y. Takikawa, and O. Hikosaka (2004). Dopamine neurons can represent context-dependent prediction error. *Neuron 41*(2), 269–80.

Otmakhova, N. A. and J. E. Lisman (1996). D1/d5 dopamine receptor activation increases the magnitude of early long-term potentiation at ca1 hippocampal synapses. *J Neurosci 16*(23), 7478–86.

Overton, P. and D. Clark (1992). Iontophoretically administered drugs acting at the n-methyl-d-aspartate receptor modulate burst firing in a9 dopamine neurons in the rat. *Synapse 10*(2), 131–40.

Overton, P. G., C. D. Richards, M. S. Berry, and D. Clark (1999). Long-term potentiation at excitatory amino acid synapses on midbrain dopamine neurons. *Neuroreport 10*(2), 221–6.

Pan, W. X. and B. I. Hyland (2005a). Pedunculopontine tegmental nucleus controls conditioned responses of midbrain dopamine neurons in behaving rats. *J Neurosci 25*(19), 4725–32.

Pan, W. X. and B. I. Hyland (2005b). Pedunculopontine tegmental nucleus controls conditioned responses of midbrain dopamine neurons in behaving rats. *J Neurosci 25*(19), 4725–32.

Parker, J. G., L. S. Zweifel, J. J. Clark, S. B. Evans, P. E. Phillips, and R. D. Palmiter (2010). Absence of nmda receptors in dopamine neurons attenuates dopamine release but not conditioned approach during pavlovian conditioning. *Proc Natl Acad Sci U S A 107*(30), 13491–6.

Ravel, S. and B. J. Richmond (2006). Dopamine neuronal responses in monkeys performing visually cued reward schedules. *Eur J Neurosci 24*(1), 277–90.

Richfield, E. K., J. B. Penney, and A. B. Young (1989). Anatomical and affinity state comparisons between dopamine d1 and d2 receptors in the rat central nervous system. *Neuroscience 30*(3), 767–77.

Robinson, D. L., M. L. Heien, and R. M. Wightman (2002). Frequency of dopamine concentration transients increases in dorsal and ventral striatum of male rats during introduction of conspecifics. *J Neurosci 22*(23), 10477–86.

Robinson, D. L., P. E. Phillips, E. A. Budygin, B. J. Trafton, P. A. Garris, and R. M. Wightman (2001). Sub-second changes in accumbal dopamine during sexual behavior in male rats. *Neuroreport 12*(11), 2549–52.

Roesch, M. R., D. J. Calu, and G. Schoenbaum (2007). Dopamine neurons encode the better option in rats deciding between differently delayed or sized rewards. *Nat Neurosci 10*(12), 1615–24.

Satoh, T., S. Nakai, T. Sato, and M. Kimura (2003). Correlated coding of motivation and outcome of decision by dopamine neurons. *J Neurosci 23*(30), 9913–23.

Schultz, W. (1998). Predictive reward signal of dopamine neurons. *J Neurophysiol 80*(1), 1–27.

Suaud-Chagny, M. F., K. Chergui, G. Chouvet, and F. Gonon (1992). Relationship between dopamine release in the rat nucleus accumbens and the discharge activity of dopaminergic neurons during local in vivo application of amino acids in the ventral tegmental area. *Neuroscience 49*(1), 63–72.

Swanson, L. W. (1982). The projections of the ventral tegmental area and adjacent regions: a combined fluorescent retrograde tracer and immunofluorescence study in the rat. *Brain Res Bull 9*(1-6), 321–53.

Tobler, P. N., C. D. Fiorillo, and W. Schultz (2005). Adaptive coding of reward value by dopamine neurons. *Science 307*(5715), 1642–5.

Ungless, M. A., P. J. Magill, and J. P. Bolam (2004). Uniform inhibition of dopamine neurons in the ventral tegmental area by aversive stimuli. *Science 303*(5666), 2040–2.

Ungless, M. A., J. L. Whistler, R. C. Malenka, and A. Bonci (2001). Single cocaine exposure in vivo induces long-term potentiation in dopamine neurons. *Nature 411*(6837), 583–7.

Vorel, S. R., X. Liu, R. J. Hayes, J. A. Spector, and E. L. Gardner (2001). Relapse to cocaine-seeking after hippocampal theta burst stimulation. *Science 292*(5519), 1175–8.

Waelti, P., A. Dickinson, and W. Schultz (2001). Dopamine responses comply with basic assumptions of formal learning theory. *Nature 412*(6842), 43–8.

Zweifel, L. S., E. Argilli, A. Bonci, and R. D. Palmiter (2008). Role of nmda receptors in dopamine neurons for plasticity and addictive behaviors. *Neuron 59*(3), 486–96.

Zweifel, L. S., J. G. Parker, C. J. Lobb, A. Rainwater, V. Z. Wall, J. P. Fadok, M. Darvas, M. J. Kim, S. J. Mizumori, C. A. Paladini, P. E. Phillips, and R. D.

Palmiter (2009). Disruption of nmdar-dependent burst firing by dopamine neurons provides selective assessment of phasic dopamine-dependent behavior. *Proc Natl Acad Sci U S A 106*(18), 7281–8.

Chapter 3

Mice Lacking Dopamine Neuron NMDARs Show Impaired Acquisition of a Binary Choice Auditory Discrimination Despite Normal Response Vigor

This chapter describes the generation of a line of transgenic mice lacking, specifically in dopamine neurons, the obligatory NMDA receptor subunit, NR1. Previous characterizations of mice lacking NMDARs in dopamine neurons show a selective reduction of burst-firing in dopamine neurons, the mode of dopamine firing proposed to serve as a reward prediction error or "teaching signal" (Schultz, 1998). By comparison, previous reports of mice with increased "tonic" dopamine firing have described enhanced motivation in the absence of new learning (Cagniard et al., 2006), suggesting dissociable functions for burst and tonic firing modes of dopamine neurons. Here we describe the development of an auditory binary choice task and stimuli that lend themselves to efficient learning as well as morphing. Chapter 4 will further de-

scribe the use of morphed stimuli for the purpose of modulating the difficulty of a discrimination. Here, we report that mice lacking NMDARs in dopamine neurons demonstrate impaired learning in a two-alternative forced choice task, despite normal response vigor.

3.1 Introduction

Dopamine has been described as serving a dual function in the development of reward related behaviors, as both a retroactive reinforcement signal of reward-preceding memory traces (Schultz, 1998), and a proactive energizer of approach behavior (Wise, 2004).

Behavioral Assessments of Dopamine Firing Modes in Rodent. Midbrain dopamine neurons generate distinct tonic and burst firing patterns (Grace and Bunney, 1984). The contributions of phasic and tonic dopamine firing modes to reward contingent learning paradigms have been difficult to dissect. Two recent mouse models have provided a new method for comparison and potential dissociation of functions these firing modes may subserve. Mice characterized as having enhanced tonic firing rates demonstrate enhanced motivation in the absence of new learning (Cagniard et al., 2006). By contrast, mice lacking dopamine neuron NMDARs show a reduction in burst-firing of dopamine neurons accompanied by impairments in conditioned place preference and a visually cued t-maze task (Zweifel et al., 2008, 2009). Conversely, Tsai, et. al. recently induced conditioned place preference in mice by approximating phasic activation of dopamine neurons using optogenetic stimulation, while emulating tonic firing was not sufficient to drive learning (Tsai et al., 2009). Further reports of mice lacking dopamine neuron NMDARs have detailed a 3-fold reduction in phasic dopamine levels in response to task relevant stimuli (Parker et al., 2010) and a 6-fold reduction upon stimulation of the PPTg (Zweifel et al., 2009), the largely glutamatergic afferent structure known to induce dopamine burst-firing (Pan and Hyland, 2005).

Prediction Error Signaling in Rodents. While studies of phasic dopamine activations in primate have fueled a prominent hypothesis of dopamine as an error signal of discrepancies between actual and expected reward information, rodent studies have recently generated several related findings. Voltammetry studies of dopamine release profiles measured in the striatum reveal that phasic dopamine release in rodents occurs in a manner consistent with descriptions in primate (Stuber et al., 2008; Parker et al., 2010; Flagel et al., 2010). Task relevant dopamine transients are observed, initially to rewards, and eventually to reward-predictive cues. In a departure from this widely held view, in some cases, reward reponses in the rodent persist unchanged during learning (Parker et al., 2010; Flagel et al., 2010). These differences could arise from (sometimes very) different task parameters or training time periods, they could be the result of different learning or response strategies favored across species, or they could be the result of individual differences.

Prediction Errors Elicited in a Binary-Choice Task. While reward prediction error like signaling has been observed by voltammetry in conditioning tasks, Roesch, et al. recorded from dopamine neurons in rats engaged in a binary choice conditioning task similar to the wealth of dopamine primate literature (Roesch et al., 2007). By repeatedly reversing reward size or delay, reward prediction error signaling could be reliably and repeatedly induced as the rat engaged each reversal block.

An odor-cued two-alternative forced choice task was developed in the rodent by Uchida and Mainen (Uchida and Mainen, 2003). This task lends itself to generating and recording robust reward prediction error signals as shown by Schoenbaum and colleagues in an equivalent odor-cued task. Given characterizations in recent literature demonstrating the selective decrease in burst-firing in mice lacking NMDARs in dopamine neurons, and the recent demonstrations in rodent of robust reward prediction error signaling, we were interested to investigate, in an equivalent two-choice task to that developed in rat, whether mice lacking dopamine neuron NMDARs would demonstrate learning deficits.

3.2 Results

In order to investigate the role of dopamine neuron NMDARs in learning (Chapter 3), the expression of biases in decision-making (Chapter 4), and measures of speed and accuracy (Chapter 5) in a two-alternative forced choice auditory discrimination task, we used a genetic strategy to inactivate NMDARs in dopamine neurons. Inactivation in dopamine neurons of the obligatory subunit of the NMDA receptor, *Grin1* (NR1), blocks long-term potentiation at glutamatergic synapses onto dopamine neurons. In addition, it has recently been reported to result in a selective reduction in dopamine neuron burst firing and has been employed as a method for behavioral assessment of phasic dopamine (Zweifel et al., 2009).

3.2.1 Generation of Mice Lacking NMDARs in Dopamine Neurons

DAT-Cre recombination pattern is restricted to dopamine neurons. In the work described in this thesis, a line of transgenic mice is used in which Cre recombinase is targeted to the dopamine transporter (*Slc6a3*) locus (Zhuang et al., 2005). In addition, a line of mice is used in which a portion of the *Grin1* gene is flanked by *loxP* recognition sequences ($Grin1^{f/+}$) such that Cre-mediated excision of the floxed region renders the resulting NR1 subunit and the NMDA receptor, non-functional (Tsien et al., 1996). Crossing $Slc6a3^{+/Cre}$ mice with a *lacZ* reporter line of mice (Soriano, 1999) results in robust expression of β-galactosidase in regions of the midbrain rich in dopamine neurons of the SNc (Fig. 3-1a) and VTA (Fig. 3-1b, Supplementary Fig. 3-6). Fluorescent immunohistochemistry of β-galactosidase, the enzyme product of *lacZ* and reporter of Cre-mediated recombination, shows exclusive colocalization with dopamine marker tyrosine hydroxylase (TH), demonstrating that Cre-mediated recombination in the midbrain is occurring in dopamine neurons (Fig. 3-1c).

Breeding strategy to generate mice lacking NMDARs in dopamine neurons. Due to a high rate of ectopic Cre-mediated recombination among com-

pound *Slc6a3*$^{+/Cre}$ and homozygous floxed *Grin1* transgenic mice as assayed by PCR of tail DNA, we generated control and knockout mice equivalent to those previously characterized. Both control and knockout mice retain one functional *Grin1* and *Slc6a3* allele, except in knockout mice in which the second floxed allele is susceptible to Cre-mediated inactivation in dopamine neurons.

It has been suggested that the DAT promoter drives Cre expression transiently in germ cells (Zweifel et al., 2008). We investigated further whether germ-line deletion can be assumed or whether a more problematic mosaic pattern of deletion is likely to occur. We bred male and female *Slc6a3*$^{+/Cre}$ mice with homozygous *Grin1*$^{f/f}$ mice. *Slc6a3*$^{+/Cre}$ positive offspring of this generation (F1) are uniformly heterozygous for the floxed *Grin1* allele (Supplementary Fig. 3-7). Fifty percent of both male and female mice tested positive for the targeted Cre transgene by PCR. Male and female *Slc6a3*$^{+/Cre}$ positive offspring from this generation (F1) were again bred with *Grin1*$^{f/f}$ homozygous for the floxed allele mice, maintaining the female or male as the Cre carrier according to the first generation cross. DNA of F1 and F2 offspring was compared by PCR of tail DNA to assess recombination of the floxed *Grin1* allele. Ectopic recombination appears in F2 but not in F1 offspring. This indicates that ectopic recombination does not occur after the fertilization of a *Slc6a3*^{Cre} positive egg with sperm carrying a floxed *Grin1* allele, or vice versa. In other words, our breeding strategy can rely on the germ-cell recombination of the floxed *Grin1* allele, and therefore a homogeneous background genotype, rather than mosaic recombination. Because a *Grin1* null genotype is lethal, viable F2 offspring positive for germ-cell deletion must retain one intact *Grin1* allele. However, since the subsequent generation (F2) is riddled with offspring whose tail DNA tests positive for recombination of the floxed *Grin1* allele, recombination occurs at some stage of gametogenesis in the compound transgenic mouse (mice whose gametes carry both *Slc6a3*$^{+/Cre}$ and floxed *Grin1* alleles). Interestingly, we see no difference in the rates of ectopically recombined F2 offspring generated from female and male Cre-carriers. Therefore, to ensure control and knockout mice were of comparable genotype and in order to maintain consistency with previous characterizations, F1 *Slc6a3*$^{+/Cre}$ male and female mice were

crossed with $Grin1^{f/+}$ mice to generate control, $Slc6a3^{+/Cre};Grin1^{\Delta/+}$ and knockout, $Slc6a3^{+/Cre};Grin1^{\Delta/f}$ experimental mice (referred to hereafter as DAT/NR1 control and DAT/NR1 knockout mice, or simply control and knockout mice).

Reduction in NR1 expression occurs in TH expressing region of knockout mice. A decrement in signal of an in situ cDNA probe against NR1 mRNA is seen in the midbrain region. In adjacent sections, this region shows hybridization of a probe against dopamine neuron marker, tyrosine hydroxylase (Fig. 3-2). No gross differences are apparent between genotypes in other brain structures (Supplementary Fig. 3-8).

3.2.2 Two-alternative forced choice behavioral task results

Two-alternative forced choice task design. A two-alternative forced choice olfactory discrimination task has previously been demonstrated to elicit reward prediction errror signaling of dopamine neurons in rat (Roesch et al., 2007). Training mice in an olfactory two-alternative forced choice task results in robust and rapid associative learning and odor discrimination (Supplementary 3-9). However, due to a large population of olfactory bulb dopamine neurons, cues other than olfactory are necessary when employing a mouse line in which dopamine specific promoters are used to drive transgene expression. In this task, a trial is initiated when the mouse pokes and breaks an IR beam in the center port. This elicits the delivery of one of two cues which persists until the mouse exits the center port. Poking the side port associated with this cue results in a water reward.

3.2.3 Rates of Acquisition

DAT/NR1 knockout mice show delayed acquisition of two-choice task.

During training on a two-alternative forced choice task using auditory stimuli, DAT/NR1 knockout mice demonstrate a pronounced acquisition deficit in achieving equal performance accuracy to controls. Control mice require between two and

three weeks of training to achieve performance criterion (two consecutive days of 70% performance). Knockout mice require roughly twice as long to achieve this level of performance. Survival analysis of the percentage of mice to achieve the performance criterion by a given training session confirms a significant difference between control and DAT/NR1 knockout mice (Fig. 3-4b, $P<0.001$, log-rank test).

3.2.4 Rates of Responding

DAT/NR1 knockout mice show comparable trial initiation rate and reaction time to controls.

Impaired acquisition by knockout mice of the two-choice task could be due to deficits in associative learning, perceptual discrimination, or deficits in motivation or locomotion. No differences between genotype were seen in time spent from entry to exit from the cue port (Fig. 3-5a), movement time from the cue port to reward port (Fig. 3-5b), or latency to initiate trials following correct trials (Fig. 3-5c), as quantified in Fig. 3-5d (respectively, $P=0.12$, $P=0.94$, $P=0.08$, by unpaired t-tests). These results suggest that mice lacking dopamine neuron NMDARs retain normal locomotor function and do not show reduced motivation for acquiring rewards. These findings are consistent with previous reports of learning impairments in equivalent DAT/NR1 knockout mice in the absence of the motor and motivational deficits frequently encountered with coarser perturbations of dopamine circuitry.

3.3 Discussion

Here we described the generation of a line of transgenic mice lacking, specifically in dopamine neurons, the obligatory NMDA receptor subunit, NR1. Using an auditory two-cue alternative forced choice task to test associative learning and complex auditory stimuli that lend themselves to efficient learning as well as morphing, we report

that mice lacking dopamine neuron NMDARs demonstrate impaired learning in a two-alternative forced choice task. Despite a prominent deficit in acquisition of the binary discrimination, mice demonstrate no difference in measures of locomotion and response vigor.

These findings are consistent with previous reports of learning impairments in these knockout mice in the absence of the motor and motivational deficits frequently encountered upon coarser perturbations of dopamine circuitry. Despite slower learning, knockout mice eventually achieve performance equivalent to control mice.

One suggested mechanism by which these firing modes may confer differential function is by differential activation of high and low affinity dopamine receptors in dopamine target regions (Richfield et al., 1989). Specifically, low affinity dopamine D1 receptors requiring higher concentrations of dopamine are implicated in learning as well as synaptic plasticity in dopamine target regions (Dalley et al., 2005; Goto and Grace, 2005; Frey et al., 1990; Huang and Kandel, 1995; Otmakhova and Lisman, 1996).

While NMDARs contribute to the phasic activation of dopamine neurons, they also mediate synaptic plasticity at glutamatergic dopamine afferents (Bonci and Malenka, 1999). It is possible that an NMDAR-mediated rearrangement of synaptic weights onto dopamine neurons enables or contributes to the burst-firing of these neurons. NMDARs would thereby, in effect, gate afferent inputs such that only those providing correlated plasticity-inducing activity would effect bursts in dopamine neurons.

While studies suggest a dissociable role for phasic dopamine firing in learning, and for tonic firing in motivation, interaction exists between these processes. Learning rates increase with increased food and water deprivation, for instance, which also enhances responding in break point analyses and other measures of response vigor. However, as demonstrated in the Cagniard study, when calibrating task difficulty such that learning is equivalent between control and experimental mouse cohorts, it is possible to uncover an increased threshold of responding (break point) in mice with enhanced tonic dopamine transmission, suggesting a dissociable role for tonic firing in motivation (Cagniard et al., 2006).

Some reports of learning related deficits (Engblom et al., 2008) and task-relevant dopamine responses in mice lacking dopamine neuron NMDARs (Parker et al., 2010), on the surface, offer an inconsistent view of the role of dopamine neuron NMDARs in learning. However, a common thread has emerged that deficits in these mice may be revealed as a function of task difficulty, such that Pavlovian conditioned approach training can be acquired normally by mice lacking NMDARs and overtraining can obscure deficits in conditioned place preference, but visually-cued t-maze tasks, or shorter periods of training can reveal acquisition deficits. Our results provide the most complex reward contingent learning paradigm that DAT/NR1 knockout mice have been tested in at this time, and the largest deficit in task acquisition.

3.4 Methods

3.4.1 Generation of Mice Lacking NMDARs in Dopamine Neurons

Slc6a3$^{+/Cre}$ male and female mice were crossed with *Grin1*$^{f/+}$ mice to generate control, *Slc6a3*$^{+/Cre}$;*Grin1*$^{\Delta/+}$ and knockout,*Slc6a3*$^{+/Cre}$;*Grin1*$^{\Delta/f}$ experimental mice (see breeding strategy section of Results). We employed a *Slc6a3*$^{+/Cre}$ knock-in line (gift from X. Zhuang, University of Chicago) (Zhuang et al., 2005) and floxed *Grin1*$^{f/f}$ line of mice generated in-house (Tsien et al., 1996). This work uses the same mouse lines and an equivalent breeding strategy to arrive at the genotypes described in prior characterizations (Zweifel et al., 2008, 2009) of mice lacking NMDARs in dopamine neurons.

3.4.2 Histology

Mice were transcardially perfused with 4% paraformaldehyde (PFA) in 0.1 M sodium phosphate buffer (PB). For X-Gal staining the brains were then removed and post-fixed for 2 hours in 4% PFA at 4°C. Coronal sections (50 μm thick) were cut on a Vibratome and collected in PB. Sections were first incubated in 0.1 M PB con-

taining 0.01% SDS, 0.02% NP-40, 2 mM $MgCl_2$ at 4°C for15 minutes, followed by the β-galactosidase reaction in 1xPBS pH 8.0 containing 0.5 mg/ml Xgal, 5 mM $K_4Fe(CN)_6 \bullet 3H_2O$, 5 mM $K_3Fe(CN)_6$, 2 mM $MgCl_2$ at 37°C for 18-24 hours. Sections were counterstained with Nuclear Fast Red.

3.4.3 Immunohistochemistry

For double immunofluorescent staining, brains were post-fixed in 4% paraformaldehyde overnight, and 50 μm Vibratome sections were prepared. Sections were then incubated in 50% EtOH in PBS, rinsed and incubated with 10% normal goat serum at room temperature for 1 hour followed by incubation at 4°C overnight with gentle shaking in anti-β-galactosidase polyclonal antibody (1/2000; Cappel) with 3% normal goat serum. After rinsing, the sections were then incubated with a biotinylated anti-rabbit IgG (1/200; Jackson, IL) at room temperature for 1 hour, and then with Alexa555-conjugated streptavidin for 1 hour at room temperature. After rinsing, sections were again incubated with 10% normal goat serum at room temperature for 1 hour followed by incubation at 4°C overnight with gentle shaking in anti-tyrosine hydroxylase monclonal antibody (1/1000; Chemicon/Millipore) with 3% normal goat serum. After rinsing, the sections were incubated in Alexa488-conjugated anti-mouse IgG (1/500; Molecular Probes) at room temperature for 1 hour. Fluorescent images were captured.

3.4.4 In Situ Hybridization

In situ hybridization was carried out as described previously((Nakazawa et al., 2002)). In brief, brains were removed and frozen fresh in OCT solution. 10 μm parasagital sections were prepared in a cryostat and mounted onto pre-coated glass slides. Sections were post fixed with 4% paraformaldehyde in PBS for 15 min, and treated with 10 μg/ml proteinase K at 37°C for 30 min followed by 0.2 M HCl for 10 min. After rinsing, sections were further incubated in 0.25% acetic anhydride and 0.1 M triethanolamine for 10 min to avoid non-specific binding of the probe. Following

dehydration with ethanol, hybridization was performed at 55°C for 18 hours in a hybridization buffer containing 50% formamide. For detection of the mouse NR1 mRNAs, a complementary RNA (cRNA) probe, derived from the AvrII-SphI 0.4-kb antisense DNA fragment of rat NR1 cDNA containing from exon 13 to exon 16 (5), was labeled with [33P]UTP (5x105 cpm), and added to the hybridization buffer. For detection of the mouse TH mRNAs, a complementary RNA (cRNA) probe was labeled with [33P]UTP (5x105 cpm), and added to the hybridization buffer. The brain sections were serially washed at 55C with a set of SSC buffers of decreasing strength, the final strength being 0.2x and then treated with RNase A (12.5 g/ml) at 37°C for 30 min. The sections were exposed to hyper-beta max for 2 days and were dipped in nuclear emulsion followed by exposure to X-ray film for 3-4 weeks.

3.4.5 Behavior

Behavior experiments were conducted in the Harvard Department of Molecular and Cellular Biology. Mice were housed in plastic homecages with laboratory bedding (1-2 mice/cage) and with a 12:12 hour light/dark cycle. All experiments were conducted by scientists blind to the genotypes of the animals. 10 control mice and 12 knockout mice between 20 and 44 weeks of age were trained to discriminate two auditory cues in a two-alternative forced choice paradigm.

Water restriction/handling/habituation: Mice were weighed and water restricted for 1 day prior to habituation. To habituate mice to behavioral chambers and the experimenter, mice were handled for two minutes each and placed in behavioral chambers for 15 minutes the first day and 5 minutes the second day. For the duration of the experiment, mice were given access to water for 40 minutes every 24 hours. Early in training, additional water was provided as needed to ensure mice did not fall below 85% body weight.

Mouse approach behavior was shaped for 5-7 sessions to the contingencies of a two-alternative choice paradigm. The first day consisted of 20 trials of a progressive ratio followed by 20 trials of a variable schedule of reinforcement in which mice learned to retrieve water from the two side ports of three adjacent nose poke ports. For 4

to 6 additional sessions, mice learned to first elicit a cue by poking the center poke in order to elicit water from either side port. A cue sampling time requirement was progressively increased from 0-0.4 seconds and reward available duration was progressively decreased from 10 to 4 seconds during this time. Mice were then trained to discriminate two complex tones for 14 to 45 sessions. For discrimination training, a trial was initiated upon the breaking of an IR beam by a nose poke into the center port of three adjacent ports. Following a 200-500ms delay (uniformly distributed), mice were presented with one of two complex tones. Auditory cues were presented until the mouse exited the center port. Entry into the correct side port within 4 seconds resulted in immediate delivery of a 4-10 μl water drop. Trials in which mice did not remain in the center port long enough to elicit a cue were not considered valid trials and are not represented in our analyses. Trials in which a choice was attempted but in the incorrect side port are considered error trials. Error trials were followed by a progressively increasing 3-10 second timeout in order to prevent rapid guessing. Trial reinitiation latency is therefore reported for correct trials.

3.4.6 Auditory Stimuli

Complex tones comprised of three harmonic components with the same base frequency were generated using a custom Matlab script. To enable later morphing, both stimuli that were used here for discrimination training were generated such that all components have the same base frequency. Mice learned to discriminate complex tones comprised of three harmonic components centered at 3 kHz and 7.5 kHz and delivered at 85 decibels. For morphing, the amplitude ratio of the two spectral peaks (around 3 kHz and 7.5 kHz) was varied.

Bibliography

Bonci, A. and R. C. Malenka (1999). Properties and plasticity of excitatory synapses on dopaminergic and gabaergic cells in the ventral tegmental area. *J Neurosci 19*(10), 3723–30.

Cagniard, B., J. A. Beeler, J. P. Britt, D. S. McGehee, M. Marinelli, and X. Zhuang (2006). Dopamine scales performance in the absence of new learning. *Neuron 51*(5), 541–7.

Dalley, J. W., K. Laane, D. E. Theobald, H. C. Armstrong, P. R. Corlett, Y. Chudasama, and T. W. Robbins (2005). Time-limited modulation of appetitive pavlovian memory by d1 and nmda receptors in the nucleus accumbens. *Proc Natl Acad Sci U S A 102*(17), 6189–94.

Engblom, D., A. Bilbao, C. Sanchis-Segura, L. Dahan, S. Perreau-Lenz, B. Balland, J. R. Parkitna, R. Lujan, B. Halbout, M. Mameli, R. Parlato, R. Sprengel, C. Luscher, G. Schutz, and R. Spanagel (2008). Glutamate receptors on dopamine neurons control the persistence of cocaine seeking. *Neuron 59*(3), 497–508.

Flagel, S. B., T. E. Robinson, J. J. Clark, S. M. Clinton, S. J. Watson, P. Seeman, P. E. Phillips, and H. Akil (2010). An animal model of genetic vulnerability to behavioral disinhibition and responsiveness to reward-related cues: implications for addiction. *Neuropsychopharmacology 35*(2), 388–400.

Frey, U., H. Schroeder, and H. Matthies (1990). Dopaminergic antagonists prevent long-term maintenance of posttetanic ltp in the ca1 region of rat hippocampal slices. *Brain Res 522*(1), 69–75.

Goto, Y. and A. A. Grace (2005). Dopamine-dependent interactions between limbic and prefrontal cortical plasticity in the nucleus accumbens: disruption by cocaine sensitization. *Neuron 47*(2), 255–66.

Grace, A. A. and B. S. Bunney (1984). The control of firing pattern in nigral dopamine neurons: single spike firing. *J Neurosci 4*(11), 2866–76.

Huang, Y. Y. and E. R. Kandel (1995). D1/d5 receptor agonists induce a protein synthesis-dependent late potentiation in the ca1 region of the hippocampus. *Proc Natl Acad Sci U S A 92*(7), 2446–50.

Nakazawa, K., M. C. Quirk, R. A. Chitwood, M. Watanabe, M. F. Yeckel, L. D. Sun, A. Kato, C. A. Carr, D. Johnston, M. A. Wilson, and S. Tonegawa (2002). Requirement for hippocampal ca3 nmda receptors in associative memory recall. *Science 297*(5579), 211–8.

Otmakhova, N. A. and J. E. Lisman (1996). D1/d5 dopamine receptor activation increases the magnitude of early long-term potentiation at ca1 hippocampal synapses. *J Neurosci 16*(23), 7478–86.

Pan, W. X. and B. I. Hyland (2005). Pedunculopontine tegmental nucleus controls conditioned responses of midbrain dopamine neurons in behaving rats. *J Neurosci 25*(19), 4725–32.

Parker, J. G., L. S. Zweifel, J. J. Clark, S. B. Evans, P. E. Phillips, and R. D. Palmiter (2010). Absence of nmda receptors in dopamine neurons attenuates dopamine release but not conditioned approach during pavlovian conditioning. *Proc Natl Acad Sci U S A 107*(30), 13491–6.

Richfield, E. K., J. B. Penney, and A. B. Young (1989). Anatomical and affinity state comparisons between dopamine d1 and d2 receptors in the rat central nervous system. *Neuroscience 30*(3), 767–77.

Roesch, M. R., D. J. Calu, and G. Schoenbaum (2007). Dopamine neurons encode

the better option in rats deciding between differently delayed or sized rewards. *Nat Neurosci 10*(12), 1615–24.

Schultz, W. (1998). Predictive reward signal of dopamine neurons. *J Neurophysiol 80*(1), 1–27.

Soriano, P. (1999). Generalized lacz expression with the rosa26 cre reporter strain. *Nat Genet 21*(1), 70–1.

Stuber, G. D., M. Klanker, B. de Ridder, M. S. Bowers, R. N. Joosten, M. G. Feenstra, and A. Bonci (2008). Reward-predictive cues enhance excitatory synaptic strength onto midbrain dopamine neurons. *Science 321*(5896), 1690–2.

Tsai, H. C., F. Zhang, A. Adamantidis, G. D. Stuber, A. Bonci, L. de Lecea, and K. Deisseroth (2009). Phasic firing in dopaminergic neurons is sufficient for behavioral conditioning. *Science 324*(5930), 1080–4.

Tsien, J. Z., D. F. Chen, D. Gerber, C. Tom, E. H. Mercer, D. J. Anderson, M. Mayford, E. R. Kandel, and S. Tonegawa (1996). Subregion- and cell type-restricted gene knockout in mouse brain. *Cell 87*(7), 1317–26.

Uchida, N. and Z. F. Mainen (2003). Speed and accuracy of olfactory discrimination in the rat. *Nat Neurosci 6*(11), 1224–9.

Wise, R. A. (2004). Dopamine, learning and motivation. *Nat Rev Neurosci 5*(6), 483–94.

Zhuang, X., J. Masson, J. A. Gingrich, S. Rayport, and R. Hen (2005). Targeted gene expression in dopamine and serotonin neurons of the mouse brain. *J Neurosci Methods 143*(1), 27–32.

Zweifel, L. S., E. Argilli, A. Bonci, and R. D. Palmiter (2008). Role of nmda receptors in dopamine neurons for plasticity and addictive behaviors. *Neuron 59*(3), 486–96.

Zweifel, L. S., J. G. Parker, C. J. Lobb, A. Rainwater, V. Z. Wall, J. P. Fadok, M. Darvas, M. J. Kim, S. J. Mizumori, C. A. Paladini, P. E. Phillips, and R. D.

Palmiter (2009). Disruption of nmdar-dependent burst firing by dopamine neurons provides selective assessment of phasic dopamine-dependent behavior. *Proc Natl Acad Sci U S A 106*(18), 7281–8.

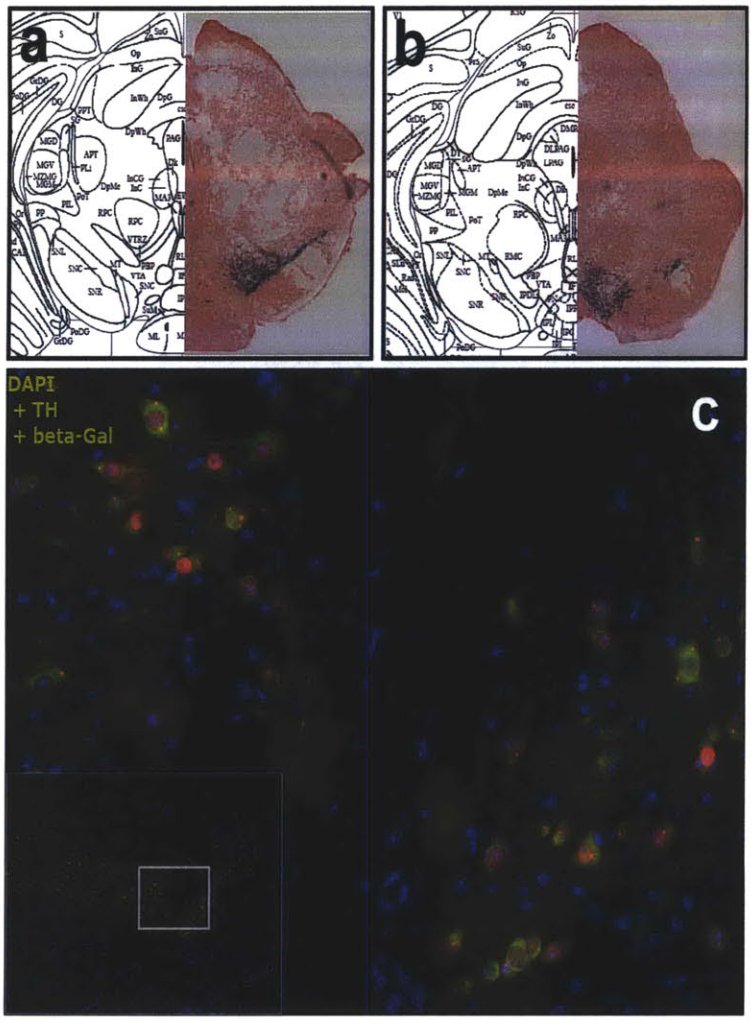

Figure 3-1: **DAT-Cre recombination pattern is restricted to dopamine neurons.** *Slc6a3*$^{+/Cre}$ mouse line crossed with ROSA26-*loxP*-STOP-*loxP*-*lacZ* reporter mouse line results in Cre-mediated recombination restricted to tyrosine hydroxylase expressing neurons. A) X-gal staining of midbrain sections shows reporter recombination in SNc (A) and VTA (B) nuclei. C) Fluorescent immunohistochemistry shows Cre-mediated reporter expression β-galactosidase reporter (red) colocalized with and dopaminergic marker, tyrosine hydroxylase, (green). Nuclear DAPI stain (blue) indicates no reporter expression outside of tyrosine hydroxylase cells.

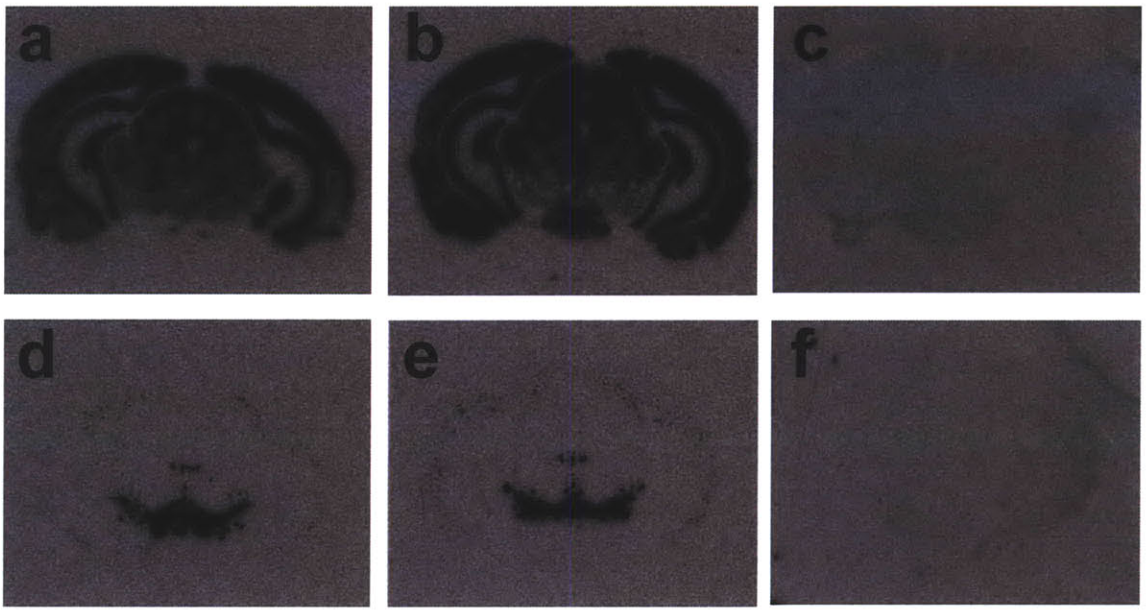

Figure 3-2: **NMDAR expression is reduced in midbrain dopaminergic nuclei.** Images of coronal sections after in situ hybridization with a 33P-labeled NR1 cDNA probe. A) DAT/NR1 control NR1 expression in a midbrain section; adjacent section shows tyrosine hydroxylase positive signal (D). B) Expression of NR1 in DAT/NR1 knockout is reduced in the midbrain region positive for tyrosine hydroxylase signal. C) Sense cDNA control probe against NR1 and tyrosine hydroxylase (D).

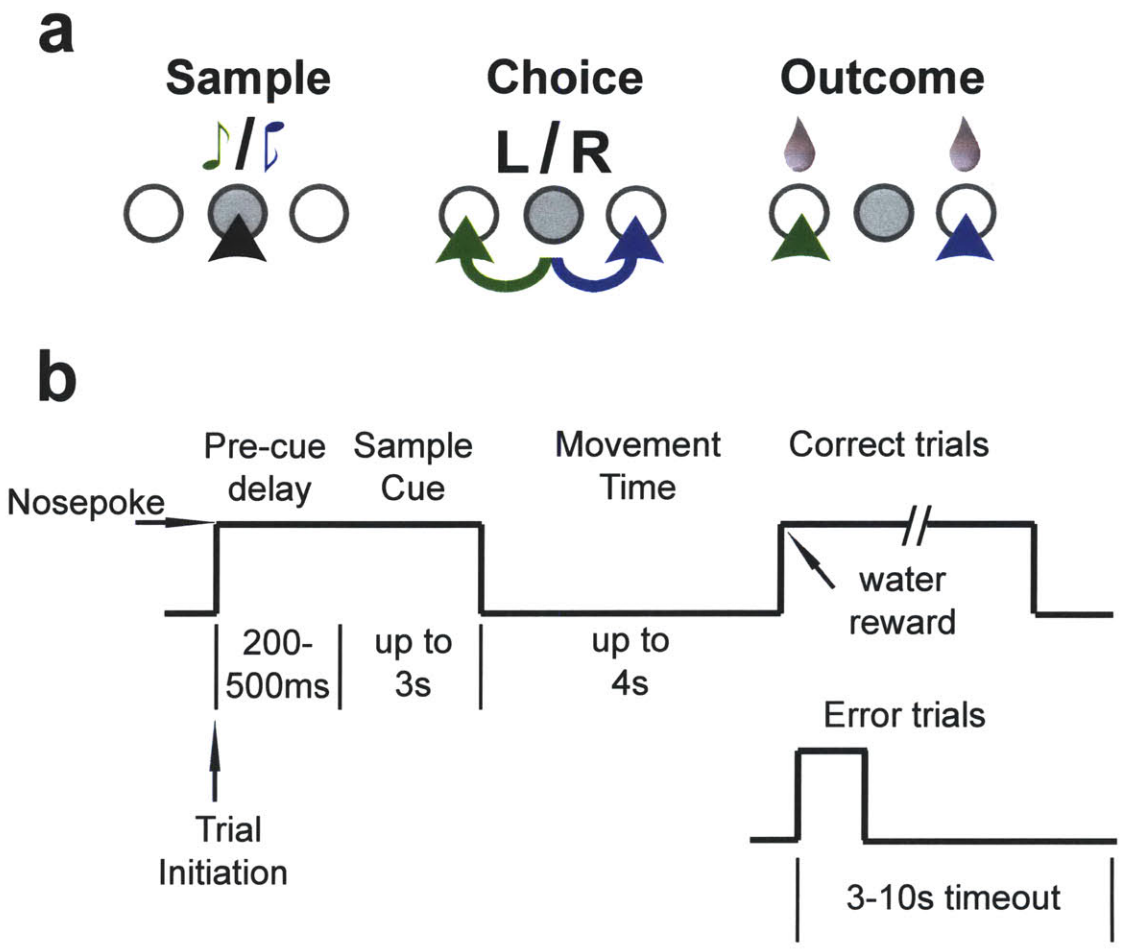

Figure 3-3: **Auditory two-alternative forced choice task design for mice.** A) Schematic of task design. B) Temporal description of task design. Two auditory cues indicate the availability of a reward following a correct choice of the associated side port. A valid trial is initiated by poking into the center port until a cue is presented. A 200-500ms delay precedes the onset of one of two auditory cues. The cue is presented until the mouse exits the center port. A water reward is delivered immediately upon correctly poking the associated side port. Error trials are followed by a progressively increasing timeout.

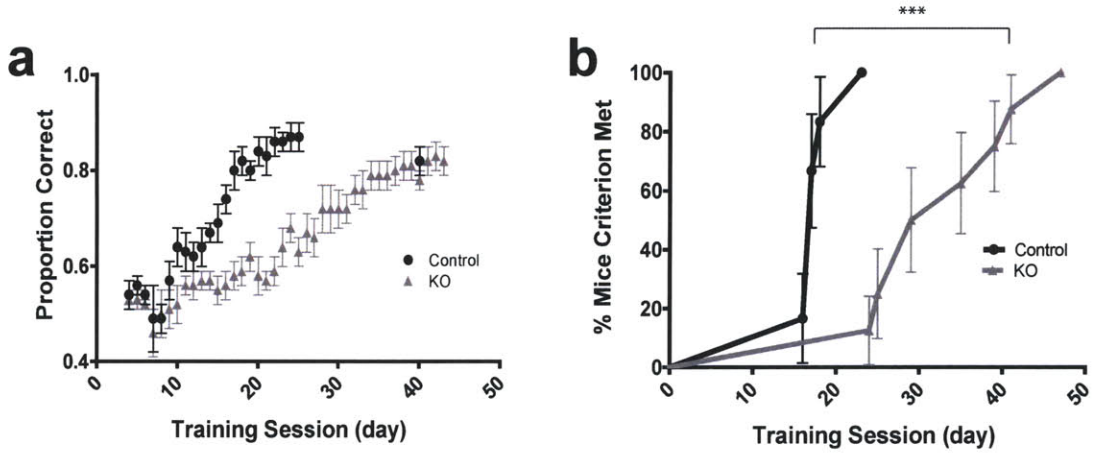

Figure 3-4: **DAT/NR1 knockout mice show impaired learning of two-choice task.** Comparison of control and DAT/NR1 knockout mice in a two-alternative forced choice task reveals a prominent acquisition deficit in mice lacking NMDARs in dopamine neurons. A) Behavioral performance across sessions. B) Percentage of mice that achieved criterion by session. $^{*}P<0.005$. Data shown, mean±s.e.m.

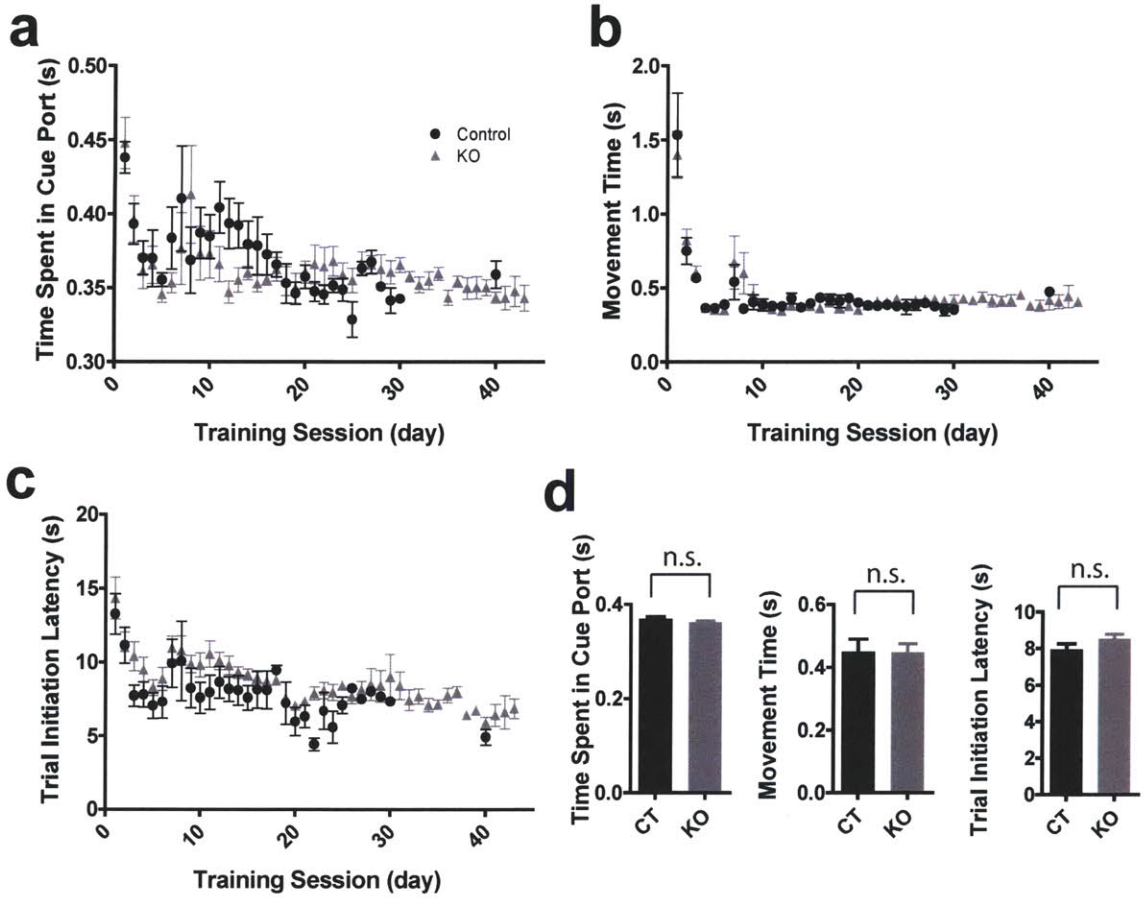

Figure 3-5: **DAT/NR1 knockout mice do not exhibit locomotor or motivational deficits.** A) Time spent in the cue port is not different between DAT/NR1 control and knockout mice. B) Time spent moving from cue port to the reward port is not different between control and knockout mice. C) Latency to initiate a trial by poking the cue port is not different between control and knockout mice. D) Summary statistics of A-C. n.s., not significant (P>0.05). Data shown, mean±s.e.m.

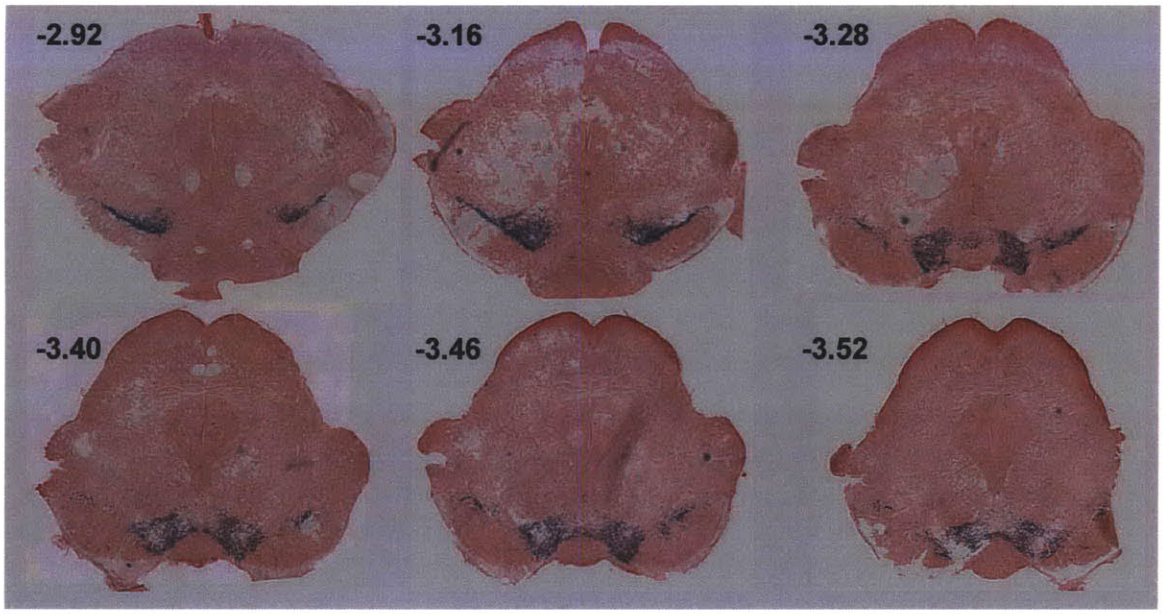

Figure 3-6: Supplementary Figure. **DAT-Cre mediated recombination of lacZ reporter in midbrain.** DAT-Cre mouse line crossed with ROSA26-lacZ reporter mouse line. X-gal stain indicates Cre-mediated recombination in midbrain sections. Sections, shown rostral to caudal) show pattern of recombination consistent with dopaminergic nuclei. Numbers indicate approximate distance posterior from bregma.

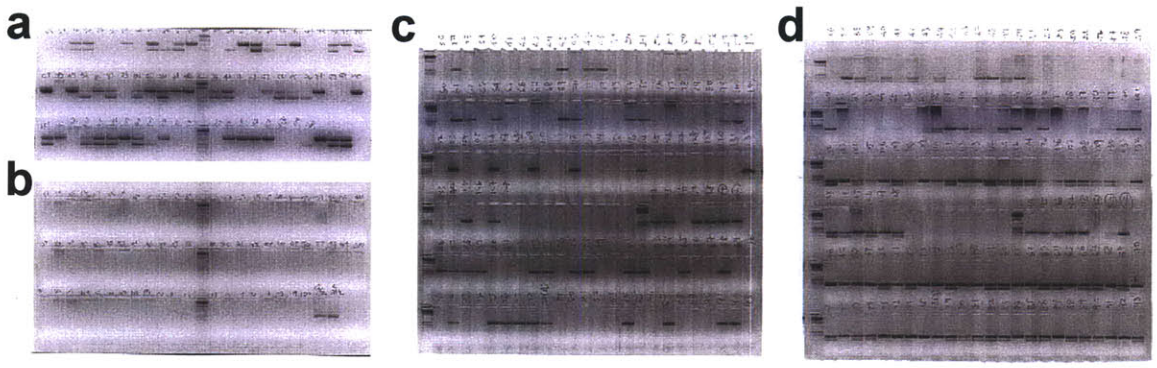

Figure 3-7: Supplementary Figure. **DAT-Cre mediated floxed NR1 ectopic recombination occurs in germ cells.** A-B) Genotyping by PCR of tail DNA of F1 progeny resulting from seven male DAT-Cre carriers and seven female DAT-Cre carriers crossed with ffNR1. Each gel well represents genotyping result of one mouse. A) Cre positive progeny occur at expected 50% rate (500bp Cre band; 1kb control band). B) The same F1 mice show no evidence of ectopic recombination (500bp band indicates ectopic recombination; two positive control samples bottom right). Identical DNA samples were used in panels A and B demonstrating the viability of the DNA used in panel B; two positive control samples (panel B bottom right of gel) demonstrate the viability of the primer set used to detect ectopic recombination of floxed NR1 allele. C-D) Genotyping progeny (F2) of male and female DAT-Cre positive F1 offspring crossed with ffNR1 demonstrates D) evidence of ectopic recombination in F2 generation and D) approximate expected rates of floxed NR1 alleles in F2 generation (50% $NR1^{f/f}$; 50% $NR1^{f/+}$).

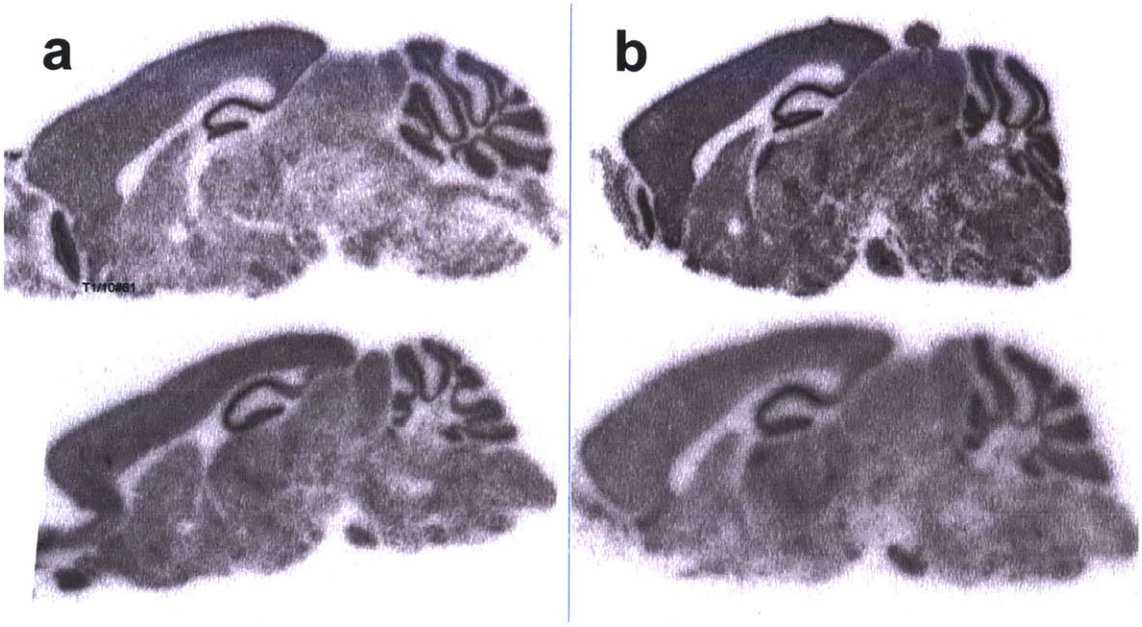

Figure 3-8: Supplementary Figure. **NMDAR expression appears normal throughout brain regions of DAT/NR1 knockout.** Images of sagittal sections of control (A) and DAT/NR1 knockout (B) mice after in situ hybridization with a 33P-labeled NR1 cDNA probe. No gross differences are apparent in NR1 expression level in brain structures of DAT/NR1 knockout compared with control mice.

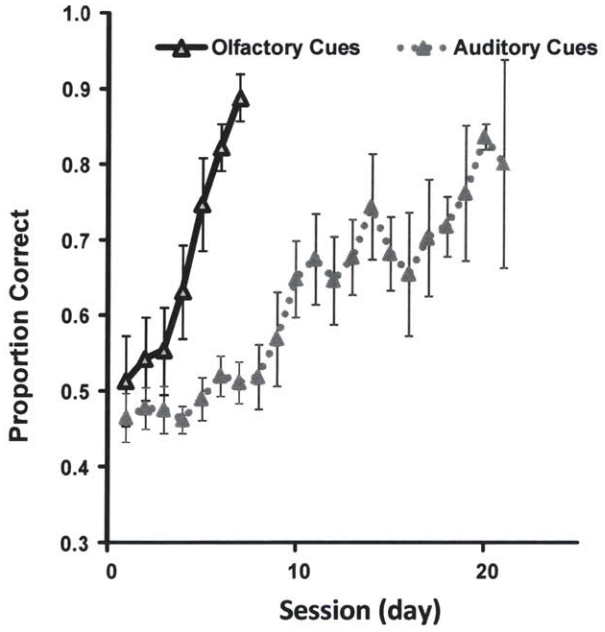

Figure 3-9: Supplementary Figure. **Olfactory versus auditory binary choice acquisition speed in mice.** Comparison of olfactory and auditory acquisition in a pilot experiment with wildtype mice tested in identical task designs. Mice learned to discriminate either caproic acid and hexanol or 3 kHz and 15 kHz pure tone stimuli (n=4 olfactory and 4 auditory trained *wt* mice). In this task, the trial duration was progressively increased across sessions. In the final task design, complex tones and a progressively increasing timeout following error trials were used. (The use of stimuli more complex than pure tones and a timeout following error trials were the result of helpful advice from K. Borges, G. Otazu and others in the laboratory of Tony Zador at Cold Spring Harbor Laboratory.)

Chapter 4

Dopamine Neuron NMDARs Modulate an Influence of Prior Success Difficulty on Decisions

Studies dating back to those culminating in Thorndike's Law of Effect have demonstrated the influence of prior choice parameters on future decisions (Thorndike, 1911, 1933). Recent observations in rat in an olfactory binary choice task developed in the Mainen and Uchida labs (Uchida and Mainen, 2003) have identified an influence of the degree of difficulty of prior trials on the degree of response bias in subsequent decisions (manuscript in preparation). We report this influence in mice challenged by varying degrees of discrimination difficulty in an auditory-cued binary choice task. Using mice engineered to selectively lack functional NMDA receptors in dopamine neurons, we report that the presence of this receptor is necessary for the difficulty-dependent modulation of the influence of prior successes on subsequent decisions.

4.1 Introduction

Dopamine is thought to serve as a teaching signal in reward contingent learning. Updating the reward predictive value of cues is fundamental to shaping adaptive patterns of behavior and decision-making. Midbrain dopamine neurons are

widely reported to signal errors conveying discrepancies between predicted and actual reward, and, in some cases, punishment (Mirenowicz and Schultz, 1994; Montague et al., 1996; Schultz, 1998; Bayer and Glimcher, 2005; D'Ardenne et al., 2008; Fiorillo et al., 2003; Hollerman and Schultz, 1998; Matsumoto and Hikosaka, 2009; Morris et al., 2006; Pan et al., 2005; Roesch et al., 2007; Tobler et al., 2005; Ungless et al., 2004; Waelti et al., 2001). Phasic dopamine responses to unexpected rewards and reward predictive cues (Satoh et al., 2003; Nakahara et al., 2004; Bayer and Glimcher, 2005; Tobler et al., 2005; Morris et al., 2006; Ravel and Richmond, 2006; Roesch et al., 2007; Kobayashi and Schultz, 2008) are broadcast widely to brain structures where dopamine may contribute to the updating of decision parameters including the predictive value of cues.

Varying stimulus difficulty in a binary perceptual discrimination task elicits reward predictive cue responses in dopamine neurons in primate. Perceptual discrimination tasks have long used predictive cues of varying discrimination difficulty to gain insights about perceptual information processing, categorization and decision-making in primate (Newsome and Pare, 1988; Newsome et al., 1989; Shadlen and Newsome, 2001; Freedman et al., 2001) and more recently in rodent (Uchida and Mainen, 2003; Feierstein et al., 2006; Kepecs et al., 2008). Recent investigations in primate of cue responses of dopamine neurons using such perceptually difficult discriminations identified a late phase of the dopamine cue response that covaries with the degree of discrimination difficulty and therefore the reward probability (Nomoto et al., 2010).

Binary choice tasks elicit reward prediction error signals in dopamine neurons in rodent. Dopamine neuron responses to unexpected rewards and reward predictive cues have been demonstrated in rodent in auditory cued conditioning paradigms (Hyland et al., 2002; Pan and Hyland, 2005), conjunctive (auditory and visual) cued conditioning paradigms (Stuber et al., 2008), as well as odor cued binary choice tasks (Roesch et al., 2007; Takahashi et al., 2009).

Prior trial difficulty in a binary choice task influences subsequent choices in rat. An odor-based binary choice task, inspired by those used as cardinal assays of perceptual processing in primate, was previously developed for the study of olfactory processing in rat (Uchida and Mainen, 2003; Feierstein et al., 2006). Observations of choice behavior in this task by the Uchida and Mainen labs (manuscript in preparation) identify an influence of the discrimination difficulty of prior trials on subsequent decisions. Specifically, the degree of discrimination difficulty in prior trials predicts the degree of a response bias on subsequent trials. Given the proposed role of dopamine as a teaching signal in associative learning, we hypothesized an influence of phasic dopamine signaling in the differential modulation of this response bias. We propose that these biases represent the differential updating by dopamine of the reward predictive value of reward associated cues.

We report the development of an auditory-cued binary choice task as well as morphed auditory cues for the study of response biases in mouse. To test whether dopamine may play a role in the differential response biases observed following successes of varying difficulty, we adapted for the mouse a binary choice task and stimuli of varying discrimination difficulty. We chose to use auditory stimuli due to a population of olfactory bulb dopamine neurons affected in transgenic mouse lines relying on dopamine neurons specific promoters.

We report an influence in mouse of prior decision parameters on subsequent decisions. The present study extends the findings of Uchida and Mainen to the genetically accessible mouse model system, in particular, for assessment of response biases in a mouse model of reduced phasic dopamine signaling (Zweifel et al., 2009). Here we describe the extension of the binary choice task described in Chapter 3 to include morphed stimuli: combinations of the two previously learned auditory stimuli. Using these stimuli, we replicate in mice the finding that the degree of difficulty of a prior success predicts the degree of response bias in the subsequent trial. Specifically, larger response biases follow more difficult successes.

We report modulation by the dopamine system of the influence of prior decision parameters on subsequent decisions. Using mice engineered to selectively lack NMDA receptor function in dopamine neurons, we examined the role of dopamine signaling in the updating of behavioral responses according to prior decision parameters. This genetic perturbation has previously been demonstrated result in a reduction in dopamine neuron burst-firing.

Two sets of findings are reported here. First, mice challenged with complex auditory stimulus discriminations show greater biases in subsequent decisions depending on the difficulty of the previous decision. Second, mice lacking dopamine neuron NMDARs lack differential modulation of response biases following decisions of varying difficulty. Specifically, mice lacking dopamine neuron NMDARs show no difference in response biases following difficult versus easy decisions.

4.2 Results

4.2.1 Auditory binary choice paradigm for mice.

Binary choice paradigm optimized for mice. In order to investigate the influence of prior decision parameters on subsequent decisions, 10 DAT/NR1 control and 12 DAT/NR1 knockout mice were trained to discriminate two auditory stimuli as described in Chapter 3. Mice lacking dopamine neuron NMDA receptors were delayed in their acquisition of this discrimination, but eventually achieved control levels of performance. Once both groups achieved equivalent performance, mice were introduced to a phase of the task in which morphs of the learned stimuli were presented. One cue from a set of six morphed stimuli was pseudorandomly presented in each trial. Each of the six stimuli was jittered by 0-5% in order to facilitate categorization based on a consistent set of stimulus features, ie. in order to prevent memorization based on irrelevant stimulus specific features (Freedman, et. al 2001). As in Chapter 3, mice initiated trials with nose pokes to the center of three adjacent ports thereby eliciting one of the six auditory stimuli (Figure 4-1). In order for a trial to be con-

sidered valid, mice were required to remain in the center port for a pre-cue delay of 200-500 ms (uniformly distributed) prior to the onset of the cue. Cue presentation persisted until the mouse withdrew its nose from the center port. Poking the side port associated with the presented cue resulted in delivery of a water reward. Trials could be initiated every four seconds regardless of trial outcome.

Complex auditory stimuli. To learn whether the influence of prior decision difficulty on subsequent decisions generalizes to mice and to the auditory modality, we first developed auditory stimuli that lend themselves to efficient acquisition as well as morphing. We developed complex tones, each comprised of three harmonic frequencies. These two complex stimuli share the same fundamental frequency, but have three component harmonic frequencies centered either at 3kHz or 7.5kHz. In order to achieve morphs of the original stimuli, harmonic components of both stimuli were combined, and the amplitudes of the spectral peaks varied (Figure 4-2).

4.2.2 Influence of prior decisions on current decisions in mice.

It has long been reported that choices followed by reward tend to be repeated, a process described by Thorndike as representing the "stamping in" of an association in his "Law of Effect" (Thorndike, 1911, 1933). With greater repetition of rewarded choices (as the animal learns reward contingencies), the reward may become predictable. A hallmark of phasic dopamine reward responses is the diminished responding to rewards as they become predictable. In addition, with repetition, stimuli that reliably precede rewards gain predictive value, a process known to be correlated with phasic dopamine neuron responses to reward predictive cues. In order to modulate the predictive nature of a cue, we varied the difficulty of the stimulus discrimination in a binary choice task, as this has recently been demonstrated to differentially engage phasic dopamine neuron responses to reward predictive cues (Nomoto et al., 2010). The difficulty of discrimination determines the performance of the animal, ie. the probability of reward, and therefore, the predictive value of the reward predictive cue. Because dopamine neurons are known to fire phasic responses based on the predictive value of reward predictive cues, and because phasic dopamine is suggested to

be involved in learning and updating the value of such cues, we were interested in whether an influence of reward history would be evident in the choices made by mice in our auditory binary choice task.

Prior successes and errors differentially influence subsequent choices.

Performance diminishes with increased discrimination difficulty. We first describe the influence of trial history in control mice presented with morphed stimuli of various discrimination difficulties. Plotting the performance of mice in terms of the proportion of their choices made in the "A" direction, demonstrates that mice made reliable choices in the "A" direction in response to 95% "A" stimuli and in the "B" direction in response to 5% "A" stimuli (95% "B" stimuli). Performance diminished in response to morphs that lie closer to the 50% category boundary (Fig. 4-3), black average curves). Stimuli are referred to hereafter as 95% A, 65% A, 35% A, 5% A to indicate stimulus direction and difficulty.

Mice are biased in the direction of a previous success. By segregating data according to prior success (Fig. 4-3a) or prior error (Fig. 4-3b) and further segregating according to prior stimulus identity (indicated by line color), a prominent influence of prior success is made apparent. In particular, control mice showed a bias in the direction of a previous reward (Fig. 4-3a), but not in the direction of a previous error (Fig. 4-3b). For instance, prior successes in the "A" direction (green 65% A curve and blue 95% A curve) predict a shift in the proportion of choices made in the "A" direction, whereas prior successes in the "B" direction (yellow 35% A curve and red 5% A curve) predict a shift in the proportion of choices made in the "B" direction.

Difficulty of prior success influences subsequent choices.

Mice are more biased following a difficult success. Interestingly, we observed that the *difficulty* of a prior success modulates this bias in the direction of a previous reward (Fig. 4-3, line color). In other words, prior difficult successes pre-

dict a greater bias in the direction of a previous reward than prior easy successes. Specifically, curves representing prior difficult stimuli (green 65% A curve and yellow 35% A curve) show greater shifts in the direction of a prior success than curves representing prior easy stimuli (blue 95% A curve and red 5% A curve). Data segregated according to prior errors show no detectable bias in response to prior trial parameters (Fig. 4-3b). (Note: the existence of far fewer error trials reduces the statistical power and, therefore, increases the possibility of incorrectly accepting the null hypothesis, that no difference exists between distributions following errors.)

Correcting for selection bias. Segregating data according to prior outcome may introduce a selection bias. For instance, prior successes may be preferentially preceded by prior successes. The influence of prior successes and errors is replotted in Fig. 4-4 for comparison with the influence of the population of trials preceding them. The influence on the current trial of trials *preceding* prior successes and prior errors are shown in Fig. 4-4b and Fig. 4-4e, respectively. A small bias of $\text{trials}_{n-2...m}$ is seen when data is segregated according to prior success (Fig. 4-4b). In order to correct for selection biases introduced by trials preceding trial_{n-1}, the contribution of $\text{trials}_{n-2...m}$ is subtracted from all further analyses shown in this chapter. The subtraction of this selection bias only reduces the significance level of some analyses, but does not alter any conclusions. Even after accounting for the influence of $\text{trials}_{n-2...m}$, the isolated influence of immediately prior successes still predicts a response bias in the direction of the prior success (Fig. 4-4c) and the influence of immediately prior errors remains small (Fig. 4-4f). In order to quantify the contribution of prior success difficulty on subsequent trials, we collapsed trials across both directions because we found that the influence of prior reward direction on subsequent choice was symmetric. As shown in Fig. 4-5, decisions are biased more by prior difficult successes than prior easy successes (difficulty of prior success is indicated along the x-axis). Decisions are also influenced by the difficulty of the current stimulus. Current easy decisions are relatively resistant to the influence of prior reward direction compared with current difficult decisions. However, while the influence of prior direction diminishes when current decisions are easy, the influence of *prior difficulty* is seen regardless of current

difficulty. Results of a two-way ANOVA (prior difficulty by current difficulty) confirm significant main effects of both prior difficulty ($F_{2,54}$=6.64, P=0.0026) and current difficulty ($F_{2,54}$=4.34, P=0.023) on choices following successful trials in control mice. No interaction between factors was detected ($F_{4,54}$=0.20, P=0.94).

To summarize, we found that control mice show a biased response depending on the outcome, direction, and difficulty of the previous trial.

Mice lacking dopamine neuron NMDARs are not differentially influenced by the difficulty of prior success.

We next compared the influences of prior choice parameters observed in control mice with mice engineered to lack functional NMDA receptors in dopamine neurons (DAT/NR1 knockout mice), a genetic perturbation previously shown to result in a specific decrement in burst-firing of dopamine neurons (Zweifel et al., 2009). Because dopamine neurons are known to fire phasic responses based on the predictive value of reward predictive cues, we hypothesized that prior reward history would have a diminished influence on DAT/NR1 knockout mice. While we found that control mice were more biased following difficult successes than easy successes, DAT/NR1 knockout did not show a differential influence of prior difficulty on subsequent choices (Fig. 4-6b). Quantification of the influence of prior and current discrimination difficulty by a two-way ANOVA in DAT/NR1 knockout mice (genotype by prior difficulty) identified main effects of genotype ($F_{1,40}$=7.00, P=0.015), and prior difficulty ($F_{2,40}$=8.83, P=0.0007) (Fig. 4-6). The interaction effect was not significant ($F_{2,40}$=1.87, P=0.17). Post-hoc analyses using Bonferroni adjusted alpha levels of 0.0055 (0.5/9) confirmed a significantly larger influence of prior difficult success than prior easy success in subsequent choices of control mice, but no differential effects of prior difficulty on subsequent choices in mice lacking NMDARs in dopamine neurons.

Current decision difficulty influences choice bias in both control and DAT/NR1 knockout mice.

Current decision difficulty determines influence of prior difficulty of success. While only control mice show a significant influence of prior difficulty on choice bias, both control and DAT/NR1 knockout mice demonstrate a significant influence of current trial difficulty on choice bias. Specifically, in both genotypes, easier decisions are less susceptible to the influence of prior success parameters (Fig. 4-7 seen in the decrease in bias across current difficulties, shades of gray and blue). DAT/NR1 knockout mice show a main effect of current trial difficulty but not of prior trial difficulty. (Fig. 4-7b; Fig. 4-7a is replotted for comparison.) A two-way analysis of variance (current by prior difficulty) indicates that DAT/NR1 knockout mice show a main effect of current trial difficulty only. DAT/NR1 knockout mice do not show a significant effect of prior difficulty ($F_{2,66}$=2.38, P=0.10). No interaction between factors was detected ($F_{4,66}$=0.1.10, P=0.36). (Fig. 4-7b). Results of post-hoc analyses of knockout mice show significantly less bias in the direction of a prior reward when the current decision is easy than difficult ($F_{2,66}$=5.96, P=0.0062). Therefore, like control mice, DAT/NR1 knockout mice are less susceptible to the influence of prior reward direction when the current trial is easy. Unlike control mice, there is no differential influence of the *difficulty* of prior decisions on subsequent decisions.

Prior errors do not influence decisions in control or DAT/NR1 knockout mice.

Prior errors show no influence on current decisions in control and DAT/NR1 knockout mice. While both control and DAT/NR1 knockout mice show an influence of prior reward direction, neither control mice nor DAT/NR1 knockout mice show an influence of prior error (Fig. 4-8). Results of a two-way ANOVA (genotype by prior difficulty) indicate no significant main effects of genotype ($F_{1,40}$=2.49, P=0.13) or prior error difficulty ($F_{2,40}$=2.00, P=0.15). No interaction between factors was detected ($F_{2,40}$=0.41, P=0.67). In addition, neither control nor DAT/NR1 knockout mice demonstrate a significant influence of prior error difficulty on choice bias, even when data is segregated by current trial difficulty (Fig. 4-9). Results of a two-way ANOVA (current difficulty by prior difficulty) in-

dicate no significant main effects of current difficulty ($F_{2,66}$=0.57, P=0.57) or prior difficulty ($F_{2,66}$=2.21, P=0.12) were found in control or DAT/NR1 knockout mice. No significant interaction between factors ($F_{4,66}$=0.79, P=0.54) was found in control or DAT/NR1 knockout mice.

We were curious whether the larger influence of prior success seen in DAT/NR1 knockout mice is the result of a lower average performance. In other words, with performance held constant, we wondered if DAT/NR1 knockout mice would still show a larger magnitude choice bias than controls. Plotting magnitude of choice bias against average performance revealed no difference between control and DAT/NR1 knockout mice, suggesting that the larger magnitude choice bias seen in DAT/NR1 knockout mice arises from In addition, comparing mice well matched in average performance eliminated differences in the magnitude of choice bias between genotype. By contrast, the graded influence of prior difficulty remains a significant difference between control and DAT/NR1 knockout mice.

4.2.3 Temporal Dynamics of Influences of Prior Decisions

Our observation that the larger choice bias in DAT/NR1 knockout mice recedes to control levels when matched for average performance prompted our interest in the temporal dynamics of the influence of the difficulty of prior success.

The influence of prior success diminishes with learning.

We compared the degree of response bias during the first half of training with the degree of response bias in the last half. As mice gained experience, their average performance improved (Fig. 4-10, black curves). Interestingly, with improved performance, mice showed a diminished response bias toward the direction of prior rewards. This suggests that a process of refinement is at play, honing responses such that the history of a past reward holds less sway on a decision than current trial parameters.

In order to further visualize the dynamics of this behavioral refinement, we tallied biased responses and plotted them against a tally of opportunities for biased responses

(Fig. 4-11). To get at the effect, we restricted our analysis to occasions when a mouse faced a difficult choice, but in the opposite direction from a prior difficult or prior easy success. For instance, in prior sections we have shown that following a difficult success in the A (or B) direction, mice are biased to choose the same A (or B) direction again, especially given another difficult trial. Mice thereby incur errors with greater frequency on trials in the opposite direction of a prior success. In other words, mice will underperform (compared to their average) when faced with difficult choices following difficult contralateral successes. Mice will overperform (compared to their average) when faced with difficult choices following difficult ipsilateral successes. For this reason, we looked to difficult successes followed by contralateral difficult cues, or easy successes followed by contralateral difficult cues for a measure of bias. In this measure, a line with a slope of one would indicate that all trials of this contralateral sequence were successful, and therefore lines approaching a slope of one indicate the diminishing bias of prior rewards. We then compared the slopes of lines for easy and difficult prior successes in both genotypes.

In this analysis, we find that control mice, as before, show greater bias following difficult than following easy successes. We again observe no difference between the influence of prior difficult and easy successes in knockout mice. Adding to our previous findings, we can now see that when normalized by opportunities for bias (in effect normalizing for experience), knockout mice show a degree of bias equivalent to the largest bias seen in control mice, ie. to prior difficult successes. These results were confirmed in a two-way analysis of variance with repeated measures comparing slopes of prior difficult and prior easy curves in control and knockout mice (genotype by prior morph difficulty). Doing so revealed a main effect of prior morph difficulty ($F_{1,20}$=17.04, P<0.001), such that control mice showed significantly higher slope (indicating diminished bias) following prior easy successes. No significant effect of genotype was found in this analysis ($F_{1,20}$=4.21, P=0.054). However, a significant interaction between factors was detected ($F_{1,20}$=4.65, P=0.043), confirming also that the effect of prior morph difficulty was greater in the control than knockout genotype.

This finding suggests that knockout mice show an equivalent degree of bias to

control mice when this measure is normalized for experience, albeit with no gradation according to prior difficulty. This finding also suggests that the lack of differential bias in knockout mice is not due simply to a slower rate of onset of differential bias. Although it is possible that knockout mice may eventually show differential response biases following prior difficult and prior easy successes, it appears that while the degree of maximum response bias (in this case to prior difficult success) scales with average performance and keeps pace with control mice when normalized for performance, the differential rates of diminishing response biases seen in controls is not apparent in knockout mice even when normalizing for the degree of experience with biasing opportunities.

In summary, our results demonstrate that current decisions are influenced by the outcome of a prior decision. In particular, decisions are biased in the direction of prior rewards.

In addition, current decisions are influenced by the *difficulty* of prior decisions. Specifically, the more difficult a prior success, the larger the influence of prior reward direction in biasing a current decision.

In addition, we report that the influence of prior decision *difficulty* shown here in control mice, is not seen in mice lacking dopamine neuron NMDARs, a genetic perturbation previously demonstrated to result in reduced burst-firing of dopamine neurons. We also demonstrate that current easy decisions are less susceptible to the influences of prior trial parameters than current difficult decisions, a finding which spanned genotype.

Finally, we demonstrate that the biasing influence of a prior success recedes with experience (learning) in a manner independent of dopamine. However, while the overall influence of prior successes diminishes, the influence of prior easy successes diminishes faster than the influence of prior difficult successes in control mice.

Our findings provide behavioral evidence that mice with intact phasic dopamine signaling update the predictive value of cues at differential rates corresponding to the magnitude of phasic dopamine responses known to be elicited by differentially reward predictive stimuli.

4.2.4 Behavioral Response Time Measures

Given the relationship between discrimination difficulty and response time, we wondered if mice were spending longer sampling difficult auditory cues than easy cues. Analysis using paired comparisons of median response times to pooled easy (5A and 95A pooled) and pooled difficult (35A and 65A) stimuli demonstrated no difference between time spent sampling difficult and easy stimuli in control or mutant mice. In our analysis of median cue sampling time, we restricted trials analyzed to those above a 150 ms threshold (Fig. 4-12 top row). In order to assess if thresholding had influenced our observation of a lack of difference between response times to easy and difficult stimuli, we checked the distributions of pooled reaction time data from all mice for differences. Here we also observed no difference between distributions of cue sampling of easy and difficult stimuli.

In order to determine if pooling responses across the easy and difficult stimuli obscured an influence of individual stimuli, we compared responses to each individual morph (Fig. 4-13). No difference was found between morphs or between genotypes for time spent sampling the cue. Results of a two-way ANOVA (genotype by cue sampling time) confirm no significant effects of either genotype ($F_{1,100}$=0.43, P=0.5216) or stimulus identity ($F_{5,100}$=0.12, P=0.12). No interaction between factors was detected ($F_{5,100}$=0.90, P=0.94).

We wondered if a differential influence of cue sampling time might increase across training (Fig. 4-14). Segregating data based on the first half of sessions (referred to as "Early") and the second half of sessions (referred to as "Late"; 8-10 sessions each), we found no influence in controls or mutants in either early and late sessions. Results of a two-way ANOVA (genotype by cue sampling time) in the early sessions found no significant effects of genotype ($F_{1,100}$=0.98, P=0.33) or stimulus identity ($F_{5,100}$=1.57, P=0.18). No interaction between factors was detected ($F_{5,100}$=0.15, P=0.98). Results of a two-way ANOVA (genotype by cue sampling time) in the late sessions found no significant effects of genotype ($F_{1,100}$=0.14, P=0.71) or stimulus identity ($F_{5,100}$=0.27, P=0.92). No interaction between factors was de-

tected ($F_{5,100}$=0.46, P=0.80).

4.3 Discussion

Our results demonstrate that current decisions are influenced by the outcome of a prior decision. In particular, decisions are biased in the direction of prior rewards. In addition, current decisions are influenced by the *difficulty* of prior decisions. Specifically, the more difficult a prior success, the larger the influence of prior reward direction in biasing a current decision. In addition, we report that the influence of prior decision difficulty is shown here in control mice, is reduced in mice lacking dopamine neuron NMDARs, a genetic perturbation previously demonstrated to result in reduced burst-firing in dopamine neurons. Finally, we demonstrate that current easy decisions are less susceptible to the influences of prior trial parameters than current difficult decisions, a finding which spanned genotype. A proposed model and alternative explanations are discussed in the following chapter.

For more than a century, reaction time measures have served as a proxy for brain 'processing' or 'computational load', and have been assayed in an effort to rank neural computations, and decipher what neural processes may be independent. The trade-off between speed and accuracy has been studied empirically and modeled extensively. Regarding reaction time measures, the findings made here are two-fold. First, we find no differences in any response measure between control and DAT/NR1 knockout mice. These observations are reminiscent of the findings presented in Chapter 3 that control and DAT/NR1 mice do not exhibit differences in response latency, movement time or cue sampling time during initial acquisition of two tone discrimination. This is despite severe deficits in acquisition of the task. In addition, a number of associative learning assays of mice lacking NMDARs in dopamine neurons, taken together, suggest that as difficulty of the task is increased, so is the observed difference between performance of control and knockout mice (see Chapter 2. Background). While knockout mice show a large deficit in acquiring an auditory two-choice task (Chapter 3) and while their performance climbs more slowly than controls when faced with morphs of the two

learned cues, their response times remain remarkably stable regardless of difficulty. That difficulty of discrimination does not reveal impairments in knockout mice is consistent with an interpretation of the acquisition deficits as an associative learning deficit rather than a deficit in perceptual discrimination learning.

However, the second finding reported here is that difficult stimuli do not elicit longer cue sampling times than easier stimuli. This may be the result of our experiment and equipment design, and future studies can be designed to address more directly whether this is a feature of the strategy or exploratory nature of mice, or an equipment-related anomaly.

In summary, our findings provide new insights into the far-reaching and specific nature of dopamine neuron NMDARs in these behavioral assessments of learning, decision-making and response times. The requirement of NMDARs in the generation of normal dopamine neuron burst-firing makes this mouse a remarkable new tool for testing hypotheses regarding dopamine neuron burst-firing. Here we have tested the hypothesis that dopamine subserves learning in an associative auditory discrimination task. While mice lacking dopamine neuron NMDARs show dramatic deficits in acquiring a binary choice task, they show no difference in measures of response times and motivation. In addition, we report that the influence of prior decision *difficulty* shown here in control mice, is not seen in mice lacking dopamine neuron NMDARs. Finally, in measurements of cue sampling and movement times, we again find no difference between genotypes in response time measures. These findings together suggest that locomotor and motivational functions are not impaired in mice with reduced dopamine neuron burst-firing. In addition, perceptual measures including time sampling an array of auditory stimuli is not different in these mice. These findings together are consistent with a specific role for dopamine neuron burst-firing in proper credit assignment to appropriate reward predictive cues such that updating of those cues can guide and promote adaptive behavior.

4.4 Methods

4.4.1 Auditory Discrimination Task

Behavior experiments were conducted in the Harvard Department of Molecular and Cellular Biology. Mice were housed in plastic homecages with laboratory bedding (1-2 mice/cage) and with a 12:12 hour light/dark cycle. All experiments were conducted by scientists blind to the genotypes of the animals. 10 control mice and 12 knockout mice between 20 and 44 weeks of age were trained to discriminate two auditory cues in a two-alternative forced choice paradigm.

Water restriction/handling/habituation: Mice were weighed and water restricted for 1 day prior to habituation. To habituate mice to behavioral chambers and the experimenter, mice were handled for two minutes each and placed in behavioral chambers for 15 minutes the first day and 5 minutes the second day. For the duration of the experiment, mice had access to water for 45 minutes every 24 hours. Additional water was provided to ensure mice did not fall below 85% initial body weight.

Mouse approach behavior was shaped for 5-7 sessions to the contingencies of a two-alternative choice paradigm and subsequently trained to discriminate two complex tones as described previously (Chapter 3.4.5). Trials were initiated upon the breaking of an IR beam by a nose poke into the center port of three adjacent ports. Following a 200-500ms delay (uniformly distributed), mice were presented with one of two complex tones. Auditory cues were presented until the mouse exited the center port. Entry into the correct side port within 4 seconds resulted in immediate delivery of a 4-10 μl water drop. Trials in which mice did not remain in the center port long enough to elicit a cue were not considered valid trials and are not represented in our analyses. Trials in which a choice was attempted but in the incorrect side port are considered error trials. Error trials were followed by a progressively increasing 3-10 second timeout in order to prevent rapid guessing. Trial reinitiation latency is therefore reported for correct trials.

4.4.2 Auditory Stimuli

Auditory stimuli were generated using a custom Matlab script as described in Chapter 3. To vary discrimination difficulty, two parameters were varied, the harmonic frequency, and a number between 0 and 100 that defines the morph. Morphed stimuli are complex tones comprised of 6 components with the same base frequency (fundamental frequency). While the fundamental frequency remains the same, the amplitude ratio of the two spectral peaks (around 3 kHz and 7.5 kHz) is varied.

Bibliography

Bayer, H. M. and P. W. Glimcher (2005). Midbrain dopamine neurons encode a quantitative reward prediction error signal. *Neuron 47*(1), 129–41.

D'Ardenne, K., S. M. McClure, L. E. Nystrom, and J. D. Cohen (2008). Bold responses reflecting dopaminergic signals in the human ventral tegmental area. *Science 319*(5867), 1264–7.

Feierstein, C. E., M. C. Quirk, N. Uchida, D. L. Sosulski, and Z. F. Mainen (2006). Representation of spatial goals in rat orbitofrontal cortex. *Neuron 51*(4), 495–507.

Fiorillo, C. D., P. N. Tobler, and W. Schultz (2003). Discrete coding of reward probability and uncertainty by dopamine neurons. *Science 299*(5614), 1898–902.

Freedman, D. J., M. Riesenhuber, T. Poggio, and E. K. Miller (2001). Categorical representation of visual stimuli in the primate prefrontal cortex. *Science 291*(5502), 312–6.

Hollerman, J. R. and W. Schultz (1998). Dopamine neurons report an error in the temporal prediction of reward during learning. *Nat Neurosci 1*(4), 304–9.

Hyland, B. I., J. N. Reynolds, J. Hay, C. G. Perk, and R. Miller (2002). Firing modes of midbrain dopamine cells in the freely moving rat. *Neuroscience 114*(2), 475–92.

Kepecs, A., N. Uchida, H. A. Zariwala, and Z. F. Mainen (2008). Neural correlates, computation and behavioural impact of decision confidence. *Nature 455*(7210), 227–31.

Kobayashi, S. and W. Schultz (2008). Influence of reward delays on responses of dopamine neurons. *J Neurosci 28*(31), 7837–46.

Matsumoto, M. and O. Hikosaka (2009). Two types of dopamine neuron distinctly convey positive and negative motivational signals. *Nature 459*(7248), 837–41.

Mirenowicz, J. and W. Schultz (1994). Importance of unpredictability for reward responses in primate dopamine neurons. *J Neurophysiol 72*(2), 1024–7.

Montague, P. R., P. Dayan, and T. J. Sejnowski (1996). A framework for mesencephalic dopamine systems based on predictive hebbian learning. *J Neurosci 16*(5), 1936–47.

Morris, G., A. Nevet, D. Arkadir, E. Vaadia, and H. Bergman (2006). Midbrain dopamine neurons encode decisions for future action. *Nat Neurosci 9*(8), 1057–63.

Nakahara, H., H. Itoh, R. Kawagoe, Y. Takikawa, and O. Hikosaka (2004). Dopamine neurons can represent context-dependent prediction error. *Neuron 41*(2), 269–80.

Newsome, W. T., K. H. Britten, and J. A. Movshon (1989). Neuronal correlates of a perceptual decision. *Nature 341*(6237), 52–4.

Newsome, W. T. and E. B. Pare (1988). A selective impairment of motion perception following lesions of the middle temporal visual area (mt). *J Neurosci 8*(6), 2201–11.

Nomoto, K., W. Schultz, T. Watanabe, and M. Sakagami (2010). Temporally extended dopamine responses to perceptually demanding reward-predictive stimuli. *J Neurosci 30*(32), 10692–702.

Pan, W. X. and B. I. Hyland (2005). Pedunculopontine tegmental nucleus controls conditioned responses of midbrain dopamine neurons in behaving rats. *J Neurosci 25*(19), 4725–32.

Pan, W. X., R. Schmidt, J. R. Wickens, and B. I. Hyland (2005). Dopamine cells respond to predicted events during classical conditioning: evidence for eligibility traces in the reward-learning network. *J Neurosci 25*(26), 6235–42.

Ravel, S. and B. J. Richmond (2006). Dopamine neuronal responses in monkeys performing visually cued reward schedules. *Eur J Neurosci 24*(1), 277–90.

Roesch, M. R., D. J. Calu, and G. Schoenbaum (2007). Dopamine neurons encode the better option in rats deciding between differently delayed or sized rewards. *Nat Neurosci 10*(12), 1615–24.

Satoh, T., S. Nakai, T. Sato, and M. Kimura (2003). Correlated coding of motivation and outcome of decision by dopamine neurons. *J Neurosci 23*(30), 9913–23.

Schultz, W. (1998). Predictive reward signal of dopamine neurons. *J Neurophysiol 80*(1), 1–27.

Shadlen, M. N. and W. T. Newsome (2001). Neural basis of a perceptual decision in the parietal cortex (area lip) of the rhesus monkey. *J Neurophysiol 86*(4), 1916–36.

Stuber, G. D., M. Klanker, B. de Ridder, M. S. Bowers, R. N. Joosten, M. G. Feenstra, and A. Bonci (2008). Reward-predictive cues enhance excitatory synaptic strength onto midbrain dopamine neurons. *Science 321*(5896), 1690–2.

Takahashi, Y. K., M. R. Roesch, T. A. Stalnaker, R. Z. Haney, D. J. Calu, A. R. Taylor, K. A. Burke, and G. Schoenbaum (2009). The orbitofrontal cortex and ventral tegmental area are necessary for learning from unexpected outcomes. *Neuron 62*(2), 269–80.

Thorndike, E. (1911). Animal intelligence: Experimental studies (new york: Macmillan).

Thorndike, E. (1933). A proof of the law of effect. *Science 77*, 173–175.

Tobler, P. N., C. D. Fiorillo, and W. Schultz (2005). Adaptive coding of reward value by dopamine neurons. *Science 307*(5715), 1642–5.

Uchida, N. and Z. F. Mainen (2003). Speed and accuracy of olfactory discrimination in the rat. *Nat Neurosci 6*(11), 1224–9.

Ungless, M. A., P. J. Magill, and J. P. Bolam (2004). Uniform inhibition of dopamine neurons in the ventral tegmental area by aversive stimuli. *Science 303*(5666), 2040–2.

Waelti, P., A. Dickinson, and W. Schultz (2001). Dopamine responses comply with basic assumptions of formal learning theory. *Nature 412*(6842), 43–8.

Zweifel, L. S., J. G. Parker, C. J. Lobb, A. Rainwater, V. Z. Wall, J. P. Fadok, M. Darvas, M. J. Kim, S. J. Mizumori, C. A. Paladini, P. E. Phillips, and R. D. Palmiter (2009). Disruption of nmdar-dependent burst firing by dopamine neurons provides selective assessment of phasic dopamine-dependent behavior. *Proc Natl Acad Sci U S A 106*(18), 7281–8.

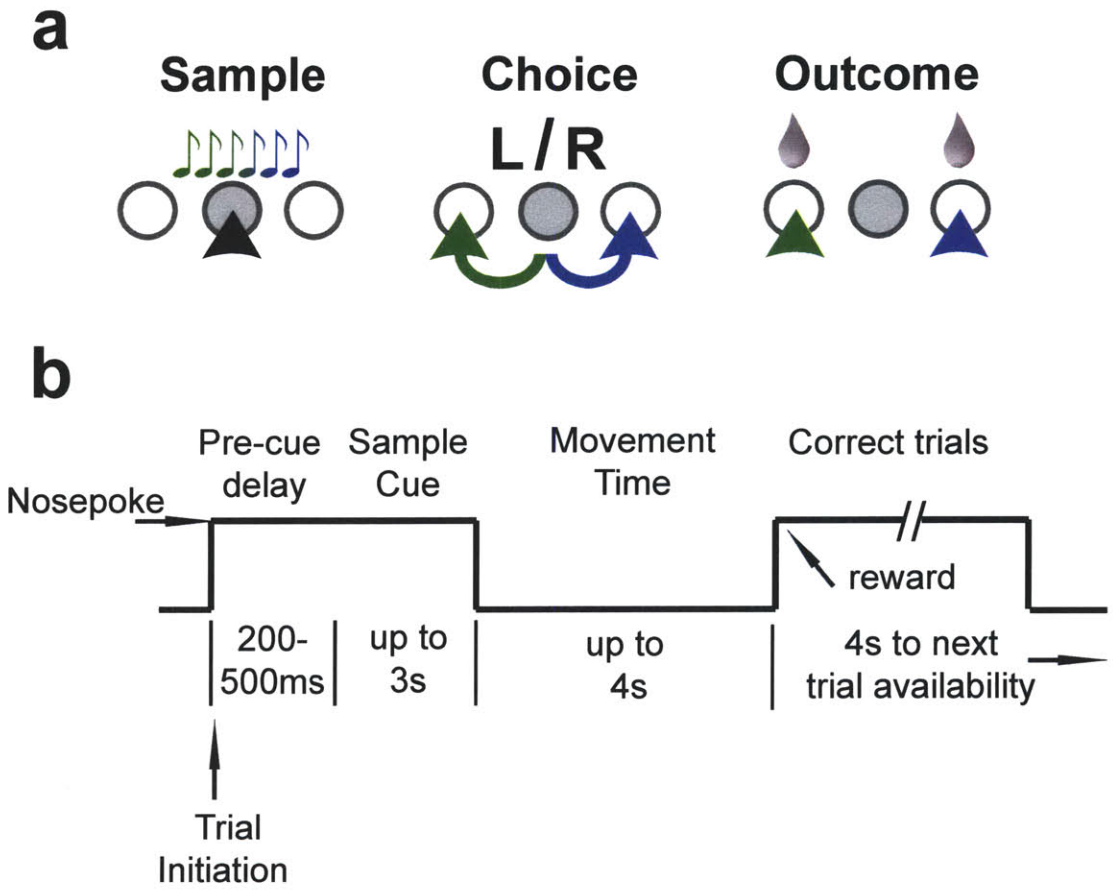

Figure 4-1: **Morphed auditory stimuli are presented in a two-alternative forced choice task design for mice.** Morphs of two previously learned auditory complex tones indicate reward availability at the associated side port. A trial is initiated by poking the center port. After a 200-500ms delay, one of 6 morphed auditory cues is delivered. Cue presentation is maintained until the mouse exits the center port. A water reward is delivered upon correctly poking the associated side port. A new trial can be initiated every 4 seconds.

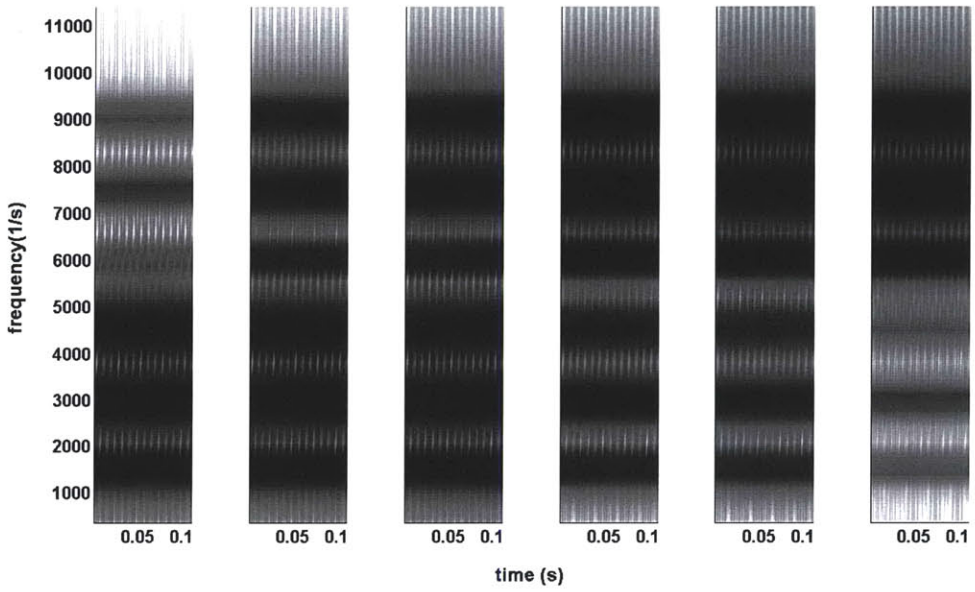

Figure 4-2: **Morphed auditory stimuli.** Morphed stimuli are complex tones comprised of 6 components with the same base frequency (fundamental frequency). While the fundamental frequency remains the same, the amplitude ratio of the two spectral peaks (around 3 kHz and 7.5 kHz) is varied.

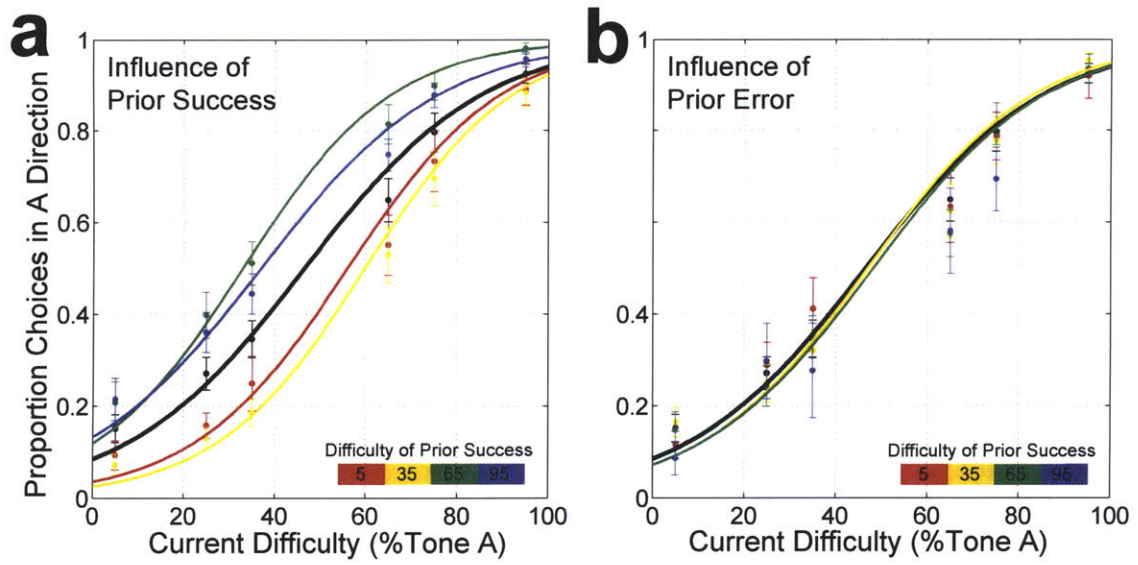

Figure 4-3: **Prior success and prior error differentially influences subsequent choice.** Control mice presented with morphed stimuli of various discrimination difficulties show a biased response depending on the outcome, direction, and difficulty of the previous trial. Performance is indicated on the y-axis as the proportion of choices made in the direction of tone "A". The x-axis indicates the morphed stimulus presented on a current trial (trial_n) according the percentage of tone "A". Color indicates data segregated based on the identity of the morphed stimulus presented in the previous trial (trial_{n-1}). Average performance on all trials is shown in black; data points represent mean±s.e.m. Lines represent univariate logistic regressions based on regression coefficients determined for individual mice and averaged across mice. A-B) The influence of prior trial outcome is shown in the two panels: the left panel shows the influence of a prior success, the right panel shows the influence of a prior error. Mice make reliable choices in the A direction in response to 95% A stimuli and in the B direction in response to 5% A stimuli (95% B stimuli) and show diminished performance in response to morphs that lie closer to the 50% category boundary. The influence of prior direction and prior difficulty is indicated by line color. A) Prior successes in the A direction (green 65% A curve and blue 95% A curve) are shifted in the A direction and vice versa. In addition, curves representing prior difficult stimuli (green 65% A curve and yellow 35% A curve) are more shifted in the direction of a prior success than curves representing prior easy stimuli (blue 95% A curve and red 5% A curve). B) Data segregated according to prior errors show no detectable bias in response to prior trial parameters. (Note: the existence of far fewer error trials reduces the statistical power and, therefore, increase the possibility of incorrectly accepting the null hypothesis, that no difference exists between distributions following errors.)

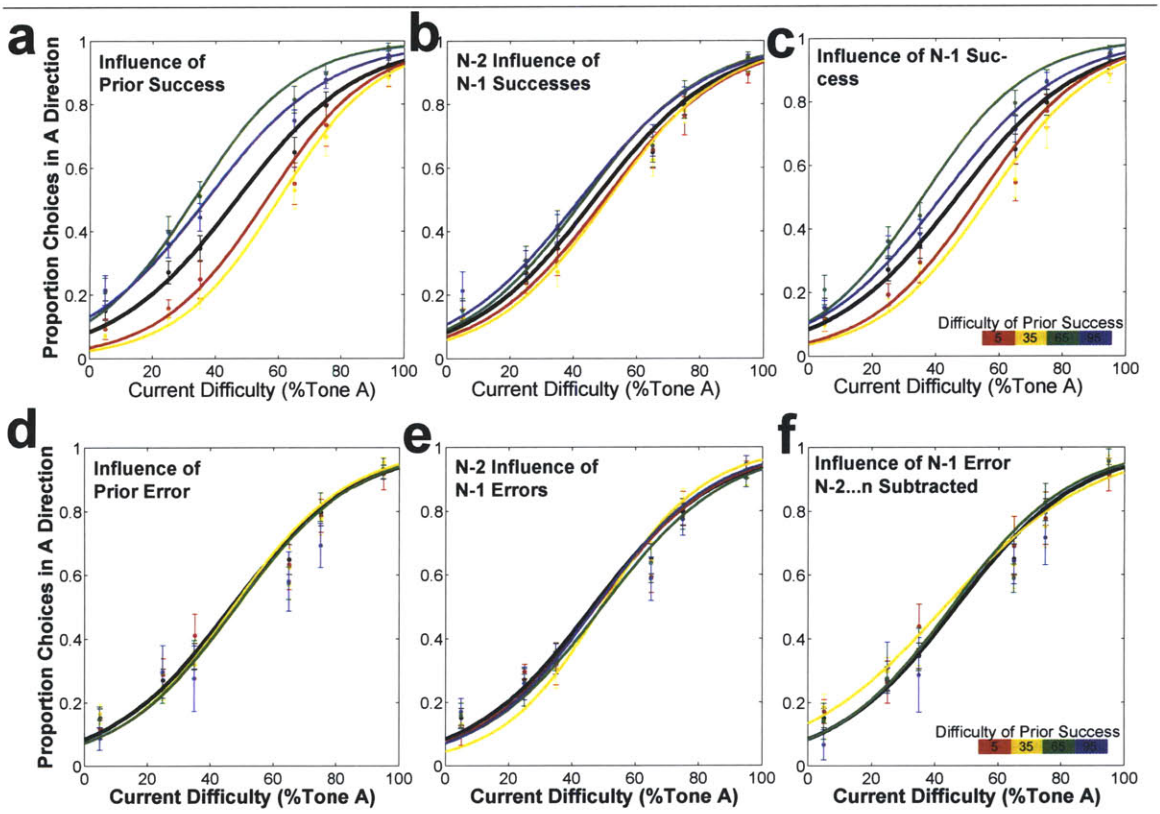

Figure 4-4: **Success of the immediately prior trial predicts a response bias in the subsequent choice.** Segregating data according to prior outcome may introduce a selection bias. For instance, prior successes may be preferentially preceded by prior successes. A, D) The influence of prior successes (A) and errors (D) is replotted for comparison with the influence of trials preceding them. B, E) The influence on the current trial of trials preceding prior successes (B) and prior errors (E). In order to account for selection biases introduced by trials preceding trial$_{n-1}$, the contribution of (trials$_{n-2...m}$) is subtracted. C, F) After accounting for the influence of trials$_{n-2...m}$, the isolated influence of the immediately prior success still predicts a response bias in the direction of the prior trial (C) and the influence of immediately prior errors remains small (F).

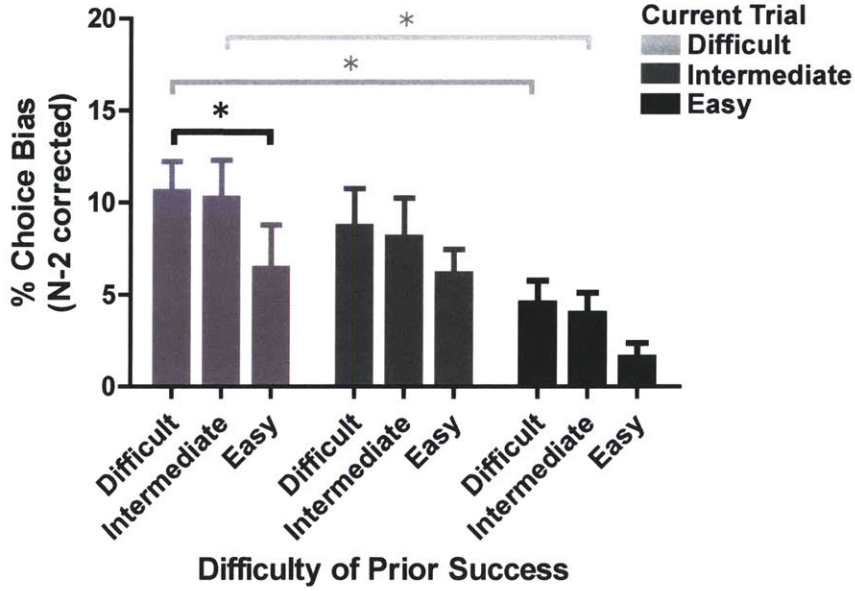

Figure 4-5: **Quantification of influence of prior success difficulty on subsequent decisions.** Decisions are biased more by prior difficult successes than prior easy successes (difficulty of prior success indicated along x-axis). Decisions are also biased (in the direction of the previous reward) by the difficulty of the current stimulus as seen within groups (within shades of gray). Current easy decisions are relatively resistant to influence of prior reward direction than current difficult decisions as seen in comparing across groups (black and light gray levels). Shades of gray indicate current discrimination difficulty: light gray, difficult current discrimination; medium grey, current discrimination of intermediate difficulty; black, current easy discrimination. Results of two-way ANOVA (current difficulty by prior difficulty) indicate significant main effects of both prior and current discrimination difficulty. Results of post-tests are indicated by $^{*}P<0.05$. Data shown, mean±s.e.m.

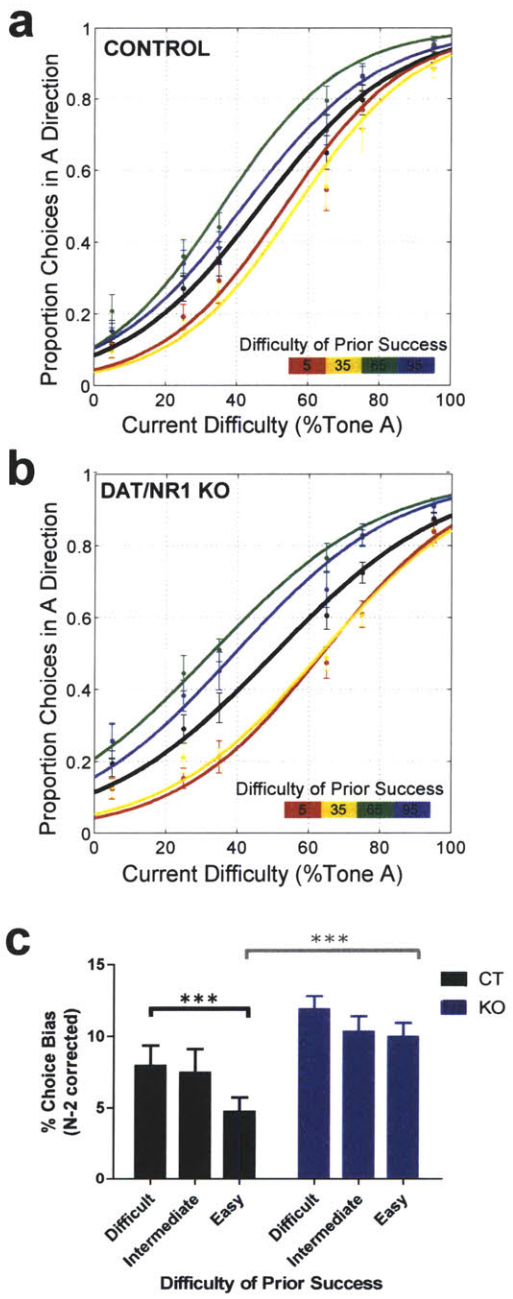

Figure 4-6: **Difficulty of prior success influences current decisions in a manner dependent on dopamine neuron NMDARs.** While both control and DAT/NR1 knockout mice show an influence of prior reward direction, control mice (A) show a graded influence of prior success difficulty on current decisions compared with DAT/NR1 knockout mice (B). C) Quantification comparing the influence of prior success difficulty across genotypes. The influence of prior success on current decisions is modulated by dopamine neuron NMDARs. Significant main effects of genotype and prior success difficulty (two-way ANOVA). Results of post-hoc analyses indicated according to $^{*}P<0.05$, $^{**}P<0.01$, $^{***}P<0.005$. Data shown, mean±s.e.m.

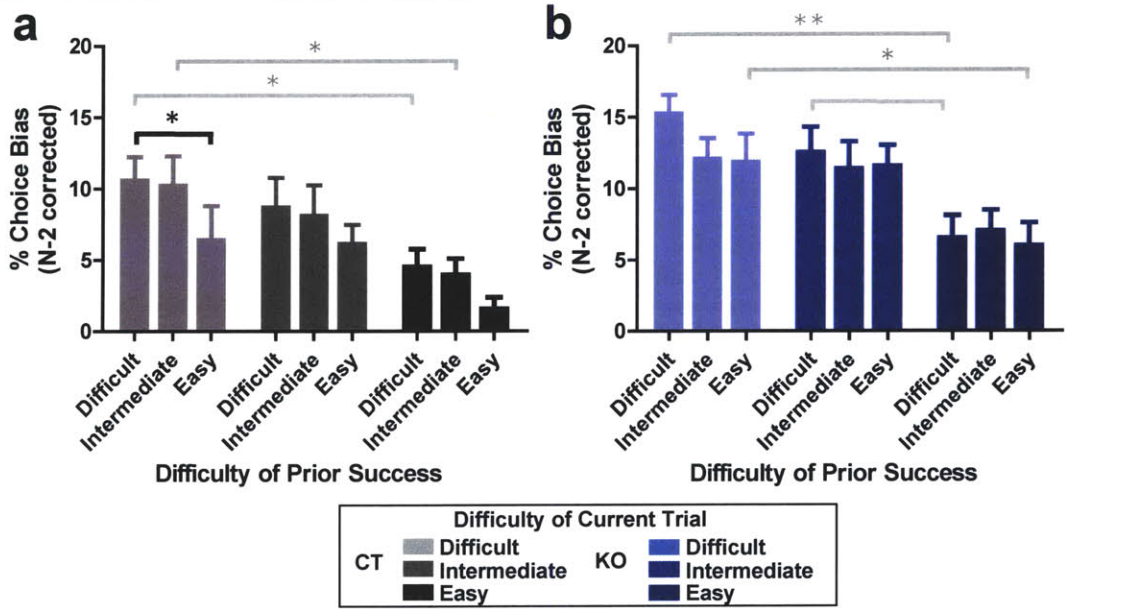

Figure 4-7: **Current decision difficulty influences choice bias in both control and DAT/NR1 knockout mice.** A, B) While only control mice show a significant influence of prior difficulty on choice bias, both control and DAT/NR1 knockout mice demonstrate a significant influence of current trial difficulty on choice bias. Specifically, in both genotypes, easier decisions are less susceptible to the influence of prior success parameters (direction of prior reward) as seen in the decrease in bias across shades of gray and blue. Shades of gray or blue indicate difficulty of current trial. A) Control mice show a main effect of current trial difficulty and prior success difficulty. B) DAT/NR1 knockout mice show a main effect of current trial difficulty but not of prior trial difficulty. Results of two-way ANOVA (current by prior difficulty) indicate significant main effects in control mice of both prior success difficulty and current trial difficulty; knockout mice show a main effect of current trial difficulty. Results of post-tests indicated by $^{*}P<0.05$, $^{**}P<0.01$. Data shown, mean±s.e.m.

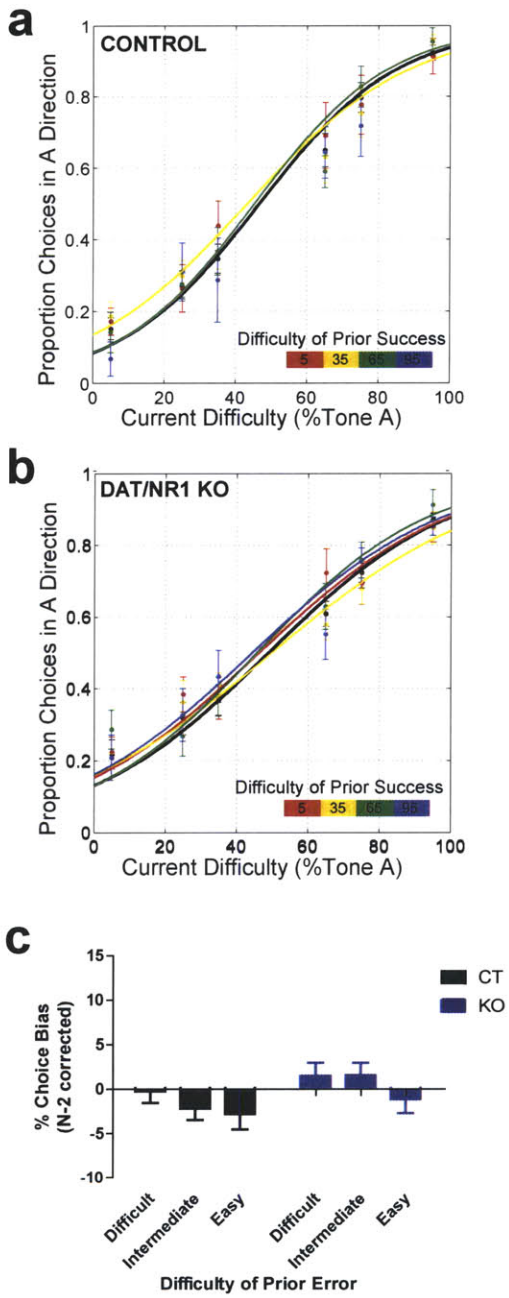

Figure 4-8: **Difficulty of prior error shows no significant influence on current decisions regardless of prior difficulty or genotype.** While both control and DAT/NR1 knockout mice show an influence of prior reward direction, neither control mice (A) nor DAT/NR1 knockout mice (B) show an influence of prior error (prior error direction or prior error difficulty). C) Quantification comparing the influence of prior error difficulty across genotypes. Results of two-way ANOVA (genotype by prior difficulty) indicate no significant main effects or interaction effects of genotype or prior error difficulty. Note: only regression curves of prior difficult errors are plotted in control (A) panel due to insufficient easy error trial data to support maximum likelihood estimations of regression coefficients. Data shown, mean±s.e.m.

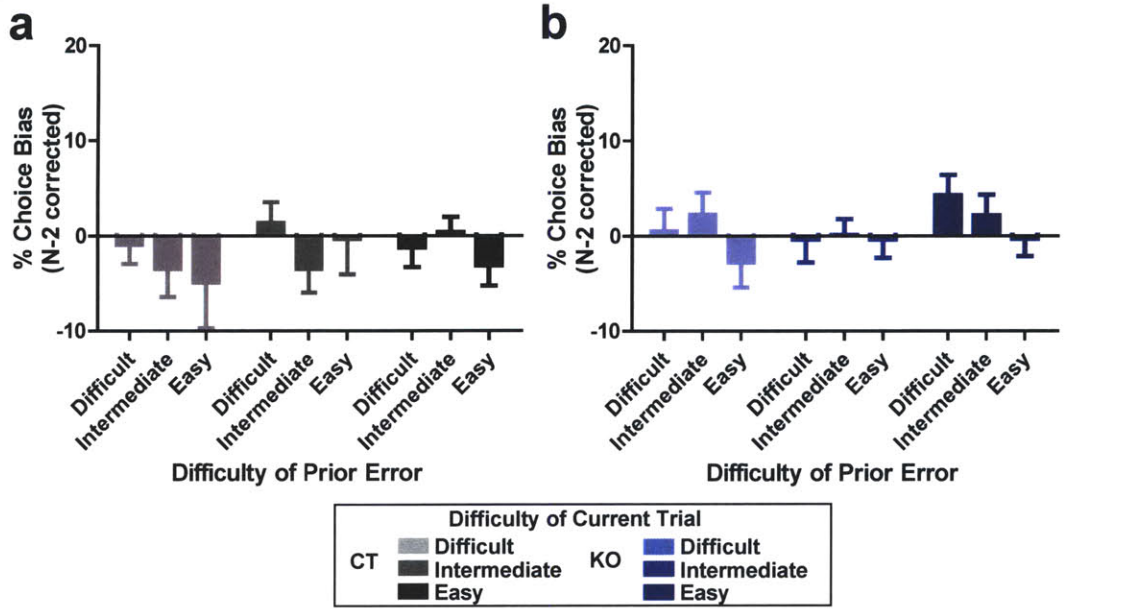

Figure 4-9: **Prior errors show no influence on current decisions regardless of prior or current decision difficulty.** A, B) Neither control nor DAT/NR1 knockout mice demonstrate a significant influence of prior error difficulty on choice bias, even when data is segregated by current trial difficulty. Results of two-way ANOVA (current difficulty by prior difficulty) indicate no significant main effects nor interaction effects in control mice or DAT/NR1 knockout mice. Data shown, mean±s.e.m.

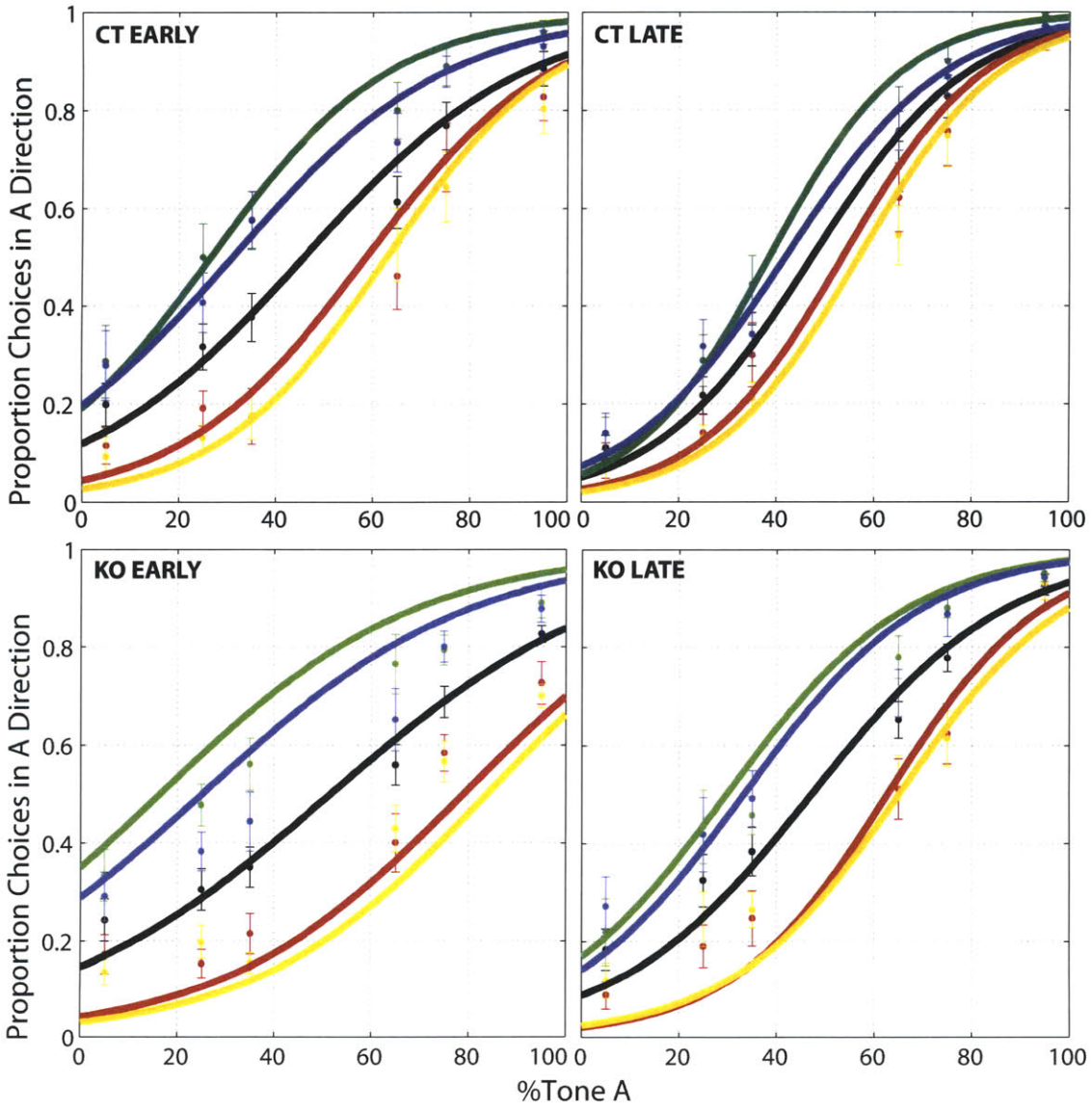

Figure 4-10: **Choice bias diminishes with experience.** Choice bias diminishes with experience faster following easy successes but not in the absence of dopamine neuron NMDARs.

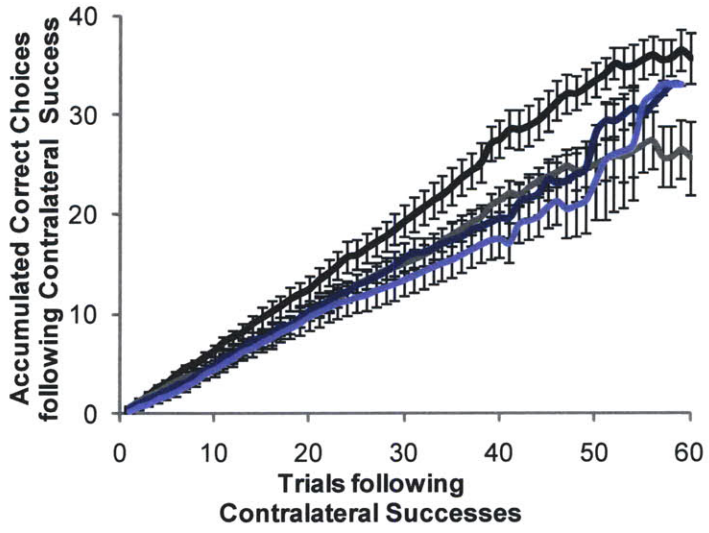

Figure 4-11: **Choice bias diminishes with experience.** Choice bias diminishes with experience faster following easy successes but not in the absence of dopamine neuron NMDARs. Chart shows a running total of biased responses plotted against a running total of opportunities for biased responses. Black and gray indicate influence on control of prior successes that were easy (black) and difficult (gray). Blue shades indicate influence on control of prior successes that were easy (dark blue) and difficult (light blue).

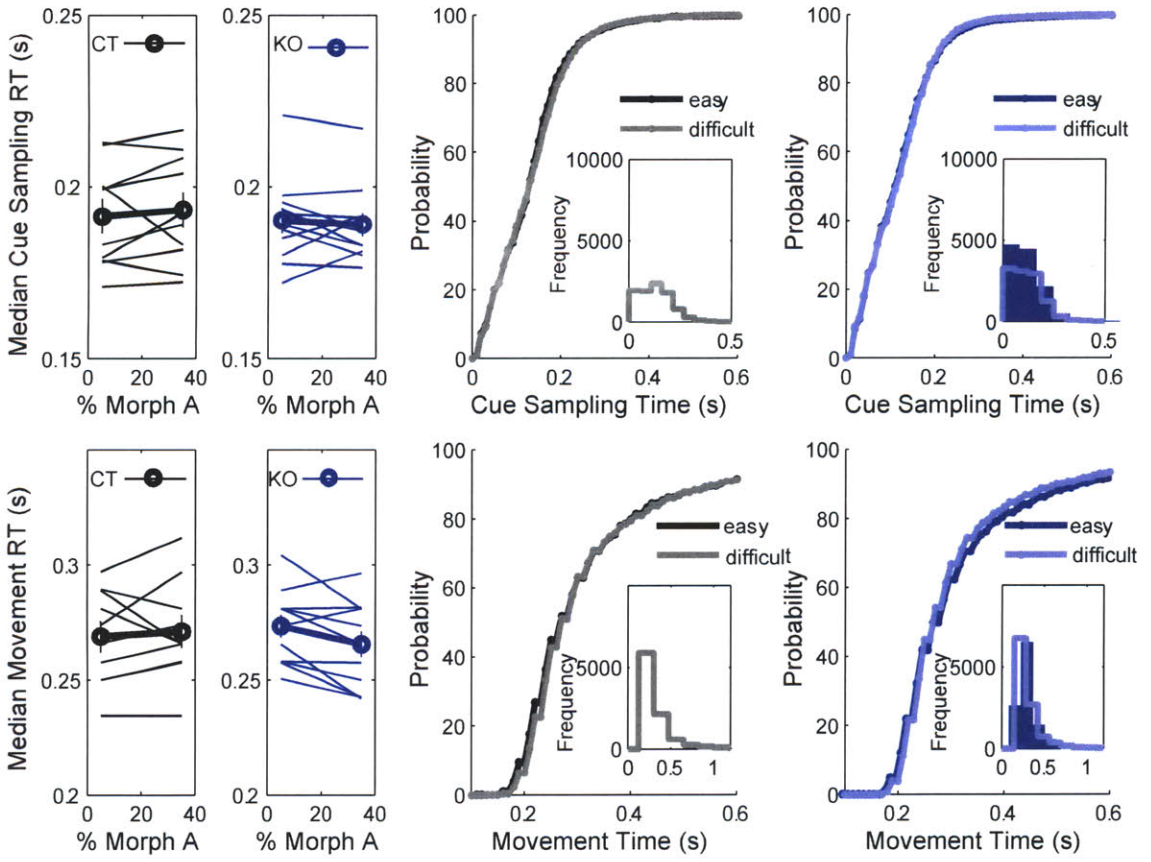

Figure 4-12: **Response Times: Cue Sampling Time and Movement Time.** Control mouse shown in black; DAT/NR1 knockout mouse shown in blue. Cue sampling time data shown on top row; movement time data shown on bottom row. Cue sampling time is measured as time elapsing from the onset of the cue to exiting the center port (cue sampling port). (A, B) Cue sampling time for control (A) and knockout (B) mice for each morph in binary choice task. (C-D) Cumulative distribution functions comparing distributions shown in histogram insets of cue sampling times for easy (dark line) and difficult (light line) decisions for control (C) and knockout (D) mice. (E-H) Movement time is measured as time elapsing from exiting the center (cue sampling) port to entering one of the two side (reward) ports. 'Easy' refers to trials pooled from the furthest two morphs from the 50% morph category boundary. 'Difficult' refers to trials pooled from the two morphs closest to 50% morph category boundary. (E,F) Median movement time of individual mice (lines) and averages (circles) in 'Easy' and 'Difficult' trials for control (black) and knockout (blue) mice in a binary choice bias task. (G,H) Cumulative distribution functions comparing distributions shown in histogram insets of movement times for easy (dark line) and difficult (light line) decisions for control (G) and knockout (H) mice.

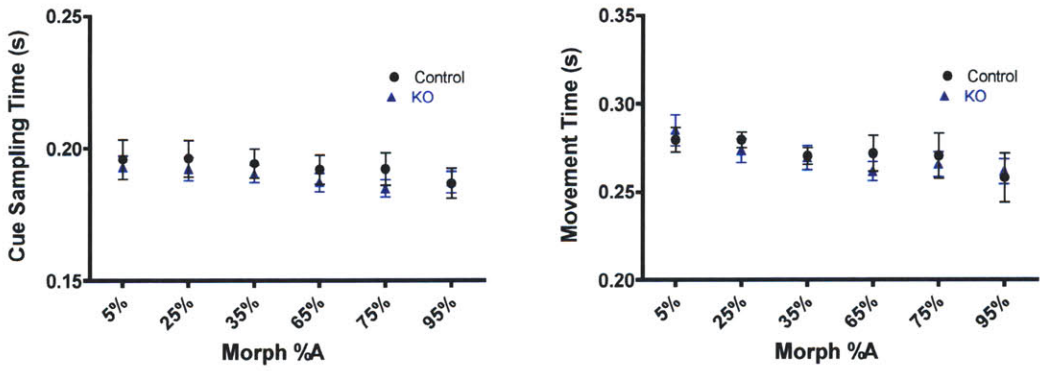

Figure 4-13: **Cue Sampling Time and Movement Time.** Control mouse shown in black; DAT/NR1 knockout mouse shown in blue. Comparison of control (black) and knockout (blue) mice in cue sampling time (A) and movement time (B) for each morph.

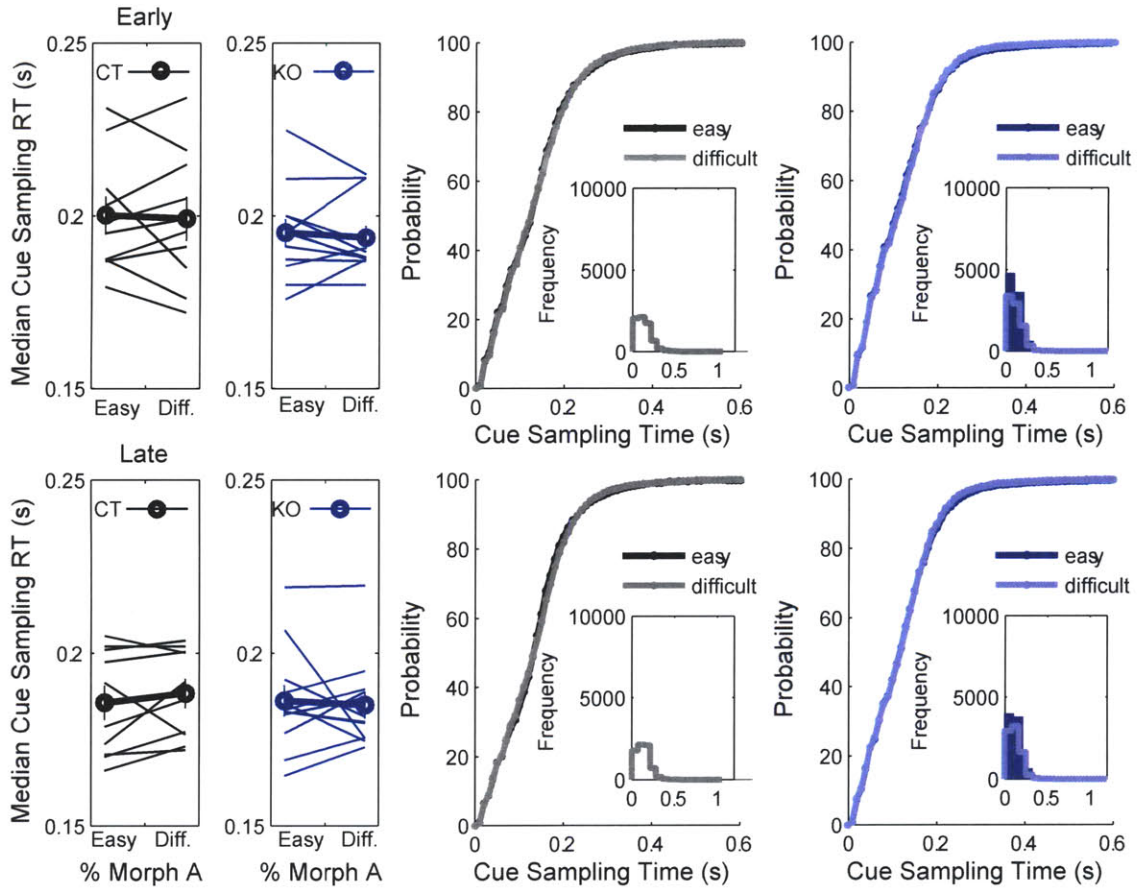

Figure 4-14: **Cue Sampling Time: Early vs. Late.** Control mouse shown in black; DAT/NR1 knockout mouse shown in blue. 'Early' data shown on top row; 'Late' data shown on bottom row. Cue sampling time is measured as time elapsing from the onset of the cue to exiting the center port (cue sampling port). (A, B) Comparison of cue sampling time for control (black) and knockout (blue) mice for each morph in early choice bias task (A), and late choice bias task (B). (C-F) Cumulative distribution functions comparing distributions shown in histogram insets of cue sampling times for easy (dark line) and difficult (light line) decisions for control (C, D) and knockout (E, F) mice.

Chapter 5

A Proposed Role for Dopamine Neuron NMDARs in Reward History-Dependent Response Biases

With repetition of stimulus-reward pairings, stimuli that reliably precede rewards gain predictive value, a process known to be correlated with phasic dopamine neuron responses to reward predictive cues. In keeping with Thorndike's classical formulation of the "Law of Effect" (Thorndike, 1911), we have observed, in mice, that prior outcomes influence subsequent choices in the form of a response bias in the direction of successful outcomes. In keeping with a role for the graded nature of a prediction error "teaching signal," we observe, by varying the difficulty of stimulus discrimination, the graded modulation of this response bias.

A hallmark of phasic dopamine reward responses is the graded nature of reward-response magnitude showing diminished responding as rewards become predictable. According to theory, the discrepancy between predicted and actual reward should drive learning. However, whether learning occurs in a graded manner depending on the magnitude of dopamine signaling is not clear.

We were able to test this idea using a behavioral model of updating in which mice show varying degrees of learning (updating) depending on the difficulty of discrimination. Our finding, that the graded effect of difficulty is greatly reduced in knockout mice, supports the hypothesis that dopamine regulates learning in a manner dependent on the magnitude of prediction errors.

We initially hypothesized that the magnitude of dopamine burst-firing to rewards mediates reward-history dependent biases, such that unexpected rewards (success following a difficult discrimination) would result in a large response bias, and relatively expected rewards (success following an easy discrimination) would result in a smaller response bias. We therefore expected that DAT/NR1 knockout mice, previously shown to have reduced levels of dopamine neuron burst-firing would show limited reward-history dependent bias. Instead, we find that mice lacking dopamine neuron NMDARs are as biased as control mice following difficult successes. However, in keeping with the basis for our original hypothesis, we find that mice lacking dopamine neuron NMDARs show a reduction in the graded nature of this response bias, such that the influence of prior difficult and prior easy successes is not significantly different. (Formally, this is a failure to reject the null hypothesis that the influences of easy and difficult prior successes are the same in mutant mice. In the absence of a formal statistical power analysis, we point to the significant difference between the small influence of prior easy successes in control mice, and the significantly larger influence of prior easy successes in DAT/NR1 knockout mice to demonstrate our point statistically.)

Because DAT/NR1 knockout mice, to our surprise, retain a large bias in response to prior successes, we propose that dopamine burst-firing is needed to *remove* this bias, ie. dopamine is needed to refine cue-response associations such that prior outcomes no longer bear irrelevant influence on current decisions (Thorndike, 1933; Walton et al., 2010). We propose that the graded nature of the response bias in control mice reflects the graded speed at which dopamine refines stimulus-response associations. We propose that DAT/NR1 knockout mice still exhibit a large bias in response to prior successes because they don't have sufficient dopamine burst-firing to refine it

away. The observation that DAT/NR1 knockout mice ultimately *do* show a reduction in bias (albeit more slowly or to a lesser degree than in control mice) is informed by our initial studies that these mice also eventually learn a binary choice discrimination task, as described in Chapter 3, albeit more slowly than control mice. We suspect that residual levels of burst-firing or the normal levels of background and tonic dopamine neuron firing in knockout mice may suffice to drive eventual learning of the binary choice task described in Chapter 3 and eventually reduce reward-history dependent biases as described here. In summary, we propose that dopamine plays a role in freeing decision-making from the influence of prior decisions, by promoting the assignment of appropriate credit to relevant and causal stimuli in a decision (Fig. 5-1).

According to this interpretation, dopamine does not mediate the initial response bias and our study provides no explanation for what mechanisms may drive this bias. Literature investigating win-stay strategies and ego- versus allo-centric strategies may inform on the mechanism by which a win-stay strategy, such as the one seen here, comes about. Win-stay strategies are thought to be a dorsal lateral striatally-mediated response strategy, as opposed to an allocentric hippocampal place strategy or a win-shift response strategy thought to recruit ventral striatal circuits (Wise, 2004).

Our proposal that dopamine is required to reduce the influence of reward history is fueled by the literature describing DAT/NR1 knockout mice as showing reduced dopamine neuron burst-firing (Zweifel et al., 2009; Parker et al., 2010). However, an alternative hypothesis, that we cannot rule out, proposes that dopamine neuron burst-firing, in fact, mediates a reward-history driven bias. According to this model, either dopamine neuron burst-firing in DAT/NR1 knockout mice eventually achieves normal levels during the initial training of two auditory cues, as described in Chapter 3, after which it is available to drive response biases as in control mice, or the reduced burst-firing levels of DAT/NR1 knockout mice are sufficiently large to reach some threshold needed to incur the same large response bias seen in controls. According to this model, we might expect that dopamine neurons develop sufficiently strong responses to both easy and difficult rewards, but that burst-firing does not reduce with

pairing to a predictive stimulus, and remaining high to both easy and difficult stimuli (Fig. 5-2). In a well-trained animal dopamine levels can affect striatal synchrony and are thereby thought to gate corticostriatal inputs and modulate action selection. Because striatal excitability is heavily influenced by D1 receptor expressing medium spiny neurons (Costa et al., 2007), and because phasic dopamine firing kinetics preferentially activate D1 receptor signaling in the striatum (Richfield et al., 1989), this possibility is a viable alternative, although not as parsimonious with known demonstrations of reduced burst firing in DAT/NR1 knockout mice.

These models could be distinguished by recording from dopamine neurons (an effort underway in collaboration with Corey Puryear). The models could also be distinguished by optogenetic stimulation in mutant and control mice during trial relevant stimuli. Optogenetic stimulation of dopamine neurons in mutant mice during the time of a reward would allow subsequent analysis of whether a) this caused *reduction* in the influence of a prior success in support of our proposed interpretation or b) this caused *enhancement* of the influence of a prior success in support of the latter described alternative hypothesis (Fig. 5-2, H_2 panel).

A possible anatomical circuit would comprise the following: 1. PPTg activation drives burst-firing of dopamine neurons to salient events such as rewards and cues. Burst-firing of dopamine neurons depends on the activation of NMDARs, perhaps the recruiting and building from the rearrangement of synaptic weights by NMDAR-dependent LTP, such that salient rewards and relevant stimuli increasingly effectively drive burst-firing. By whatever mechanism (charge transfer of the NMDAR or NMDAR-dependent LTP), burst-firing is assumed in our interpretation to be reduced in dopamine neurons of DAT/NR1 knockout mice.

Explanatory Models: Target region dopamine release refines stimulus-response associations, or primes actions for selection.

Refinement for Appropriate Credit-Assignment Model. Dopamine release, likely in the striatum, enables refinement of stimulus-response associations (for in-

stance amygdala-striatal or cortico-striatal synapses), so that with learning, motor response is driven by the appropriate cue and not influenced by prior trials (Fig. 5-2, H_1 panel).

Action Selection Model. Alternatively, dopamine release, likely in the striatum, may cause short-lived priming of a response circuit via residual dopamine or a short-term facilitation or plasticity from prior trials. This priming of a particular directional response circuit may cause a bias in the direction of prior trials which is slowly overcome due to the gradual reduction in magnitude of the phasic dopamine reward response as rewards become increasingly predicted (Fig. 5-2, H_2 panel).

Future studies aimed at distinguishing explanatory models. Future studies aimed at discriminating between these two proposed models include recordings of dopamine neurons in control and DAT/NR1 knockout mice during this task. This will be informative as to the relative degree of burst-firing between genotypes, especially if burst-firing in DAT/NR1 knockout mice occurs in keeping with our alternative hypothesis, such that normal phasic responses are observed to primary rewards. If, however, we observe the expected reduction in dopamine neuron burst-firing in DAT/NR1 knockout mice, an interpretation may be complicated by the potential for a smaller dopamine response in knockout mice to mediate a bias by achieving a critical threshold or by compensatory mechanisms in target regions.

A more definitive test of these models may be achieved by the rescue of dopamine neuron burst-firing in DAT/NR1 knockout mice (if burst-firing levels are indeed reduced) by optogenetic stimulation triggered at the time of reward delivery. As described in the first, "refinement of credit-assignment" model, behavioral analysis of the influence of this rescued dopamine neuron burst-firing may cause a faster reduction in response bias (and gradation of this reduction in bias if calibration of a graded optogenetic stimulation proves possible).

Alternatively, optogenetic stimulation triggered at the time of reward delivery may cause an enhancement in response bias in the direction of prior successes. In

this case, optogenetic stimulation in *control* mice of dopamine neurons at the time of easily attained (expected) rewards should result a renewed influence of these prior easy rewards. Further studies by electrophysiological and optogenetic methods may uncover influences of cue responses in this behavior.

In summary, this study is the first demonstration in the genetically accessible mouse model system of quantitative behavioral dissection of the role of dopamine in reward-history dependent responding. Here we tested the idea whether learning occurs in a graded manner depending on the magnitude of dopamine signaling using a behavioral model of updating in which mice show varying degrees of learning (updating) depending on the difficulty of discrimination. Our finding that the effect of difficulty is greatly reduced in knockout mice supports the hypothesis that dopamine regulates learning in a manner dependent on the magnitude of prediction errors. Given this assumption, our interpretation of these findings is that dopamine refines the associative strength between stimulus and response such that reward history no longer interferes with current decisions.

Bibliography

Costa, R. M., R. Gutierrez, I. E. d. Araujo, M. R. P. Coelho, A. D. Kloth, R. R. Gainetdinov, M. G. Caron, M. A. L. Nicolelis, and S. A. Simon (2007). Dopamine levels modulate the updating of tastant values. *Genes, Brain and Behavior 6*(4), 314–320.

Parker, J. G., L. S. Zweifel, J. J. Clark, S. B. Evans, P. E. Phillips, and R. D. Palmiter (2010). Absence of nmda receptors in dopamine neurons attenuates dopamine release but not conditioned approach during pavlovian conditioning. *Proc Natl Acad Sci U S A 107*(30), 13491–6.

Richfield, E. K., J. B. Penney, and A. B. Young (1989). Anatomical and affinity state comparisons between dopamine d1 and d2 receptors in the rat central nervous system. *Neuroscience 30*(3), 767–77.

Thorndike, E. (1911). Animal intelligence: Experimental studies (new york: Macmillan).

Thorndike, E. (1933). A proof of the law of effect. *Science 77*, 173–175.

Walton, M. E., T. E. Behrens, M. J. Buckley, P. H. Rudebeck, and M. F. Rushworth (2010). Separable learning systems in the macaque brain and the role of orbitofrontal cortex in contingent learning. *Neuron 65*(6), 927–39.

Wise, R. A. (2004). Dopamine, learning and motivation. *Nat Rev Neurosci 5*(6), 483–94.

Zweifel, L. S., J. G. Parker, C. J. Lobb, A. Rainwater, V. Z. Wall, J. P. Fadok, M. Darvas, M. J. Kim, S. J. Mizumori, C. A. Paladini, P. E. Phillips, and R. D. Palmiter (2009). Disruption of nmdar-dependent burst firing by dopamine neurons provides selective assessment of phasic dopamine-dependent behavior. *Proc Natl Acad Sci U S A 106*(18), 7281–8.

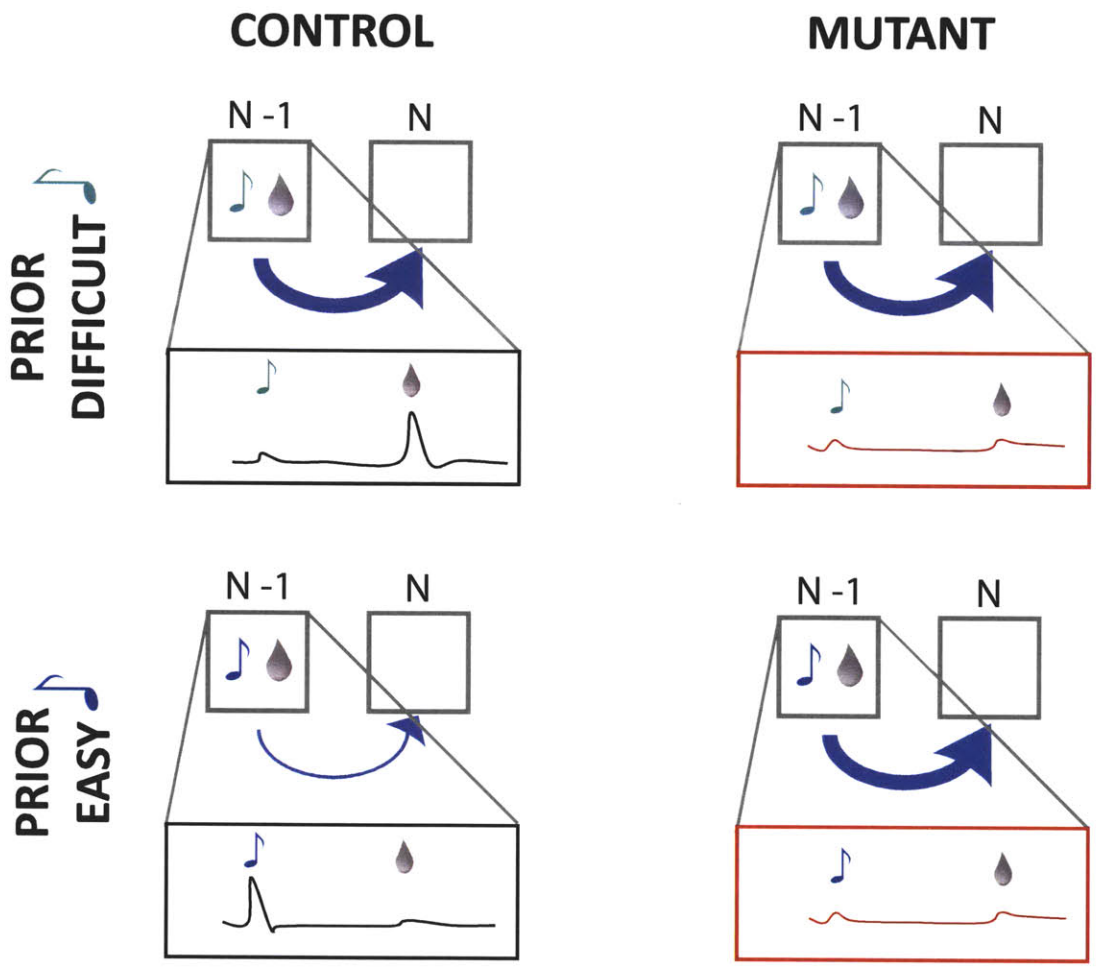

Figure 5-1: **Observed biases and proposed phasic dopamine responses.** Observed biases and proposed phasic dopamine responses. Varying degrees of bias observed on trial_N following difficulty (greenish-blue note) and easy (blue note) successful (indicated by water reward) trials_{N-1} are indicated by arrow size. Proposed phasic dopamine responses are indicated for control (left, inside black boxes) and knockout (right inside red boxes). Because DAT/NR1 knockout mice retain a large bias in response to prior successes, we propose that dopamine burst-firing is needed to *remove* this bias, ie. dopamine is needed to refine stimulus-response associations such that prior outcomes no longer bear irrelevant influence on current decisions. We propose that the graded nature of the response bias in control mice reflects the graded speed at which dopamine refines stimulus-response associations, and that the cue-related phasic dopamine activity reflects the degree to which these associations have been refined (and bias lessened). We propose that DAT/NR1 knockout mice still exhibit a large bias in response to prior successes because they don't have sufficient dopamine burst-firing to refine it away. In summary, we propose that dopamine plays a role in freeing decision-making from the influence of prior decisions, by promoting the assignment of appropriate credit to relevant and causal stimuli in a decision.

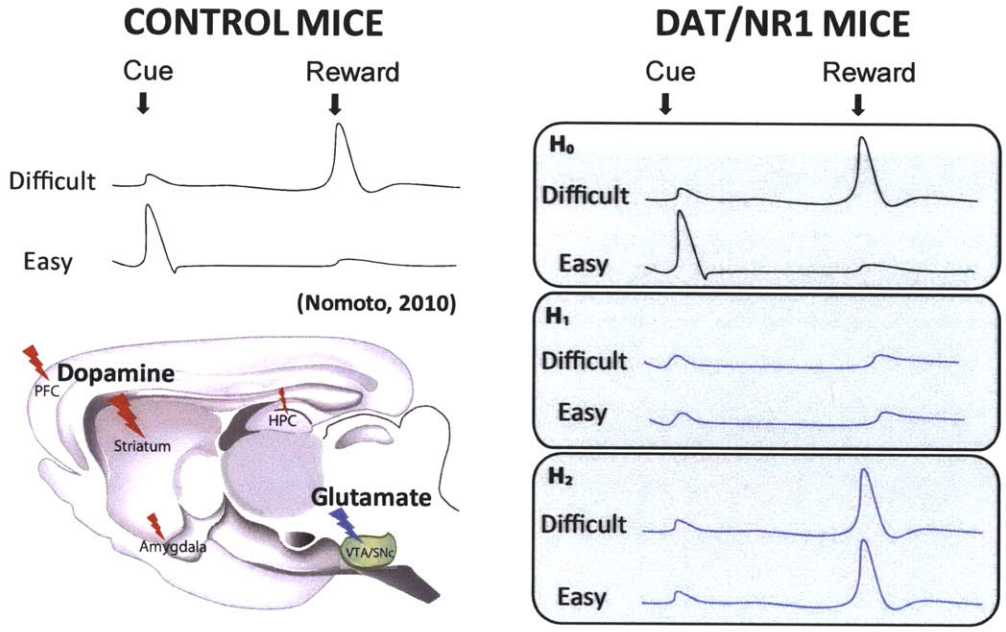

Figure 5-2: **Proposed and alternative task-relevant phasic dopamine burst-firing.** Proposed and alternative task-relevant phasic dopamine burst-firing. We propose that dopamine neuron burst-firing is needed to free decisions from the irrelevant influence of reward history. We propose that mutants still have bias because they don't have sufficient dopamine burst-firing required to reduce this influence. According to this hypothesis, recording from dopamine neurons during this task would be expected to reveal that phasic dopamine responses in mutants are reduced compared with control mice (H_1). An alternative hypothesis (H_2) proposes that dopamine burst-firing mediates the bias. According to this hypothesis, recording from dopamine neurons, would reveal that DAT/NR1 knockout mice eventually developed sufficient dopamine responses to rewards, and that these dopamine responses determine the magnitude of bias on subsequent trials. These hypotheses could be further tested by using optogenetic stimulation in mutant mice. Optogenetic stimulation of dopamine neurons in mutant mice during the time of a reward would allow subsequent analysis of whether a) this causes *reduction* in the influence of a prior success in keeping with H_1 or b) this causes *enhancement* of the influence of a prior success in keeping with H_2.

Appendix A

Circuit Genetic Approaches to the Study of Dopamine Function: A strategy for viral vector delivery and conditional targeting of shRNA-mediated gene knockdown and gene rescue in midbrain dopamine neurons

A.1 Introduction

Neuromodulatory nuclei of the brainstem receive a convergence of many afferent structures and send divergent projections to a wide array of target structures. Dopaminergic midbrain nuclei are one example of a neuromodulatory system known to subserve many functions. The many functions of dopamine result at least in part from the diversity of target structures, the diversity of afferent structures, and the multiple

modes of neuronal firing they exhibit. Circuit genetic approaches for the dissection of dopamine function have been eagerly adopted with recent advances in recombinant viral vector and optogenetic approaches, used in combination with Cre-expressing mouse lines. RNAi-based strategies provide a complementary addition to the array of tools available for circuit dissection. Conditional viral knockdown strategies are well suited for dissection of dopamine circuitry. Viral-mediated cell-type specific targeting of gene knockdown provides a novel approach to questions that cannot be addressed by more traditional approaches.

We describe a knockdown method that can provide spatial and temporal restriction for use in cases where inducible conditional transgenic mouse lines do not exist, and when promoter fragments small enough and specific enough for viral-mediated Cre delivery to specific brain regions are not available. We demonstrate viral delivery of a Cre-mediated recombination-dependent shRNA to dopamine neurons with the possibility for monitoring recombination.

A.2 Results

A Cre-dependent construct design and shRNA against *lacZ* that was previously used in the generation of a viable transgenic mouse line (Hitz et al., 2007) was modified by integrating a promoter and fluorophore between flanking *loxP* sites and the shRNA sense and antisense stems (Fig. A-1a). Two polII promoters driving fluorophores were used such that Cre-mediated recombination would result in the excision of only one fluorophore. *In vitro* assays in cultured HEK293T cells of fluorescence following Cre-mediated excision of the *loxP* flanked fluorophore revealed an unmasking effect of the other fluorophore possibly due to promoter competition between the two polII promoters (Fig. A-1b). Additional modifications were made for the purpose of packaging the construct in an AAV8 viral vector.

Titration of virus and a timecourse was performed in order to optimize knockdown efficacy. It was found that 500μl of a 1X10 ^{12} pfu/mL viral dilution resulted in robust knockdown efficacy in the absence of apoptotic markers for at least 3 weeks (Data

not shown).

Stereotactic injections of a pre-recombined version into *Slc6a3*$^{+/Cre}$*;floxed-ROSA26-lacZ* mice (Soriano, 1999) demonstrated dramatic reduction in levels of β-galactosidase activity in dopamine neurons, as seen by X-gal stain in injected and non-injected brain hemispheres one week following injection (Fig. A-2b versus Fig. A-2a). The same titer AAV8 packaged with GFP was injected to determine if viral expression alone could account for the depression in X-gal staining. One week following injection β-galactosidase activity was normal (Fig. A-2e GFP-injected versus Fig. A-2f AAV8-loxP-shLacZ injected) demonstrating that viral load alone could not account for this reduction.

In order determine if the reduction in β-galactosidase activity following AAV8-loxP-shLacZ injection could be due to the loss dopamine cells, we fluorescently immunostained sections for tyrosine hydroxylase, a marker of dopamine neurons, ECFP to indicate virally transduced neurons, and β-galactosidase (Fig. A-3). The reduction in β-galactosidase was also apparent by fluorescent immunhistochemistry and was not matched by tyrosine hydroxylase reduction, although a smaller reduction was seen, a possible indication of off-target effects, the result of viral load, or interferon response (Fig. A-4).

We found no evidence of cell death in TUNEL stained sections compared with DNAse treated positive control sections and negative control sections (Fig. A-5). Three concentrations of DNAse were used to ensure an appropriate positive control for comparison; the intermediate concentration is shown here.

We conclude that AAV8-delivery of shRNAs to dopamine neurons in combination with a conditional transgenic mouse line provides a possible additional approach for genetic dissection strategies. While we do see evidence of potential off-target effects with this construct, this my be a function of siRNA design and not the viral delivery method. Future studies will combine this approach with shRNAs designed and optimized for minimizing off-target effects.

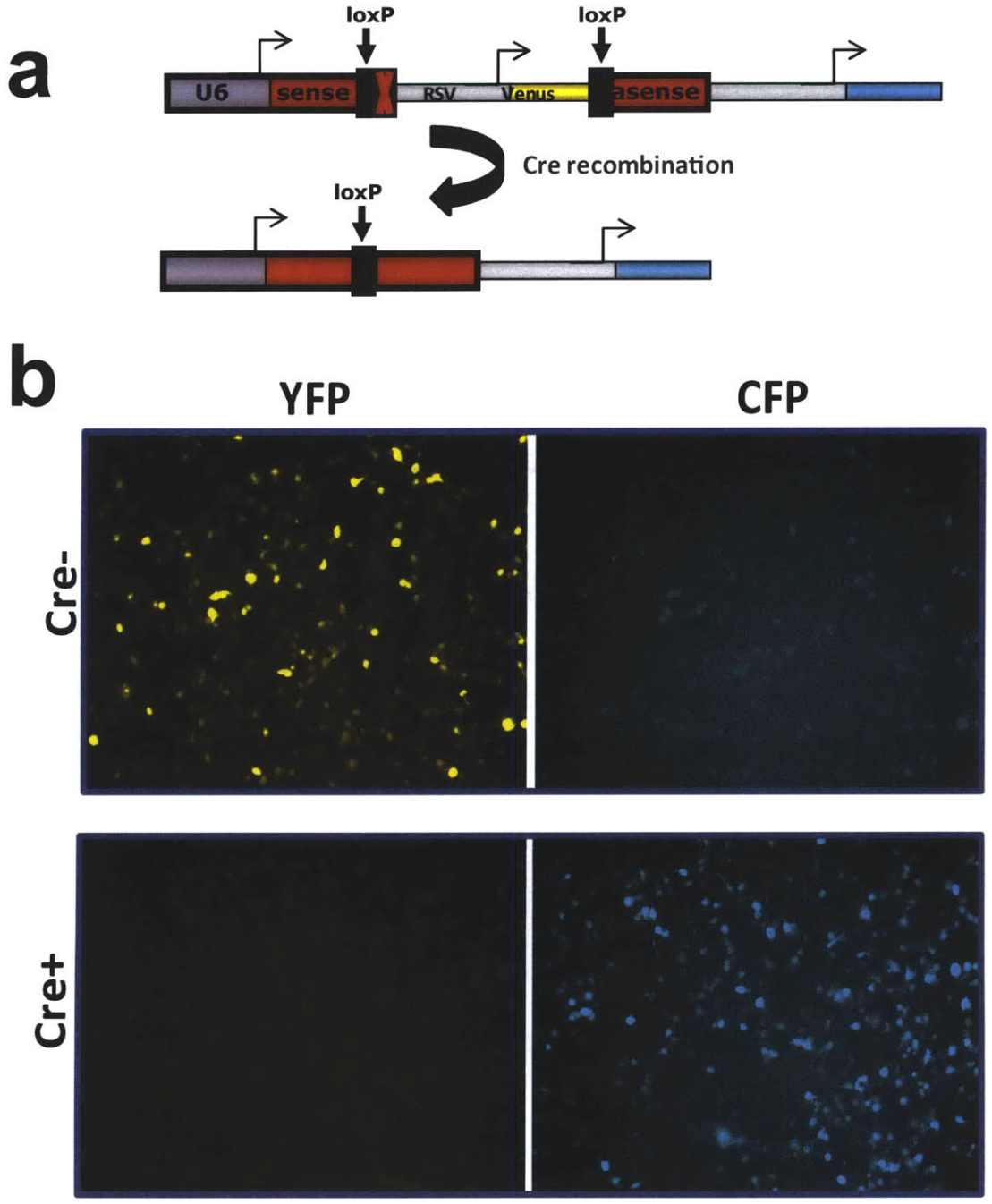

Figure A-1: **Cre recombines *lox-STOP-lox-shRNA* construct *in vitro*.** In vitro assay of Cre-mediated recombination following transfection of HEK293 cells with Cre plasmid and *LSL-shRNA* plasmid demonstrates excision of RSV promoter and EYFP. Unmasking of ECFP expression may be the result of promoter competition between two polII promoters, RSV and human Syn1.

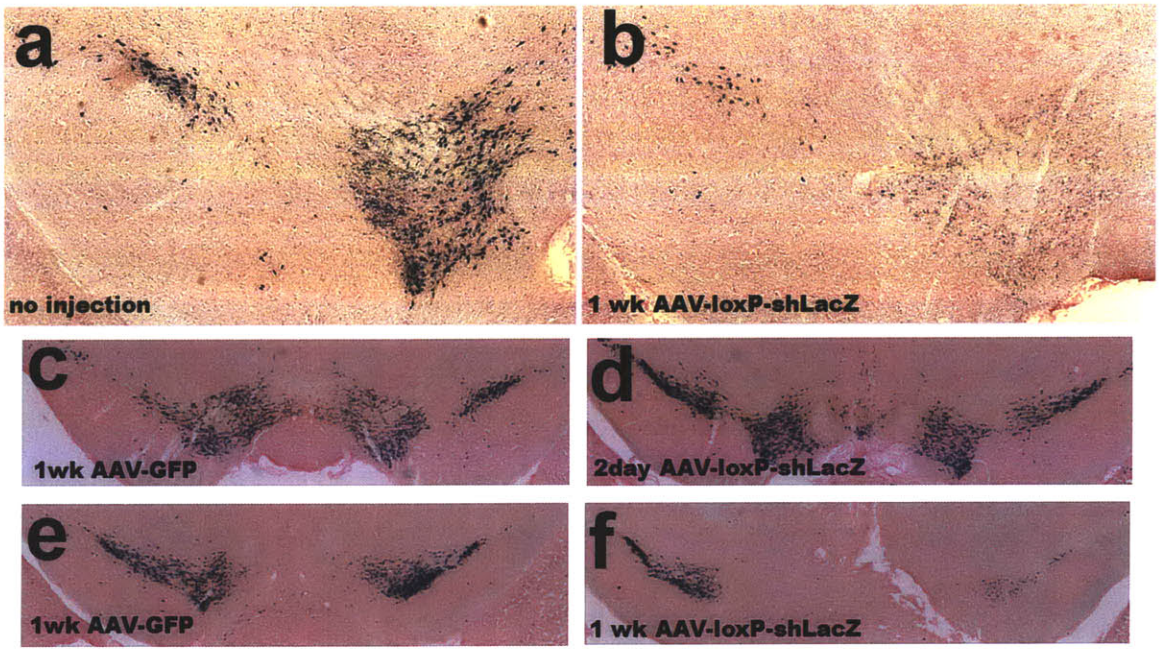

Figure A-2: **AAV8-*loxP-shLacZ* knocks down β-galactosidase expression in vivo.** In *Slc6a3*$^{+/Cre}$*;floxed-ROSA26-lacZ* mice, reduced X-gal staining is seen in AAV8-*loxP-shLacZ* injected tissue (b,f) one week after injection, but not the contralateral side to the injection (a). No reduction is seen 2 days after injection (d), nor in mice having received a sham injection of AAV8 packaged with the fluorophore alone (c,e). Comparable experimental mice are paired horizontally.

A.3 Discussion

RNAi-based approaches to circuit dissection provide a method of circuit-specific study of gene function, or a strategy for genetic modification to effect a functional change. For instance, loss of functional NMDARs in dopamine neurons results in a reduction of dopamine neuron burst-firing (Zweifel et al., 2009). Reduction of the dopamine transporter (DAT) results in functional elevation of tonic firing levels (Cagniard et al., 2006). These examples highlight the potential for RNAi-based circuit dissection strategies.

However, RNAi-based approaches can be fraught with complexity due to the potential for off-target effects, induction of interferon response, and apoptotic responses to high viral expression of these small RNAs. *In vivo* RNAi studies require extensive

Figure A-3: **AAV8-*loxP-shLacZ* knocks down β-galactosidase expression in vivo.** In *Slc6a3*$^{+/Cre}$*;floxed-ROSA26-lacZ* mice, reduced X-gal staining is seen in AAV8-*loxP-shLacZ* injected tissue (b,f) one week after injection, but not the contralateral side to the injection (a). No reduction is seen 2 days after injection (d), nor in mice having received a sham injection of AAV8 packaged with the fluorophore alone (c,e). Comparable experimental mice are paired horizontally.

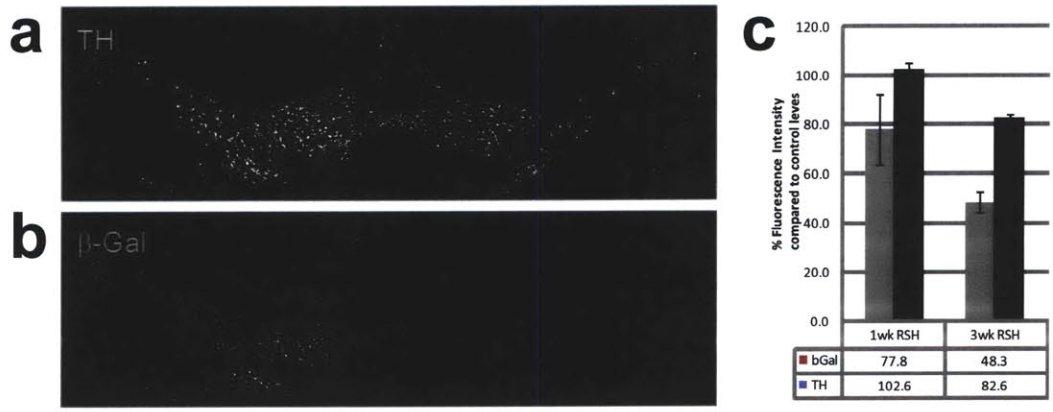

Figure A-4: **AAV8-*loxP-shLacZ* knocks down β-galactosidase expression in vivo.** In *Slc6a3*$^{+/Cre}$*;floxed-ROSA26-lacZ* mice, reduced X-gal staining is seen in AAV8-*loxP-shLacZ* injected tissue (b,f) one week after injection, but not the contralateral side to the injection (a). No reduction is seen 2 days after injection (d), nor in mice having received a sham injection of AAV8 packaged with the fluorophore alone (c,e). Comparable experimental mice are paired horizontally.

controls at a number of stages including the screening of at least three siRNAs in cell culture for knockdown efficacy, ideally primary cultures of the cell-type of interest, assaying the expression of several non-target genes for evidence of off-target effects, comparing candidate siRNA sequences with scrambled versions of the siRNA seed region or, better, demonstrating the knockdown resistance of a target cDNA construct modified with silent mutations in the region of siRNA hybridization, and confirming behavioral phenotypes with at least two shRNAs (Cullen, 2006). Use with viral delivery requires additional titration to ensure non-toxic expression levels and assessment of the timecourse of efficacy. Pre-screening and siRNA libraries can minimize the search space and improve experimental design and outcomes.

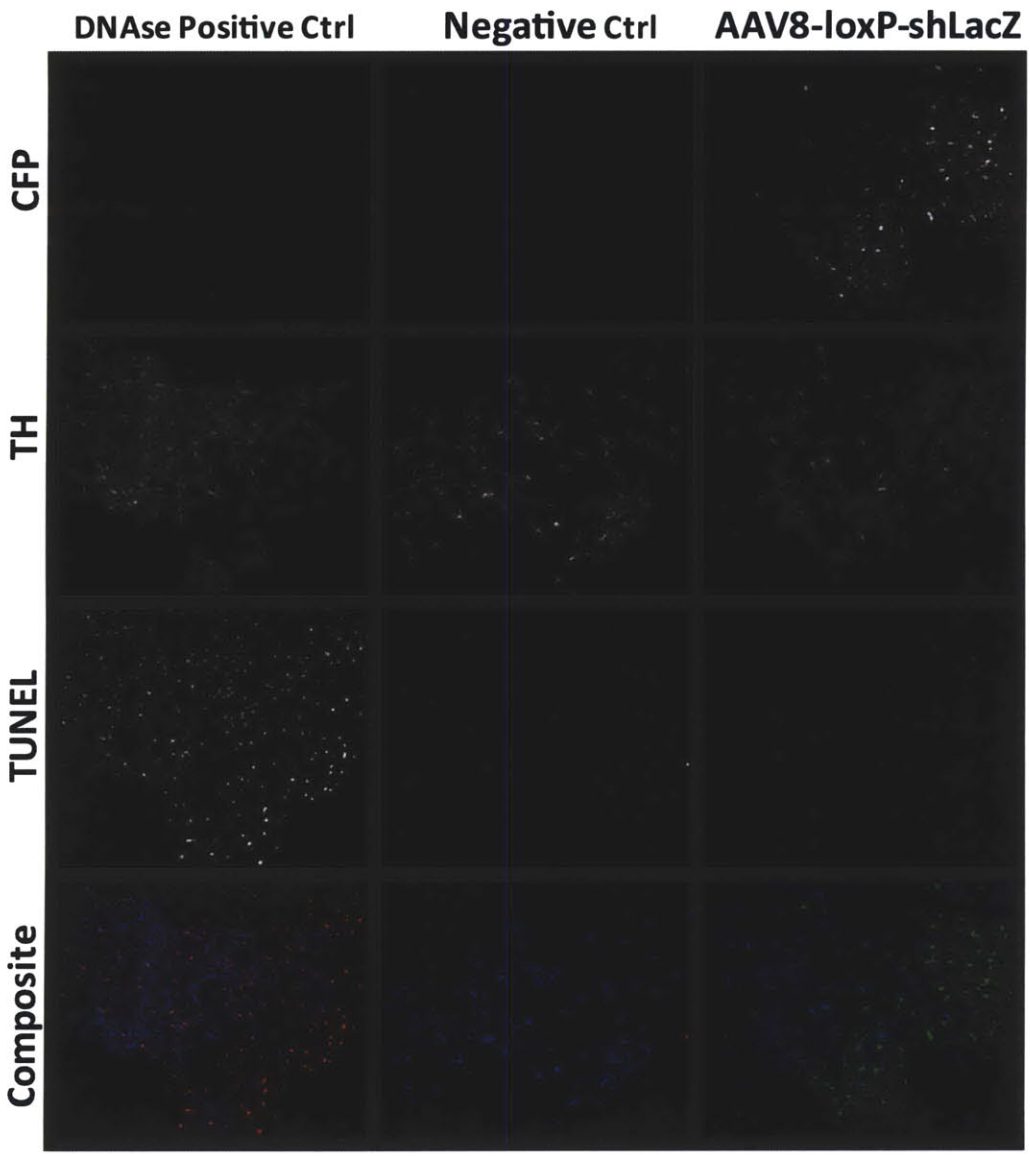

Figure A-5: **AAV8-loxP-shLacZ does not induce cell death.** TUNEL staining was done to assess apoptotic activity at 2 weeks post- AAV8-shLacZLoxP injection. ECFP (indicating AAV-shLacZLoxP expression), TH and TUNEL staining was done on sections treated with DNAse a), sections from an uninjected side b), and sections from a AAV-shLacZLoxP injected littermate c). TUNEL signal appears equivalent to negative control levels.

A.4 Methods

A.4.1 Mice

Slc6a3$^{+/Cre}$*;floxed-ROSA26-lacZ* mice (Soriano, 1999) were used to assess *in vivo* knockdown efficiency.

A.4.2 Viral vector preparation

Lentiviral vectors were packaged using a self-inactivating vector engineered with the human synapsin1 promotor, a woodchuck hepatitis virus posttranscriptional regulatory element (WRE) and pseudotyped with the vesicular stomatitis virus glycoprotein (VSVG) (all packaging plasmids gifts from Carlos Lois, MIT) as described in (Lois et al., 2002). Adeno-associated viral vectors were packaged by the MGH Viral Vector Core Facility, Charlestown, MA. Constructs were cloned into either FUGW for lentiviral production or 1114.5 AAV-CMV/Hsyn backbone for AAV production.

A.4.3 Construct design and subcloning

Pre-designed siRNA sequences (Ambion/Applied Biosystems, Austin, TX) against six regions of *Grin1* were ordered as oligos (Integrated DNA Technologies, Coralville, IA). PCR expression cassettes of each siRNA downstream of a U6 and H1 promoter element were generated using the Silencer Select (Ambion/Applied Biosystems, Austin, TX) for comparison of efficiency with both promoters.

A conditional shRNA construct against *lacZ*, a gift from Reinhard Kuhn (Hitz et al., 2007), was modified to incorporate a rous sarcoma virus (RSV) promoter and EYFP fluorophore in place of the original neomycin spacer sequence. This shRNA-fluorophore cassette was cloned into the FUGW and 1114.5 backbones and packaged as lentiviral and AAV vectors, respectively.

A.4.4 Surgery

All surgical procedures were performed under aseptic conditions. To induce anesthesia, adult mice (>25g) were anesthetized by IP injection of 0.5-0.7 cc avertin (20mg/ml solution, prepared from tert-amyl alcohol and 2-2-2 Tribromoethanol, Sigma). Buprenorphine was given as a subcutaneous injection prior to surgery at 0.05 mg/kg. A 100nl to 1ml volume of viral solution was injected into the ventral midbrain 2.6mm caudal to bregma, 0.5mm lateral to the midline and 4.6mm ventral. The opening of the brain were closed with non-toxic dental adhesive (Vetbond, Henry Schein) and sutures. To prevent skin infection, a neomycin solution was applied and animals were placed singly in a cage with infrared illumination to prevent hypothermia. Animals were housed alone for one week, and provided with food and water ad-libitum. Animals were monitored daily for 3 days post-operative, and weekly thereafter. At the end of the 14 day-3 month experiment period, brain tissue was used in post-hoc histology experiments. For histology experiments, animals were anesthesized with an overdose of avertin (a triple dose of that used for surgery), and perfused intracardially with paraformaldehyde.

A.4.5 Histology

Mice were transcardially perfused with 4% paraformaldehyde (PFA) in 0.1 M sodium phosphate buffer (PB). For X-Gal staining the brains were then removed and post-fixed for 2 hours in 4% PFA at 4°C. Coronal sections (50 μm thick) were cut on a Vibratome and collected in PB. Sections were first incubated in 0.1 M PB containing 0.01% SDS, 0.02% NP-40, 2 mM $MgCl_2$ at 4°C for15 minutes, followed by the β-galactosidase reaction in 1xPBS pH 8.0 containing 0.5 mg/ml Xgal, 5 mM $K_4Fe(CN)_6 \bullet 3H_2O$, 5 mM $K_3Fe(CN)_6$, 2 mM $MgCl_2$ at 37°C for 6 hours. Sections were counterstained with Nuclear Fast Red.

A.4.6 Immunohistochemistry

For triple immunofluorescent staining, brains were post-fixed in 4% paraformaldehyde overnight, and 50 μm Vibratome sections were prepared. Sections were then incubated in 50% EtOH in PBS, rinsed and incubated with 10% normal goat serum at room temperature for 1 hour followed by incubation at 4°C overnight with gentle shaking in chicken anti-β-galactosidase antibody, 1/5000, Abcam with 3% normal goat serum. After rinsing, the sections were then incubated with a biotinylated anti-rabbit IgG (1/200; Jackson, IL) at room temperature for 1 hour, and then with Alexa555-conjugated streptavidin (1:200, Jackson Immunolabs) for 1 hour at room temperature. After rinsing, sections were again incubated with 10% normal goat serum at room temperature for 1 hour followed by incubation at 4°C overnight with gentle shaking in rabbit anti-GFP (1:1000, Abcam) and anti-tyrosine hydroxylase monoclonal antibody (1:1000, Chemicon/Millipore) with 3% normal goat serum. After rinsing, the sections were incubated in Alexa488-conjugated anti-chicken IgG and Alexa633-conjugated anti-mouse IgG (1:400, Molecular Probes) at room temperature for 1 hour. Fluorescent images were captured.

A.4.7 TUNEL Staining

For quadruple staining with terminal deoxynucleotidyl transferase-mediated dUTP-biotin in situ nick labeling (TUNEL) stain as well as GFP, beta-galactosidase and tyrosine hydroxylase immunohistochemisty, brains were post-fixed in 4% paraformaldehyde overnight, and 50 μm Vibratome sections were prepared. Sections were then incubated for two minutes in 0.1% TritonX100 and 0.1% sodium citrate, rinsed and incubated for 1 hour at 37°C with TUNEL labeling solution (In Situ Cell Death Detection, Roche Applied Sciences). Positive controls were generated using DNAse (Promega) at three concentrations, 0.1, 0.06 and 0.004 U/μml. TUNEL staining was following by immunofluorescent staining for GFP and TH. Sections were incubated in 10% normal goat serum in PBS for 1 hour at room temperature. Sections were then incubated overnight at 4°C in a solution according to the concentrations listed previ-

ously of primary antibodies against rabbit anti-GFP, chicken anti-beta-galactosidase and mouse anti-tyrosine hydroxylase. After rinsing, sections were incubated for 1 hour at room temperature in Alexa350-conjugated anti-mouse IgG, Alexa633-conjugated anti-chicken IgG and Alexa488-conjugated anti-rabbit IgG. Fluorescent images were captured.

Bibliography

Cagniard, B., J. A. Beeler, J. P. Britt, D. S. McGehee, M. Marinelli, and X. Zhuang (2006). Dopamine scales performance in the absence of new learning. *Neuron 51*(5), 541–7.

Cullen, B. R. (2006). Enhancing and confirming the specificity of rnai experiments. *Nat Methods 3*(9), 677–81.

Hitz, C., W. Wurst, and R. Kuhn (2007). Conditional brain-specific knockdown of mapk using cre/loxp regulated rna interference. *Nucleic Acids Res 35*(12), e90.

Lois, C., E. J. Hong, S. Pease, E. J. Brown, and D. Baltimore (2002). Germline transmission and tissue-specific expression of transgenes delivered by lentiviral vectors. *Science 295*(5556), 868–72.

Soriano, P. (1999). Generalized lacz expression with the rosa26 cre reporter strain. *Nat Genet 21*(1), 70–1.

Zweifel, L. S., J. G. Parker, C. J. Lobb, A. Rainwater, V. Z. Wall, J. P. Fadok, M. Darvas, M. J. Kim, S. J. Mizumori, C. A. Paladini, P. E. Phillips, and R. D. Palmiter (2009). Disruption of nmdar-dependent burst firing by dopamine neurons provides selective assessment of phasic dopamine-dependent behavior. *Proc Natl Acad Sci U S A 106*(18), 7281–8.

Appendix B

Presynaptic Regulation of Quantal Size by the Vesicular Glutamate Transporter VGLUT1

Wilson NR, Kang J, Hueske EV, Leung T, Varoqui H, Murnick JG, Erickson JD, Liu G. (2005). ***Journal of Neuroscience. 25(26)*****, 6221-34.**

Cellular/Molecular

Presynaptic Regulation of Quantal Size by the Vesicular Glutamate Transporter VGLUT1

Nathan R. Wilson,[1] Jiansheng Kang,[1] Emily V. Hueske,[1] Tony Leung,[1] Helene Varoqui,[2] Jonathan G. Murnick,[1] Jeffrey D. Erickson,[2] and Guosong Liu[1]

[1]Department of Brain and Cognitive Sciences, Picower Center for Learning and Memory, and The Institute of Physical and Chemical Research (RIKEN)–Massachusetts Institute of Technology Neuroscience Center, Massachusetts Institute of Technology, Cambridge, Massachusetts 02139-4307, and [2]Neuroscience Center, Louisiana State University Health Sciences Center, New Orleans, Louisiana 70112

A fundamental question in synaptic physiology is whether the unitary strength of a synapse can be regulated by presynaptic characteristics and, if so, what those characteristics might be. Here, we characterize a newly proposed mechanism for altering the strength of glutamatergic synapses based on the recently identified vesicular glutamate transporter VGLUT1. We provide direct evidence that filling in isolated synaptic vesicles is subject to a dynamic equilibrium that is determined by both the concentration of available glutamate and the number of vesicular transporters participating in loading. We observe that changing the number of vesicular transporters expressed at hippocampal excitatory synapses results in enhanced evoked and miniature responses and verify biophysically that these changes correspond to an increase in the amount of glutamate released per vesicle into the synaptic cleft. In addition, we find that this modulation of synaptic strength by vesicular transporter expression is endogenously regulated, both across development to coincide with a maturational increase in vesicle cycling and quantal amplitude and by excitatory and inhibitory receptor activation in mature neurons to provide an activity-dependent scaling of quantal size via a presynaptic mechanism. Together, these findings underscore that vesicular transporter expression is used endogenously to directly regulate the extent of glutamate release, providing a concise presynaptic mechanism for controlling the quantal efficacy of excitatory transmission during synaptic refinement and plasticity.

Key words: VGLUT1; glutamate release; quantal size; homeostatic; excitatory; vesicular transporter

Introduction

A continuing goal of synaptic physiology is to uncover the features of synaptic structure that most dramatically influence synaptic strength. In excitatory glutamatergic synapses, remarkable progress has been made in detailing the postsynaptic factors that regulate synaptic efficacy (Malenka and Nicoll, 1999; Sheng and Kim, 2002). However, comparatively less has been done to identify corresponding presynaptic mechanisms that influence postsynaptic activation by governing the amount of transmitter released (Atwood and Karunanithi, 2002; Liu, 2003). Nevertheless, recent studies of central synapses have demonstrated that normal transmitter release can be insufficient to fully activate postsynaptic receptors (Bekkers et al., 1990; Liu and Tsien, 1995; Silver et al., 1996; Forti et al., 1997; Liu et al., 1999; Mainen et al., 1999; McAllister and Stevens, 2000), and variability in excitatory quantal size is increasingly considered to be significantly attributable to presynaptic fluctuations in transmitter release (Liu et al., 1999; Hanse and Gustafsson, 2001; Franks et al., 2003). Therefore, it is worthwhile to consider what presynaptic molecular mechanisms might influence the amount of glutamate released into the synaptic cleft and whether such mechanisms might be endogenously controlled to provide additional modes of synaptic regulation.

Recent work has demonstrated that artificial perturbations can alter excitatory transmission by modulating the amount of glutamate released from synaptic vesicles. In particular, either disrupting electrochemical proton gradients that drive the loading of transmitter into vesicles before release (Zhou et al., 2000) or making additional glutamate available for loading (Ishikawa et al., 2002; Yamashita et al., 2003) are both effective at changing the degree of postsynaptic activation during transmission.

We hypothesize that postsynaptic activation is similarly controlled by endogenous presynaptic mechanisms via the expression of the vesicular glutamate transport protein (VGLUT1), which is now known to underlie the transport of glutamate into excitatory vesicles (Bellocchio et al., 2000; Takamori et al., 2000). Functional work has recently demonstrated that perturbations to VGLUT1 expression can influence the strength of excitatory transmission, with knocking out VGLUT1 in particular leading to a profound reduction in excitatory signaling (Fremeau et al., 2004; Wojcik et al., 2004). VGLUT1 thus seems well poised as a control point for regulating synaptic transmission, although its precise mode of action in synaptic transmission remains unchar-

Received July 22, 2004; revised May 10, 2005; accepted May 12, 2005.

This work was supported by The Institute of Physical and Chemical Research (RIKEN)–Massachusetts Institute of Technology Neuroscience Center Grant MH58880 to G.L. and by National Institutes of Health Grants NS37342 (G.L.), 1P29RR16816 (H.V.), and NS36936 (J.D.E.). N.R.W. was supported by a predoctoral fellowship from the National Science Foundation. We thank Dr. Bing Li for culture assistance, Dr. Yasunori Hayashi for insightful discussions, and Dr. Morgan Sheng for helpful suggestions.

Correspondence should be addressed to Dr. Guosong Liu, Picower Center for Learning and Memory, E18-218, Massachusetts Institute of Technology, Cambridge, MA 02139-4307. E-mail: liu@mit.edu.

DOI:10.1523/JNEUROSCI.3003-04.2005

 0270-6474/05/256221-14$15.00/0

acterized, and its propensity for meaningful regulation is unreported. Indeed, although properties of cholinergic (Song et al., 1997) and aminergic (Pothos et al., 2000) vesicular transporters have now been examined as well, whether the expression of any vesicular transporter can be controlled endogenously to facilitate activity-dependent plasticity has not been explored.

The present work thus aims to more fully characterize the manner by which VGLUT1 expression is able to influence synaptic function and to elucidate whether neurons actually make use of this machinery endogenously, to presynaptically modulate the function of excitatory signaling. The characterizations of VGLUT1 described below, along with the specific expression of VGLUT1 in brain areas associated with adult plasticity (Fremeau et al., 2001; Liu, 2003), suggest an intriguing role for the regulation of vesicular transport in facilitating the functional dynamic range of glutamatergic synapses.

Materials and Methods

Synaptic vesicle purification and uptake. Synaptic vesicles were purified from 30 g of adult rat cerebral cortex (including hippocampus), using the procedure of Hell et al. (1988), and stored at −80°C until use. Vesicles were thawed on ice and diluted in sucrose buffer (320 mM sucrose, 10 mM HEPES, pH 7.4) to a protein concentration of 250 μg/ml (Pierce Bradford assay using BSA as a standard; Pierce, Rockford, IL). Aliquots (100 μl) were mixed with 50 μl of KCl solution (8 mM) in uptake buffer (110 mM potassium tartrate, 20 mM HEPES, 2 mM $MgSO_4$, pH 7.4) and preincubated for 5 min at 37°C in the presence or absence of the specific inhibitors Rose Bengal (RB) or trypan blue (TB). Uptake was initiated by the addition of 50 μl of uptake buffer containing 20 mM Na2-ATP, 0.9 μM ^{3}H-glutamate (51 Ci/mmol; NEN, Boston, MA), and various concentrations of unlabeled glutamate and allowed to proceed at 37°C for 0.5–15 min. To terminate the uptake, tubes were placed in an ice/water slurry, and the vesicle suspensions were filtered under vacuum through GF/F filters prewetted with uptake buffer and washed with 8 ml of ice-cold uptake buffer. The radioactivity bound to the filter was solubilized in 1 ml of 1% SDS before adding 5 ml of EcoScint scintillation fluid.

VGLUT1 overexpression and functional analysis. Sequences encoding VGLUT1 (GenBank accession number U07609) (Ni et al., 1994) were cloned (Varoqui et al., 2002) and amplified using a 5′ primer containing an *Eco*RI site (ggaattccaccatggagttccggcaggaggagtttcgg) and a 3′ primer containing an *Sal*I site to remove the stop codon (actggtcgaccagtagtcccggacaggggggtggggg). After digestion with *Eco*RI and *Sal*I, the PCR product was subcloned in frame into pEGFP-N1 to produce a transporter tagged on its C terminus with enhanced green fluorescent protein (EGFP). The cDNA fusion insert was subcloned into pCDNA3.1 using *Eco*RI and *Not*I for transient heterologous expression using the vaccinia T7 hybrid system in PC12 cells as described previously (Varoqui et al., 2002). A light population of membranes containing synaptic-like microvesicles was isolated from VGLUT-expressing PC12 cells and from mock-transfected cells as described previously (Varoqui et al., 2002). Western blot analysis was then also performed as described previously (Varoqui et al., 2002). VGLUT1 transport activity was assessed by measuring ^{3}H-glutamate uptake under optimal conditions (Mg^{2+}-ATP, 5 mM; chloride ion, 4 mM) for 5 min at 32°C in the presence and absence of the H^+-uncoupler carbonyl cyanide m-chlorophenylhydrazone (CCCP; 50 μM) as in previous studies (Schafer et al., 2002; Varoqui et al., 2002).

Cultured hippocampal neurons and transfection. Hippocampi were dissected from postnatal day 1 Sprague Dawley rat pups and cultured as described previously (Liu et al., 1999). A pCDNA3.1-VGLUT1 construct (Varoqui et al., 2002) was used to transfect cells at 6–11 d *in vitro* (DIV) using the calcium phosphate method, with neurons transfected at least 2 d before observation. VGLUT-enhanced neurons were compared with control neurons from the same batches of culture, with evoked recordings age-matched from 9–11 DIV, miniature recordings measured at 10 DIV, glutamate release experiments performed at 14–16 DIV, and activity-dependence experiments at 16 DIV after 2 d of drug treatment. All experiments involving animals were approved by the Massachusetts Institute of Technology Committee on Animal Care.

Imaging and immunohistochemistry. All imaging was performed using an Olympus Fluoview confocal microscope (Olympus, Melville, NY) with a 40× planapochromatic water immersion lens (1.15 numerical aperture). Cell cultures were fixed with 4% paraformaldehyde and 4% sucrose in 1× PBS, and permeabilized with 0.5% Triton X-100 for 30 min at 22–24°C. Primary antibodies against VGLUT1 (Chemicon, Temecula, CA), synaptotagmin (American Qualex, San Clemente, CA), or synapsin I (Chemicon) were applied, followed by rinses in PBS and visualization with Alexa 488-, 546-, or 633-conjugated secondary antibodies (1/400; Molecular Probes, Eugene, OR). AM1-43 (Biotium, Richmond, CA) is a form of the styryl dye FM1-43 commonly used to visualize vesicle fusion activity (Renger et al., 2001), but with an additional aldehyde-reactive amino group at the hydrophilic end, rendering it less sensitive to fixation. Coverslips containing cultured neurons were bathed for 120 s at 22–24°C in high-K^+ solution (plus 8 μM AM1-43) and placed into Tyrode's solution [see above; plus 1 μM tetrodotoxin (TTX)] for 15 min. They were then transferred for quenching to the sulfonated b-cyclodextrin derivative ADVASEP-7 (125 μM; Biotium) for 4 min at 22–24°C. Cells were fixed immediately after staining in FSB (see above) and 0.02% glutaraldehyde for 60 min, rinsed in 1× PBS, and blocked with 0.4% saponin and 5% serum in 1× PBS. First and secondary antibodies were then applied as above. All images were collected at 1280 × 1024 pixel resolution and 4× software zoom, using a z series projection of 8–11 images taken at 0.8 μm depth intervals. An average image contained ~250 synapses.

Whole-cell recording. Whole-cell patch-clamp recordings were performed as described previously (Renger et al., 2001). Patch pipettes (3–6 MΩ) contained the following (in mM): 120 potassium gluconate, 3 KCl, 10 HEPES, 8 NaCl, 0.5 $CaCl_2$, 5 EGTA, 2 Mg^{2+}-ATP, and 0.3 GTP, pH was adjusted to 7.3 with NaOH. Perforated-patch pipettes were front-filled with a solution containing the following (in mM): 130 potassium gluconate, 4 KCl, 10 HEPES, 8 NaCl, 0.4 EGTA, pH was adjusted to 7.2 with KOH and then back-filled with the same solution containing 150 ng/ml amphotericin B (Sigma, St. Louis, MO). Extracellular solution was based on Tyrode's solution containing the following (in mM): 145 NaCl, 3 KCl, 15 glucose, 10 HEPES, 1.3–2.6 $MgCl_2$, and 1.3–2.6 $CaCl_2$ and 50 μM picrotoxin (Sigma), pH adjusted to 7.4 with NaOH. Signals were recorded under voltage clamp (−60 mV) using a MultiClamp 700A amplifier (Molecular Devices, Foster City, CA), digitized at 10 kHz, filtered at 1 kHz, and recorded using in-house software. 1,2,3,4-Tetrahydro-6-nitro-2,3-dioxo-benzo [f] quinoxaline-7-sulfonamide (NBQX; 5 μM; Sigma) was used to verify AMPA currents. TTX (1 μM; Biotium) was added for miniature EPSC (mEPSC) recordings.

Dual-cell evoked recordings. For dual cell-evoked EPSCs, a second whole-cell patch or perforated patch was achieved, and action potentials were stimulated by injecting 100–300 pA of current over 10 ms (current clamp) (see Fig. 5, or 30–80 mV over 0.5 ms (voltage clamp) (see Fig. 8). For glutamate antagonist experiments, 600 μM γ-D-glutamylglycine (γ-DGG) (Tocris Cookson, Ellisville, MO) was bath applied. For tuning of synaptic failure rates, varying concentrations of calcium (0.6–1.3 mM) and magnesium (2.6–3.4 mM) were bath applied for each connection until the apparent probability of release was low (0.4–0.1). Data was then collected after a stable baseline at a consistent failure rate was established.

Estimation of the potential for multivesicular release. The potential for multivesicular release (MVR) in our measurements was determined while assuming, first, ~10 release sites per bouton (Schikorski and Stevens, 1997) and, second, independent release between vesicles. Binomial statistics were used in which the number of vesicles undergoing fusing (N) relates to the probability that a given vesicle will fuse (p) and the number of vesicles able to fuse per bouton (N_{max}). We determined the probability of event failure as the likelihood that zero vesicles could undergo fusion: $P_{N=0} = (1 - P)^{N\max}$, using observed failure rates to estimate p. The probability of exactly one vesicle fusing, in turn, would be: $P_{N=1} = N_{max}(1 - P)^{N\max - 1}p$. As such, the probability of multivesicular release would be the likelihood per action potential that there is neither a failure nor a single release but rather that several vesicles release: $P_{N\geq 2} = 1 - P_{N=1} - P_{N=0}$, or $1 - N_{max}(1 - p)^{N\max-1}p(1 - p)^{N\max}$.

Chronic drug treatments of cultures. In treatments to chronically shift activity levels, cultures were treated continuously beginning at 14 DIV and observed at 16–17 DIV. NBQX (5 μM; Sigma), DL-2-Amino-5-phosphonopentanoic acid (AP-5; 50 μM; Tocris Cookson), or bicuculline methobromide (20 μM; Sigma) were used to block AMPA, NMDA, and $GABA_A$ receptors.

Data analysis. Analysis of electrophysiological data was performed in MiniAnalysis (Synaptosoft, Leonia, NJ) for mEPSCs, and custom scripts were written in C++ and MatLab (MathWorks, Natick, MA) for EPSCs evoked presynaptically and iontophoretically. EPSC failure rates were estimated using a threshold of ~4 pA. Such a threshold was also invoked for determining mean amplitude before γ-DGG attenuation, and an equal proportion of events was then compared after drug application to determine mean attenuation (consistent probability of release was assumed). Traces for which access resistance varied substantially or were >25 MΩ were rejected from analysis. Image analysis was performed via custom scripts written in ImagePro Plus (Media Cybernetics, Carlsbad, CA) for puncta localization and quantification. Pixels within each punctum were assigned intensity values, and the combined sum of the intensity values of a punctum, or integrated optical density (IOD), was taken as the total intensity of the punctum. VGLUT1 total intensity was measured against that of synapsin I or synaptotagmin in the same punctum. All comparisons involving multiple conditions were quantified first using ANOVA, followed by unpaired *t* tests between adjacent groups as reported, and all error bars report SEM unless otherwise noted.

Results

Loading in excitatory synaptic vesicles depends on glutamate concentration and number of available transporters

To characterize the nature by which VGLUT1 expression might impact synaptic transmission, it was first important to demonstrate that varying the parameters of glutamate transport could actually modulate the extent of vesicle filling. A possible scenario is that although different transport conditions might influence the speed of filling, vesicles eventually fill to a "set point" that is dictated by some parameter independent of transport, such as vesicle size. In contrast, if the amount of glutamate loaded into vesicles was to be specified by a dynamic equilibrium process that could be stoichiometrically influenced by the components of the loading reaction, it would allow for the modulation of vesicle filling and the consequent release of glutamate by endogenous characteristics such as transporter expression.

Previous work has assayed the loading of glutamate into PC12 cells (Bellocchio et al., 2000), the BON line of human endocrine cells (Takamori et al., 2000), and even purified synaptic vesicles at specific external glutamate concentrations (Maycox et al., 1988; Wolosker et al., 1996). However, given a recent set of insightful studies that has begun to elucidate the previously unknown range of the cytosolic glutamate concentration (Ishikawa et al., 2002; Yamashita et al., 2003), we were interested in systematically measuring the glutamate uptake equilibrium around variants of this physiological range of conditions as well as assessing the influence of transporter number in defining this equilibrium.

We therefore quantified the time course and final equilibrium of glutamate transport under different conditions using VGLUT1 synaptic vesicles isolated from rat cerebral cortex and hippocampus (Fig. 1). Observing the uptake of the vesicles of 50 μM ^{3}H-glutamate (Fig. 1*A*) revealed that vesicular transport in our system reached an equilibrium balance between transmitter influx and efflux along a similar time course to that reported previously (Maycox et al., 1988; Wolosker et al., 1996). To examine whether the number of transporters participating in loading could influence its final equilibrium, we also compared our equilibrium uptake to that occurring in the presence of Rose Bengal, an antagonist of VGLUT1 loading that is believed to interact allosterically with the transporter (Ogita et al., 2001). Because the drug is thought to noncompetitively disrupt glutamate transport at the site of loading, it offered a pharmacological means for reducing the effective number of transporters participating in uptake to examine whether the size of the available transporter pool can help determine the final amount of vesicle filling. Loading in the presence of Rose Bengal indeed exhibited a reduced equilibrium of filling (Fig. 1*A*), a property that was also observed under treatment with trypan blue, the most potent known competitive antagonist of vesicular glutamate transport (Roseth et al., 1998). Both drugs were applied at approximate IC_{50} concentrations, whereby 2 μM at either 5 or 10 min preincubation achieved complete inhibition of loading (data not shown).

By repeating these treatments under a more physiological concentration of extravesicular glutamate (1 mM) (Fig. 1*B*), we were next able to observe whether transporter activity can also

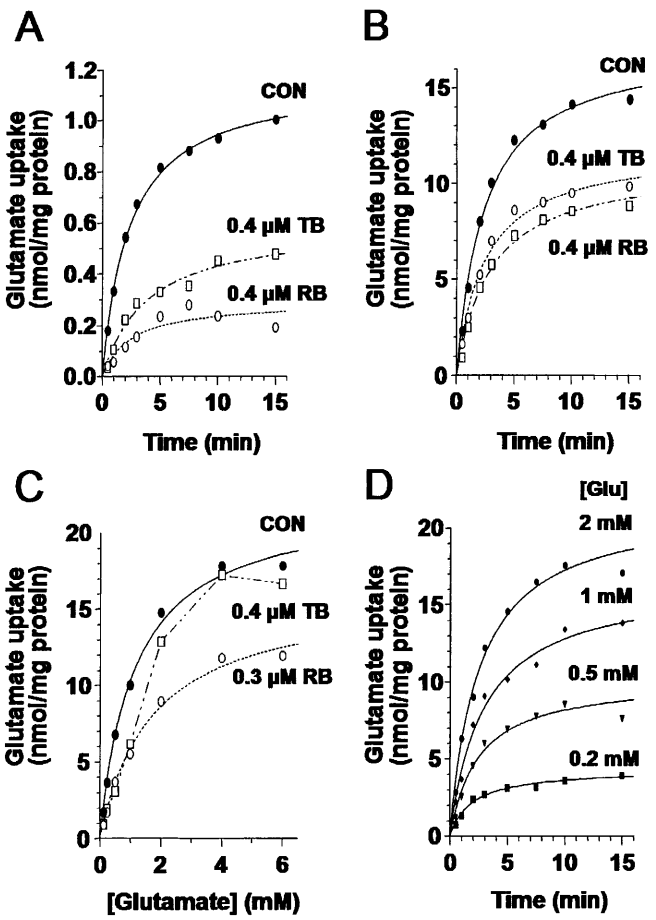

Figure 1. VGLUT1 loading in synaptic vesicles depends on glutamate concentration and the number of available transporters. ***A***, Uptake time course of 50 μM ^{3}H-glutamate by purified synaptic vesicles (●) reaches equilibrium in ~10 min. CON, Control. Uptake in the presence of either the competitive VGLUT1 inhibitor trypan blue (□) or the noncompetitive VGLUT1 inhibitor Rose Bengal (○) both fill along a similar time course but to smaller equilibrium amounts. ***B***, Uptake time course for 1 mM ^{3}H-glutamate by synaptic vesicles (●) occurs along a similar time course as in ***A*** but to a dramatically increased final equilibrium amount. Equilibrium is again reduced in the presence of either trypan blue (□) or Rose Bengal (○). ***C***, Saturation isotherm of ^{3}H-glutamate (0.06 – 6 mM) accumulation at 10 min in the presence and absence of Rose Bengal (○) or trypan blue (□). In the presence of >1 mM glutamate, the competitive trypan blue inhibition is lost while the noncompetitive Rose Bengal inhibition is maintained. ***D***, Time courses of ^{3}H-glutamate (Glu) uptake at four subsaturating concentrations of glutamate show that steady-state vesicular glutamate levels depend on the concentration of glutamate present in the medium.

influence vesicle filling at a glutamate concentration closer to what has endogenously been estimated in functional studies (Ishikawa et al., 2002). At this higher concentration of glutamate, the vesicles now filled to a higher steady-state concentration, indicating that the final extent of VGLUT1 filling depends directly on the concentration of glutamate around the vesicle and does not have an independent set point. Equilibrium filling was again reduced by the presence of either RB or TB (Fig. 1*B*), demonstrating that, also at this higher concentration, the equilibrium can be shifted by reducing the number of active transporters contributing to the loading process.

Varying the external glutamate concentration along a continuum while measuring 10 min equilibrium uptake levels (Fig. 1*C*) reveals that maximal uptake increases linearly up to 1 mM exogenous glutamate and begins to saturate at ~4–6 mM. Even at these concentrations, the extent of transporter availability is critical in determining the equilibrium value, because RB attenuates the final concentration reached for all values of external glutamate in a similar manner to TB, although competitive antagonism of TB is eventually overwhelmed as glutamate concentration is increased. Together, the results lead us to conclude that VGLUT1 vesicles are subject to a flexible degree of filling that can be influenced by both the concentration of glutamate outside of the vesicle as well as the effective number of available transporters. Aligning the time courses of loading observed under various glutamate concentrations (Fig. 1*D*) demonstrates that both the magnitude and, to a lesser degree, the rate of uptake are influenced by alterations in transport conditions.

We thus observe three properties of glutamate uptake into synaptic vesicles at physiological terminal glutamate concentrations. First, additional increases to external glutamate concentrations can enhance the amount of transmitter loaded, as predicted by the aforementioned functional work (Ishikawa et al., 2002; Yamashita et al., 2003). Second, the number of transporters available for loading can influence the final loading equilibrium, even at glutamate concentrations above the physiological range. Third, vesicle filling is a slow process, requiring minutes to reach completion, which could indicate an importance of changes to the vesicle loading rate, in addition to the loading amount, in determining physiological synaptic transmission.

Transporter overexpression in PC12 cells and hippocampal synapses

If VGLUT1 vesicles do not merely accumulate transmitter until full but rather have their speed and amount of filling determined by an equilibrium process that is subject to the available concentration of transmitter and transporter, we were interested in examining whether this equilibrium could also be shifted in a more physiological context. Therefore, we next attempted to vary the amount of vesicular transporters expressed in the synaptic terminals of neurons to examine the resulting consequences for glutamate release in endogenous synaptic transmission.

To characterize the functional relationship between VGLUT1 expression and excitatory synaptic transmission, we attempted to overexpress the transporter at hippocampal synaptic terminals. We created two expression constructs for delivery into neurons: one for wild-type VGLUT1 (WT) and another tagging VGLUT1 with the reporter GFP at its C terminus. To verify the effectiveness of our constructs in enhancing VGLUT1 expression, PC12 cells were transiently transfected as described previously for VGLUT2 (Varoqui et al., 2002) and the recently identified VGLUT3 (Schafer et al., 2002). A Western blot analysis (Fig. 2*A*) using a guinea pig antibody specific for VGLUT1 (Schafer et al., 2002) reveals that although mock-transfected cells (M) did not express detectable levels of VGLUT1, single immunoreactive bands of appropriate size were observed for PC12 cells transfected with either the wild-type VGLUT1 or the VGLUT-GFP fusion (+GFP) constructs. The fusion protein had an ~26 kb higher molecular weight than wild-type VGLUT1 because of the additional mass of the fused EGFP. To check the functionality of these newly synthesized proteins, we observed whether transfection of our constructs into PC12 cells gave rise to glutamate transport by assaying for radioactive glutamate uptake in the presence of magnesium-ATP and chloride ions to activate transporter function (Fig. 2*B*). Here, both WT and GFP-tagged (+GFP) constructs demonstrated successful transport of ^{3}H-glutamate into a light population of membranes, a function that was found to be inhibited by the proton uncoupler CCCP. CCCP-sensitive uptake in this and similar preparations of vesicles is considered a valid indicator of the H^+-dependent uptake of glutamate (Takamori et al., 2000, 2002). Although notable levels of uptake were not observed in mock-transfected cells (Mock), uptake capacity for both constructs was found to be comparable with those reported previously for VGLUT1 (Bellocchio et al., 2000; Takamori et al., 2000) as well as for VGLUT2 and VGLUT3 (Schafer et al., 2002; Varoqui et al., 2002). We therefore concluded that our constructs were effective for increasing VGLUT1 protein levels and enhancing glutamate transport.

We next examined whether VGLUT1 protein levels could be enhanced at the synaptic terminals of hippocampal neurons. This requires not only an increase in the production of VGLUT1 protein in transfected neurons but also that the VGLUT1 generated from our constructs contain the correct targeting sequence to be transferred to synaptic terminals effectively. We examined VGLUT1 targeting by transfecting neurons with the VGLUT1-GFP fusion construct and visualizing protein localization. Here, confocal imaging of the fluorescent-tagged protein (Fig. 2*C*, top) showed that new protein was successfully targeted to the synaptic terminals, where it accumulated in discrete puncta colocalized with the presynaptic bouton label FM4–64 and was not observable in dendrites. In contrast, when GFP was cotransfected separately from VGLUT1 to fully label neurons overexpressing the protein for later experiments (Fig. 2*C*, bottom), the GFP diffused evenly throughout the cell, with no specific targeting to synaptic terminals. We therefore conclude that overexpressed VGLUT1 can be targeted to hippocampal synapses.

Although the fusion construct proved useful for establishing the targeting of overexpressed protein to synaptic terminals, we chose to use wild-type VGLUT1 for the subsequent functional characterizations to avoid any modification of VGLUT1 structure that could perturb insertion at the vesicular membrane or disrupt potential endogenous regulation at the terminal. It was then necessary to verify that our VGLUT1/GFP cotransfection also succeeded in increasing total VGLUT1 protein levels at the synaptic terminal. Figure 2*D* shows immunolabeled VGLUT1 occurring within synaptic terminals marked with synapsin I along axons cotransfected with GFP and VGLUT1 (top images) or transfected with GFP alone (bottom images). We found that VGLUT1 puncta appeared more intense in synapses occurring on the GFP-labeled transfected axon than in neighboring puncta occurring off the GFP axon (top images). As an additional control demonstrating that GFP transfection alone did not enhance VGLUT1 levels per synaptic terminal, the above comparison was repeated with GFP axons lacking VGLUT1 cotransfection, again versus neighboring GFP-negative terminals (Fig. 2*D*, bottom images). In this case, there did not appear to be an appreciable

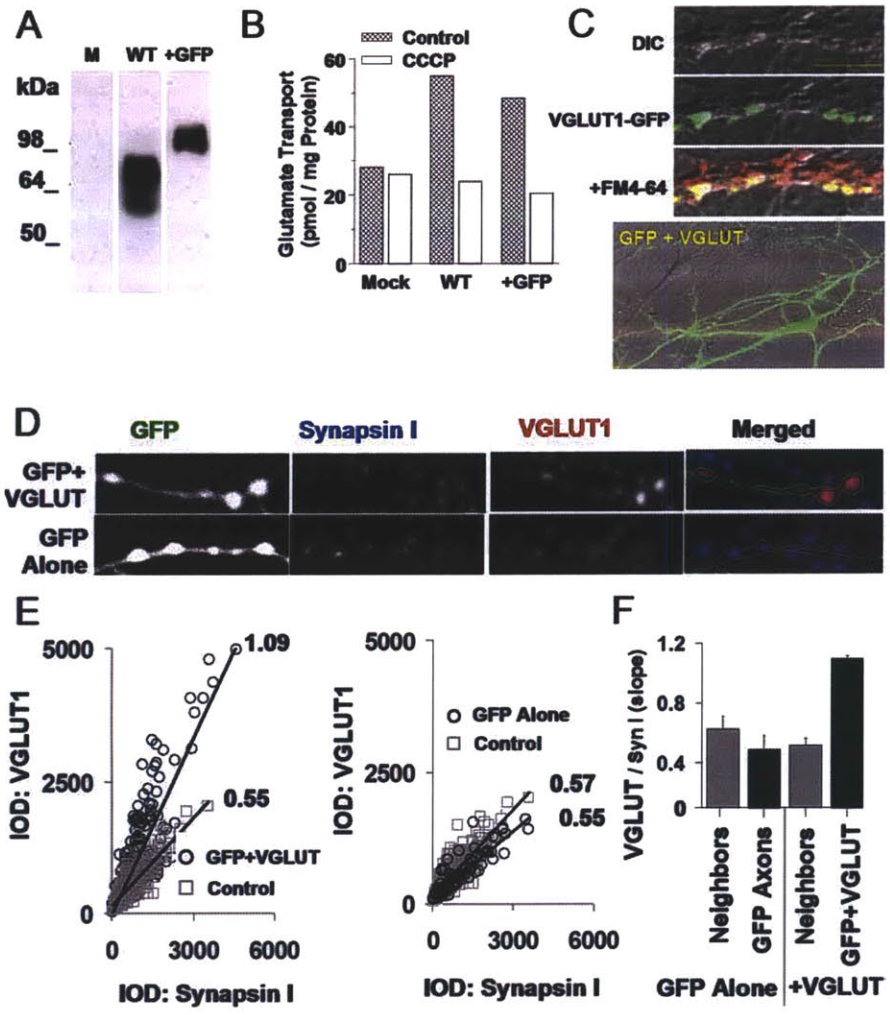

Figure 2. Overexpression of VGLUT1 in PC12 cells and hippocampal synapses. ***A***, Expression of both wild-type VGLUT1 (WT) and GFP-tagged VGLUT1 (+GFP) constructs in PC12 cells reveals single immunoreactive bands of appropriate size for wild-type and EGFP-tagged proteins as visualized by Western blot analysis. Mock-transfected cells (M) did not contain immunoreactivity. ***B***, Both constructs succeeded in facilitating CCCP-sensitive glutamate loading into PC12 cells, whereas mock transfection (Mock) did not. ***C***, Top, Overexpressed VGLUT1-GFP fusion protein localized to synaptic terminals (top) as shown by colocalization of the fusion protein (green) with FM4–64 (red). Scale bar, 10 μm. Bottom, Wild-type VGLUT1 cotransfected with GFP clearly labels the morphology of transfected neurons. DIC, Differential interference contrast. ***D***, Double-immunostaining for synapsin I and VGLUT1 along GFP-labeled hippocampal axons. VGLUT1 intensity was higher in axons expressing GFP plus VGLUT (top images) than in axons expressing GFP alone (bottom images). ***E***, Ratio of VGLUT1 IOD to synapsin I IOD at individual synapses. Ratios were higher along axons transfected with GFP plus VGLUT (left; 278 transfected synapses, 576 control synapses) than axons transfected with GFP alone or adjacent nontransfected synapses from the same area (right; 92 transfected synapses, 422 control synapses). ***F***, Summary data across multiple coverslips (total, $n = 8$) for data in ***E***. GFP plus VGLUT1 cotransfection results in augmented VGLUT1 protein levels per synapse.

difference in the size or intensities of VGLUT1 puncta occurring on or off the GFP-labeled axon.

The absolute amount of VGLUT1 per synapse is determined by both the number of synaptic vesicles and the average amount of VGLUT1 protein per vesicle. It was important to discern whether any increase in VGLUT1 levels that we observed was indeed attributable to a specific change in the concentration of VGLUT1 across the synapse and not just a general increase in the size or density of the vesicle pool. Because synapsin I intensity provides a measure of the concentration of a second protein associated with vesicles, we used the ratio of VGLUT1 to synapsin I to determine the available amount of transporter protein independently of fluctuations in the number of vesicles or the synaptic area. Figure 2*E* demonstrates a quantification of this measure, which utilizes the IOD of VGLUT1 and synapsin I to compare the expression levels of the two proteins. Synapses from axons transfected with both GFP and VGLUT1 show a nearly twofold increase in the VGLUT1/synapsin I IOD ratio compared with neighboring synaptic terminals (Fig. 2*E*, GFP+VGLUT, left plot). GFP alone axons, in contrast, did not show noticeably larger VGLUT1/synapsin I IOD ratios than in neighboring terminals (Fig. 2*E*, GFP Alone, right plot). Repeating this measure across multiple coverslips demonstrates a consistent increase in the targeting of VGLUT1 protein to synapses as a result of GFP plus VGLUT1 cotransfection (Fig. 2*F*), with no increase in VGLUT1 protein at neighboring synapses in the same neuronal network. We therefore conclude that our constructs were capable of effectively targeting elevated levels of VGLUT1 protein to the synaptic terminals of our hippocampal cultures.

VGLUT1 overexpression enhances AMPA receptor-mediated responses and decreases evoked failure rate

Having demonstrated a successful elevation of VGLUT1 protein levels in synaptic terminals, we examined the physiological consequences for functional synaptic transmission. Traditional electrophysiological methods record events postsynaptically, such that postsynaptic genetic manipulations have the possibility of influencing all recorded events. Presynaptic modifications, however, are more difficult to assay, because they require strict differentiation over which terminals are contributing to measured events. To solve this problem, we used dual whole-cell patch clamp, evoking an action potential in a presynaptic cell under current clamp while recording the resulting EPSCs mediated by AMPA receptors in a neighboring postsynaptic cell under voltage clamp (Fig. 3*A*, traces). Using confocal microscopy (Fig. 3*A*, image), we could distinguish presynaptic cells that were transfected with VGLUT1 by their coexpressed GFP label, as opposed to control neurons that did not express GFP. A common paradigm was to elicit transmission from a VGLUT1 neuron to a control neuron and then, as an independent control, evoke synaptic transmission under reverse configuration to compare reciprocal transmission. Figure 3*B* shows evoked synaptic transmission in a reciprocally connected pair of neurons (top), where stimulating a VGLUT-enhanced neuron evoked an EPSC that was an average of 92% larger than that evoked from the control neuron in the reverse direction (left traces). Normalizing these traces to the same peak amplitude (Fig. 3*B*, right traces) revealed a similar average time course. Visualizing the distribution of events evoked from this reciprocal pair (Fig. 3*C*) reveals a rightward shift in the VGLUT+ distribution relative to control ($p < 0.0001$; Kolmogorov–Smir-

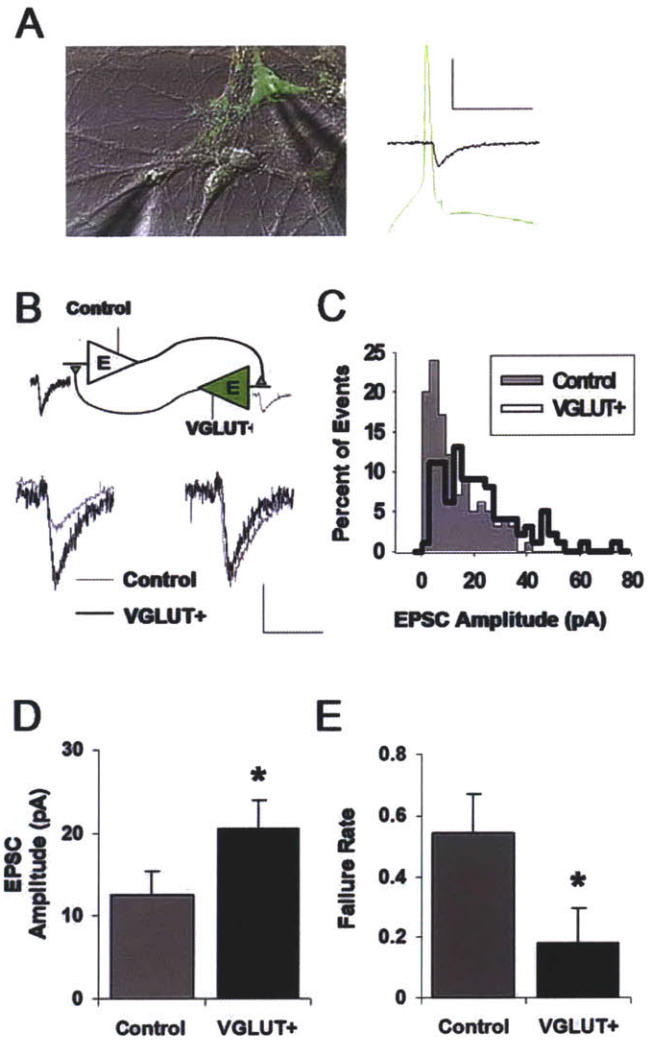

Figure 3. Enhanced excitatory synaptic transmission via VGLUT1 overexpression. ***A***, Experimental paradigm: dual whole-cell patch clamp is achieved between a VGLUT1-overexpressing VGLUT+ neuron cotransfected with GFP (green) and a nontransfected control neuron (clear). An action potential is evoked in one neuron of the pair under current clamp at 0.3 Hz, and the resulting EPSC is recorded in the other neuron under voltage clamp. Calibration: 50 pA, 50 ms. ***B***, EPSC responses evoked in a reciprocally connected pair of VGLUT+ and control neurons. Average EPSCs (left traces) contrast the responses evoked from each type of presynaptic neuron. Calibration: 10 pA, 20 ms. Normalizing these traces to the same peak amplitude (right traces) reveals a similar time course. ***C***, Distribution of EPSC amplitudes observed in the reciprocal pair shown in ***B***. Events from a VGLUT+ presynaptic neuron tend to comprise a right-shifted distribution that differs in shape from its control counterpart. ***D***, Summary data for the effect of presynaptic VGLUT1 overexpression on EPSC amplitude: mean amplitude measured across multiple pairs is significantly higher for VGLUT+ ($*p < 0.05$; unpaired *t* test; $n = 7$ control; $n = 7$ VGLUT+). ***E***, Summary data for the effect of overexpression on failure rate of evoked transmission; probability of receiving a postsynaptic response to presynaptic stimulation is increased by VGLUT1 overexpression ($*p = 0.03$; unpaired *t* test).

nov test), and, on average, control events were consistently exceeded by their VGLUT+ counterparts in EPSC amplitude (12.5 ± 2.9 vs 20.5 ± 3.4, respectively; $p < 0.05$, unpaired *t* test; $n = 7$ pairs control, 7 pairs VGLUT+) (Fig. 3*D*).

Of potential interest, VGLUT+ transmission also exhibited an unexpected decrease in the failure rate of synaptic transmission (0.54 ± 0.11 vs 0.18 ± 0.13, respectively; $p = 0.03$ unpaired *t* test) (Fig. 3*E*), suggesting that transporter overexpression leads to an increase in either of the following: (1) the number of release events that are large enough to elicit detectable AMPA receptor-mediated responses, or (2) the probability that a vesicle will be released after an action potential.

VGLUT1 overexpression enhances quantal synaptic transmission

Increases in evoked synaptic transmission after VGLUT1 overexpression could be a result of changes in the number of synaptic terminals, the probability of release per terminal, or the individual quantal size of response following each release. Therefore, we next examined whether quantal transmission is impacted by VGLUT1 overexpression by monitoring miniature synaptic transmission under bath application of tetrodotoxin to block action potentials and ensure spontaneous, single-vesicle release in control versus VGLUT1-overexpressing neurons. The difficulty in interpreting this experiment, of course, is that not all presynaptic terminals in a recorded neuron can be successfully transfected. Our strategy then was to rely first on a high-transfection rate (~25%) and, from this population, select areas of the coverslip unusually dense in transfected cells and their axons (Fig. 4*A*, bottom image). Under this condition, for a given recorded neuron, a perceptible proportion of presynaptic terminals should contain higher levels of VGLUT1. Comparing responses observed here (VGLUT+) with responses collected in a completely nontransfected coverslip (control), we attempted to assay for detectable changes in quantal transmission.

mEPSCs recorded from neurons in areas rich in VGLUT+ terminals were larger than those recorded in cells devoid of enhanced terminals. Comparing distributions from sample VGLUT+ and control neurons indicated a rightward shift of amplitudes in the VGLUT+ cultures (Fig. 4*B*) ($p < 0.001$; Kolmogorov–Smirnov test), whereas aligning sample and average traces (Fig. 4*C*) further emphasized the difference. On average, the size of mEPSCs from the neurons with VGLUT1 transfection was 31% larger than that of neurons in the control group (13.6 ± 0.6 vs 17.8 ± 2.2, respectively; $p = 0.04$ unpaired *t* test; $n = 5$ cells control, 8 cells VGLUT+) (Fig. 4*D*). In Figure 4*D*, we also compared the effects of VGLUT transfection in miniature versus evoked synaptic transmission. Control mEPSCs and EPSCs were similar in amplitude, suggesting that evoked EPSCs most likely originated from single synapses. Interestingly, although EPSCs evoked from transfected terminals were 64% larger than control, VGLUT+ mEPSCs only increased by 31%. This difference is expected from the fact that the VGLUT+ mean mEPSC amplitude was calculated from a population of events that included both VGLUT-enhanced and control terminals, and also given likely differences in detectability between evoked and spontaneous transmission (Zhou et al., 2000). Examining mEPSC frequency between the two pools of cells revealed no significant change (1.89 ± 0.54 vs 1.55 ± 0.56, respectively; $p = 0.33$; unpaired *t* test) (Fig. 4*E*). Similarly to what we observed in evoked transmission, no change was observed in the time course of control and VGLUT-enhanced spontaneous transmission (data not shown), suggesting that VGLUT1 overexpression did not induce detectable changes in postsynaptic receptor properties.

VGLUT-enhanced transmission results from increased glutamate release per vesicle

Changes in evoked and quantal transmission after VGLUT1 overexpression could be a result of either presynaptic changes in cleft glutamate concentration or postsynaptic changes in receptor number or properties. Therefore, we next investigated whether the observed enhancement to evoked and miniature excitatory transmission following VGLUT1 overexpression was a result of

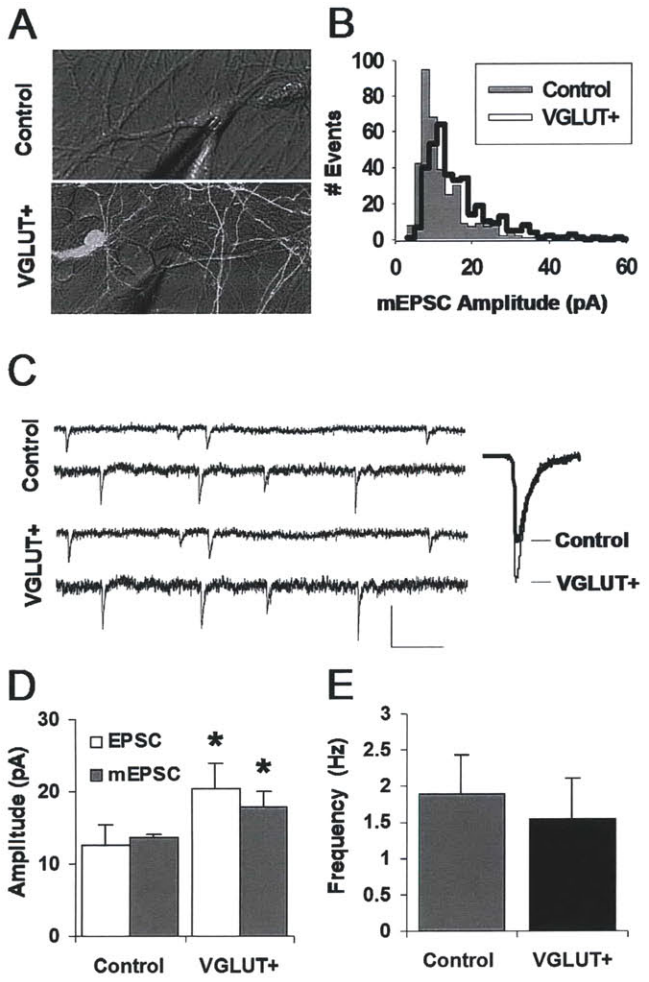

Figure 4. Effects of VGLUT1 overexpression on quantal excitatory transmission. ***A***, mEPSCs were recorded postsynaptically via a whole-cell patch clamp in the presence of TTX in either a network completely lacking VGLUT1 overexpression (Control) or from a subregion of a transfected network visually determined to be dense in overexpressing neurons (VGLUT+). ***B***, Distributions of mEPSC amplitudes observed in the neurons shown in ***A***. VGLUT+ events tend to be right-shifted relative to the control event distribution. ***C***, Sample mEPSCs from cells recorded in control and VGLUT+, which in this case are an average of 48% larger in the VGLUT+ recording. Calibration: 25 pA, 150 ms. ***D***, Average mEPSC amplitude for neurons recorded in each group shows an increase in VGLUT+ mean event amplitude (*$p = 0.04$; unpaired t test). mEPSC data are aligned with the EPSC amplitude data from Figure 3*C*. ***E***, No significant difference between control and VGLUT+ neurons is observed for mEPSC frequency (shown here) or rise and decay time kinetics (data not shown). Error bars indicate SEM.

an increased amount of glutamate released from synaptic vesicles. To assess the extent of glutamate release during synaptic transmission, we made use of a previously established pharmacological approach (Liu et al., 1999; Wadiche and Jahr, 2001). The low-affinity antagonist γ-DGG competes with glutamate for postsynaptic AMPA receptors, such that it partially attenuates glutamatergic release events at hippocampal synapses. Because of the competitive nature of its interaction with glutamate, the degree of its attenuation is inversely related to the amount of glutamate being released, such that it can be used as a quasidirect indicator of the extent of glutamate release (Liu et al., 1999). By recording EPSCs and determining the extent of γ-DGG attenuation, we could obtain a relative metric of the amount of glutamate involved in a population of synaptic release events.

Therefore, we repeated our dual whole-cell patch-clamp procedure (Fig. 3), this time with perforated patches to obtain long-duration recordings. We evoked EPSCs from either control or VGLUT-enhanced presynaptic neurons and then applied γ-DGG to measure the impact of the antagonist on the transmission. By repeatedly evoking transmission at a regular interval, it was possible to establish a baseline amplitude that could then be reliably attenuated by the perfusion of 600 μM γ-DGG (Fig. 5*A*), a concentration that we found optimal for partial attenuation of typical transmission (Fig. 5*B*). A comparison of average traces from before and after antagonist application (Fig. 5*C*) at both control synapses (left traces) and VGLUT-enhanced synapses (right traces) depicts sample attenuation of control and VGLUT-enhanced transmission. As shown, the efficacy of γ-DGG in EPSC attenuation was weaker at synapses containing higher levels of VGLUT1. On the whole, γ-DGG reduced the size of control EPSCs by 51%, in contrast to 31% in VGLUT-transfected pairs (Fig. 5*D*) (control vs VGLUT+; 51 ± 5 vs 31 ± 11%, respectively; $p < 0.05$, unpaired t test; $n = 10$ pairs control, 6 pairs VGLUT+). This line of experiments provides direct evidence that the VGLUT-enhanced synaptic transmission that we observed is indeed a result of enhanced presynaptic glutamate release from synaptic terminals.

The amount of glutamate released by synaptic terminals can be varied by changes to the amount of glutamate released per vesicle, which is likely because VGLUT1 can impact vesicle loading (Fig. 1). However, we cannot rule out the possibility that VGLUT1 overexpression is instead altering the probability of release of the terminals, which in turn could impact the likelihood of multiple vesicles fusing simultaneously at the same terminal (multivesicular release) (Tong and Jahr, 1994; Oertner et al., 2002). To directly distinguish between these two possibilities, we repeated the above γ-DGG attenuation experiments in a low probability of release condition, in which divalent cation concentrations were systematically varied until the observed transmission evoked not only approximated the quantal size (Fig. 4*D*) but also exhibited a high-failure rate. If a low proportion of stimuli results in the release of vesicles, then the proportion of stimuli that fosters multivesicular release will be exceedingly low. If vesicles release independently of one another as is widely assumed and synaptic boutons could be comprised of ~10 vesicles (Schikorski and Stevens, 1997), then the probability of a given EPSC involving two or more vesicles can be determined using binomial statistics (see Materials and Methods), and MVR will be minimized when probability of release is low and failure rates are high. Evoked synaptic transmission in control and VGLUT+ pairs was thus tuned for a high level of baseline failures in each individual pair using different ratios of calcium and magnesium concentrations, as depicted in Figure 5*E*. As shown in Figure 5*F*, the average failure rate of transmission used in these experiments was 0.64 for control pairs and 0.79 for VGLUT+ pairs. Therefore, during transmission in these experiments, an upper bound for the incidence of MVR (assuming synapses with 10 sites) was ~7 and 3%, respectively, and the majority of synaptic transmission should have been mediated by single vesicle release events. If the synapses in our study had even fewer release sites, then the likelihood of MVR would have been still further reduced.

Once such a low probability of release (P_r) condition had been achieved in each connection, we measured γ-DGG attenuation. In this new condition, favoring the release of single vesicles, γ-DGG attenuation in control versus VGLUT+ pairs were again significantly disparate (Fig. 5*D*) (control, low P_r vs VGLUT+, low P_r, 52 ± 7 vs 29 ± 14%, respectively; $p < 0.05$, unpaired t test; $n = 5$ pairs control, 5 pairs VGLUT+). Notably, even when the failure rates were made to differ dramatically between control

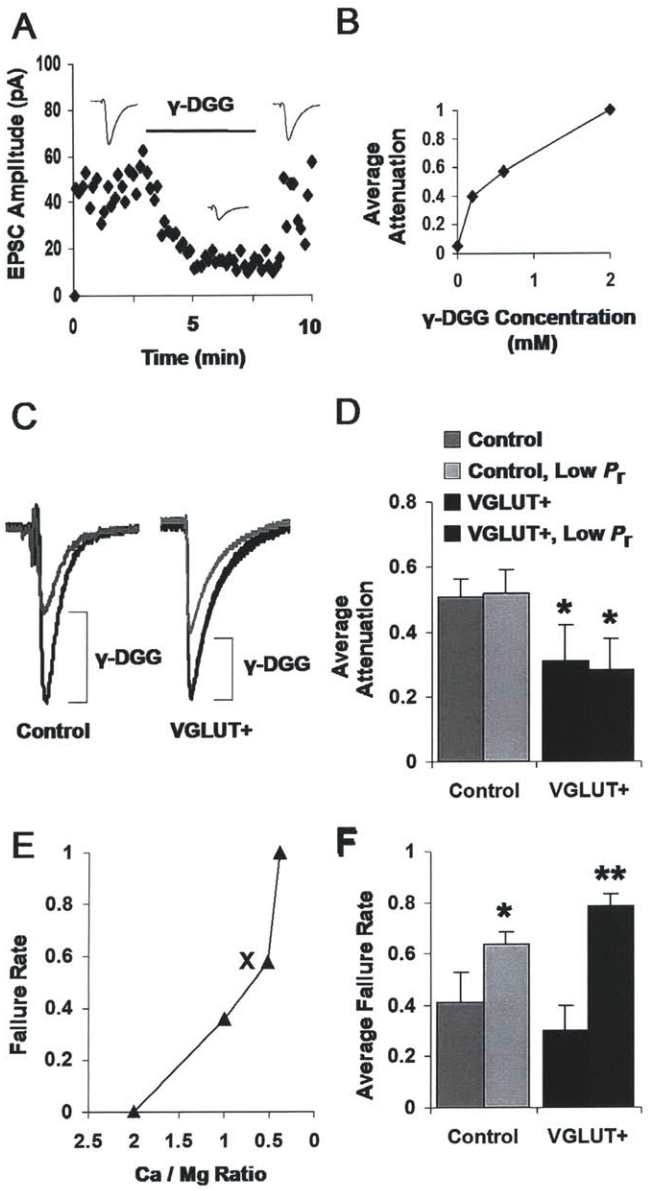

Figure 5. Enhanced per vesicle glutamate release via VGLUT1 overexpression. ***A***, Sample application of the competitive glutamate antagonist γ-DGG (600 μM) while evoking EPSCs at 0.3 Hz between a pair of neurons. Dots represent an average of three EPSCs. ***B***, Dose–response curve measuring the degree of EPSC attenuation by different concentrations of the competitive glutamate antagonist γ-DGG. ***C***, Typical attenuation of control versus VGLUT-mediated EPSCs by 600 μM γ-DGG. Median traces from single connections, normalized by predrug amplitudes for direct comparison, are shown. Bottom traces depict the γ-DGG normalized to the height of their predrug counterpart for comparison of kinetics. ***D***, Summary data of γ-DGG attenuation across all observed connections: VGLUT-mediated transmission is significantly less attenuated than control-mediated transmission (*$p < 0.05$; unpaired *t* test; control vs VGLUT+ bars). Summary data for γ-DGG attenuation acquired under intentionally reduced probability of release conditions are also shown (Control, Low P_r vs VGLUT+, Low P_r bars; see Results). Here, VGLUT-mediated transmission is again significantly less attenuated than control-mediated transmission (*$p < 0.05$; unpaired *t* test). Average failure rates used during each condition are depicted in ***F***. ***E***, Examples of tuning the failure rate of synaptic transmission by varying divalent cation concentrations for low P_r experimental conditions. The ratio of calcium/magnesium concentrations is varied while failure rate is measured until failure rate is sufficiently high to ensure a significant number of single vesicle events. The marker (X) denotes the condition in which γ-DGG attenuation data were acquired. ***F***, Average failure rates used during normal P_r and low P_r experiments summarized in ***D***. Failure rates were intentionally increased during the low P_r experiments for both control (*$p < 0.05$; unpaired *t* test) and VGLUT+ (**$p < 0.01$; unpaired *t* test) conditions.

and control, low P_r (0.41 ± 0.12 vs 0.64 ± 0.05; $p < 0.05$; unpaired *t* test) (Fig. 5*F*, left bars) and between VGLUT+ and VGLUT+, low P_r (0.30 ± 0.10 vs 0.79 ± 0.05; $p < 0.01$; unpaired *t* test) (Fig. 5*F*, right bars), similar degrees of γ-DGG attenuation were observed regardless of these manipulations to failure rate. Thus, VGLUT1 overexpression impacts the amount of glutamate released from single vesicles.

VGLUT1 expression is developmentally regulated

Although the above results demonstrate the potential of VGLUT1 regulation to alter synaptic transmission and establish the molecule as a limiting step for controlling glutamate release, we were interested in ascertaining whether this control point was used endogenously as a physiological mechanism for regulating synaptic transmission. In particular, our previous work (Renger et al., 2001) indicates that developing synapses exhibit several presynaptic functional differences from mature ones, including a reduced number of docking vesicles and less active vesicle cycling, that are rectified during maturation. Given that VGLUT1 can influence transmitter release (Fig. 5), we were interested in determining whether an additional maturational change might involve a developmental increase in VGLUT1 expression.

To monitor the developmental regulation of VGLUT1, quantitative immunohistochemistry was used to determine the amount of transporter expressed at each stage of development (Fig. 6). Immunostaining in mature hippocampal cultures (>14 DIV) depicts the transporter as discrete puncta that are tightly colocalized with synaptotagmin (Fig. 6*A*). Repeating this procedure across various stages of development reveals that expression of the transporter appears to markedly increase at later stages compared with earlier ones. This maturation results in an increased proportion of synapses expressing detectable levels of VGLUT1 (Fig. 6*B*) ($n = 11$ images for each group; 6 vs 9 DIV, $p < 0.001$, unpaired *t* test; 9 vs 20 DIV, $p < 0.01$; no significant change between 20 and 27 DIV). Of the synapses expressing detectable levels of the transporter, the ratio of VGLUT1 and synaptotagmin IODs per synapse also exhibits a graded increase across development (Fig. 6*C*) (6 vs 9 DIV, $p < 0.01$, unpaired *t* test; 9 vs 20 DIV, $p < 0.01$; no significant change between 20 and 27 DIV), indicating that the amount of VGLUT1 protein expressed per synaptic terminal is developmentally upregulated.

Given that VGLUT1 is upregulated within synapses across development, we were interested in identifying functional changes that could potentially be related to its gradual expression. One of our observations is that the peak amplitude of quantal excitatory synaptic currents seemed to undergo a strengthening as synapses matured during development (Fig. 6*D*), a trend that was significant across all populations of recorded neurons. mEPSC mean amplitude increased from 7.9 ± 1.3 pA at 8 DIV to 11.1 ± 0.9 pA at 10 DIV to 14.3 ± 0.9 pA by 15 DIV (Fig. 6*E*) ($n = 8$, 8, and 6 cells, respectively; $p < 0.05$; unpaired *t* test), thus mirroring a developmental increase that has been reported in the brainstem for AMPA receptor-mediated mEPSCs (Ishikawa et al., 2002). Although this effect could also coincide with changes in the number and conductance properties of postsynaptic receptors, the significant increase of VGLUT1 protein expressed in synaptic terminals during this period (Fig. 6*C*) could also contribute, at least in part, to this observed maturational change. Although a significant developmental increase was observed for mEPSC frequency between 10 and 15 DIV (8 DIV, 0.20 ± 0.004 Hz; 10 DIV, 0.31 ± 0.10 Hz; 15 DIV, 1.20 ± 0.45 Hz; $p < 0.05$; unpaired *t* test) (Fig. 6*F*), given our findings on the lack of influence of VGLUT1 expression on mEPSC frequency (Fig. 4*E*), we

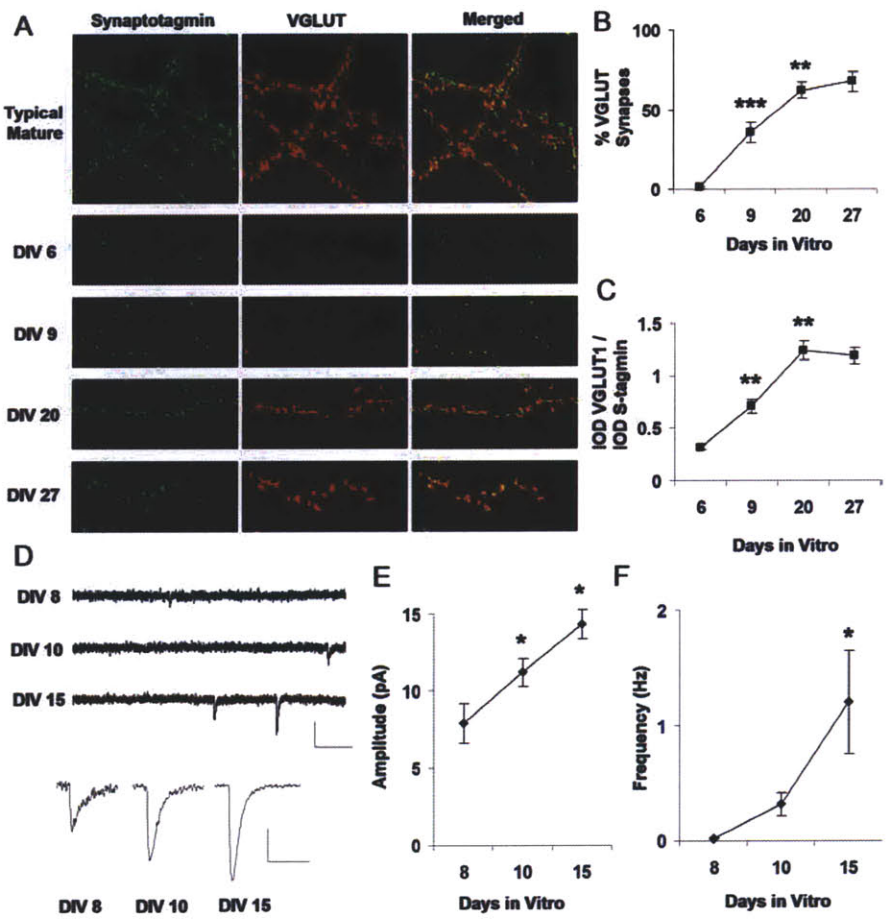

Figure 6. VGLUT1 expression is developmentally regulated and coincides with a developmental change in quantal amplitude. ***A***, Immunolabeling of VGLUT1 and the synaptic marker synaptotagmin Ia across development. ***B***, Average proportion, at various developmental stages, of synaptotagmin-labeled puncta that exhibit detectable levels of VGLUT1 protein. Average proportion of VGLUT synapses increases significantly from 6 to 9 DIV (***$p < 0.001$; unpaired t test) and from 9 to 20 DIV (**$p < 0.01$). ***C***, Average IOD for synapses already expressing detectable levels of VGLUT1. The ratio of VGLUT1 IOD to synapsin I IOD per synapse increases significantly across development from 6 to 9 DIV (**$p < 0.01$; unpaired t test) and from 9 to 20 DIV. ***D***, Miniature excitatory currents (mEPSCs) recorded at different stages of development. Calibration: 15 pA, 150 ms. Bottom traces represent an average of a population of events acquired from a single cell at each developmental stage. Calibration: 5 pA, 25 ms. ***E***, Mean mEPSC amplitude ($n = 8$, 8, and 6 cells at 8, 10, and 15 DIV, respectively) increases significantly during development (*$p < 0.05$; unpaired t test). ***F***, Mean mEPSC frequency also increases significantly between 10 and 15 DIV (*$p < 0.05$).

cannot necessarily conclude that VGLUT1 participates in this phenomenon.

VGLUT1 expression is coordinated with the onset of functional vesicle cycling

Previous work in our group (Renger et al., 2001) has shown that silent synapses can arise in part from incomplete activation of postsynaptic AMPA receptors by a diminished presynaptic release of glutamate. The work demonstrated that conversion from silent to functional transmission could correspond to the developmentally regulated onset of "functional" vesicle cycling and the uptake of the FM1-43 styryl dye (Betz and Bewick, 1992). Thus, there is a developmental delay in FM uptake at early stages of development and now a delay in VGLUT1 expression as well (Fig. 6). We therefore asked whether the delays were coordinated, and whether the developmental time course of VGLUT1 expression might be synchronized with the maturation of vesicle cycling. It seemed sensible that as vesicle cycling matures, the functional capacity of transmitter loading needs to be upregulated accordingly to prevent the release of synaptic vesicles with insignificant transmitter content.

To examine whether such features of presynaptic maturation might be coordinated, it was necessary to concurrently compare the functional capacity of presynaptic terminals with their structural protein content. We made use of AM1-43, a fixable version of FM1-43, to label the functional presynaptic terminals, and followed up with an immunostaining procedure to check the level of desired presynaptic proteins (Renger et al., 2001). It has been shown that the amount FM dye taken up during stimulation can provide an index of the functional capacity of presynaptic terminals. The ability to visualize a fixable version together with immunolabeled protein allowed us to simultaneously measure both VGLUT1 expression levels across development and the developmental onset of functional vesicle cycling. As shown by imaging VGLUT1, AM1-43, and the synaptic vesicle protein synapsin I (Syn I) at the same synaptic terminals (Fig. 7*A*), AM1-43 uptake begins appearing at a similar stage of development as VGLUT1 expression. Figure 7*B–D* quantifies these developmental changes in a population of synapses, again using IOD as a measure of protein expression. Despite a relatively constant level of synapsin I staining across development (Fig. 7*B*), VGLUT1 expression (Fig. 7*C*) appeared to increase in tandem with the onset of AM1-43 labeled functional vesicle cycling (Fig. 7*D*). In general, the ratio of VGLUT1/Syn I increases from 8 to 15 DIV ($p < 0.001$; unpaired t test) and from 10 to 15 DIV ($p < 0.001$) in parallel with the ratio of AM1-43/Syn I ($p < 0.01$; $P < 0.05$) measured at the same synapses (Fig. 7*E*). We thus conclude that the maturation of transporter expression and delivery is jointly coordinated with functional vesicle cycling, a coupling that could be designed to help guarantee the efficient loading of transmitter as vesicle cycling becomes more active.

Activity-dependent plasticity of glutamate release and VGLUT1 expression in mature circuits

Exciting work by others (Turrigiano et al., 1998; Burrone et al., 2002; Thiagarajan et al., 2002) has demonstrated recently that excitatory synapses undergo activity-dependent plasticity in quantal size in response to global changes in network activity. Mechanisms have been proposed to begin to explain this change in quantal size, including changes in postsynaptic receptor number (O'Brien et al., 1998; Watt et al., 2000; Wierenga et al., 2005). Given that molecules responsible for specifying the quantal size postsynaptically, such as AMPA receptors, appear to be critically regulated during activity-dependent synaptic scaling, we decided to examine whether VGLUT1 expression might provide a com-

plementary presynaptic mechanism by which quantal size can be coordinately regulated via endogenous, homeostatic control.

We therefore measured VGLUT1 expression levels per synaptic terminal by again taking the IOD ratio of VGLUT1 to synapsin I at each immunolabeled synapse as before but now comparing between untreated control cultures versus cultures that were preincubated for 48 h in 20 μM bicuculline (BIC) for the purpose of chronically increasing activity levels by blocking $GABA_A$ receptor-mediated inhibitory currents (Turrigiano et al., 1998) (Fig. 8*A*). We observed that chronic increases in activity levels (BIC) led to a significant reduction in synaptic VGLUT1 expression relative to control values (0.75 ± 0.06 control vs 0.95 ± 0.03 BIC; $p = 0.02$; unpaired t test; $n = 8$ images, 4482 synapses control; $n = 7$ images, 4464 synapses BIC) (Fig. 8*B*). We then attempted the exact opposite condition, chronically blocking AMPA and NMDA-type excitatory receptors by applying either 5 μM NBQX or 50 μM AP-5 to effectively decrease activity levels through each one of these pathways (Thiagarajan et al., 2002; Liu, 2004) and measuring the resulting expression levels of VGLUT1. Here, although we observed a robust increase in VGLUT1 in response to chronic NMDA receptor blockade (Fig. 8*A*,*B*), a less prominent increase and a surprising variability were disclosed in response to AMPA receptor blockade (supplementary data, available at www.jneurosci.org as supplemental material). This dichotomy was confirmed by replicating the experiments for NBQX and AP-5 many times. NMDA receptor blockade, however, resulted in increased VGLUT1 expression across every instance tested and, in the experiment presented in Figure 8, *A* and *B*, increased VGLUT1/Syn I levels by 35 ± 4% relative to controls ($p < 0.001$; unpaired t test; $n = 10$ images, 6120 synapses control; $n = 8$ images, 6532 synapses AP-5).

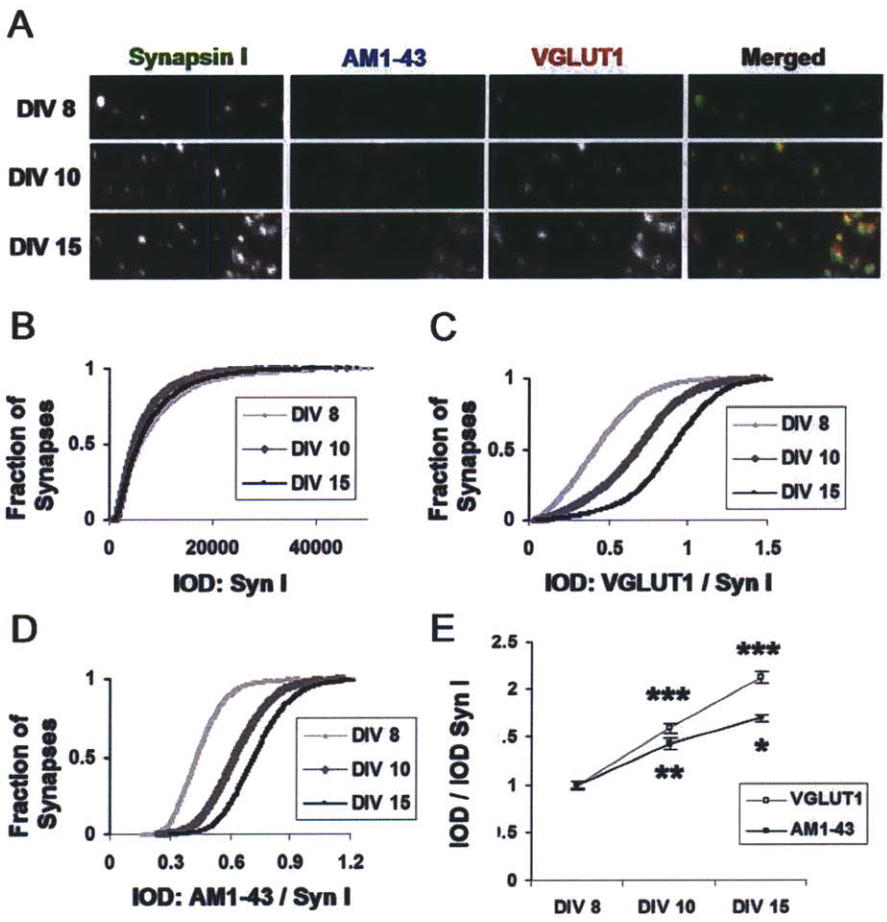

Figure 7. VGLUT1 expression is coordinated with the onset of functional vesicle cycling. ***A***, Triple immunostaining for VGLUT1, the functional bouton marker AM1-43, and the vesicle protein synapsin I. ***B***, IOD per synapse for synapsin I, an additional vesicle protein, remains relatively stable through development. ***C***, ***D***, Synaptic IOD for VGLUT1 and AM1-43 appears to undergo a developmental change. ***E***, Mean synaptic integrated optical density per image. Comparing VGLUT1 and AM1-43 intensity levels (with each normalized to synapsin I levels in the same synapse) demonstrates a significant and coordinated increase in VGLUT1 and AM1-43 staining across development. (***$p < 0.001$; **$p < 0.01$; *$p < 0.05$; unpaired t tests). Syn I, Synapsin I.

Thus, VGLUT1 expression appears to be capable of bidirectional endogenous regulation in response to changes in activity patterns, which could provide a mechanism for presynaptic terminals to coordinate functionally with activity-dependent changes to their postsynaptic partners. To verify that such changes to expression levels indeed had functional implications, we next measured whether glutamate release was also changing as a result of the activity-dependent VGLUT1 regulation. To examine activity-driven changes in glutamate release, we repeated our competitive antagonism protocol applied previously (Fig. 5), again in mature hippocampal cultures, except that in this case, one set of cultures was preincubated for 48 h in either 20 μM BIC or 50 μM AP-5. In these experiments, the cleft glutamate concentration at nontreated synapses appeared to be similar to that observed previously (Fig. 5*D*), with an ~50% reduction in evoked postsynaptic current in response to 600 μM γ-DGG (Fig. 8*C*, gray symbols, *D*, middle traces). However, bicuculline-treated synapses were significantly more sensitive to the antagonist (Fig. 8*C*, white symbols, *D*, left traces) and led to 47% more attenuation than control (76 ± 4 vs 51 ± 3%; $p = 0.03$; unpaired t test; $n = 4$ pairs BIC, 4 pairs control) (Fig. 8*E*), indicating that the bicuculline-treated terminals released less glutamate, thus rendering their transmission more susceptible to the effects of the antagonist. To examine whether a comparable change in glutamate release was also observed in the opposite direction following a treatment that upregulates VGLUT1, we repeated this comparison with chronically treated AP-5 cultures. Here, we observed that the antagonist was significantly less effective on AP-5-treated transmission (Fig. 8*C*, black symbols, *D*, right traces), whereby the γ-DGG block was reduced by 65% in AP-5 synapses compared with control transmission (20 ± 8% AP-5 vs 61 ± 5% control; $p < 0.01$; unpaired t test; $n = 6$ pairs AP-5, 6 pairs control) (Fig. 8*E*).

Because the activity-dependent changes that altered vesicular glutamate release (Fig. 8*C–E*) also impacted VGLUT1 expression (Fig. 8*A*,*B*), and because our previous data demonstrate a causal relationship between VGLUT1 expression and glutamate release, we interpret our observed changes in glutamate release under BIC and AP-5 treatments to occur primarily as a direct consequence of the altered VGLUT1 expression. However, if synaptic terminals can at times undergo multivesicular release from single

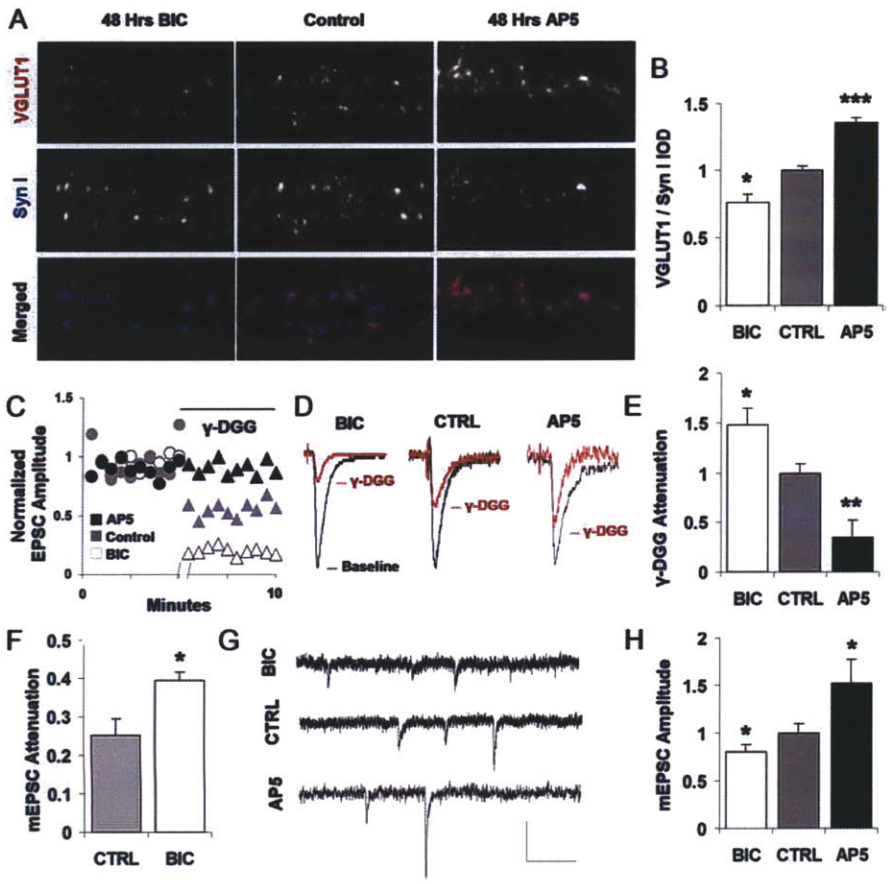

Figure 8. Activity-dependent plasticity of VGLUT1 expression and glutamate release. ***A***, Double immunostaining for VGLUT1 and the vesicle protein synapsin I after 48 h of incubation with either BIC to block $GABA_A$ receptors and increase neuronal activity or AP-5 to block NMDA receptors and decrease neuronal calcium flux. ***B***, Mean VGLUT1 expression (VGLUT1 IOD normalized by synapsin I IOD at the same synapse) was reduced following chronic $GABA_A$ receptor blockade (*$p = 0.02$; unpaired *t* test; values scaled to control) and enhanced by chronic NMDA receptor blockade (***$p < 0.001$; unpaired *t* test; values scaled to control). ***C***, Comparison of EPSC amplitude attenuation by 600 μM γ-DGG in control, BIC, and AP-5-treated cultures. Each data point represents an average of three adjacent sampled EPSCs (0.2 Hz). Representative pre-DGG and post-DGG baselines, normalized to their respective predrug levels for comparison, are shown. ***D***, Typical attenuation of control, BIC, and AP-5-treated EPSCs by 600 μM γ-DGG in the paired connection exhibiting median attenuation for the group. Traces are EPSCs averaged from multiple samples of a single connection, normalized by predrug amplitudes for direct comparison. ***E***, Summary data of γ-DGG attenuation across multiple connections: BIC-treated transmission is significantly more attenuated than nontreated control transmission (*$p < 0.05$; unpaired *t* test; values scaled to control). AP-5-treated transmission is significantly less attenuated than nontreated control transmission ($p < 0.01$; unpaired *t* test; values scaled to control). ***F***, γ-DGG attenuation measured in mEPSCs as an additional control. BIC-treated transmission is significantly more attenuated by γ-DGG application than nontreated control mEPSCs (*$p < 0.05$; unpaired *t* test), indicating that observed changes in glutamate release correspond to differences in per vesicle glutamate release. ***G***, Sample mEPSCs from bicuculline-treated, control, or AP-5-treated cultures. Calibration: 15 pA, 150 ms. ***H***, Mean mEPSC amplitude is significantly reduced in BIC-treated cultures compared with nontreated control cultures and is significantly elevated in AP-5-treated cultures (*$p < 0.05$; unpaired *t* test). CTRL, Control; Syn I, synapsin I.

release sites, then the cleft glutamate concentration could also be altered in part by changes to the number of vesicles released from single terminals. This is possible given evidence that the probability of release, and thus the prevalence of MVR-mediated changes to cleft glutamate concentration, can be modified by perturbations to network activity levels (Murthy et al., 2001). As an additional control to further verify that these changes correspond to changes to the loading of single vesicles, we also measured the cleft glutamate concentration during spontaneous, miniature EPSCs in the bicuculline-treated transmission (Fig. 8*F*). Here, we observed that median γ-DGG attenuation was significantly increased relative to controls (Fig. 8*F*) (25 ± 4% control vs 39 ± 2% BIC; $p = 0.02$; unpaired *t* test), although the attenuations observed in the mEPSCs were less than those in the EPSCs, presumably because of the detection problems associated with spontaneous transmission when it is pharmacologically reduced (Zhou et al., 2000), which likely serves to underestimate the attenuation in the control condition and, to a greater degree, the smaller amplitude bicuculline-treated condition. Even with this detection problem, significant changes in the amount of glutamate released from single vesicles were observed between the two treatments.

To verify that activity-induced changes to VGLUT1 expression were also accompanied by changes to quantal synaptic efficacy, we quantified the amplitude of spontaneous mEPSCs. Here, we observed that in bicuculline-treated transmission, mEPSC amplitude was significantly reduced compared with control transmission (Fig. 8*G*, top trace, *H*) ($n = 6$ control; $n = 4$ BIC; $p = 0.04$; unpaired *t* test), whereas in AP-5-treated transmission, mEPSC amplitude was increased by 52% from control transmission (Fig. 8*G*, bottom trace, *H*) ($n = 7$ control; $n = 6$ AP-5; $p = 0.03$; unpaired *t* test). Thus, in both cases, activity-induced changes to VGLUT1 expression are accompanied by changes to quantal synaptic efficacy.

As such, chronic changes to either levels of activity or calcium flux alter vesicular transporter expression in a manner that is accompanied by relevant changes to physiological transmission. Endogenous control over VGLUT1 provides one mechanism by which an observed presynaptic scaling of glutamate release could be coordinated with a concomitant scaling of postsynaptic sensitivity (Watt et al., 2000).

Discussion

For neurons to be able to make use of VGLUT1 expression to modulate transmission makes specific predictions on a set of issues that remain controversial at glutamatergic synapses. By following the impact of transporter number through vesicle loading (Fig. 1), glutamate release (Fig. 5), and postsynaptic receptor activation (Figs. 3, 4), we provide new evidence in support of a flexibility in excitatory vesicle filling (Atwood and Karunanithi, 2002) and a nonsaturation of hippocampal synapses (Auger and Marty, 2000; Liu, 2003). In addition, although it remains undemonstrated whether presynaptic mechanisms endogenously contribute to regulating the quantal efficacy of excitatory transmission, we show that VGLUT1 expression can confer some properties of this regulation to excitatory synapses.

Vesicle loading depends on the number of available VGLUT1 transporters

It is imaginable that vesicles set in a low concentration of glutamate might simply continue filling until they have reached a set

point level of saturation (Sulzer and Pothos, 2000), such that adding transporters could influence the speed but not the final concentration of glutamate uptake. The work presented here indicates that VGLUT1 vesicles do not fill to an invariant set point, and that reducing the pool of participating transporters (Fig. 1) reduces the equilibrium value of uptake, although it still cannot be resolved whether this is accomplished by changing the intravesicular concentration of transmitter or, instead, the structural capacity of the vesicle (Bruns et al., 2000; Colliver et al., 2000; Sulzer and Edwards, 2000; Karunanithi et al., 2002).

VGLUT1 overexpression enhances excitatory synaptic transmission via an increase in glutamate released per vesicle

We then found that it was possible to traffic additional functional VGLUT1 protein to synaptic terminals (Fig. 2), where we consequently observed larger evoked and spontaneous excitatory currents (Figs. 3, 4) as a result of an increased cleft glutamate concentration (Fig. 5). We provide direct verification that vesicular transport is able to exploit receptor nonsaturation at the level of single vesicles via a shift in the cleft glutamate concentration. An additional finding of some surprise was that VGLUT1 overexpression resulted in a decrease in evoked failure rate (Fig. 3*E*). This could suggest that in addition to enhancing the amount of glutamate deposited per release event, VGLUT1 expression might also be able to influence the likelihood that such release events will occur. Interestingly, another recent study reports that loss of VGLUT1 expression results in a substantially depleted pool of synaptic vesicles at excitatory terminals (Fremeau et al., 2004). Such a relationship between VGLUT1 expression and likelihood of release could depend on either the presence of the transporter itself or on the extent of filling that it facilitates.

It is also important to consider whether VGLUT1 expression could contribute to synaptic efficacy by influencing not only the amount of filling but also the rate (Sulzer and Pothos, 2000). This is especially plausible given two recent studies into the nature of vesicle cycling (Aravanis et al., 2003; Gandhi and Stevens, 2003), which confirmed a "kiss-and-run" type of release that involves the brief fusion and rapid reuse of synaptic vesicles. Such efficiency in cycling would place high demands on vesicle filling to prevent the "firing of blanks" via the exocytosis of "empty" vesicles. Although the precise speed of vesicle filling in the endogenous context can only be estimated, loading in vesicles isolated from the brain (Fig. 1) (Maycox et al., 1988; Wolosker et al., 1996) as well as loading in BON and PC12 cell lines (Bellocchio et al., 2000; Takamori et al., 2000) have been shown to involve a relatively slow process (several minutes), compared with the rapid process of vesicle reuse (~20 s) (Aravanis et al., 2003). A rapid turnover of vesicles could thus result in a depleted synaptic response, and an increasing degree of transporter expression may be important for ensuring a match between the speed of transmitter loading and the functional capacity of the release machinery. Indeed, VGLUT1 is upregulated in close register with the increase of vesicle cycling that occurs during synaptic maturation (Fig. 7) and downregulated during activity-dependent scaling (Fig. 8) in parallel with a reduction in probability of vesicle release (Murthy et al., 2001).

Vesicular transporter expression is endogenously regulated

We found that transporter levels are modified endogenously across development (Fig. 6) and by levels of activity (Fig. 8). If vesicular transporters do contribute meaningfully to synaptic transmission, it would not be surprising to find them amid a molecular ensemble of similar versatility to that in the postsynaptic density (PSD) (Sheng and Kim, 2002). Molecular studies at inhibitory synapses, for example, have recently uncovered a direct association between the vesicular GABA transporter, VGAT, and the synthetic enzyme GAD65 (Jin et al., 2003), suggesting that transmitter synthesis may be functionally coupled to vesicle loading. The fact that VGLUT1 expression is coordinated with the onset of functional vesicle cycling (Fig. 7) could, in turn, suggest a conjunctive signal that couples fusion with adequate filling to ensure that increasingly active vesicles are able to release meaningful quantities of transmitter, perhaps in coordination with a growing pool of receptors postsynaptically.

Similarly, a negative-feedback relationship between certain forms of synaptic activity and VGLUT1 expression, which adjusts glutamate release in response to either circuit excitability or calcium influx (Fig. 8), could provide a presynaptic means for maintaining a stable degree of activity in the face of changing input levels (Turrigiano and Nelson, 2000) in a manner congruent with other recently uncovered postsynaptic mechanisms (O'Brien et al., 1998; Watt et al., 2000; Thiagarajan et al., 2002). Chronic blockade or enhancement of synaptic activity has been shown previously to lead to compensatory shifts in the size of the readily releasable pool and the number of presynaptic active zones (Murthy et al., 2001). This observation has supported a "size principle" (Harris and Stevens, 1989; Pierce and Lewin, 1994; Schikorski and Stevens, 1997) in which functional changes in morphology can correspond to changes in the size of the presynaptic terminal or PSD. It is possible that an activity-driven scaling of presynaptic terminal size (Murthy et al., 2001) is similarly accompanied by alterations in transporter expression per vesicle (Fig. 8) to provide a presynaptic shift in quantal efficacy that coincides with the known activity-driven changes in probability of release. In contrast, although blocking inhibitory receptors was effective at scaling VGLUT1, we were surprised to find that blocking NMDA receptors triggered a more profound regulation than that observed while blocking AMPA receptors. This suggests that VGLUT1 regulation, at least in hippocampal synapses, may be more sensitive to calcium flux than postsynaptic membrane depolarization, although other regimes of regulation may be more prominent in cortical synapses (Watt et al., 2000; Pratt et al., 2003) depending on the layer of cortex and which vesicular transporter is expressed.

Most likely, additional work will elucidate a range of distinct modes by which vesicular transport contributes to the dynamics of synaptic efficacy as well as distinct isoforms by which those contributions are made. Independent regulation of VGLUT1 and its recently identified isoforms VGLUT2 (Fremeau et al., 2001; Takamori et al., 2001; Varoqui et al., 2002) and VGLUT3 (Fremeau et al., 2002; Schafer et al., 2002) could offer, in particular, exciting clinical possibilities. The first mutations to the VGLUT1 ortholog *eat-4* in *Xenopus* have revealed the importance of vesicular transport in both short-term (Rankin and Wicks, 1995) and long-term (Rose et al., 2002) memory. Future studies into the regulation of transmitter loading and release should thus discern new principles by which adaptations on both sides of the synapse are coordinated to ensure a cohesive robustness of memory.

References

Aravanis AM, Pyle JL, Tsien RW (2003) Single synaptic vesicles fusing transiently and successively without loss of identity. Nature 423:643–647.

Atwood HL, Karunanithi S (2002) Diversification of synaptic strength: presynaptic elements. Nat Rev Neurosci 3:497–516.

Auger C, Marty A (2000) Quantal currents at single-site central synapses. J Physiol (Lond) 526:3–11.

Bekkers JM, Richerson GB, Stevens CF (1990) Origin of variability in quantal size in cultured hippocampal neurons and hippocampal slices. Proc Natl Acad Sci USA 87:5359–5362.

Bellocchio EE, Reimer RJ, Fremeau Jr RT, Edwards RH (2000) Uptake of glutamate into synaptic vesicles by an inorganic phosphate transporter. Science 289:957–960.

Betz WJ, Bewick GS (1992) Optical analysis of synaptic vesicle recycling at the frog neuromuscular junction. Science 255:200–203.

Bruns D, Riedel D, Klingauf J, Jahn R (2000) Quantal release of serotonin. Neuron 28:205–220.

Burrone J, O'Byrne M, Murthy VN (2002) Multiple forms of synaptic plasticity triggered by selective suppression of activity in individual neurons. Nature 420:414–418.

Colliver TL, Pyott SJ, Achalabun M, Ewing AG (2000) VMAT-mediated changes in quantal size and vesicular volume. J Neurosci 20:5276–5282.

Forti L, Bossi M, Bergamaschi A, Villa A, Malgaroli A (1997) Loose-patch recordings of single quanta at individual hippocampal synapses. Nature 388:874–878.

Franks KM, Stevens CF, Sejnowski TJ (2003) Independent sources of quantal variability at single glutamatergic synapses. J Neurosci 23:3186–3195.

Fremeau RT, Troyer MD, Pahner I, Nygaard GO, Tran CH, Reimer RJ, Bellocchio EE, Fortin D, Storm-Mathisen J, Edwards RH (2001) The expression of vesicular glutamate transporters defines two classes of excitatory synapse. Neuron 31:247–260.

Fremeau Jr RT, Burman J, Qureshi T, Tran CH, Proctor J, Johnson J, Zhang H, Sulzer D, Copenhagen DR, Storm-Mathisen J, Reimer RJ, Chaudhry FA, Edwards RH (2002) The identification of vesicular glutamate transporter 3 suggests novel modes of signaling by glutamate. Proc Natl Acad Sci USA 99:14488–14493.

Fremeau Jr RT, Kam K, Qureshi T, Johnson J, Copenhagen DR, Storm-Mathisen J, Chaudhry FA, Nicoll RA, Edwards RH (2004) Vesicular glutamate transporters 1 and 2 target to functionally distinct synaptic release sites. Science 304:1815–1819.

Gandhi SP, Stevens CF (2003) Three modes of synaptic vesicular recycling revealed by single-vesicle imaging. Nature 423:607–613.

Hanse E, Gustafsson B (2001) Quantal variability at glutamatergic synapses in area CA1 of the rat neonatal hippocampus. J Physiol (Lond) 531:467–480.

Harris KM, Stevens JK (1989) Dendritic spines of CA 1 pyramidal cells in the rat hippocampus: serial electron microscopy with reference to their biophysical characteristics. J Neurosci 9:2982–2997.

Hell JW, Maycox PR, Stadler H, Jahn R (1988) Uptake of GABA by rat brain synaptic vesicles isolated by a new procedure. EMBO J 7:3023–3029.

Ishikawa T, Sahara Y, Takahashi T (2002) A single packet of transmitter does not saturate postsynaptic glutamate receptors. Neuron 34:613–621.

Jin H, Wu H, Osterhaus G, Wei J, Davis K, Sha D, Floor E, Hsu CC, Kopke RD, Wu JY (2003) Demonstration of functional coupling between gamma-aminobutyric acid (GABA) synthesis and vesicular GABA transport into synaptic vesicles. Proc Natl Acad Sci USA 100:4293–4298.

Karunanithi S, Marin L, Wong K, Atwood HL (2002) Quantal size and variation determined by vesicle size in normal and mutant *Drosophila* glutamatergic synapses. J Neurosci 22:10267–10276.

Liu G (2003) Presynaptic control of quantal size: kinetic mechanisms and implications for synaptic transmission and plasticity. Curr Opin Neurobiol 13:324–331.

Liu G (2004) Local structural balance and functional interaction of excitatory and inhibitory synapses in hippocampal dendrites. Nat Neurosci 7:373–379.

Liu G, Tsien RW (1995) Properties of synaptic transmission at single hippocampal synaptic boutons. Nature 375:404–408.

Liu G, Choi S, Tsien RW (1999) Variability of neurotransmitter concentration and nonsaturation of postsynaptic AMPA receptors at synapses in hippocampal cultures and slices. Neuron 22:395–409.

Mainen ZF, Malinow R, Svoboda K (1999) Synaptic calcium transients in single spines indicate that NMDA receptors are not saturated. Nature 399:151–155.

Malenka RC, Nicoll RA (1999) Long-term potentiation—a decade of progress? Science 285:1870–1874.

Maycox PR, Deckwerth T, Hell JW, Jahn R (1988) Glutamate uptake by brain synaptic vesicles. Energy dependence of transport and functional reconstitution in proteoliposomes. J Biol Chem 263:15423–15428.

McAllister AK, Stevens CF (2000) Nonsaturation of AMPA and NMDA receptors at hippocampal synapses. Proc Natl Acad Sci USA 97:6173–6178.

Murthy VN, Schikorski T, Stevens CF, Zhu Y (2001) Inactivity produces increases in neurotransmitter release and synapse size. Neuron 32:673–682.

Ni B, Rosteck Jr PR, Nadi NS, Paul SM (1994) Cloning and expression of a cDNA encoding a brain-specific Na^+-dependent inorganic phosphate cotransporter. Proc Natl Acad Sci USA 91:5607–5611.

O'Brien RJ, Kamboj S, Ehlers MD, Rosen KR, Fischbach GD, Huganir RL (1998) Activity-dependent modulation of synaptic AMPA receptor accumulation. Neuron 21:1067–1078.

Oertner TG, Sabatini BL, Nimchinsky EA, Svoboda K (2002) Facilitation at single synapses probed with optical quantal analysis. Nat Neurosci 5:657–664.

Ogita K, Hirata K, Bole DG, Yoshida S, Tamura Y, Leckenby AM, Ueda T (2001) Inhibition of vesicular glutamate storage and exocytotic release by Rose Bengal. J Neurochem 77:34–42.

Pierce JP, Lewin GR (1994) An ultrastructural size principle. Neuroscience 58:441–446.

Pothos EN, Larsen KE, Krantz DE, Liu Y, Haycock JW, Setlik W, Gershon MD, Edwards RH, Sulzer D (2000) Synaptic vesicle transporter expression regulates vesicle phenotype and quantal size. J Neurosci 20:7297–7306.

Pratt KG, Watt AJ, Griffith LC, Nelson SB, Turrigiano GG (2003) Activity-dependent remodeling of presynaptic inputs by postsynaptic expression of activated CaMKII. Neuron 39:269–281.

Rankin CH, Wicks SR (1995) Mutations of the *Caenorhabditis elegans* brain-specific inorganic phosphate transporter *eat-4* affect habituation of the tap-withdrawal response without affecting the response itself. J Neurosci 15:2434–2444.

Renger JJ, Egles C, Liu G (2001) A developmental switch in neurotransmitter flux enhances synaptic efficacy by affecting AMPA receptor activation. Neuron 29:469–484.

Rose JK, Kaun KR, Rankin CH (2002) A new group-training procedure for habituation demonstrates that presynaptic glutamate release contributes to long-term memory in *Caenorhabditis elegans*. Learn Mem 9:130–137.

Roseth S, Fykse EM, Fonnum F (1998) Uptake of L-glutamate into synaptic vesicles: competitive inhibition by dyes with biphenyl and amino- and sulphonic acid-substituted naphthyl groups. Biochem Pharmacol 56:1243–1249.

Schafer MK, Varoqui H, Defamie N, Weihe E, Erickson JD (2002) Molecular cloning and functional identification of mouse vesicular glutamate transporter 3 and its expression in subsets of novel excitatory neurons. J Biol Chem 277:50734–50748.

Schikorski T, Stevens CF (1997) Quantitative ultrastructural analysis of hippocampal excitatory synapses. J Neurosci 17:5858–5867.

Sheng M, Kim MJ (2002) Postsynaptic signaling and plasticity mechanisms. Science 298:776–780.

Silver RA, Cull-Candy SG, Takahashi T (1996) Non-NMDA glutamate receptor occupancy and open probability at a rat cerebellar synapse with single and multiple release sites. J Physiol (Lond) 494:231–250.

Song H, Ming G, Fon E, Bellocchio E, Edwards RH, Poo M (1997) Expression of a putative vesicular acetylcholine transporter facilitates quantal transmitter packaging. Neuron 18:815–826.

Sulzer D, Edwards R (2000) Vesicles: equal in neurotransmitter concentration but not in volume. Neuron 28:5–7.

Sulzer D, Pothos EN (2000) Regulation of quantal size by presynaptic mechanisms. Rev Neurosci 11:159–212.

Takamori S, Rhee JS, Rosenmund C, Jahn R (2000) Identification of a vesicular glutamate transporter that defines a glutamatergic phenotype in neurons. Nature 407:189–194.

Takamori S, Rhee JS, Rosenmund C, Jahn R (2001) Identification of differentiation-associated brain-specific phosphate transporter as a second vesicular glutamate transporter (VGLUT2). J Neurosci 21:RC182(1–6).

Takamori S, Malherbe P, Broger C, Jahn R (2002) Molecular cloning and functional characterization of human vesicular glutamate transporter 3. EMBO Rep 3:798–803.

Thiagarajan TC, Piedras-Renteria ES, Tsien RW (2002) α- and βCaMKII. Inverse regulation by neuronal activity and opposing effects on synaptic strength. Neuron 36:1103–1114.

Tong G, Jahr CE (1994) Multivesicular release from excitatory synapses of cultured hippocampal neurons. Neuron 12:51–59.

Turrigiano GG, Nelson SB (2000) Hebb and homeostasis in neuronal plasticity. Curr Opin Neurobiol 10:358–364.

Turrigiano GG, Leslie KR, Desai NS, Rutherford LC, Nelson SB (1998) Activity-dependent scaling of quantal amplitude in neocortical neurons. Nature 391:892–896.

Varoqui H, Schafer MK, Zhu H, Weihe E, Erickson JD (2002) Identification of the differentiation-associated Na^+/PI transporter as a novel vesicular glutamate transporter expressed in a distinct set of glutamatergic synapses. J Neurosci 22:142–155.

Wadiche JI, Jahr CE (2001) Multivesicular release at climbing fiber-Purkinje cell synapses. Neuron 32:301–313.

Watt AJ, van Rossum MC, MacLeod KM, Nelson SB, Turrigiano GG (2000) Activity coregulates quantal AMPA and NMDA currents at neocortical synapses. Neuron 26:659–670.

Wierenga CJ, Ibata K, Turrigiano GG (2005) Postsynaptic expression of homeostatic plasticity at neocortical synapses. J Neurosci 25:2895–2905.

Wojcik SM, Rhee JS, Herzog E, Sigler A, Jahn R, Takamori S, Brose N, Rosenmund C (2004) An essential role for vesicular glutamate transporter 1 (VGLUT1) in postnatal development and control of quantal size. Proc Natl Acad Sci USA 101:7158–7163.

Wolosker H, de Souza DO, de Meis L (1996) Regulation of glutamate transport into synaptic vesicles by chloride and proton gradient. J Biol Chem 271:11726–11731.

Yamashita T, Ishikawa T, Takahashi T (2003) Developmental increase in vesicular glutamate content does not cause saturation of AMPA receptors at the calyx of held synapse. J Neurosci 23:3633–3638.

Zhou Q, Petersen CC, Nicoll RA (2000) Effects of reduced vesicular filling on synaptic transmission in rat hippocampal neurones. J Physiol (Lond) 525:195–206.

Appendix C

LAR receptor protein tyrosine phosphatases in the development and maintenance of excitatory synapses.

Dunah AW, Hueske E, Wyszynski M, Hoogenraad CC, Jaworski J, Pak DT, Simonetta A, Liu G, Sheng M. (2005). ***Nature Neuroscience. 8(4),*** **458-67.**

nature neuroscience

LAR receptor protein tyrosine phosphatases in the development and maintenance of excitatory synapses

Anthone W Dunah[1,3], Emily Hueske[1], Michael Wyszynski[1,3], Casper C Hoogenraad[1], Jacek Jaworski[1,2], Daniel T Pak[1,3], Alyson Simonetta[1,2], Guosong Liu[1] & Morgan Sheng[1,2]

Leukocyte common antigen–related (LAR) family receptor protein tyrosine phosphatases (LAR-RPTP) bind to liprin-α (SYD2) and are implicated in axon guidance. We report that LAR-RPTP is concentrated in mature synapses in cultured rat hippocampal neurons, and is important for the development and maintenance of excitatory synapses in hippocampal neurons. RNA interference (RNAi) knockdown of LAR or dominant-negative disruption of LAR function results in loss of excitatory synapses and dendritic spines, reduction of surface AMPA receptors, impairment of dendritic targeting of the cadherin–β-catenin complex, and reduction in the amplitude and frequency of miniature excitatory postsynaptic currents (mEPSCs). Cadherin, β-catenin and GluR2/3 are tyrosine phosphoproteins that coimmunoprecipitate with liprin-α and GRIP from rat brain extracts. We propose that the cadherin-β-catenin complex is cotransported with AMPA receptors to synapses and dendritic spines by a mechanism that involves binding of liprin-α to LAR-RPTP and tyrosine dephosphorylation by LAR-RPTP.

The AMPA subtype of glutamate receptors mediates fast excitatory synaptic transmission, and regulated trafficking of AMPA receptors is a mechanism for controlling synaptic strength[1,2]. The individual subunits of AMPA receptors (GluR1–4) interact with specific sets of intracellular proteins[1,3,4]. The C-termini of GluR2/3 subunits bind to the fifth PDZ domain of the GRIP/ABP family of multi-PDZ proteins[5–7]. GRIP likely assembles a large protein complex associated with AMPA receptors[8]. For example, GRIP binds via PDZ6 to the C-terminus of liprin-α proteins, and this interaction is important for the surface expression and synaptic targeting of AMPA receptors in hippocampal neurons[9].

In turn, liprin-α proteins bind to the LAR-RPTPs, which are best known for their role in regulating axon guidance in *Drosophila*[10]. The mammalian LAR-RPTP family includes LAR, PTPδ and PTPσ[10]. The extracellular regions of LAR-RPTP contain three N-terminal immunoglobulin-like domains and a variable number of fibronectin type III–like domains[11], suggesting that these phosphatases may function as receptors for cell surface or extracellular matrix proteins[10]. The intracellular region of LAR contains two tandem phosphatase domains: the membrane proximal domain (D1), which has phosphatase activity, and the distal phosphatase domain (D2), which is devoid of catalytic activity but may regulate the substrate specificity of LAR[12,13]. LAR-RPTPs are normally cleaved post-translationally into two non-covalently linked subunits: an extracellular E-subunit with the immunoglobulin-like and fibronectin III–like domains, and a P-subunit containing the phosphatase domains plus a short ectodomain and the transmembrane segment[11,14,15].

Liprin-α proteins bind to the D2 domain of LAR-RPTPs and colocalize with LAR-RPTP at focal adhesions in cultured cell lines[15–18]. Liprin-α (also known as SYD2) is required for normal presynaptic differentiation in *C. elegans*[19]. In *Drosophila*, DLAR and liprin-α colocalize in the neuromuscular junction (NMJ), and both are required for normal NMJ morphology[20]. In mammalian synapses, however, the functional significance of liprin-α and LAR-RPTP is unknown.

Cell adhesion molecules are crucial for the formation and maturation of neuronal synapses[21]. Perhaps the most intensively studied group of these molecules is the cadherin family of homophilic cell adhesion molecules, which are implicated in synaptic plasticity and the morphogenesis of dendritic spines, the postsynaptic compartment that houses excitatory synapses[22–25]. The full adhesive function of cadherins requires the binding of cadherin to the cytoplasmic proteins β-catenin and α-catenin, which mediate anchorage to the actin cytoskeleton[26]. The interaction of β-catenin with cadherin is regulated by tyrosine phosphorylation[27], and LAR has been reported to coimmunoprecipitate with the cadherin–β-catenin complex in PC12 cells and to stimulate tyrosine dephosphorylation of β-catenin[28]. Such evidence suggests a possible involvement of LAR in the regulation of cell adhesion. In neurons, tyrosine dephosphorylation of β-catenin is correlated with the translocation of β-catenin to dendritic spines[25], but the tyrosine phosphatase responsible is unknown.

Here we report that LAR-RPTP is concentrated at excitatory synapses of cultured hippocampal neurons. Disruption of LAR-RPTP function, disruption of its protein interactions, or both impair the dendritic targeting of cadherin and β-catenin and reduce the density of

[1]The Picower Center for Learning and Memory, RIKEN-MIT Neuroscience Research Center, and [2]Howard Hughes Medical Institute, Massachusetts Institute of Technology, Cambridge, Massachusetts 02139, USA. [3]Present addresses: Department of Neurology, MassGeneral Institute for Neurodegenerative Disease, Harvard Medical School and Massachusetts General Hospital, Charlestown, Massachusetts 02129, USA (A.W.D.); Amgen, Thousand Oaks, California 91320, USA (M.W.); Department of Pharmacology, Georgetown University School of Medicine, Washington, DC 20007, USA (D.T.P). Correspondence should be addressed to M.S. (msheng@mit.edu).

Published online 6 March 2005; doi:10.1038/nn1416

excitatory synapses and spines, correlating with suppression of mEPSCs. In the brain, cadherin and β-catenin are substantially associated with the GRIP–liprin-α–AMPA receptor protein complex, and β-catenin is tyrosine dephosphorylated *in vitro* by LAR. We suggest that LAR-RPTPs contribute to synapse morphogenesis by regulating the synaptic delivery of a protein complex that is scaffolded by GRIP and liprin-α and that includes AMPA receptors and cadherin–β-catenin.

RESULTS

LAR-RPTP expression in brain and localization in neurons

Rabbit polyclonal antibody D5013 was raised against the phosphatase domain D1 of human LAR—a domain that is highly conserved among LAR-RPTPs. On immunoblots of COS-7 cells transfected with LAR or its close relatives PTPδ and PTPσ, D5013 antibody reacted with multiple species, including a top band of ~220–230 kDa (**Fig. 1a**, arrow) that presumably corresponds to the full-length protein (LAR, 220 kDa[14]; PTPδ, 220 kDa[29]; and PTPσ 230 kDa[30]). The multiple smaller bands probably arise from proteolysis of LAR-RPTPs, as no signal was observed in untransfected COS-7 cells. In rat cerebral cortex, the LAR antibody recognized a major band of M_r ~85 kDa, which is likely to represent the P-subunit containing the transmembrane and intracellular regions of LAR, PTPδ and/or PTPσ (**Fig. 1a,b**, arrowhead). Because D5103 recognizes PTPδ and PTPσ as well as LAR, we use the term 'LAR-RPTP' to include all three members of the LAR subfamily.

The ~220 kDa LAR polypeptide shifted to a lower molecular weight upon treatment with glycosidase PNGaseF (**Fig. 1b**, arrow), supporting the idea that it represents the full-length protein. PNGaseF also reduced the size of NMDA receptor subunit NR2B, a known N-linked glycoprotein[31] (**Fig. 1b**). The ~85 kDa band was unaffected (**Fig. 1b**, arrowhead), consistent with it being the P-subunit of LAR-RPTP.

Immunoblotting showed that LAR-RPTP proteins were widely expressed in different regions of the rat CNS (**Fig. 1c**), and at higher levels in postnatal day 7 (P7) brain than in adult (P45) brain (**Fig. 1d**), consistent with mRNA expression data[32]. The ~85 kDa LAR-RPTP band showed the biochemical fractionation pattern expected for an integral membrane protein (**Fig. 1e**). We noted the presence of LAR-RPTP in P3 (microsomes and light membranes) and LP2 (synaptic vesicle–enriched fraction), which is similar to GRIP, liprin-α and GluR2/3 fractionation patterns in the brain[33,34]. LAR-RPTP was enriched in postsynaptic density (PSD) fractions, though to a lesser extent than PSD-95 (**Fig. 1f**).

At 7 d *in vitro* (DIV7), LAR-RPTP showed a fine punctate immunostaining in cell bodies and dendrites of cultured hippocampal neurons and only partial colocalization with PSD-95 or with bassoon, a protein expressed in the presynaptic active zone. With neuronal maturation, an increasing fraction of LAR puncta became synaptically localized, and an increasing percentage of synapses showed detectable LAR staining (**Supplementary Fig. 1** online). The percentage of LAR clusters that colocalized with PSD-95 clusters was 54.1 ± 4.8% (DIV21) and 21.2 ± 2.4% (DIV7); the percentage that colocalized with bassoon was 52.8 ± 4.3% (DIV21) and 23.1 ± 3.6% (DIV7). In contrast, 68 ± 3.7% of PSD-95 clusters and 57.6 ± 5.3% of bassoon clusters at DIV21 colocalized with LAR-RPTP; 24.8 ± 4.1% of PSD-95 and 28.2 ± 6.1% of bassoon clusters at DIV7 colocalized with LAR-RPTP. The immunocytochemical data and biochemical findings are consistent with LAR-RPTP being enriched at excitatory synapses but more widely distributed in neurons than PSD-95.

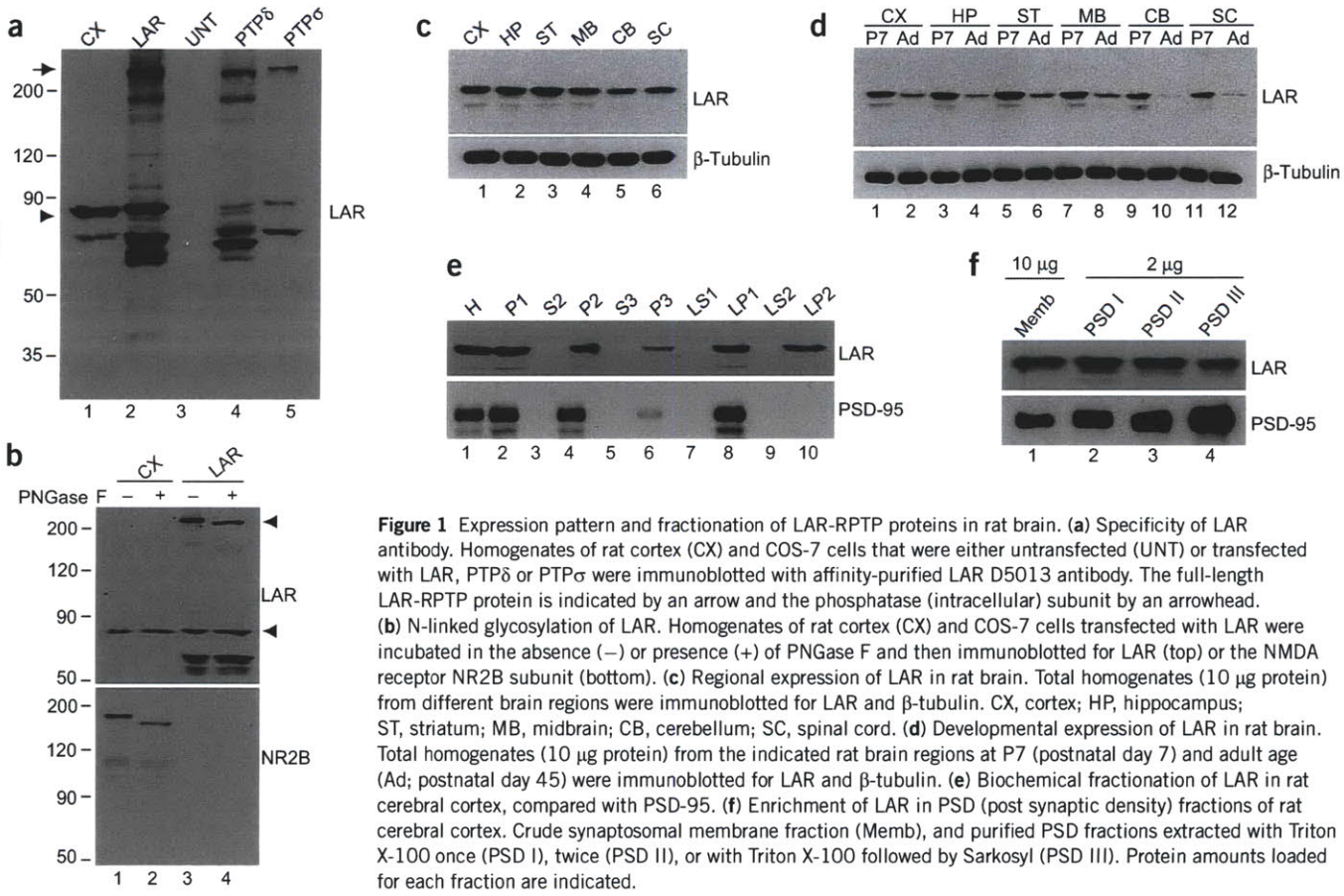

Figure 1 Expression pattern and fractionation of LAR-RPTP proteins in rat brain. (**a**) Specificity of LAR antibody. Homogenates of rat cortex (CX) and COS-7 cells that were either untransfected (UNT) or transfected with LAR, PTPδ or PTPσ were immunoblotted with affinity-purified LAR D5013 antibody. The full-length LAR-RPTP protein is indicated by an arrow and the phosphatase (intracellular) subunit by an arrowhead. (**b**) N-linked glycosylation of LAR. Homogenates of rat cortex (CX) and COS-7 cells transfected with LAR were incubated in the absence (–) or presence (+) of PNGase F and then immunoblotted for LAR (top) or the NMDA receptor NR2B subunit (bottom). (**c**) Regional expression of LAR in rat brain. Total homogenates (10 μg protein) from different brain regions were immunoblotted for LAR and β-tubulin. CX, cortex; HP, hippocampus; ST, striatum; MB, midbrain; CB, cerebellum; SC, spinal cord. (**d**) Developmental expression of LAR in rat brain. Total homogenates (10 μg protein) from the indicated rat brain regions at P7 (postnatal day 7) and adult age (Ad; postnatal day 45) were immunoblotted for LAR and β-tubulin. (**e**) Biochemical fractionation of LAR in rat cerebral cortex, compared with PSD-95. (**f**) Enrichment of LAR in PSD (post synaptic density) fractions of rat cerebral cortex. Crude synaptosomal membrane fraction (Memb), and purified PSD fractions extracted with Triton X-100 once (PSD I), twice (PSD II), or with Triton X-100 followed by Sarkosyl (PSD III). Protein amounts loaded for each fraction are indicated.

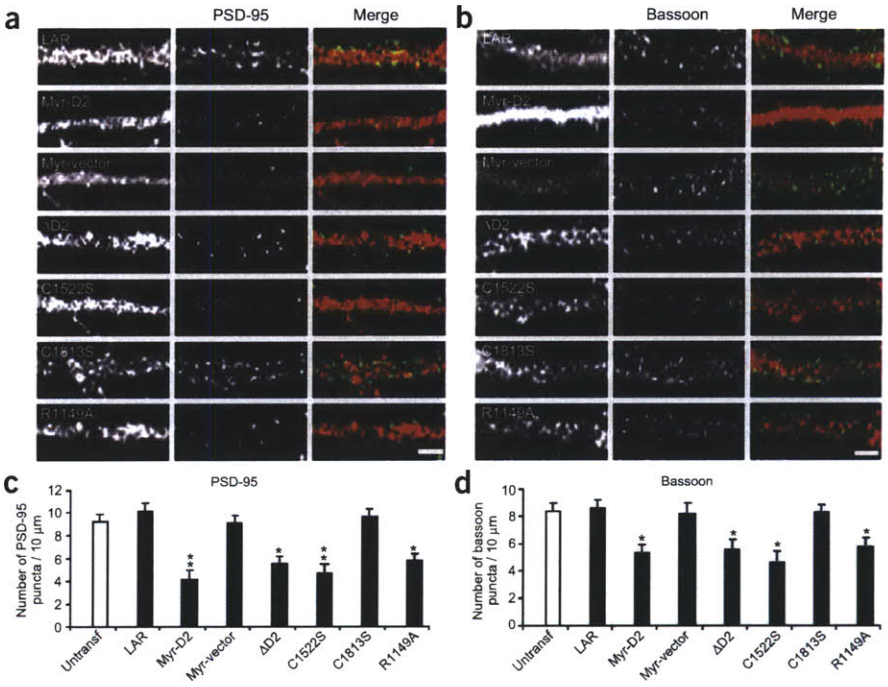

Figure 2 Overexpression of LAR interfering constructs reduces the number of excitatory synapses. (**a**,**b**) Hippocampal neurons were transfected at DIV13 with the indicated LAR constructs and double-labeled at DIV18 for transfected LAR construct (red) and endogenous PSD-95 (**a**, green) or Bassoon (**b**, green). Individual dendritic segments are shown in grayscale for individual channels, and in color for merged green and red channels. Scale bar, 4 μm. (**c**,**d**) Quantification of endogenous PSD-95 (**c**) or bassoon (**d**) cluster density in hippocampal neurons overexpressing LAR constructs. Histograms (mean ± s.e.m.) show the density of puncta per 10 μm dendrite in transfected cells, compared to untransfected cells (Untransf) in the same microscopic field. (*$P < 0.05$; **$P < 0.01$).

LAR mutant constructs reduce synapse density

To address the functional role of LAR-RPTP in the formation and maintenance of synapses, we generated a series of deletion and point mutants of LAR (tagged with hemagglutinin (HA) or Myc epitope) to act as dominant interfering constructs when overexpressed in neurons (**Supplementary Fig. 1**). Overexpression of the isolated D2 domain (fused to a myristoylation motif for membrane association (Myr-D2)) or of LAR with the D2 domain deleted (ΔD2) should disrupt the interaction of endogenous LAR-RPTPs and liprin-α. The C1522S mutation in the D1 domain inactivates the catalytic activity of this domain, whereas the corresponding mutation in the D2 domain (C1813S) should have no effect on the tyrosine phosphatase activity of LAR[12]. The R1149A mutation alters the arginine residue required for LAR proprotein cleavage, thus preventing post-translational maturation of LAR[14]. All LAR mutant constructs expressed at the expected molecular sizes in COS-7 cells (data not shown).

Hippocampal neurons were transfected with the LAR mutant constructs at approximately DIV12–13 and analyzed 5 d later (DIV17–18) by immunostaining (**Fig. 2a**,**b**). The linear density of PSD-95 clusters (a marker of excitatory synapses) was reduced by ~40–50% in neurons transfected with constructs that interfered with LAR–liprin-α binding (Myr-D2 or ΔD2), LAR phosphatase activity (C1522S) or LAR cleavage (R1149A) (**Fig. 2a**,**c**). Punctate staining for bassoon also decreased, although to a lesser degree (30–40%) (**Fig. 2b**,**d**). Wild-type LAR, Myr-Vector or C1813S did not significantly affect the puncta density of PSD-95 (**Fig. 2a**,**c**) or bassoon (**Fig. 2b**,**d**). Surface $GABA_A$ receptors (a marker of inhibitory synapses) were unaltered by any of the tested LAR constructs (**Supplementary Fig. 1**). These results indicate that the catalytic activity and D2-mediated interactions of LAR-RPTP are important for the development and/or maintenance of excitatory synapses.

LAR mutant constructs reduce dendritic spine density

To outline the morphology of dendrites, hippocampal neurons were cotransfected at DIV13 with green fluorescent protein (GFP) along with the LAR dominant-negative constructs. The density of spines (defined as protrusions of 1–4 μm in length that showed a clear 'head') at DIV18 was reduced by those mutant constructs that disrupt LAR–liprin-α binding, inactivate LAR phosphatase activity, or prevent LAR proprotein processing (**Fig. 3a**,**b**). Spine density was unaffected by overexpression of wild-type LAR or C1813S (**Fig. 3a**,**b**). The mean length and width of remaining spines, and the density of filopodia (protrusions of 1–4 μm in length lacking a head), were not substantially different in neurons overexpressing any of the LAR constructs (data not shown).

A similar reduction in spine density was observed when hippocampal neurons were transfected with the same LAR mutant constructs at DIV7 and the constructs were overexpressed for 5 d (**Supplementary Fig. 2** online), during the period when spine formation is just beginning in cultured neurons. This result suggests that LAR-RPTP may be important for the formation of spines.

To address this question more directly, we followed the fate of spines by time-lapse imaging. Neurons were transfected at DIV12 with either β-gal (control) or LAR dominant-negative mutant Myr-D2, and the same cells were imaged 24 and 72 h after transfection to detect the cotransfected GFP. Overall spine density during this 48-h period increased slightly in control neurons but decreased in Myr-D2–transfected cells (**Fig. 3c**,**d**). Further analysis showed that the decrease in spine density in Myr-D2–transfected neurons was caused both by reduced addition of new spines and by increased loss of existing spines (**Fig. 3e**). Taken together, these results imply that LAR and its D2-dependent functions are important for both the formation and maintenance of dendritic spines, correlating with their crucial role in the development of excitatory synapses.

We have previously shown that disrupting the interaction between liprin-α and GRIP inhibits surface expression and synaptic clustering of AMPA receptors[9]. We tested whether the GRIP–liprin-α interaction was also important for spine development by overexpressing liprin-α1A, a C-terminal splice variant of liprin-α1 that cannot bind to GRIP[9]. Indeed, liprin-α1A decreased the density of dendritic spines, whereas liprin-α1 (which can bind GRIP) had no effect (**Fig. 3a**,**b**; **Supplementary Fig. 2**). Thus, disrupting the binding of liprin-α to GRIP had similar effects on synapse morphology as did disrupting LAR activity or binding of liprin-α to LAR.

Associated with the depletion of excitatory synapses, surface levels of endogenous AMPA receptor GluR1 and GluR2 subunits

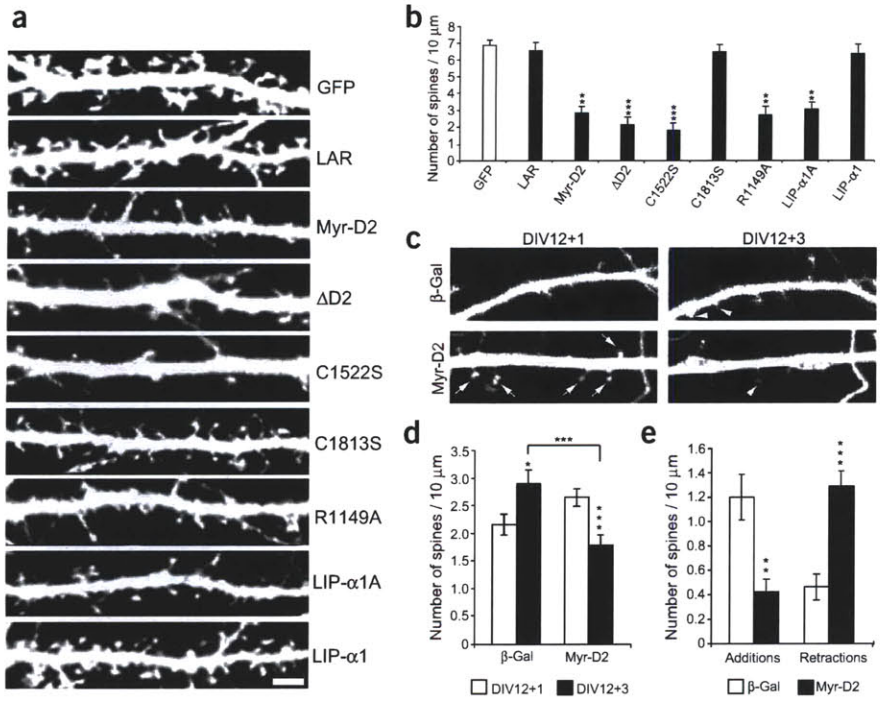

Figure 3 LAR interfering constructs decrease the density of dendritic spines. (**a**) Cultured hippocampal neurons were transfected at DIV13 with either GFP alone or GFP plus the indicated LAR or liprin-α constructs, and double-labeled at DIV18 for GFP (to visualize neuron morphology) and the transfected proteins. Scale bar, 8 μm. (**b**) Spines per 10 μm dendrite length in neurons transfected as in **a**. Histograms show mean ± s.e.m. (>13 neurons analyzed for each construct). (*$P < 0.05$; **$P < 0.01$; ***$P < 0.001$). (**c**) Representative time-lapse images of the same dendritic segment of live neurons transfected with control vector (β-gal) or Myr-D2 mutant LAR construct, visualized by cotransfected GFP at 1 d (DIV12+1) or 3 d after transfection (DIV12+3). Arrows indicate spines that were lost, and arrowheads indicate spines that were added during the intervening 2-d period. (**d**) Overall spine density at 1 d and 3 d after transfection. (**e**) Spine additions and retractions in neurons transfected with β-gal or Myr-D2 (*$P < 0.05$; **$P < 0.01$; ***$P < 0.001$).

(**Supplementary Fig. 3** online) and the density of GluR1 and GluR2 clusters (data not shown) were greatly reduced on dendrites of neurons transfected with LAR constructs Myr-D2, ΔD2, C1522S and R1149A.

We reasoned that if the inhibitory effects of the LAR mutant constructs on dendritic spines and synapse density resulted from a specific dominant-negative mechanism, then they should be at least partially rescued by overexpression of wild-type LAR. Indeed, cotransfection with wild-type LAR partially prevented the Myr-D2– or C1522S–induced reduction of surface GluR2 and PSD-95 puncta (**Supplementary Fig. 4** online).

RNAi knockdown of LAR-RPTP in hippocampal neurons

We next used RNAi to interfere with the production of endogenous LAR, PTPδ and PTPσ, which are all expressed in hippocampus[32]. We showed using COS-7 cells that multiple RNAi plasmids were effective, and gene specific, in reducing protein expression of rat LAR, PTPδ or PTPσ (**Supplementary Fig. 5** online). Hippocampal neurons were transfected for 3 d with single, double or triple combinations of RNAi plasmids targeting LAR, PTPδ and PTPσ, as well as β-galactosidase (β-gal), to visualize the transfected cell (**Fig. 4**). Neurons expressing any single LAR-RPTP RNAi plasmid, or any combination of them, showed a lower density of spines and PSD-95 puncta than did vector (pSUPER)-transfected cells (**Fig. 4**). The LAR-RPTP RNAi–transfected neurons also showed a substantial decrease in the surface staining intensity of AMPA receptor subunit GluR2 (data not shown).

In general, the inhibition of PSD-95, spine density and surface GluR2 was strongest with triple, followed by double and then single, RNAi against LAR-RPTP members. Vector control (pSUPER) and RNAi against zinc transporter ZnT3 (which is expressed in hippocampal neurons) had no significant effect on the density of PSD-95 clusters, spines or GluR2 surface expression (**Fig. 4a–c**). In 'rescue' experiments, cotransfection of wild-type LAR substantially inhibited the effect of RNAi of PTPδ or PTPσ on PSD-95 cluster density (**Fig. 4a,b**). The effect of LAR-RNAi on PSD-95 clusters was not rescued by wild-type LAR overexpression, presumably because the transfected LAR was still susceptible to the RNAi knockdown (**Fig. 4a,b**). These data provide strong evidence that the effects of LAR-RPTP RNAi are specific.

We made scatter plots of individual transfected neurons to examine the relationship between the degree of LAR-RPTP knockdown (measured by LAR-RPTP immunostaining intensity on dendrites) and density of PSD-95 clusters and dendritic spines (**Fig. 4d,e**). These scatter plots show a wide variation in the degree of LAR-RPTP knockdown induced by particular combinations of RNAi plasmids, perhaps owing in part to variable cotransfection of multiple plasmids. Nevertheless, reduction in LAR-RPTP staining was positively correlated with the number of LAR-RPTP family members targeted by RNAi (which was greatest with triple, followed by double and then single, RNAi). Furthermore, there was a strong correlation between the level of LAR-RPTP knockdown and the density of PSD-95 clusters and dendritic spines (**Fig. 4d,e**). These RNAi results corroborate the conclusion from dominant-negative experiments that LAR-RPTP is required for the normal density of spines and excitatory synapses.

Effect of LAR mutant constructs on synaptic function

To analyze the effects of LAR dominant-negative constructs on synaptic function, we quantified mEPSCs, which represent synaptic responses to spontaneous quantal release of neurotransmitter (**Fig. 5**). Hippocampal neurons overexpressing Myr-D2 or C1552S showed a lower peak amplitude and frequency of mEPSCs than did cells expressing GFP alone (**Fig. 5c,d**). The decreased mEPSC amplitude is generally taken to signify a reduced postsynaptic AMPA receptor response. The lower frequency of mEPSCs could be attributable to the reduced density of excitatory synapses in these cells, but presynaptic effects resulting from postsynaptic expression of LAR mutants cannot be excluded. Overexpression of wild-type LAR did not affect mEPSC amplitude but significantly increased the mEPSC frequency (**Fig. 5c,d**). The latter result was unexpected, given that LAR overexpression had little effect on the morphological density of synapses. Overall, the electrophysiological data bolsters the conclusion that postsynaptic function of LAR-RPTP is important for supporting

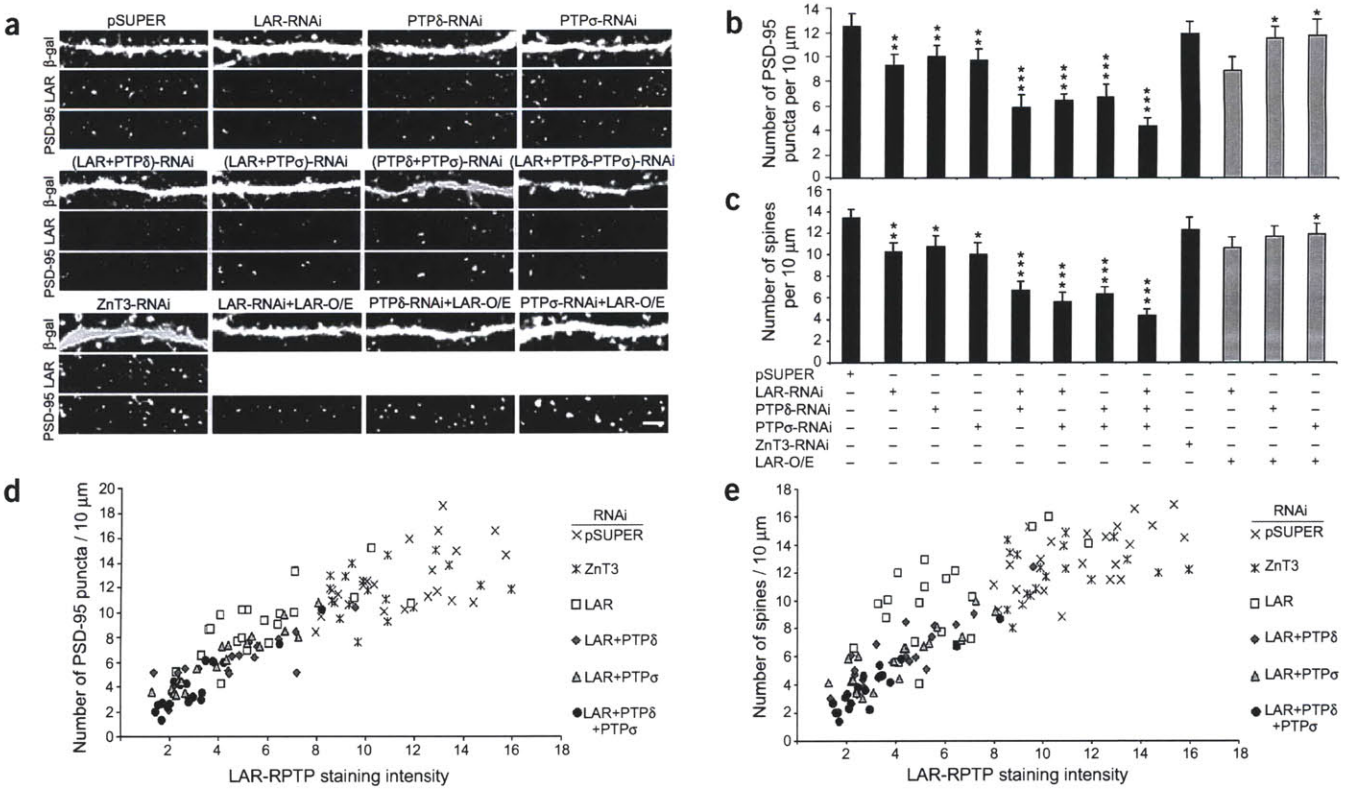

Figure 4 RNAi knockdown of LAR-RPTP reduces the density of synapses and spines. (**a**) Hippocampal neurons were cotransfected at DIV13 with β-galactosidase (β-gal) and either empty vector (pSUPER) or RNAi plasmids against LAR, PTPδ, PTPσ or ZnT3, in single, double or triple combinations, as indicated. 'LAR-O/E' indicates cotransfection with plasmid expressing wild-type LAR. At DIV16, neurons were stained for β-gal (to outline dendrite morphology), endogenous LAR and PSD-95, as indicated. Representative dendritic segments are shown. Scale bar, 8 μm. (**b**,**c**) Quantification of number of PSD-95 puncta and dendritic spines per 10 μm dendrite length in neurons transfected with RNAi constructs as in **a**. Histograms show mean ± s.e.m. (20 neurons analyzed for each condition). (*$P < 0.05$, **$P < 0.01$, ***$P < 0.001$). *P* values are calculated relative to pSUPER control for all conditions except the LAR-O/E 'rescue' experiments, which are calculated relative to RNAi alone. (**d**,**e**) Scatter graph of LAR-RPTP staining intensity of individual neurons from **b** and **c**, plotted against the number of PSD-95 clusters (**d**) and spine density (**e**) in those same neurons.

the surface expression of AMPA receptors and a normal density of excitatory synapses.

Phosphatase activity of LAR targets β-catenin to spines

Tyrosine dephosphorylation of β-catenin is associated with its accumulation in dendritic spines[25], but the tyrosine phosphatase responsible is unknown. We tested the hypothesis that LAR-RPTP mediates the recruitment of β-catenin to spines.

When transfected in neurons alone or with a β-galactosidase control, GFP-tagged β-catenin showed a punctate distribution in the cell body, dendritic shafts and spines (**Fig. 6a**)[25]. Cotransfection of LAR mutant C1522S caused loss of GFP–β-catenin signal from dendrites and accumulation of GFP–β-catenin in the cell body (**Fig. 6**). Dendritic targeting of GFP–β-catenin was also inhibited by overexpression of LAR mutants Myr-D2, ΔD2, R1149A and liprin-α1A (which lacks GRIP binding) but was unaffected by wild-type LAR, C1813S or liprin-α1 (**Fig. 6a,b**). These results indicate that the accumulation of GFP–β-catenin in dendrites and spines depends on LAR-RPTP phosphatase activity and on interactions between GRIP, liprin-α and LAR-RPTP.

To test whether the distribution of endogenous β-catenin is also regulated by its phosphorylation state, we applied a protein tyrosine phosphatase inhibitor (pervanadate) or protein tyrosine kinase inhibitor (genistein) to hippocampal neurons for 1 h. Genistein enhanced synaptic localization of β-catenin as shown by increased colocalization with PSD-95 (**Fig. 7**). Pervanadate, which should increase tyrosine phosphorylation of β-catenin, reduced the colocalization of β-catenin and PSD-95 and increased the number of β-catenin puncta inside dendritic shafts (**Fig. 7**). These findings confirm that synaptic localization of β-catenin is regulated by the opposing actions of tyrosine kinases and phosphatases[25].

We also examined the effect of LAR mutants on endogenous β-catenin and cadherin. Hippocampal neurons transfected with constructs that perturbed LAR–liprin-α binding, LAR phosphatase activity or LAR cleavage reduced the dendritic clusters of β-catenin and cadherin (**Supplementary Fig. 3**). Liprin-α1A had a similar inhibitory effect, whereas wild-type LAR, liprin-α1 and Myr-Vector did not change β-catenin or cadherin clustering (**Supplementary Fig. 3**). We conclude that LAR-RPTP, and interactions between LAR-RPTP, liprin-α and GRIP, are involved in the synaptic recruitment of the cadherin–β-catenin complex. These results support the idea that tyrosine dephosphorylation of β-catenin is mediated by LAR-RPTP.

β-catenin associates with GRIP–liprin-α–GluR2/3 in brain

Because AMPA receptor recruitment to synapses relies similarly on LAR–liprin-α–GRIP interactions (see above and ref. 9), we hypothesized that β-catenin might be assembled together with AMPA receptors in the liprin-α–GRIP protein complex and therefore transported together to synapses by the same mechanisms.

To test this hypothesis, we performed coimmunoprecipitation experiments with deoxycholate (DOC) extracts of rat cerebral cortex

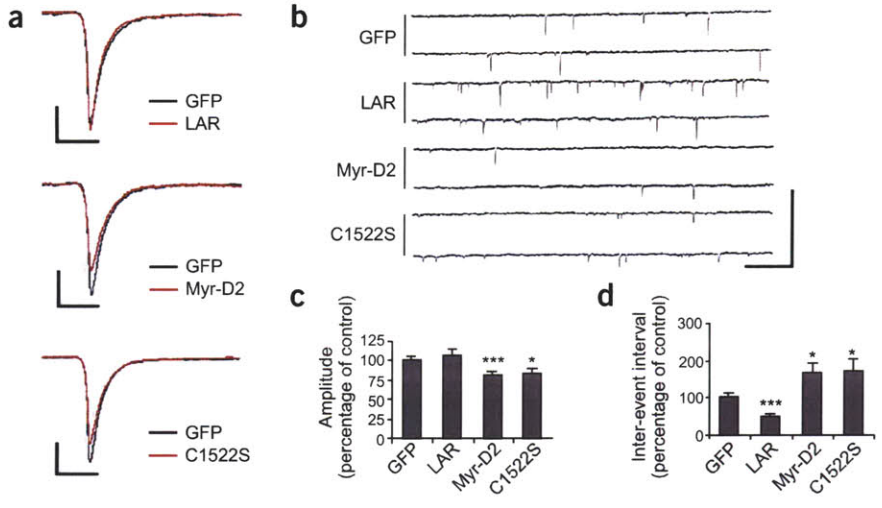

Figure 5 Effects of dominant-negative LAR constructs on synaptic function. Hippocampal neurons in dissociated culture were cotransfected with GFP alone or in combination with wild-type LAR, Myr-D2 or C1522S. (**a**) Averaged traces showing the effect of wild-type LAR, Myr-D2 and C15522S mutants (red trace) on the time course and peak amplitude of mEPSCs compared with control cells transfected with GFP only (black trace). Scales: 20 ms, 5 pA (LAR); 20 ms, 5 pA (Myr-D2); 20 ms, 6 pA (C1522S). (**b**) Representative recordings of AMPA receptor–mediated mEPSCs from neurons at DIV15 (transfected at DIV11 with the indicated constructs). Scale: 1,000 ms, 50 pA. (**c**,**d**) Quantification of mEPSC peak amplitude and mEPSC inter-event interval from hippocampal neurons transfected with the indicated constructs. Histograms show mean ± s.e.m. (>14 neurons analyzed for each construct; $^{*}P < 0.05$, $^{***}P < 0.001$).

(**Fig. 8**). Consistent with our earlier study[9], GluR2/3 and GRIP were robustly coprecipitated with the antibody to liprin-α (anti–liprin-α; **Fig. 8a**, lane 8), as were GluR2/3 and liprin-α with anti-GRIP (**Fig. 8a**, lane 11). In addition, liprin-α and GRIP antibodies also precipitated β-catenin and cadherin (**Fig. 8a**, lanes 8, 11). There was substantial coimmunoprecipitation of β-catenin with liprin-α and GRIP antibodies even when the coimmunoprecipitation of LAR in the same reaction was negligible (**Fig. 8a**, top row). Thus it is unlikely that cadherin–β-catenin association with liprin–GRIP is mediated by LAR. As negative controls, the NMDA receptor subunit NR2B was not coprecipitated by GRIP or liprin-α antibodies, and none of the analyzed proteins were precipitated by non-immune rabbit IgG (**Fig. 8a**, lane 2). These biochemical data imply that some fraction of β-catenin and cadherin is present in the liprin-α–GRIP complex, together with AMPA receptors.

We have previously shown that LAR-RPTP could be coimmunoprecipitated with liprin-α-GRIP, but only upon chemical cross-linking of brain extracts[9]. In DOC rat brain extracts, the coimmunoprecipitation of liprin-α, GRIP and GluR2/3 with LAR D5013 antibodies was close to background; nevertheless, β-catenin and cadherin were found in these LAR immunoprecipitates (**Fig. 8a**, lane 5), consistent with a previous study in PC12 cells[28]. These biochemical data suggest that one pool of cadherin–β-catenin is associated with the GRIP–liprin-α complex independently of LAR-RPTP, and another pool of β-catenin–cadherin is associated with LAR-RPTP independently of GRIP–liprin-α.

β-Catenin is a substrate of LAR-RPTP

To test whether native β-catenin is phosphorylated on tyrosine, phosphotyrosine-containing proteins were immunoprecipitated from SDS-denatured adult rat brain extracts with anti-phosphotyrosine (PY20) and immunoblotted for β-catenin and other proteins (**Fig. 8b**). β-catenin was precipitated by PY20, and this precipitation was competed by excess phosphotyrosine but not by phosphoserine, indicating that β-catenin contains phosphotyrosine (**Fig. 8b**).

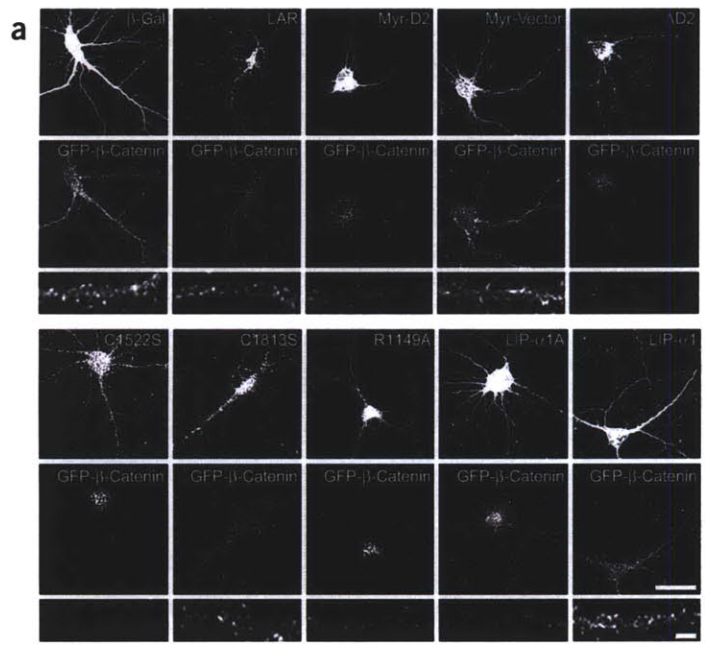

Figure 6 Overexpression of LAR and liprin-α interfering constructs disrupt the localization of exogenous GFP–β-catenin. (**a**) Cultured hippocampal neurons were cotransfected with GFP-tagged β-catenin (GFP–β-catenin) and β-galactosidase (β-gal) or the indicated LAR or liprin-α constructs. Neurons were double-labeled for the transfected proteins and GFP. Higher-magnification panels show GFP–β-catenin in individual dendritic segments. (**b**) Quantification of the dendrite/cell body distribution of GFP–β-catenin. Histograms (mean ± s.e.m.) show the dendrite/cell body ratio of staining intensity per area of GFP–β-catenin. The dendrites and cell bodies of neurons expressing GFP–β-catenin were carefully traced. The average fluorescence staining intensity of the traced regions was measured and expressed in arbitrary units of fluorescence per square area. Scale bars: upper panels, 40 μm; bottom panels, 4 μm. ($^{*}P < 0.05$, $^{**}P < 0.01$.)

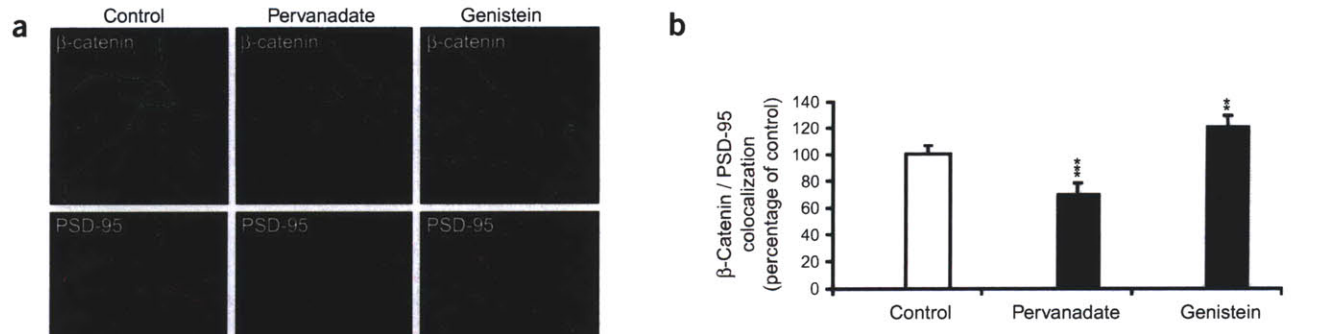

Figure 7 Effect of protein tyrosine phosphatase and tyrosine kinase inhibitors on synaptic localization of endogenous β-catenin. (**a**) Hippocampal neurons at DIV20 were left untreated (control) or treated for 1 h with pervanadate (200 μM) or genistein (100 μM), and then double-labeled for endogenous β-catenin (green) and PSD-95 (red). Higher magnifications of individual dendritic segments are shown at bottom. Scale bars: 80 μm in upper panels, 8 μm in bottom panels. (**b**) Quantification (mean ± s.e.m.) of colocalization of endogenous β-catenin clusters with PSD-95 clusters in hippocampal neurons treated with pervanadate or genistein, normalized to control untreated neurons. (**$P < 0.01$; ***$P < 0.001$.)

Similar results were obtained for cadherin and GluR2/3. We estimate that ~5–10% of β-catenin, cadherin and LAR, and ~2% of GluR2/3, are tyrosine phosphorylated in the adult rat brain, compared to ~10% for NR2B, a known tyrosine phosphoprotein[35] (**Fig. 8b**). Liprin-α, GRIP, NR1, and PSD-95 were not detectably tyrosine phosphorylated in this assay (**Fig. 8b**). Thus cadherin, β-catenin and GluR2/3, whose synaptic targeting is regulated by LAR-RPTP, are tyrosine phosphorylated in the brain, making them plausible substrates for LAR-RPTP.

Can LAR directly dephosphorylate β-catenin? Wild-type LAR, C1522S and C1813S mutants were expressed in and immunopurified from COS-7 cells and incubated with tyrosine-phosphorylated β-catenin immunoprecipitated from transfected COS-7 cells treated with pervanadate. The tyrosine phosphorylation of β-catenin (quantified by immunoblotting with anti-PY20, relative to total β-catenin signal) was reduced by incubation with wild-type and C1813S LAR, but not with the C1522S mutant that lacks phosphatase activity (**Fig. 8c,d**).

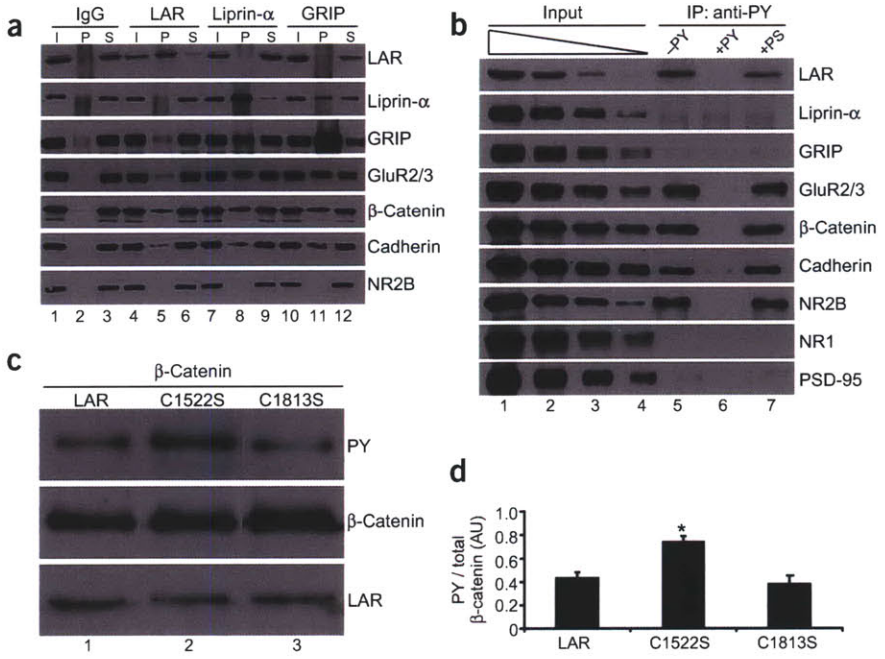

Figure 8 Association and tyrosine phosphorylation of cadherin, β-catenin, liprin-α, GRIP, AMPA receptors and LAR-RPTP in rat brain. (**a**) Coimmunoprecipitation (co-IP) of cadherin, β-catenin, liprin-α, GRIP, GluR2/3 and LAR-RPTP from rat cortex. Extracts were immunoprecipitated with non-immune rabbit IgG or antibodies indicated at top. Each IP reaction is shown in three lanes: I, input to IP reaction; P, precipitated pellet; and S, supernatant remaining after IP (10% of each loaded). Probed proteins are indicated at right. (**b**) Tyrosine phosphorylation of cadherin, β-catenin and GluR2/3 in rat brain. Precipitates (lanes 5–7) from anti-phosphotyrosine IP (–PY, without phosphotyrosine; +PY, 5 mM phosphotyrosine; +PS, 5 mM phosphoserine) were immunoblotted for the indicated proteins. Lanes 1–4 show successive twofold dilutions of input, used as calibration for estimating percentage tyrosine phosphorylation of the proteins. The following fractions of input and immunoprecipitate were loaded in the first lane of input (lane 1) and in the IP (lanes 5–7) for the specified proteins: LAR, GRIP, liprin-α, 5% and 40%; β-catenin and cadherin, 5% and 10%; NR2B, NR1 and PSD-95, 2.5% and 10%; GluR2/3, 1% and 10%. (**c**) LAR dephosphorylates β-catenin *in vitro*. Myc-tagged wild-type, C1522S or C1813S LAR proteins were overexpressed in and immunoprecipitated from COS-7 cells, and incubated with β-catenin–GFP immunopurified from transfected COS cells treated with pervanadate as described in Methods. (**d**) Quantification of β-catenin dephosphorylation by LAR mutants. Histograms (mean ± s.e.m.; $n = 3$) show ratio of signal for tyrosine-phosphorylated (PY) β-catenin divided by total β-catenin signal (arbitrary units of integrated immunoblot density) in the presence of wild-type LAR, C1522S or C1813S ($P = 0.009$).

These results demonstrate that, at least *in vitro*, β-catenin can serve as a direct substrate for LAR tyrosine phosphatase.

DISCUSSION

LAR function in synapse morphogenesis

Our dominant-interfering experiments show that in cultured hippocampal neurons, the normal density of excitatory synapses and dendritic spines depend on (i) tyrosine phosphatase activity of LAR-RPTP, (ii) protein interactions mediated by the LAR D2 domain (the binding site of liprin-α), (iii) endoproteolytic cleavage of LAR and (iv) protein interactions mediated by the extreme C-terminus of liprin-α (the binding site of GRIP). The importance of LAR-RPTPs in the postsynaptic cell is confirmed by single and multiplex RNAi, which show a correlation between LAR-RPTP protein knockdown and the loss of synapses and dendritic spines. The functional role of LAR-RPTP in synapses is further corroborated by electrophysiological studies: amplitude and frequency of mEPSCs are diminished when LAR activity is disrupted in the postsynaptic cell.

It is uncertain how disruption of LAR cleavage would lead to a dominant-negative effect, but proteolytic processing is known to regulate subcellular distribution of LAR-RPTPs, which might be important for enzymatic activity and substrate specificity[15]. Nevertheless, the R1149A LAR mutant was expressed on the surface of transfected neurons (data not shown). We do not exclude the possibility that the C1522S mutant acts as a dominant negative by 'substrate trapping' of proteins whose actual dephosphorylation is irrelevant to the normal function of LAR. However, the same phenotype was obtained with other LAR mutants that should not cause substrate trapping, as well as by specific RNAi of LAR-RPTPs. Therefore, there seems little doubt that LAR-RPTP activity is important for synapse morphogenesis and function.

In addition to the liprin-α family of proteins[16–18], a rho/rac guanine nucleotide exchange factor named Trio can interact with the D2 domain of LAR[36]. It is therefore possible that the LAR constructs Myr-D2 and ΔD2 are perturbing additional interactions beyond liprin-α. Genetic deletion or RNAi knockdown of liprin-α proteins (which are encoded by four genes) would help clarify this issue. Similarly, it could be argued that the liprin-α1A effect could be due to interference with any interaction mediated by the C-terminus of liprin-α1, although in this case, the only known binding partner is GRIP/ABP. With these caveats noted, it is notable how multiple constructs that interfere in different ways with LAR function, LAR-liprin-α interaction or liprin-α-GRIP interaction elicit similar morphological effects on synapses. Thus, we conclude that the development and maintenance of excitatory synapses requires the function of LAR-RPTP and is most likely to require the specific interactions between LAR-RPTP, liprin-α, and GRIP.

Because the dominant-negative LAR constructs could act on any of the LAR family of RPTPs, these experiments cannot distinguish whether one or all LAR-family phosphatases are involved in synapse and spine morphogenesis. However, the RNAi data imply that all three members of the LAR-RPTP family have overlapping functions in hippocampal neurons and contribute significantly to the regulation of synapse density.

Another important conclusion of this study is that LAR-RPTP function and LAR–liprin-α–GRIP interactions are also crucial for the dendritic targeting of β-catenin and cadherin. Tyrosine phosphorylation of β-catenin reduces its association with cadherin[37], whereas tyrosine dephosphorylation promotes accumulation of β-catenin in dendritic spines[25]. We find that LAR-RPTP is enriched in synapses and that β-catenin is a direct substrate of LAR tyrosine phosphatase *in vitro*. Our results implicate LAR-RPTP as the specific tyrosine phosphatase responsible for dephosphorylation and synaptic recruitment of β-catenin.

AMPA receptors and β-catenin in the liprin-α–GRIP complex

LAR-RPTP phosphatase activity and LAR–liprin-α–GRIP interactions are important for the dendritic targeting of the cadherin–β-catenin complex and AMPA receptors. Moreover, cadherin–β-catenin and AMPA receptors are coimmunoprecipitated to a substantial degree with liprin-α and GRIP. We propose that a subpopulation of cadherin–β-catenin and GluR2/3 are assembled in the same protein 'packet' by GRIP–liprin-α scaffolds and that this protein complex is targeted to postsynaptic sites by a common mechanism involving tyrosine dephosphorylation by LAR-RPTP. Immunoelectron microscopic and/or biochemical evidence that AMPA receptors and cadherin–β-catenin coexist in the same membrane vesicles are needed to support this hypothesis.

The specific interaction between liprin-α and the D2 domain of LAR-RPTP provides a mechanism for the recruitment of the GRIP–liprin-α protein complex to LAR-RPTP, which is concentrated in synapses. As a result, components of the GRIP–liprin-α complex (such as β-catenin) become subject to tyrosine dephosphorylation by the D1 domain of LAR-RPTP, resulting in accumulation of β-catenin in spines. Because tyrosine dephosphorylation enhances the interaction between β-catenin and cadherin, LAR-RPTP promotes not only the synaptic accumulation of β-catenin but also the cell adhesion function of the cadherin–β-catenin complex at synapses, leading to growth of the synapse and spine.

GluR2/3 is also tyrosine phosphorylated in neurons, and tyrosine phosphorylation is correlated with loss of surface AMPA receptors[38]. It remains to be determined whether AMPA receptor accumulation in synapses is regulated by tyrosine dephosphorylation of GluR2/3 by LAR-RPTPs. In any case, both the cadherin–β-catenin complex and GluR2 can promote growth and/or stabilization of synapses and dendritic spines[24,39]. Thus, the recruitment of the cadherin–β-catenin complex and AMPA receptors to synapses by LAR-RPTP could explain why LAR-RPTP phosphatase activity and D2 interactions are important for normal synapse and spine morphogenesis.

Coordination of synapse morphology and function

There is a good correlation between the size of the dendritic spine head, the strength of postsynaptic response, and the abundance of AMPA receptors in the synapse[40]. AMPA receptors themselves might contribute to the coordinate regulation of morphology and function, because the GluR2 subunit, through its N-terminal extracellular domain, promotes spine growth[39]. Our findings here provide another potential mechanism for matching synapse growth with synaptic potentiation, namely the coordinate recruitment to synapses of 'structural' molecules (cadherin–β-catenin adhesion complex) and 'functional' molecules (AMPA receptor channels) by the action of LAR-RPTP (see also ref. 25).

Another highly correlated feature of excitatory synapses is the size of PSD and presynaptic active zone[41,42]. The molecular mechanisms that match presynaptic and postsynaptic size and shape are unclear, but trans-synaptic protein-protein interactions are good candidates. Cadherins are attractive as presynaptic-postsynaptic matchmakers because they function as homophilic adhesion molecules and are present on both sides of the synapse[43,44]. The coordinate recruitment of the cadherin–β-catenin complex with AMPA receptors to postsynaptic sites could generate a retrograde 'growth promoting' signal to the presynaptic terminal through trans-synaptic homophilic interactions of cadherin[25].

In this respect, it is noteworthy that LAR-RPTP, liprin-α and GRIP are also present in axons and presynaptic sites[7,9], where they probably have functions analogous to those in dendrites. It is possible that the cadherin–β-catenin complex is transported to the presynaptic membrane by the same liprin-α–GRIP–LAR-RPTP system as proposed for the dendritic compartment. Consistent with a presynaptic role for these proteins, studies in *Drosophila* and *C. elegans* have shown that LAR and liprin-α mutants are defective in growth of the synapse, structure of the active zone and efficacy of neurotransmitter release[19,20]. In *Drosophila* NMJ development, liprin-α is required for LAR function but not required for the synaptic localization of LAR[20]. These genetic findings suggest that liprin-α acts 'downstream' of LAR and are consistent with our model in which liprin-α links LAR to its tyrosine phosphatase substrates through specific protein-protein interactions.

METHODS

Antibodies. Rabbit polyclonal LAR-RPTP antibodies (D5013) were raised against a fusion protein of the human LAR phosphatase domain D1 (amino acids 1315–1607) and affinity purified. Affinity-purified rabbit anti-GRIP[7,45], anti-liprin[9], anti-NR2B[46] and mouse anti-PSD-95 (ref. 47) were previously described. Details of other antibodies used in this study are in the **Supplementary Methods** online.

DNA constructs. The mammalian expression constructs for LAR[14], liprin-α1 and liprin-α1A[16] have been described. To generate the mammalian expression construct encoding domain D2 of LAR (Myr HA-D2), a DNA cassette encoding in tandem a HA epitope tag (YPYDVPDYA) and myristoylation modification sequence (MGQSLTTHA) was generated by PCR using two overlapping oligonucleotides and inserted into the polylinker region of the mammalian expression vector pGW1 (CMV promoter). The D2 domain of LAR (amino acids 1614–1881) was amplified by PCR and subcloned in frame downstream of the HA tag and myristoylation modification sequence. The phosphatase D2 domain deletion mutant (ΔD2), and LAR mutants containing cysteine-to-serine (C1522S and C1813S) and arginine-to-alanine (R1149A) missense mutations, were generated by site-directed mutagenesis using the QuikChange system (Stratagene).

Immunocytochemistry of hippocampal neurons. Surface staining of endogenous receptors was performed as previously described[9] using antibodies recognizing extracellular regions of AMPA receptor subunit GluR1 (Oncogene), GluR2 or $GABA_A$ receptor β-subunit (Chemicon). Transfected proteins were labeled with anti-HA (1 μg ml^{-1}) or anti-Myc antibodies (1 μg ml^{-1}).

Live imaging of hippocampal neurons. Time-lapse images were acquired by using LSM510 confocal system on Axiovert microscope (Zeiss). During confocal scanning, neurons were kept on a 37 °C microscope stage incubator in 5% CO_2. To avoid neuronal toxicity, the intensity of the argon laser was minimized and the images were taken at maximum speed. Between imaging sessions, the neurons were placed back in the incubator. The position of neurons on the coverslip was retained by LSM software for subsequent imaging.

Electrophysiology. Rat hippocampal neurons were transfected at DIV10–11 using calcium phosphate. Whole-cell recordings were obtained at room temperature (23–25 °C) from GFP-fluorescent spindle-shaped pyramidal neurons at DIV14–15. Cells were recorded in Tyrode's solution containing (in mM) NaCl, 124; KCl, 5; $CaCl_2$, 2; $MgCl_2$, 1; glucose, 30; and HEPES, 25 (pH 7.4 with NaOH). Tetrodotoxin (1 μm), picrotoxin (50 μm) and AP5 (20 μM) were added to block action potentials, GABAergic transmission and NMDA receptor–mediated mEPSC components, respectively. Intracellular pipette solution contained (mM) potassium gluconate, 120; KCl, 3; HEPES, 10; NaCl, 8,000; $CaCl_2$, 500; EGTA, 5; magnesium ATP, 2 and GTP, 0.03. Recordings were made with an Axon Instruments 200B amplifier with a 1-kHz Bessell low-pass filter. Miniature EPSCs were detected by custom software using a template-matching algorithm[48]. Once all mEPSCs were located, their peak amplitudes and intervals were calculated.

Coimmunoprecipitation studies. Sodium deoxycholate extracts of rat cortex were immunoprecipitated with non-immune rabbit immunoglobulins (IgG) or with antibodies to LAR, liprin-α, and GRIP, as previously described[9] and were probed for LAR, liprin-α, GRIP, GluR2/3, β-catenin, cadherin, and NR2B.

Tyrosine phosphorylation studies. Boiled SDS extracts of rat cortex were immunoprecipitated with phosphotyrosine antibody (PY20) as previously described[49] in the absence or presence of phosphotyrosine (5 mM) or phosphoserine (5 mM) as indicated across the top of **Figure 8b,** and were probed for LAR, liprin-α, GRIP, GluR2/3, β-catenin, cadherin, NR2B, NR1 and PSD-95.

***In vitro* tyrosine phosphatase assay.** Wild-type LAR, LAR mutants C1522S and C1813S (Myc-tagged) and β-catenin (GFP-tagged) were individually expressed in COS-7 cells. A day after transfection, cells were serum-starved and the β-catenin–expressing cells were treated with 200 μm pervanadate for 15 min. Deoxycholate extracts of transfected cells were precipitated with anti-Myc (LAR, C1522S and C1813S) or anti-GFP antibodies and washed as previously described[7]. Immunoprecipitated β-catenin was eluted with 50 mM glycine, pH 2.5, neutralized with 1.0 M Tris-HCl, pH 8.5 and incubated with the immunoprecipitated LAR, C1522S or C1813S proteins (on protein A–Sepharose beads) for 30 min at 25 °C. Reactions were terminated by the addition of sample buffer. Tyrosine phosphorylation of β-catenin was detected by immunoblotting with anti-phosphotyrosine antibody (PY20); and total β-catenin protein with anti-GFP antibody and for total LAR protein (the full-length 220-kDa protein is shown in **Figure 8c**) using anti-Myc antibody.

LAR-RPTP RNA interference in hippocampal neurons. RNAi sequences consisted of nucleotides 5′-GAAAGTCAGCTCCCAGCGC-3′ of rat LAR mRNA (NM_019249), 5′-GTGCCGGCTAGAAACTTGT-3′ of rat PTPδ mRNA (NM_233065), and 5′-GCCACACACCTTCTATAAC-3′ of rat PTPσ mRNA (NM_019140). The complementary oligonucleotides were annealed and inserted into the pSuper vector (Oligoengine)[50]. The efficiency and specificity of the various RNAi plasmids for knockdown of LAR, PTPδ and PTPσ were determined by cotransfection in COS-7 cells (**Supplementary Fig. 5**).

Image analysis and quantification. Confocal images of single- and double-transfected neurons were obtained using a Zeiss 63× (NA 1.4) objective with sequential acquisition settings at the maximal resolution of the confocal (1280 × 1024 pixels). Each image was a *z*-series of 7–12 images averaged 2–3 times with a Kalman filter and taken at 0.75-μm depth intervals. The resultant stack was 'flattened' into a single image using a maximum projection. The confocal microscope settings were kept the same for all scans. Morphometric analysis and quantification were done using MetaMorph image analysis software (Universal Imaging). Dendrites from transfected and untransfected cells were randomly selected and carefully traced, and the average intensity of surface fluorescence staining was then determined for the traced regions. Intensity measurements are expressed in arbitrary units of fluorescence per square area. For spine morphology studies, individual spines on dendrites were manually traced, and the maximum length and head width of each spine was automatically measured by computer and logged into Microsoft Excel. Blind conditions were used for the morphometric quantification of acquired images.

For quantification of GFP-tagged β-catenin signal (**Fig. 6**), we randomly selected and manually traced the dendrites and cell bodies of transfected neurons, and the average GFP staining intensity expressed in arbitrary units of fluorescence per square area was determined for the traced regions and computed as the ratio of dendrites to cell bodies (**Fig. 6b**).

Note: Supplementary information is available on the Nature Neuroscience website.

ACKNOWLEDGMENTS

The authors thank M. Streuli for kind gifts of LAR, liprin-α1 and liprin-α1A expression constructs, and S. Rudolph-Correia and B. Li for expert help. M.S. is an Investigator of the Howard Hughes Medical Institute.

COMPETING INTERESTS STATEMENT

The authors declare that they have no competing financial interests.

Received 13 December 2004; accepted 2 February 2005
Published online at http://www.nature.com/natureneuroscience/

1. Malinow, R. & Malenka, R.C. AMPA receptor trafficking and synaptic plasticity. *Annu. Rev. Neurosci.* **25**, 103–126 (2002).
2. Bredt, D.S. & Nicoll, R.A. AMPA receptor trafficking at excitatory synapses. *Neuron* **40**, 361–379 (2003).
3. McGee, A.W. & Bredt, D.S. Assembly and plasticity of the glutamatergic postsynaptic specialization. *Curr. Opin. Neurobiol.* **13**, 111–118 (2003).
4. Sheng, M. & Lee, S.H. AMPA receptor trafficking and the control of synaptic transmission. *Cell* **105**, 825–828 (2001).
5. Dong, H. *et al.* GRIP: a synaptic PDZ domain-containing protein that interacts with AMPA receptors. *Nature* **386**, 279–284 (1997).
6. Srivastava, S. *et al.* Novel anchorage of GluR2/3 to the postsynaptic density by the AMPA receptor-binding protein ABP. *Neuron* **21**, 581–591 (1998).
7. Wyszynski, M. *et al.* Association of AMPA receptors with a subset of glutamate receptor-interacting protein *in vivo*. *J. Neurosci.* **19**, 6528–6537 (1999).
8. Sheng, M. & Sala, C. PDZ domains and the organization of supramolecular complexes. *Annu. Rev. Neurosci.* **24**, 1–29 (2001).
9. Wyszynski, M. *et al.* Interaction between GRIP and liprin-alpha/SYD2 is required for AMPA receptor targeting. *Neuron* **34**, 39–52 (2002).
10. Johnson, K.G. & Van Vactor, D. Receptor protein tyrosine phosphatases in nervous system development. *Physiol. Rev.* **83**, 1–24 (2003).
11. Serra-Pages, C., Saito, H. & Streuli, M. Mutational analysis of proprotein processing, subunit association, and shedding of the LAR transmembrane protein tyrosine phosphatase. *J. Biol. Chem.* **269**, 23632–23641 (1994).
12. Streuli, M., Krueger, N.X., Thai, T., Tang, M. & Saito, H. Distinct functional roles of the two intracellular phosphatase like domains of the receptor-linked protein tyrosine phosphatases LCA and LAR. *EMBO J.* **9**, 2399–2407 (1990).
13. Tsujikawa, K. *et al.* Distinct functions of the two protein tyrosine phosphatase domains of LAR (leukocyte common antigen-related) on tyrosine dephosphorylation of insulin receptor. *Mol. Endocrinol.* **15**, 271–280 (2001).
14. Streuli, M. *et al.* Expression of the receptor-linked protein tyrosine phosphatase LAR: proteolytic cleavage and shedding of the CAM-like extracellular region. *EMBO J.* **11**, 897–907 (1992).
15. Aicher, B., Lerch, M.M., Muller, T., Schilling, J. & Ullrich, A. Cellular redistribution of protein tyrosine phosphatases LAR and PTPsigma by inducible proteolytic processing. *J. Cell Biol.* **138**, 681–696 (1997).
16. Serra-Pages, C. *et al.* The LAR transmembrane protein tyrosine phosphatase and a coiled-coil LAR-interacting protein co-localize at focal adhesions. *EMBO J.* **14**, 2827–2838 (1995).
17. Serra-Pages, C., Medley, Q.G., Tang, M., Hart, A. & Streuli, M. Liprins, a family of LAR transmembrane protein-tyrosine phosphatase-interacting proteins. *J. Biol. Chem.* **273**, 15611–15620 (1998).
18. Pulido, R., Serra-Pages, C., Tang, M. & Streuli, M. The LAR/PTP delta/PTP sigma subfamily of transmembrane protein-tyrosine-phosphatases: multiple human LAR, PTP delta, and PTP sigma isoforms are expressed in a tissue-specific manner and associate with the LAR-interacting protein LIP.1. *Proc. Natl. Acad. Sci. USA* **92**, 11686–11690 (1995).
19. Zhen, M. & Jin, Y. The liprin protein SYD-2 regulates the differentiation of presynaptic termini in *C. elegans*. *Nature* **401**, 371–375 (1999).
20. Kaufmann, N., DeProto, J., Ranjan, R., Wan, H. & Van Vactor, D. *Drosophila* liprin-alpha and the receptor phosphatase Dlar control synapse morphogenesis. *Neuron* **34**, 27–38 (2002).
21. Li, Z. & Sheng, M. Some assembly required: the development of neuronal synapses. *Nat. Rev. Mol. Cell Biol.* **4**, 833–841 (2003).
22. Tang, L., Hung, C.P. & Schuman, E.M. A role for the cadherin family of cell adhesion molecules in hippocampal long-term potentiation. *Neuron* **20**, 1165–1175 (1998).
23. Goda, Y. Cadherins communicate structural plasticity of presynaptic and postsynaptic terminals. *Neuron* **35**, 1–3 (2002).
24. Togashi, H. *et al.* Cadherin regulates dendritic spine morphogenesis. *Neuron* **35**, 77–89 (2002).
25. Murase, S., Mosser, E. & Schuman, E.M. Depolarization drives beta-Catenin into neuronal spines promoting changes in synaptic structure and function. *Neuron* **35**, 91–105 (2002).
26. Nagafuchi, A., Ishihara, S. & Tsukita, S. The roles of catenins in the cadherin-mediated cell adhesion: functional analysis of E-cadherin-alpha catenin fusion molecules. *J. Cell Biol.* **127**, 235–245 (1994).
27. Ozawa, M. & Kemler, R. Altered cell adhesion activity by pervanadate due to the dissociation of alpha-catenin from the E-cadherin.catenin complex. *J. Biol. Chem.* **273**, 6166–6170 (1998).
28. Kypta, R.M., Su, H. & Reichardt, L.F. Association between a transmembrane protein tyrosine phosphatase and the cadherin-catenin complex. *J. Cell Biol.* **134**, 1519–1529 (1996).
29. Pulido, R., Krueger, N.X., Serra-Pages, C., Saito, H. & Streuli, M. Molecular characterization of the human transmembrane protein-tyrosine phosphatase delta. Evidence for tissue-specific expression of alternative human transmembrane protein-tyrosine phosphatase delta isoforms. *J. Biol. Chem.* **270**, 6722–6728 (1995).
30. Wallace, M.J., Fladd, C., Batt, J. & Rotin, D. The second catalytic domain of protein tyrosine phosphatase delta (PTP delta) binds to and inhibits the first catalytic domain of PTP sigma. *Mol. Cell. Biol.* **18**, 2608–2616 (1998).
31. Wang, Y.H. *et al.* Characterization of NMDA receptor subunit-specific antibodies: distribution of NR2A and NR2B receptor subunits in rat brain and ontogenic profile in the cerebellum. *J. Neurochem.* **65**, 176–183 (1995).
32. Schaapveld, R.Q. *et al.* Developmental expression of the cell adhesion molecule-like protein tyrosine phosphatases LAR, RPTPdelta and RPTPsigma in the mouse. *Mech. Dev.* **77**, 59–62 (1998).
33. Lee, S.H., Valtschanoff, J.G., Kharazia, V.N., Weinberg, R. & Sheng, M. Biochemical and morphological characterization of an intracellular membrane compartment containing AMPA receptors. *Neuropharmacology* **41**, 680–692 (2001).
34. Shin, H. *et al.* Association of the kinesin motor KIF1A with the multimodular protein liprin-alpha. *J. Biol. Chem.* **278**, 11393–11401 (2003).
35. Lau, L.F. & Huganir, R.L. Differential tyrosine phosphorylation of *N*-methyl-D-aspartate receptor subunits. *J. Biol. Chem.* **270**, 20036–20041 (1995).
36. Debant, A. *et al.* The multidomain protein Trio binds the LAR transmembrane tyrosine phosphatase, contains a protein kinase domain, and has separate rac-specific and rho-specific guanine nucleotide exchange factor domains. *Proc. Natl. Acad. Sci. USA* **93**, 5466–5471 (1996).
37. Roura, S., Miravet, S., Piedra, J., Garcia de Herreros, A. & Dunach, M. Regulation of E-cadherin/Catenin association by tyrosine phosphorylation. *J. Biol. Chem.* **274**, 36734–36740 (1999).
38. Ahmadian, G. *et al.* Tyrosine phosphorylation of GluR2 is required for insulin-stimulated AMPA receptor endocytosis and LTD. *EMBO J.* **23**, 1040–1050 (2004).
39. Passafaro, M., Nakagawa, T., Sala, C. & Sheng, M. Induction of dendritic spines by an extracellular domain of AMPA receptor subunit GluR2. *Nature* **424**, 677–681 (2003).
40. Matsuzaki, M. *et al.* Dendritic spine geometry is critical for AMPA receptor expression in hippocampal CA1 pyramidal neurons. *Nat. Neurosci.* **4**, 1086–1092 (2001).
41. Harris, K.M. & Stevens, J.K. Dendritic spines of CA 1 pyramidal cells in the rat hippocampus: serial electron microscopy with reference to their biophysical characteristics. *J. Neurosci.* **9**, 2982–2997 (1989).
42. Schikorski, T. & Stevens, C.F. Quantitative ultrastructural analysis of hippocampal excitatory synapses. *J. Neurosci.* **17**, 5858–5867 (1997).
43. Yagi, T. & Takeichi, M. Cadherin superfamily genes: functions, genomic organization, and neurologic diversity. *Genes Dev.* **14**, 1169–1180 (2000).
44. Fannon, A.M. & Colman, D.R. A model for central synaptic junctional complex formation based on the differential adhesive specificities of the cadherins. *Neuron* **17**, 423–434 (1996).
45. Wyszynski, M., Kim, E., Yang, F.C. & Sheng, M. Biochemical and immunocytochemical characterization of GRIP, a putative AMPA receptor anchoring protein, in rat brain. *Neuropharmacology* **37**, 1335–1344 (1998).
46. Sheng, M., Cummings, J., Roldan, L.A., Jan, Y.N. & Jan, L.Y. Changing subunit composition of heteromeric NMDA receptors during development of rat cortex. *Nature* **368**, 144–147 (1994).
47. Kim, E., Niethammer, M., Rothschild, A., Jan, Y.N. & Sheng, M. Clustering of Shaker-type K^+ channels by interaction with a family of membrane-associated guanylate kinases. *Nature* **378**, 85–88 (1995).
48. Clements, J.D. & Bekkers, J.M. Detection of spontaneous synaptic events with an optimally scaled template. *Biophys. J.* **73**, 220–229 (1997).
49. Dunah, A.W. & Standaert, D.G. Dopamine D1 receptor-dependent trafficking of striatal NMDA glutamate receptors to the postsynaptic membrane. *J. Neurosci.* **21**, 5546–5558 (2001).
50. Brummelkamp, T.R., Bernards, R. & Agami, R. A system for stable expression of short interfering RNAs in mammalian cells. *Science* **296**, 550–553 (2002).

Appendix D

Curriculum Vita

CURRICULUM VITAE

Emily Hueske
May 2011

Personal Details

Birth Place: Berlin, Germany
Nationality: American, German
Address: 77 Massachusetts Ave, Bldg 46-5295, Cambridge MA 02139

Education

2001-present **Massachusetts Institute of Technology**
Ph.D. Brain & Cognitive Sciences
Thesis Advisor: Dr. Susumu Tonegawa, Ph.D.
Ph.D. Thesis: "A Role for Dopamine Neuron NMDA Receptors in Learning and Decision-Making."

1996-2001 **University of Texas at Austin**
B.S. Chemistry
B.A. PlanII Humanities Honors

1995-1996 **Freie Universität Berlin, Germany**
Biology, Diplom track

Research Background

2005-present Current Research - Behavioral Genetics MIT, Cambridge, MA
PhD Thesis Title: *Role of NMDARs in Dopamine Neurons in Learning and Decision-Making.*
Thesis Advisor: Dr. Susumu Tonegawa, Ph.D.

2002-2005 Cellular Electrophysiology & Imaging MIT, Cambridge, MA
Project title: *Structural and functional distribution and regulation of presynaptic vesicular transporters, VGLUT1 and VGAT in hippocampal cell types.*
Advisor: Dr. Guosong Liu, M.D., Ph.D.
Published results: Wilson NR, et. al. *J.Neurosci.* 2005 Jun 29; 25(26):6221-34.

01/00-06/01 Electrochemistry Undergraduate Research Univ of Texas, Austin, TX
Project Title: *Development and characterization of Hemispherical Hg Ultramicroelectrode for biological detection of Tl+.*
Supervisor: Dr. Alan J. Bard, Ph.D.
Results published: Mauzeroll J, Hueske E, Bard AJ. *Analytical Chemistry.* 2003 Aug 1;75(15):3880-9.

06/99-08/99 Undergraduate Research Fellowship UT Southwestern, Dallas, TX
Project Title: *Impact of HIV on the aging thymus.*
Mentor: Dr. Daniel Douek, M.D., Ph.D.

Membership in Professional Societies

2002-present Society for Neuroscience
1999-2002 American Chemical Society

Awards & Fellowships

2005 BCS Team Teaching Award
Department of Brain & Cognitive Science, MIT
2004 Poitras Research Fellowship
Massachusetts Institute of Technology
2002 NSF Graduate Fellowship Honorable Mention
National Science Foundation
2001 Presidential Graduate Fellowship
Massachusetts Institute of Technology
2001 Phi Beta Kappa
University of Texas Chapter
2001 Kolthoff Award for Young Analytical Chemist
ACS National Mtg, San Diego (11 nationally)
2000 Undergraduate Research Fellowship
University of Texas at Austin
1999 Summer Undergraduate Research Fellowship
UT Austin & UT Southwestern Medical Center

Publications

Wilson NR, Kang JS, Hueske EA, Leung T, Varoqui H, Murnick JM, Erickson J, Liu G. Presynaptic control of excitatory transmission by vesicular transporter expression. *J.Neurosci.* 2005 Jun 29;25(26):6221-34.

Dunah AW, Hueske E, Wyszynski M, Hoogenraad CC, Jaworski J, Pak DT, Simonetta A, Liu G, Sheng M. LAR receptor protein tyrosine phosphatases in the development and maintenance of excitatory synapses. *Nature Neurosci.* 2005 Apr;8(4):458-67.

Mauzeroll J, Hueske E, Bard AJ. Scanning electrochemical microscopy. 48. Hg/Pt hemispherical ultramicroelectrodes: fabrication and characterization. *Anal Chem.* 2003 Aug 1;75(15):3880-9.

Abstracts & Talks

Invited Speaker. *Circuit Genetic Approaches to Study of Dopamine Function.* MIT Department of Comparative Medicine: Continuing Education Lecture Series, July 29, 2009.

E. A. Hueske, J. S. Kang, G. Liu. Postsynaptic cell-type dependent regulation of presynaptic vesicular transporters. *2005 Meeting on Imaging Neurons and Neural Activity Poster Abstracts.* Cold Spring Harbor: CSHL Meeting, May, 2005.

E. A. Hueske, J. S. Kang, G. Liu. Structural and Functional Balance of Excitation and Inhibition in Cultured Hippocampal Neurons. 2003 *Abstract Viewer/Itinerary Planner.* Program No. 256.20. New Orleans: Society for Neuroscience, 2003. Online.

E. A. Hueske. Structural and functional balance of excitatory and inhibitory inputs to hippocampal pyramidal neurons. Talk presented at *Brain Lunch.* Department of Brain & Cognitive Sciences, MIT, Cambridge, MA. November 2002.

E. A. Hueske, J. Mauzeroll. Fabrication and characterization of Hg^{+} ultramicroelectrode for measurement of Tl^{+} currents. San Diego: American Chemical Society National Meeting, 2001.

Teaching Experience

2003-2006	**Introduction to Neuroanatomy**	MIT, Cambridge, MA
	Volunteer Instructor – MIT Educational Studies Program	
	Designed, prepared and co-taught four annual two-day high school neuroanatomy and sheep brain dissection courses. (2 instructors)	
2005	**Experimental Molecular Neurobiology**	MIT, Cambridge, MA
	Teaching Assistant – Dept. of Brain & Cognitive Sciences	
	Prepared lab materials and advised students on lecture material. Awarded BCS Team teaching award. (4 teaching assistants)	
2003	**Introduction to Neurobiology**	MIT, Cambridge, MA
	Teaching Assistant – Dept. of Brain & Cognitive Sciences	
	Advised students on lecture material. (3 teaching assistants)	
2003	**After-School Science Initiative**	EastEnd House, Cambridge, MA
	Volunteer Instructor	
	Designed, prepared and taught 8 science labs for elementary school age kids. (Taught individually).	
2002	**Introduction to Psychology**	MIT, Cambridge, MA
	Teaching Assistant – Dept. of Brain & Cognitive Sciences	
	Prepared and delivered supporting lectures for 12 weekly recitation sections. Advised on research writing and lectures. (Taught individually)	

Bibliography

Bayer, H. M. and P. W. Glimcher (2005). Midbrain dopamine neurons encode a quantitative reward prediction error signal. *Neuron 47*(1), 129–41.

Bonci, A. and R. C. Malenka (1999). Properties and plasticity of excitatory synapses on dopaminergic and gabaergic cells in the ventral tegmental area. *J Neurosci 19*(10), 3723–30.

Cagniard, B., J. A. Beeler, J. P. Britt, D. S. McGehee, M. Marinelli, and X. Zhuang (2006). Dopamine scales performance in the absence of new learning. *Neuron 51*(5), 541–7.

Chergui, K., H. Akaoka, P. J. Charlety, C. F. Saunier, M. Buda, and G. Chouvet (1994). Subthalamic nucleus modulates burst firing of nigral dopamine neurones via nmda receptors. *Neuroreport 5*(10), 1185–8.

Chergui, K., P. J. Charlety, H. Akaoka, C. F. Saunier, J. L. Brunet, M. Buda, T. H. Svensson, and G. Chouvet (1993). Tonic activation of nmda receptors causes spontaneous burst discharge of rat midbrain dopamine neurons in vivo. *Eur J Neurosci 5*(2), 137–44.

Costa, R. M. (2007). Plastic corticostriatal circuits for action learning: what's dopamine got to do with it? *Ann N Y Acad Sci 1104*, 172–91.

Cullen, B. R. (2006). Enhancing and confirming the specificity of rnai experiments. *Nat Methods 3*(9), 677–81.

Dalley, J. W., K. Laane, D. E. Theobald, H. C. Armstrong, P. R. Corlett, Y. Chudasama, and T. W. Robbins (2005). Time-limited modulation of appetitive pavlovian memory by d1 and nmda receptors in the nucleus accumbens. *Proc Natl Acad Sci U S A 102*(17), 6189–94.

D'Ardenne, K., S. M. McClure, L. E. Nystrom, and J. D. Cohen (2008). Bold responses reflecting dopaminergic signals in the human ventral tegmental area. *Science 319*(5867), 1264–7.

Di Ciano, P. and B. J. Everitt (2004). Contribution of the ventral tegmental area to cocaine-seeking maintained by a drug-paired conditioned stimulus in rats. *Eur J Neurosci 19*(6), 1661–7.

Engblom, D., A. Bilbao, C. Sanchis-Segura, L. Dahan, S. Perreau-Lenz, B. Balland, J. R. Parkitna, R. Lujan, B. Halbout, M. Mameli, R. Parlato, R. Sprengel, C. Luscher, G. Schutz, and R. Spanagel (2008). Glutamate receptors on dopamine neurons control the persistence of cocaine seeking. *Neuron 59*(3), 497–508.

Feierstein, C. E., M. C. Quirk, N. Uchida, D. L. Sosulski, and Z. F. Mainen (2006). Representation of spatial goals in rat orbitofrontal cortex. *Neuron 51*(4), 495–507.

Fields, H. L., G. O. Hjelmstad, E. B. Margolis, and S. M. Nicola (2007). Ventral tegmental area neurons in learned appetitive behavior and positive reinforcement. *Annu Rev Neurosci 30*, 289–316.

Fiorillo, C. D., P. N. Tobler, and W. Schultz (2003). Discrete coding of reward probability and uncertainty by dopamine neurons. *Science 299*(5614), 1898–902.

Flagel, S. B., T. E. Robinson, J. J. Clark, S. M. Clinton, S. J. Watson, P. Seeman, P. E. Phillips, and H. Akil (2010). An animal model of genetic vulnerability to behavioral disinhibition and responsiveness to reward-related cues: implications for addiction. *Neuropsychopharmacology 35*(2), 388–400.

Floresco, S. B., C. L. Todd, and A. A. Grace (2001). Glutamatergic afferents from

the hippocampus to the nucleus accumbens regulate activity of ventral tegmental area dopamine neurons. *J Neurosci 21*(13), 4915–22.

Floresco, S. B., A. R. West, B. Ash, H. Moore, and A. A. Grace (2003). Afferent modulation of dopamine neuron firing differentially regulates tonic and phasic dopamine transmission. *Nat Neurosci 6*(9), 968–73.

Freedman, D. J., M. Riesenhuber, T. Poggio, and E. K. Miller (2001). Categorical representation of visual stimuli in the primate prefrontal cortex. *Science 291*(5502), 312–6.

Frey, U., H. Schroeder, and H. Matthies (1990). Dopaminergic antagonists prevent long-term maintenance of posttetanic ltp in the ca1 region of rat hippocampal slices. *Brain Res 522*(1), 69–75.

Geisler, S., C. Derst, R. W. Veh, and D. S. Zahm (2007). Glutamatergic afferents of the ventral tegmental area in the rat. *J Neurosci 27*(21), 5730–43.

Goto, Y. and A. A. Grace (2005). Dopamine-dependent interactions between limbic and prefrontal cortical plasticity in the nucleus accumbens: disruption by cocaine sensitization. *Neuron 47*(2), 255–66.

Grace, A. A. and B. S. Bunney (1984a). The control of firing pattern in nigral dopamine neurons: burst firing. *J Neurosci 4*(11), 2877–90.

Grace, A. A. and B. S. Bunney (1984b). The control of firing pattern in nigral dopamine neurons: single spike firing. *J Neurosci 4*(11), 2866–76.

Hitz, C., W. Wurst, and R. Kuhn (2007). Conditional brain-specific knockdown of mapk using cre/loxp regulated rna interference. *Nucleic Acids Res 35*(12), e90.

Hollerman, J. R. and W. Schultz (1998). Dopamine neurons report an error in the temporal prediction of reward during learning. *Nat Neurosci 1*(4), 304–9.

Huang, Y. Y. and E. R. Kandel (1995). D1/d5 receptor agonists induce a protein synthesis-dependent late potentiation in the ca1 region of the hippocampus. *Proc Natl Acad Sci U S A 92*(7), 2446–50.

Hyland, B. I., J. N. Reynolds, J. Hay, C. G. Perk, and R. Miller (2002). Firing modes of midbrain dopamine cells in the freely moving rat. *Neuroscience 114*(2), 475–92.

Hyman, S. E. (2005). Addiction: a disease of learning and memory. *Am J Psychiatry 162*(8), 1414–22.

Justice, J. B., J. (1993). Quantitative microdialysis of neurotransmitters. *J Neurosci Methods 48*(3), 263–76.

Kepecs, A., N. Uchida, H. A. Zariwala, and Z. F. Mainen (2008). Neural correlates, computation and behavioural impact of decision confidence. *Nature 455*(7210), 227–31.

Kobayashi, S. and W. Schultz (2008). Influence of reward delays on responses of dopamine neurons. *J Neurosci 28*(31), 7837–46.

Lammel, S., A. Hetzel, O. Hackel, I. Jones, B. Liss, and J. Roeper (2008). Unique properties of mesoprefrontal neurons within a dual mesocorticolimbic dopamine system. *Neuron 57*(5), 760–73.

Liu, Q. S., L. Pu, and M. M. Poo (2005). Repeated cocaine exposure in vivo facilitates ltp induction in midbrain dopamine neurons. *Nature 437*(7061), 1027–31.

Lodge, D. J. and A. A. Grace (2006). The hippocampus modulates dopamine neuron responsivity by regulating the intensity of phasic neuron activation. *Neuropsychopharmacology 31*(7), 1356–61.

Lois, C., E. J. Hong, S. Pease, E. J. Brown, and D. Baltimore (2002). Germline transmission and tissue-specific expression of transgenes delivered by lentiviral vectors. *Science 295*(5556), 868–72.

Lokwan, S. J., P. G. Overton, M. S. Berry, and D. Clark (1999). Stimulation of the pedunculopontine tegmental nucleus in the rat produces burst firing in a9 dopaminergic neurons. *Neuroscience 92*(1), 245–54.

Matsumoto, M. and O. Hikosaka (2009). Two types of dopamine neuron distinctly convey positive and negative motivational signals. *Nature 459*(7248), 837–41.

McFarland, K. and P. W. Kalivas (2001). The circuitry mediating cocaine-induced reinstatement of drug-seeking behavior. *J Neurosci 21*(21), 8655–63.

Mirenowicz, J. and W. Schultz (1994). Importance of unpredictability for reward responses in primate dopamine neurons. *J Neurophysiol 72*(2), 1024–7.

Montague, P. R., P. Dayan, and T. J. Sejnowski (1996). A framework for mesencephalic dopamine systems based on predictive hebbian learning. *J Neurosci 16*(5), 1936–47.

Morris, G., A. Nevet, D. Arkadir, E. Vaadia, and H. Bergman (2006). Midbrain dopamine neurons encode decisions for future action. *Nat Neurosci 9*(8), 1057–63.

Nakahara, H., H. Itoh, R. Kawagoe, Y. Takikawa, and O. Hikosaka (2004). Dopamine neurons can represent context-dependent prediction error. *Neuron 41*(2), 269–80.

Nakazawa, K., M. C. Quirk, R. A. Chitwood, M. Watanabe, M. F. Yeckel, L. D. Sun, A. Kato, C. A. Carr, D. Johnston, M. A. Wilson, and S. Tonegawa (2002). Requirement for hippocampal ca3 nmda receptors in associative memory recall. *Science 297*(5579), 211–8.

Newsome, W. T., K. H. Britten, and J. A. Movshon (1989). Neuronal correlates of a perceptual decision. *Nature 341*(6237), 52–4.

Newsome, W. T. and E. B. Pare (1988). A selective impairment of motion perception following lesions of the middle temporal visual area (mt). *J Neurosci 8*(6), 2201–11.

Nomoto, K., W. Schultz, T. Watanabe, and M. Sakagami. Temporally extended dopamine responses to perceptually demanding reward-predictive stimuli. *J Neurosci 30*(32), 10692–702.

Otmakhova, N. A. and J. E. Lisman (1996). D1/d5 dopamine receptor activation increases the magnitude of early long-term potentiation at ca1 hippocampal synapses. *J Neurosci 16*(23), 7478–86.

Overton, P. and D. Clark (1992). Iontophoretically administered drugs acting at the n-methyl-d-aspartate receptor modulate burst firing in a9 dopamine neurons in the rat. *Synapse 10*(2), 131–40.

Overton, P. G., C. D. Richards, M. S. Berry, and D. Clark (1999). Long-term potentiation at excitatory amino acid synapses on midbrain dopamine neurons. *Neuroreport 10*(2), 221–6.

Pan, W. X. and B. I. Hyland (2005a). Pedunculopontine tegmental nucleus controls conditioned responses of midbrain dopamine neurons in behaving rats. *J Neurosci 25*(19), 4725–32.

Pan, W. X. and B. I. Hyland (2005b). Pedunculopontine tegmental nucleus controls conditioned responses of midbrain dopamine neurons in behaving rats. *J Neurosci 25*(19), 4725–32.

Parker, J. G., L. S. Zweifel, J. J. Clark, S. B. Evans, P. E. Phillips, and R. D. Palmiter (2010). Absence of nmda receptors in dopamine neurons attenuates dopamine release but not conditioned approach during pavlovian conditioning. *Proc Natl Acad Sci U S A 107*(30), 13491–6.

Ravel, S. and B. J. Richmond (2006). Dopamine neuronal responses in monkeys performing visually cued reward schedules. *Eur J Neurosci 24*(1), 277–90.

Richfield, E. K., J. B. Penney, and A. B. Young (1989). Anatomical and affinity state comparisons between dopamine d1 and d2 receptors in the rat central nervous system. *Neuroscience 30*(3), 767–77.

Robinson, D. L., M. L. Heien, and R. M. Wightman (2002). Frequency of dopamine concentration transients increases in dorsal and ventral striatum of male rats during introduction of conspecifics. *J Neurosci 22*(23), 10477–86.

Robinson, D. L., P. E. Phillips, E. A. Budygin, B. J. Trafton, P. A. Garris, and R. M. Wightman (2001). Sub-second changes in accumbal dopamine during sexual behavior in male rats. *Neuroreport 12*(11), 2549–52.

Roesch, M. R., D. J. Calu, and G. Schoenbaum (2007). Dopamine neurons encode the better option in rats deciding between differently delayed or sized rewards. *Nat Neurosci 10*(12), 1615–24.

Satoh, T., S. Nakai, T. Sato, and M. Kimura (2003). Correlated coding of motivation and outcome of decision by dopamine neurons. *J Neurosci 23*(30), 9913–23.

Schultz, W. (1998). Predictive reward signal of dopamine neurons. *J Neurophysiol 80*(1), 1–27.

Shadlen, M. N. and W. T. Newsome (2001). Neural basis of a perceptual decision in the parietal cortex (area lip) of the rhesus monkey. *J Neurophysiol 86*(4), 1916–36.

Soriano, P. (1999). Generalized lacz expression with the rosa26 cre reporter strain. *Nat Genet 21*(1), 70–1.

Stuber, G. D., M. Klanker, B. de Ridder, M. S. Bowers, R. N. Joosten, M. G. Feenstra, and A. Bonci (2008). Reward-predictive cues enhance excitatory synaptic strength onto midbrain dopamine neurons. *Science 321*(5896), 1690–2.

Suaud-Chagny, M. F., K. Chergui, G. Chouvet, and F. Gonon (1992). Relationship between dopamine release in the rat nucleus accumbens and the discharge activity of dopaminergic neurons during local in vivo application of amino acids in the ventral tegmental area. *Neuroscience 49*(1), 63–72.

Swanson, L. W. (1982). The projections of the ventral tegmental area and adjacent regions: a combined fluorescent retrograde tracer and immunofluorescence study in the rat. *Brain Res Bull 9*(1-6), 321–53.

Takahashi, Y. K., M. R. Roesch, T. A. Stalnaker, R. Z. Haney, D. J. Calu, A. R. Taylor, K. A. Burke, and G. Schoenbaum (2009). The orbitofrontal cortex and ventral tegmental area are necessary for learning from unexpected outcomes. *Neuron 62*(2), 269–80.

Thorndike, E. (1911). Animal intelligence: Experimental studies (new york: Macmillan).

Thorndike, E. (1933). A proof of the law of effect. *Science 77*, 173–175.

Tobler, P. N., C. D. Fiorillo, and W. Schultz (2005). Adaptive coding of reward value by dopamine neurons. *Science 307*(5715), 1642–5.

Tsai, H. C., F. Zhang, A. Adamantidis, G. D. Stuber, A. Bonci, L. de Lecea, and K. Deisseroth (2009). Phasic firing in dopaminergic neurons is sufficient for behavioral conditioning. *Science 324*(5930), 1080–4.

Tsien, J. Z., D. F. Chen, D. Gerber, C. Tom, E. H. Mercer, D. J. Anderson, M. Mayford, E. R. Kandel, and S. Tonegawa (1996). Subregion- and cell type-restricted gene knockout in mouse brain. *Cell 87*(7), 1317–26.

Uchida, N. and Z. F. Mainen (2003). Speed and accuracy of olfactory discrimination in the rat. *Nat Neurosci 6*(11), 1224–9.

Ungless, M. A., P. J. Magill, and J. P. Bolam (2004). Uniform inhibition of dopamine neurons in the ventral tegmental area by aversive stimuli. *Science 303*(5666), 2040–2.

Ungless, M. A., J. L. Whistler, R. C. Malenka, and A. Bonci (2001). Single cocaine exposure in vivo induces long-term potentiation in dopamine neurons. *Nature 411*(6837), 583–7.

Vorel, S. R., X. Liu, R. J. Hayes, J. A. Spector, and E. L. Gardner (2001). Relapse to cocaine-seeking after hippocampal theta burst stimulation. *Science 292*(5519), 1175–8.

Waelti, P., A. Dickinson, and W. Schultz (2001). Dopamine responses comply with basic assumptions of formal learning theory. *Nature 412*(6842), 43–8.

Walton, M. E., T. E. Behrens, M. J. Buckley, P. H. Rudebeck, and M. F. Rushworth (2010). Separable learning systems in the macaque brain and the role of orbitofrontal cortex in contingent learning. *Neuron 65*(6), 927–39.

Wise, R. A. (2004). Dopamine, learning and motivation. *Nat Rev Neurosci 5*(6), 483–94.

Zhuang, X., J. Masson, J. A. Gingrich, S. Rayport, and R. Hen (2005). Targeted gene expression in dopamine and serotonin neurons of the mouse brain. *J Neurosci Methods 143*(1), 27–32.

Zweifel, L. S., E. Argilli, A. Bonci, and R. D. Palmiter (2008). Role of nmda receptors in dopamine neurons for plasticity and addictive behaviors. *Neuron 59*(3), 486–96.

Zweifel, L. S., J. G. Parker, C. J. Lobb, A. Rainwater, V. Z. Wall, J. P. Fadok, M. Darvas, M. J. Kim, S. J. Mizumori, C. A. Paladini, P. E. Phillips, and R. D. Palmiter (2009). Disruption of nmdar-dependent burst firing by dopamine neurons provides selective assessment of phasic dopamine-dependent behavior. *Proc Natl Acad Sci U S A 106*(18), 7281–8.